

LITHOGEOCHEMISTRY AND ORIGIN OF METASEDIMENTS HOSTING
THE BROKEN HILL DEPOSIT, AGGENEYS, SOUTH AFRICA,
AND IMPLICATIONS FOR ORE GENESIS

by

RAEL DESMOND LIPSON

DOCTOR OF PHILOSOPHY

IN THE DEPARTMENT OF GEOCHEMISTRY

FACULTY OF SCIENCE

UNIVERSITY OF CAPE TOWN

APRIL 1990

The University of Cape Town has been given
the right to reproduce this thesis in whole
or in part. Copyright is held by the author.

The copyright of this thesis vests in the author. No quotation from it or information derived from it is to be published without full acknowledgement of the source. The thesis is to be used for private study or non-commercial research purposes only.

Published by the University of Cape Town (UCT) in terms of the non-exclusive license granted to UCT by the author.

ABSTRACT

The thin metasedimentary suite (< 1 000m) of supracrustal schist and quartzite at Broken Hill, Aggeneys, forms part of the Proterozoic Aggeneys Subgroup within the Namaqua Province of South Africa. The structural succession at Broken Hill comprises gneisses (not investigated in this thesis), which overlie red-coloured, nodular magnetite-bearing Namies Schist that grades downwards into mature Broken Hill Quartzites. The latter host heavy mineral layers containing detritally rounded zircons. Ore Schist lying below Broken Hill Quartzites, has similar characteristics to Namies Schist, and hosts the banded iron formation-associated Broken Hill Pb-Ag-Zn-Cu orebody. Biotite garnet schist and stringers of Garnet Quartzite within Ore Schist represent an Ore Equivalent Horizon at the same stratigraphic level as the two superposed lenses comprising the Broken Hill orebody. A Biotite Graphite Zone marks the sharp contact between Ore Schist and the green-coloured, pyrite- and graphite- bearing Shaft Schist. Lenses of Calc Silicate Rock plus Manganese Quartzite within Shaft Schist lie close to the Biotite Graphite Zone. Analyses of an extensive suite of spatially and lithologically controlled borehole core and surface outcrop samples by X-ray fluorescence spectrometry reveals a contrast between sporadically high base metal values in Namies Schist, and Shaft Schist which is chemically anomalous only in its elevated Pb content. Namies Schist at Broken Hill is therefore interpreted as predating the orebody, whereas Shaft Schist postdated the deposit. An overturned sequence is thus inferred at Broken Hill, and it can be correlated unit-for-unit with sequences at Namiesberg and Wortel (termed regional rocks) lying 25 - 30km to the east and north. A voluminous basement of potassic, siliceous, biotite gneisses underlie the supracrustal rocks.

The low MnO and high S content of the homogeneous Shaft Schist stand in contrast to the high MnO and low S character of the chemically variable Namies Schist, and viewed together with rock colour and absence or presence of magnetite, indicate that Namies Schist and the related, detrital Broken Hill Quartzites, formed in oxygenated, agitated, aqueous conditions whereas Shaft Schist developed as a black shale in an anoxic, meromictic, lagoon-like environment. Lenses of Calc Silicate Rock plus Manganese Quartzite primarily represent the precipitates from elements which had accumulated at the thermocline boundary prior to destabilization of the quiet, lagoonal conditions. The high S content of Shaft Schist and negative Ce anomaly of Calc Silicate Rock plus Manganese Quartzite show that Shaft Schist formed beneath sea water. A passive continental margin environment may be deduced from the extreme silica purity and sheet-like morphology of the quartz arenitic Broken Hill Quartzites, and from the elevated alumina concentrations of Namies Schist and Shaft Schist. Shaft Schist and Broken Hill Quartzites were probably the lagoon and beach barrier sediments, respectively, of a prograding beach barrier system, and the upward coarsening Namies Schist represents the shoreface pelites. Ore Schist probably formed as washover sediments derived from Namies Schist. The tendency for quartzite to thin southwards through Aggeneys is matched by progressively cleaner separation in that direction, of silica in quartzite from alumina in schist, indicating south-directed progradation over tens of kilometres.

Shapes of rare earth element patterns, Eu/Eu* ratios from Namies Schist, Broken Hill Quartzites and Shaft Schist, and major and trace element modelling suggest that the metasediments were derived from a weathered, granodioritic provenance. Ca removed during early provenance weathering was probably precipitated distally to form the calcic rocks south and east of Aggeneys, while removed Na remained in

solution. Detrital transport of the granodioritic residuum caused the formation of Ca- and Na- depleted, and K-, Al- and total rare earth element-enriched shales and sandstones. Ion microprobe Pb isotope dating of detrital zircons from Broken Hill Quartzites return maximum ages of 2.0Ga which confirm the post-Archaeon signatures given by low La/Th ratios and negative Eu anomalies of the metasediments. The age constraints and oxygen isotope composition of Broken Hill Quartzites are compatible with a provenance of Vioolsdrif granitoids, which crop out to the north and north-west of Aggeneys.

The average base metal and associated element concentrations of Namies Schist and Broken Hill Quartzites at Broken Hill are greater than for their correlative regional rocks, indicating the presence of a geochemical halo around the orebody. The Ore Equivalent Horizon displays a localized primary geochemical halo measureable for up to 10km distance, and most clearly defined by increasing Zn and Ba concentrations progressively nearer the orebody. "Ore Factor" scores from the Factor Analysis of Ore Schist, also increase progressively nearer ore. Together with positive heavy rare earth element anomalies of many Ore Equivalent Horizon samples, and their unusual petrography, these observations suggest that many component elements of the Ore Equivalent Horizon were of exhalative origin. Within the Ore Equivalent Horizon, higher concentrations of base metals and related elements on the west side of the Broken Hill orebody relative to the east side, and a maximum MnO concentration lying some 300m east of the orebody, suggest that the hydrothermal fluid from which ore formed moved eastwards along the sea floor.

Thermochemical modelling of Zn/Cu and Pb/Cu ratios of hydrothermal solutions in equilibrium with sphalerite, galena and chalcocite shows that higher solution pH favours greater relative Cu concentrations in

the ore fluid. Whereas the higher temperature fluids ($> 150^{\circ}\text{C}$) have relatively low Zn/Cu ratios, maximum relative Zn concentrations occur in the lowest pH and lowest temperature fluids. The four orebodies in the Aggeneys-Gamsberg area were likely to have had similar metal ratios to those present in their parent hydrothermal fluids. Using the gross Zn/Pb, Zn/Cu and Pb/Cu ratios of each deposits and thermochemical data from both this investigation and from Huston and Large (1987), it is shown that the Pb-Zn-Cu-rich Broken Hill deposit formed from fluids at ca. 280°C and a pH of 4.7 - 5.4. The Zn-rich Gamsberg deposit formed from fluids at $100 - 150^{\circ}\text{C}$ and a pH of 4.0 - 4.5. The acidic and reduced, S-bearing waters in the enclosed Gamsberg basin are contrasted with the oxidizing, SO_4 -bearing and more alkaline environment in which the Broken Hill (and Black Mountain) orebodies formed. The nature of individual basin sea water which was convected kilometres down into the crust, as well as the depth of convection, ultimately determined the proportions of metals leached from a basement which probably becomes more mafic at depth. The higher temperature, more deeply circulating, alkaline fluids which gave rise to the Black Mountain and Broken Hill deposits, leached relatively more Cu, whereas low temperature, shallowly circulating, more acidic and H_2S -rich fluids generated the Gamsberg and Big Syncline orebodies. Unrealistically large volumes of illite would be required at Aggeneys to produce a deposit of the size of Broken Hill, solely by the dehydration of sediment.

Localization of ore to the general Aggeneys-Gamsberg area where amphibolite bodies and wedges of clastic conglomerates occur, point to the likely existence of synsedimentary rift processes. Such rift faults probably focussed fluids on their return journey from depth, and sulphur and metals precipitated at or near the vents in response to falling temperature, to form stratiform orebodies on the sea floor.

The passage of hydrothermal fluid caused slight metal contamination of Namies Schist and Broken Hill Quartzites immediately below the ore time horizon. The Broken Hill orebody and geochemical halo were preserved by progradational deposition of the overlying Shaft Schist.

LITHOGEOCHEMISTRY AND ORIGIN OF METASEDIMENTS HOSTING THE BROKEN HILL
DEPOSIT, AGGENEYS, SOUTH AFRICA, AND IMPLICATIONS FOR ORE GENESIS

TABLE OF CONTENTS

	Page No.
LIST OF FIGURES IN VOLUME 2	vii
LIST OF TABLES IN VOLUME 2	xvii
DEDICATION	xx
ACKNOWLEDGEMENTS	xxi
ABBREVIATIONS	xxiv
PART A. INTRODUCTION	
1. HISTORY AND LOCATION	1
2. STUDY CONTEXT, OBJECTIVES AND METHODOLOGY	3
2.1 Study context	3
2.2 Objectives	3
2.3 Methodology	4
PART B. GEOLOGY AND PETROGRAPHY	
3. REGIONAL GEOLOGICAL SETTING	6
4. BROKEN HILL GEOLOGY AND PETROGRAPHY	12
4.1 Structure, metamorphism and lithostratigraphy	12
4.2 Broken Hill schists	14
4.2.1 Namies Schist (NS)	14
4.2.2 Shaft Schist (SS)	16
4.2.2.1 Biotite Graphite Zone (BGZ)	17
4.2.2.2 Calc Silicate Rock plus Manganese Quartzite (CSMQ)	18
4.2.3 Ore schists and orebody	18
4.3 Broken Hill Quartzites (BQ)	21
4.4 Physical dimensions	23
4.5 Conclusions	25
5. LITHOSTRATIGRAPHIC CORRELATIONS	26
5.1 Broken Hill area	26
5.2 Namiesberg, Wortel and Achab	30
5.3 Conclusions	35

PART C. GEOCHEMISTRY

6.	BROKEN HILL GEOCHEMISTRY	37
6.1	Element redistributions	37
6.1.1	Introduction	38
6.1.2	Constraints on rigorous modelling of element mobility during metamorphism	39
6.1.3	Non-rigorous modelling of element mobility during metamorphism	39
6.1.3.1	Major elements	39
6.1.3.2	K/Rb ratios	40
6.1.3.3	Pegmatite and host schist	41
6.1.3.3.1	Physical evidence	41
6.1.3.3.2	Geochemical evidence	42
6.1.3.4	Pyrite to pyrrhotite transitions	43
6.1.3.5	Oxygen isotopes	44
6.1.4	Element mobility during weathering	44
6.1.4.1	Comparison between specific selected samples (orientation study)	45
6.1.4.2	Comparison between sample groups	46
6.1.5	Discussion and conclusions	46
6.2	Namies Schist and Shaft Schist	48
6.2.1	Direct geochemical contrast between NS and SS	48
6.2.2	Element variability	49
6.2.3	R-mode factor analysis	49
6.2.4	Discriminant function analysis (DFA)	51
6.2.5	Rare earth elements (REE)	52
6.2.6	Contrasted behaviour of base metals in NS and SS	53
6.2.7	Minor lithologies and special samples	53
6.2.7.1	Calc Silicate Rock plus Manganese Quartzite (CSMQ)	53
6.2.7.2	Biotite Graphite Zone (BGZ)	54
6.2.7.3	Geochemistry of ALP054	54
6.2.7.4	Tank Hill samples	55
6.3	Ore Equivalent Horizon and Orebody	56
6.3.1	Schists	56
6.3.1.1	Geochemical characteristics	56
6.3.1.2	R-mode factor analysis	57
6.3.1.3	Discriminant function analysis	58
6.3.1.4	Rare earth elements	60
6.3.1.5	OS correlations	60
6.3.1.6	OS geochemical variations at Broken Hill	61
6.3.2	Ore Schist plus Garnet Quartzite (OS+GQ), Ore Equivalent Garnet Quartzite (OEGQ), Garnet Quartzite (GQ) and Orebody	62
6.3.2.1	Geochemical characteristics	62
6.3.2.2	Rare earth elements	64
6.3.2.3	Garnet Quartzite (GQ), Ore Equivalent Garnet Quartzite (OEGQ) and Ore Schist plus Garnet Quartzite (OS+GQ) geochemical variations at Broken Hill	65
6.3.3	Comparison with mineralized sequences	66
6.4	Broken Hill Quartzites (BQ)	67
6.4.1	Geochemical characteristics	67
6.4.2	R-mode factor analysis	69
6.4.3	Discriminant function analysis (DFA)	69
6.4.4	Rare earth elements	69

6.5	Oxygen isotopes	70
6.6	Geochemical relationships between adjacent lithologies	71
6.6.1	NS to BQ transition	71
6.6.2	OS $\delta^{18}\text{O}$ transitions	73
6.6.3	SS transitions	74
6.6.4	Ratio transitions through the succession	75
7.	REGIONAL GEOCHEMISTRY AND COMPARISON WITH BROKEN HILL	77
7.1	Regional schists	77
7.1.1	Geochemical characteristics	77
7.1.2	R-mode factor analysis	79
7.1.3	Rare earth elements	79
7.2	Regional Quartzites (RQ)	79
7.2.1	Geochemical characteristics	79
7.2.2	Rare earth elements	80
7.3	Geochemical comparisons between data sets	80
7.3.1	Methods of comparison	80
7.3.2	Comparisons for elements unrelated to the Broken Hill orebody	82
7.3.3	Comparisons for ore-related elements	83
7.3.4	Conclusions	84
PART D. GEOLOGICAL AND GEOCHEMICAL MODELLING		
8.	PROVENANCE	85
8.1	Provenance age	85
8.1.1	Rare earth elements	85
8.1.2	Uranium/lead age dating of zircons	86
8.2	State of provenance weathering	87
8.2.1	Major and trace elements	87
8.2.2	Rare earth elements	89
8.3	Provenance composition	90
8.3.1	Rare earth elements	91
8.3.2	Major and trace elements	92
8.3.3	Heavy mineral separates	94
8.4	Discussion and conclusions	95
9.	GENESIS OF THE METASEDIMENTS AND STRUCTURAL IMPLICATIONS	97
9.1	Schists: NS and SS depositional environments	97
9.1.1	Geochemical comparisons with shales	97
9.1.2	Maturity and ore-relatedness	100
9.1.3	Redox conditions	104
9.1.4	Behavior of key elements and ratios during the formation of black shales	108
9.1.4.1	Carbon, phosphorus, sulphur and copper	108
9.1.4.2	Manganese and iron	115
9.1.4.3	Vanadium and molybdenum	117
9.1.4.4	Chromium	120
9.1.4.5	Nickel and cobalt	121
9.1.4.6	Zinc and uranium	123
9.1.4.7	Rare earth elements	125
9.1.4.8	Additional ratios	126

9.1.5	Significance of ALP054 geochemistry	127
9.1.6	SS depositional rates	127
9.1.7	Calc Silicate Rock plus Manganese Quartzite (CSMQ)	128
9.1.7.1	Geochemical comparisons	129
9.1.7.2	Possible hydrothermal derivation	129
9.1.7.3	Possible authochthonous derivation	130
9.1.7.4	Preferred model for CSMQ origin	133
9.1.8	Biotite Graphite Zone (BGZ)	134
9.2	Structural geology summary	135
9.3	Quartzites: Genesis and depositional environment	137
9.3.1	Geochemical comparisons with chert and sandstone	137
9.3.2	Chert as a precursor	139
9.3.3	Sandstone as a precursor	141
9.3.3.1	Beach-barrier shoreline sands	142
9.3.3.2	Shallow marine siliclastic sandstones	144
9.3.3.3	Deltaic sandstones	145
9.3.3.4	Massive sandstone facies of turbidites	145
9.3.3.5	Fluvial sandstones	145
9.3.3.6	Lacustrinal siliclastic sandstones	146
9.3.3.7	Aeolian dunes	146
9.3.4	Genesis of heavy mineral layers	146
9.3.5	Conclusions	148
9.4	Local sedimentary genetic model	150
9.4.1	Physical environments	150
9.4.2	Geochemical differentiation	153
9.4.3	Oxygen isotopes	154
9.5	Facies variations and regional sedimentary genetic model	157
10.	GENESIS OF THE OREBODY AND ORE EQUIVALENT HORIZON	160
10.1	Distinctive physical characteristics of the Broken Hill orebody, its host rocks, and implications	160
10.2	Distinctive chemical characteristics of the Broken Hill orebody, its host rocks, and implications	162
10.2.1	Redox conditions of host rocks	162
10.2.2	Low Zn/Pb ratio and source rocks	164
10.3	Ore fluid chemistry	165
10.3.1	Zn/Pb ratio of fluid	165
10.3.2	Solubility modelling of Cu-Pb-Zn ratios	166
10.3.3	Cu-Pb-Zn ratios at Aggeneys-Gamsberg	169
10.4	Sulphur isotopes and source of sulphur	170
10.5	Basin dewatering versus deep convection of fluids	173
10.6	Ore and gangue deposition	182
10.7	Ore Equivalent Horizon (OEH)	184
10.7.1	Origin of OEH	185
10.7.2	Metal haloes and assymetry	187
10.8	Possible significance of Tank Hill	190
10.9	Rare earth elements	191

10.10	Genetic model for Aggeneys-Gamsberg orebodies and OEH	194
11.	CONCLUSIONS	202
11.1	Stratigraphy and sedimentology	202
11.2	Ore genesis and local tectonics	205
11.3	Ore halo and exploration	208
11.4	Geotectonic setting	209
PART E. APPENDICES AND REFERENCES		
12.	APPENDICES	213
APPENDIX A	SAMPLING AND ANALYTICAL TECHNIQUES	213
A.1	Sampling rationale and technique	213
A.1.1	Parameters common to borehole core and surface outcrop sampling	213
A.1.2	Borehole core samples	213
A.1.3	Surface outcrop samples	213
A.2	Analytical methods	213
A.2.1	Sample preparation	213
A.2.2	X-ray fluorescence spectrometry (XRF)	214
A.2.3	Volatile-free recalculation	214
A.2.4	Gas chromatography	215
A.2.5	Comparison between XRF and Instrumental Neutron Activation Analysis (INAA) results for rare earth elements	215
APPENDIX B	STATISTICAL TECHNIQUES	217
B.1	Correlation	217
B.2	Factor analysis	217
B.3	Discriminant function analysis (DFA)	217
APPENDIX C	ADDITIONAL PETROGRAPHIC DESCRIPTIONS	219
C.1	Namies Schist (NS)	219
C.2	Shaft Schist (SS)	219
C.2.1	Biotite Graphite Zone (BGZ)	219
C.2.2	Calc Silicate Rock plus Manganese Quartzite (CSMQ)	220
C.3	Ore Schist (OS) and Orebody	221
C.4	Broken Hill Quartzites (BQ)	222
C.5	Namies-type Schist (NTS)	223
C.5.1	NTS at Namiesberg	223
C.5.2	NTS in Achab borehole	223
C.6	Shaft-type Schist (STS)	224
C.6.1	Massive Sillimanite	224
C.6.2	Calc Silicate-type Rock plus Manganese Quartzite	224

C.7	Regional Quartzite (RQ)	225
APPENDIX D	METAMORPHISM	226
APPENDIX E	RELATIONSHIPS BETWEEN MAJOR LITHOLOGIES	227
E.1	Gneisses through NS to WQ	227
E.2	OS through SS to Plant Quartzite (PQ)	227
APPENDIX F	ORE SCHIST FACTOR SCORES RELATED TO THE OREBODY	228
APPENDIX G	LITHOGEOCHEMICAL EXPLORATION STRATEGY	229
APPENDIX H	CALCULATION OF LIMITING CASES FOR PRE-METAMORPHIC CARBON AND SULPHUR CONTENTS OF SS	230
APPENDIX I	CALCULATION OF PB/CU AND ZN/CU RATIOS IN FLUIDS	232
APPENDIX J	MASS BALANCE FOR GENERATING BROKEN HILL OREBODY USING LYDON'S DEWATERING MODEL	234
APPENDIX K	SUNDRY TABLES REFERRED TO IN THE TEXT	234
13.	REFERENCES	235

LIST OF FIGURES IN VOLUME 2

- Fig. 1.1 Major Proterozoic tectonic provinces and subprovinces of southern Africa (after Hartnady et al., 1985). Box covers Aggeneys area shown in Fig. 1.4. SCCB = Southern Cape Conductive Belt; + = Beattie magnetic anomaly (after de Beer and Meyer, 1983)
- Fig. 1.2 Aerial photograph of Broken Hill mine, looking west. The Black Mountain orebody is seen in the far distance. Photograph courtesy A. Lanham
- Fig. 1.3 Panoramic view of Broken Hill looking east. Maanhaarkop is seen in the middle distance and Gamsberg (flat-topped mountain) in the far distance
- Fig. 1.4 Locality map of southern Africa showing position of inselbergs in the Aggeneys area within the Namaqua Province. Position of Groothoek Thrust after Blignault et al. (1983, Fig. 14). BH = Broken Hill; MK = Maanhaarkop; FK = Froneman se Kop; BM = Black Mountain; PH = Plant Hill; TH = Tank Hill. Inset shows Aggeneys area relative to political boundaries
- Fig. 2.1 Conceptual representation of an orebody enveloped by its lithogeochemical halo. On the top surface are shown two idealized lithogeochemical sampling profiles for an element of interest with concentration intensity (here shown as positive) increasing both towards the centre of each profile and with proximity to the orebody. Similar profiles could be drawn down the borehole (BH) depicted, with increased geochemical response where the borehole intersects the halo. The Broken Hill orebody only measures 1 000m by 100m in outcrop. Prior knowledge of a halo which envelopes Broken Hill-type mineralization would indicate a buried deposit, or alert the explorationist when a borehole had narrowly missed the orebody
- Fig. 3.1 Map showing Subgroups of the Bushmanland Group, and Subgroups of the Okiep Group which are similar to the Aggeneys and Pella Subgroups. Modified after SACS (1980, Figs. 5.1.5 and 5.1.6)
- Fig. 3.2 Map showing the Aggeneys Subgroup and all possible correlative supracrustal successions in the Namaqua Province, and the distribution of the Little Namaqualand Suite, from Bitterfontein to Prieska (based on Blignault et al., 1983, Fig. 14; Joubert, 1986; SACS, Fig. 5.1.1 and Moore, 1986, Fig. 1.1)
- Fig. 4.1 Map of the Aggeneys area showing gross similarity of the geology between Broken Hill, Klein Kop, Maanhaarkop and Froneman se Kop. Locality plan shows relationship of Broken Hill (BH), Maanhaarkop (MK) and Froneman se Kop (FK) forming the southern limb of the Black Mountain (BM) synclinorium. Also indicated are Plant Hill (PH) and Tank Hill (TH).
- Fig. 4.2 Structural succession at Broken Hill: the idealized borehole intersection
- Fig. 4.3 Regional north south section through Broken Hill, Aggeneysberge and Black Mountain showing fold closure positions for Aggeneysberge and Black mountain projected down plunge from surface (after Lipson, 1978, Fig. 87). Location of cross section shown in Fig. 5.3
- Fig. 4.4 Structural interpretation along a section through Broken Hill and Plant Hill
- Fig. 4.5 Idealized structural section through Maanhaarkop and borehole TS11
- Fig. 4.6 Working stratigraphic column at Broken Hill
- Fig. 4.7 Photograph of NS core showing pink hue and common nodular texture

- Fig. 4.8 NS (ALP063) showing undeformed muscovite as an alteration product after folded sillimanite. Note also simplectic quartz intergrowths (dark zones in muscovite). Highly birefringent inclusion in quartz is zircon. Crossed nichols. (1cm = 100 micron)
- Fig. 4.9 Photograph of SS core showing bottle-green hue and uniformly banded texture. Note green colour of pegmatite at bottom centre
- Fig. 4.10 SS (ALP186) showing muscovite as an alteration product after biotite. Plain polarized light. (1cm = 100 micron)
- Fig. 4.11 Photograph of conglomerate at Maanhaarkop
- Fig. 4.12 Photograph of folded OEGQ layer in OS on west side of Broken Hill orebody. Note pegmatite formed between OEGQ boudins in upper limb of fold
- Fig. 4.13 Photograph of IS showing pseudo-pebbles in schist matrix. Note quartzitic band in bottom left, which has started to boudinage
- Fig. 4.14 Photograph of OES+GQ core from borehole BH112 beyond the eastern fold closure of the orebody. Note garnet-biotite composition of OES, and the intense refoliation present in the top piece of core
- Fig. 4.15 Quartzite with heavy mineral layers showing possible foreset between two subparallel bands
- Fig. 4.16 Stereoscopic X-ray radiographs of quartzite. Heavy mineral layers show ripple-like features with cusps pointing southward. Detail also shows apparent foreset "F" being truncated by apparent topset "T" at "X"
- Fig. 4.17 Stereoscopic X-ray radiographs of quartzite showing detail of possible raindrop feature located at "Z"
- Fig. 4.18 Photomicrograph of well rounded zircon concentrates from BQ (ALP227). Photograph courtesy of G. Martin
- Fig. 4.19 Heavy mineral layer in quartzite with rounded zircon (Z) the dominant mineral. (R = rutile; Ln = limonite). Photograph courtesy of G. Martin
- Fig. 5.1 Generalized geological map of Black Mountain, Tank Hill and Broken Hill
- Fig. 5.2 Photograph of Tank Hill looking south west. Note the unusual rock-types Garnet Quartzite, Green Quartzite, Massive Magnetite and Barite Magnetite Rock, all lying within the dip slope of a single stratigraphic horizon between the quartzite which forms the ridge of Tank Hill, and gneiss underlying the sand-covered flats. Quartzites in the far distance are separated from Tank Hill by a valley
- Fig. 5.3 Generalized geological map of the Aggeneys area with some selected inselbergs. Indicated are section lines through Broken Hill-Aggeneysberge (Fig. 4.3), Namiesberg (Fig. 5.4) and Wortel (Fig. 5.6)
- Fig. 5.4 Cross section through Namiesberg and borehole VG1. Abbreviations as in list at start of thesis
- Fig. 5.5 Photograph of southern limb of Namiesberg syncline showing Dark-type Quartzite overlying White-type Quartzite
- Fig. 5.6 Cross section through Wortel and borehole WTL4. Abbreviations as in list at start of thesis
- Fig. 5.7 Generalized comparative stratigraphic successions from Broken Hill, Gamsberg, Namiesberg and Wortel. Abbreviations as in list at start of thesis
- Fig. 6.1 NS and SS K vs Rb concentrations compared with various shales. See legend for shale codes
- Fig. 6.2 Photograph of schist from borehole core (touching pencil) and surface outcrop, used to test the chemical effects of surface weathering

- Fig. 6.3 Surface schist weathering orientation study. Percent variation (positive or negative) in element content is with respect to sample ALP163
- Fig. 6.4 NS and SS Zr vs SiO₂ concentrations
- Fig. 6.5 NS and SS element variations vs Al₂O₃: (a) Zr; (b) Ba; (c) Zn; (d) Cu; (e) Ni; (f) MnO; (g) Pb; (h) Co
- Fig. 6.6 NS factor analysis: (a) loadings on the six factors which cumulatively explain 93.6 % of the variance; (b) geometric representation of Factors 1, 3 and 4 which account for 64.7 % of the total variance. For purposes of clarity the elements Co, Ni, Sc, P₂O₅, V, MgO, TiO₂, Nb and Fe₂O₃ have been omitted as they may be effectively represented by the elements Al₂O₃, K₂O and Rb, as seen in Fig. 6.6 (a) above. The REE's and certain other elements are also omitted in the interests of clarity; (c) 3-D conceptual representation of the major NS factors shown in Fig. 6.6 (b) above.
- Fig. 6.7 SS factor analysis: (a) loadings on the five factors which cumulatively explain 82.6 % of the variance; (b) geometric representation of Factors 1, 3 and 4 which account for 65.6 % of the total variance. For purposes of clarity the elements Co, Ni, Sc, V, MgO, Cr and Fe₂O₃ have been omitted as they may be effectively represented by the elements Al₂O₃, K₂O and Ba, as seen in Fig. 6.7 (a) above. The REE's and certain other elements are also omitted in the interests of clarity; (c) 3-D conceptual representation of the major NS factors shown in Fig. 6.7 (b) above.
- Fig. 6.8 Shale-normalized REE patterns using the INAA analytical method: (a) NS; (b) SS. ALP057, 184 and 059 are USS; ALP158 is LSS. Average shale after Piper (1974)
- Fig. 6.9 Shale-normalized schist REE patterns, using the XRF analytical method: (a) NS from borehole BH123; (b) USS from borehole BH123; (c) LSS from boreholes BH164 and 156. Estimated Ho (Ho est.) = Y*0.0272 (see Appendix A.2.5).
- Fig. 6.10 Average shale-normalized REE patterns for the rock-types NS, USS and LSS for XRF-derived data
- Fig. 6.11 Shale-normalized REE patterns using the XRF analytical method: (a) CS; (b) MnQ (s = surface samples; c = borehole core)
- Fig. 6.12 Shale-normalized REE patterns using the INAA method for MnQ sample ALP213
- Fig. 6.13 NS, SS and BGZ Zr vs SiO₂ concentrations
- Fig. 6.14 Shale-normalized BGZ REE patterns: (a) XRF data; (b) INAA data
- Fig. 6.15 Shale-normalized REE patterns for the Tank Hill rocks using XRF-derived data. Surface NS (NSS) and SS (SSS) are shown for comparison
- Fig. 6.16 OS factor analysis: (a) including REE, with loadings on the seven factors which cumulatively explain 89.6 % of the variance; (b) excluding REE, with loadings on the 6 factors which cumulatively explain 80.9 % of the variance; (c) geometric representation of Factors 1, 2 and 3 (excluding REE) which account for 52.6 % of the total variance. For purposes of clarity the elements Rb, Cr, Co, Sc and TiO₂ have been omitted as all except Co may be effectively represented by K₂O, as seen in Fig. 6.16 (b) above. Co was omitted because it displays poor correlation with all elements (Table 6.19) and falls in Factor 6 (Fig. 6.16 (b)). The REE's are also omitted in the interests of clarity; (d) 3-D conceptual representation of the major NS factors shown in Fig. 6.16 (c) above

- Fig. 6.17 Shale-normalized INAA REE profiles of Ore Schists: (a) UFS (ALP052) and IS (ALP147); (b) HS; (c) OS surface samples west of orebody; (d) OS surface samples east of orebody, with ALP219 and ALP225 from Maanhaarkop
- Fig. 6.18 OS borehole core element variations versus distance from the orebody: (a) Zn; (b) Mn; (c) Ba
- Fig. 6.19 OS surface outcrop element and ratio variations versus distance from the orebody: (a) Zn; (b) Ba; (c) Pb; (d) Mn; (e) Mn/Mn+Fe
- Fig. 6.20 Average K/Rb and Ca/Sr (ppm/ppm) ratios for ore- and non-ore-related rocks
- Fig. 6.21 Shale-normalized INAA and XRF REE profiles for various ore-related rocks: (a) Massive Sulphide and Quartz Magnetite Rock from the Broken Hill orebody; (b) Magnetite-rich rocks from the Broken Hill orebody compared with Froneman se Kop Quartz Magnetite Rock; (c) Lower Orebody Garnet Quartzite; (d) Ore Equivalent Garnet Quartzite (ALP130 and ALP132 from Maanhaarkop); (e) Ore Schist plus Garnet Quartzite (ALP128 and ALP129 from Maanhaarkop. INAA data in (a); XRF data in (b) to (e)
- Fig. 6.22 OS+GQ and GQ element and inter-element ratio variations versus distance from the orebody: (a) Zn; (b) Pb; (c) Zn/Zn+Al; (d) Pb/Pb+K
- Fig. 6.23 Plot of Fe/Ti vs Al/(Al+Fe+Mn) ratios after Bostrom (1973). All data other than Aggeney's samples from Marchig et al. (1982). (b) is an enlargement of the area in (a) centered on average crust
- Fig. 6.24 Shale-normalized INAA and XRF REE profiles for various ore-related rocks at Aggeney's compared with metalliferous hydrothermal sediments from the Santorini caldera (1), Atlantis II Deep (2), Galapagos islands (3) and nontronite encrusting basalt on the Juan de Fuca Ridge (4). Comparisons are (a) massive sulphide (5 = ALP081, 6 = ALP110); (b) schists (5 = NS, ALP030; 6 = SS, ALP057; 7 = OS, ALP225; 8 = OS, ALP052). Profiles 1, 2 and 3 from Fleet (1984); profile 4 from Murnane and Clague (1983, sample 11b).
- Fig. 6.25 BQ element variations vs Al₂O₃: (a) Ba; (b) Pb; (c) Zn
- Fig. 6.26 Combined factor analysis for WQ and DQ: (a) excluding REE, with loadings on the five factors which cumulatively explain 92,2 % of the variance; (b) including REE with loadings on the four factors which cumulatively explain 100 % of the variance
- Fig. 6.27 Shale-normalized BQ REE patterns: (a) INAA analysis for a WQ sample; (b) XRF analyses of WQ (ALP040), DQ (ALP042) and MDS (ALP041) from borehole BH123, and MDS from Maanhaarkop (ALP125)
- Fig. 6.28 $\delta^{18}O$ (SMOW) ratios of quartz grains from different parts of the structural succession. Most samples come from borehole BH123 hence all samples have been fitted into their approximate positions within the borehole lithological column. Within the Ore and Equivalent Horizons the following infrequently used abbreviations are: UOB = Upper Orebody; LOB = Lower Orebody; QM = Quartz Magnetite; MS = Massive Sulphide
- Fig. 6.29 NS element variations down borehole BH123: (a) SiO₂, Cr and Zr; (b) Al₂O₃, K₂O, TiO₂ and CaO; (c) Ni, Nb and Co; (d) V, Rb, Sr and Sc. All elements reported in ppm except SiO₂, Al₂O₃, K₂O, TiO₂ and CaO which are in percent. X-axis represents depth in metres down the borehole. Sample numbers and rock types are shown. Zr and Cr are the only elements which do not grade smoothly across the NS-WQ boundary
- Fig. 6.30 Shale-normalized XRF-derived REE analyses from borehole BH166. Samples 1 to 5 of NS are taken progressively nearer WQ (sample 6).
- Fig. 6.31 NS Zr vs SiO₂ concentrations

- Fig. 6.32 Plots of average element concentrations of NS against MDS and DQ for each of three boreholes: (a) SiO₂; (b) Ce; (c) Zr
- Fig. 6.33 Zones over which geochemical transitions are considered in SS. Zones a. to e. referred to in the text are highlighted.
- Fig. 6.34 SS element variations down boreholes. Elements in percent are SiO₂, MnO, Na₂O, CaO, Al₂O₃, P₂O₅ and S. All other elements in ppm. X-axis represents depth in metres down the sub-vertical borehole. Sample numbers, rock types and contacts referred to in the text, are shown. Boreholes are (a) BH123; (b) BH156; (c) BH164
- Fig. 6.35 Inter-element ratios versus distance down borehole BH123: (a) Ba/Ba+Sr; (b) Rb/Rb+Sr
- Fig. 6.36 Inter-element ratios versus distance down borehole BH156: (a) Ba/Ba+Sr; (b) Rb/Rb+Sr
- Fig. 7.1 Comparison between element concentrations in Broken Hill borehole BH123 and Wortel holes WTL3 & 4: (a) Zr; (b) SiO₂; (c) Zn; (d) MnO. X-axis represents consecutive rock types down the holes plotted at equally spaced intervals. NS and SS = Broken Hill and Wortel Namies and Shaft Schists; Q = Broken Hill and Wortel quartzites; OEH = Broken Hill OEH and approximate equivalent stratigraphic schist at Wortel; CSMQ = Broken Hill CSMQ and Wortel CTSMQ
- Fig. 7.2 Shale normalized REE patterns for regional rocks compared with Broken Hill analogues, using the XRF analytical method: (a) NS compared with Wortel and Achab NTS; (b) SS compared with Wortel and Namiesberg STS; (c) CSMQ compared with Wortel CTSMQ; (d) WQ compared with Wortel WTQ; (e) MDS compared with Wortel MDTs
- Fig. 7.3 Delta diagrams showing the log ratios of mean element concentration of Broken Hill rock-types to Regional rock-types for borehole core only: (a) NS/NTS (Achab); (b) NS/NTS (Wortel); (c) SS/STS (Namiesberg); (d) SS/STS (Wortel); (e) WQ/WTQ (Wortel); (f) DQ/DTQ (Wortel); (g) DQ/DTQ (Namiesberg). Elements are those less obviously related to the orebody
- Fig. 7.4 Ratio-ratio diagrams showing the log ratios of the mean concentrations of 3 elements plotted against the log Si ratios for various suites of rocks shown: (a) Al; (b) K; (c) Fe. Legend appears with Fig. 7.5
- Fig. 7.5 Log[Al(bh)/Al(reg)] ratio plotted against the SiO₂ content of the regional rock, for the rock-types shown
- Fig. 7.6 Delta diagrams showing the log ratios of mean ore-related element concentration of Broken Hill rock-types to regional rock-types for both borehole core and surface samples: (a) NS/NTS (core); (b) NS/NTS (surface); (c) SS/STS (core); (d) MDS/MDTS (surface and core); (e) WQ/WTQ (core); (f) DQ/DTQ (core)
- Fig. 8.1 (a) Chondrite normalised NS (ALP028), SS (ALP057), and WQ (ALP067) INAA REE patterns compared with those of Australian Archaean shales (AAS) and post-Archaean Australian shales (PAAS). Chondrite values used for normalization are from Taylor and Gorton (1977). AAS analysis is from Taylor and McLennan (1981), while PAAS values come from Nance and Taylor (1976)
- Fig. 8.2 NS and SS La vs Th concentrations on plots after McLennan et al. (1983)
- Fig. 8.3 NS and SS Co/Th vs La/Sc concentrations on plots after McLennan et al. (1983). M = average Archaean mafic volcanic rocks; F = average Archaean felsic volcanic rocks
- Fig. 8.4 Concordia diagram of ion microprobe results from single zircons from WQ (after Armstrong et al., 1988)

- Fig. 8.5 Chondrite normalised BS (ALP028) REE patterns compared with those of siliceous to intermediate rocks and to PAAS. Chondrite values used for normalization are from Taylor and Gorton (1977). Granite and intermediate rock REE values are taken from Haskin et al. (1968), while PAAS values come from Nance and Taylor (1976)
- Fig. 8.6 Estimates of average crust which produced BS, using plots of: (a) K/Rb vs K; (b) Si/Al vs Al; (c) Ti vs Zr; (d) Zr vs Cr. Average rock-types annotated thus: n = NS; s = SS; N and H = calculated crust which produced NS and SS, respectively; v = data from Vinogradov (1962); k = data from Krauskopf (1979); t = data from Turekian (1972); y = data from Taylor (1964); s = shale average; c = crustal average; M = mafic rocks; I = intermediate rocks ($\text{SiO}_2 < 60\%$); G = granite ($\text{SiO}_2 > 60\%$)
- Fig. 9.1 Fields of NS and SS relative to sedimentary and igneous fields defined by de la Roche (1966) in the ternary diagram Fe_2O_3 (total)+ TiO_2 + $\text{CaO} - \text{SiO}_2 \cdot 0.73 - \text{Al}_2\text{O}_3$. Solid line passing through gabbro and granite defines the igneous trend. Ternary diagram represents the subset shown in the locality figure
- Fig. 9.2 Fields of NS and SS relative to sedimentary and igneous fields defined by de la Roche (1966) in the ternary diagram $\text{MgO} - \text{K}_2\text{O} - \text{Na}_2\text{O}$. Solid line passing through gabbro and granite defines the igneous trend. Ternary diagram represents the full field shown in the locality figure
- Fig. 9.3 Fields of NS and SS in the binary diagram $(\text{Al}-\text{K})+(\text{Fe}-\text{Mg})-4\text{Ca}$ vs $(\text{Al}-\text{K})-(\text{Fe}-\text{Mg})-2\text{Na}$ of de la Roche (1978) which shows progressive chemical changes that accompany the transformation of igneous rocks to various types of highly mature sediment
- Fig. 9.4 Fields of NS and SS relative to sedimentary and igneous fields defined by Garrels and MacKenzie (1971) in the binary diagram $\log(\text{SiO}_2/\text{Al}_2\text{O}_3)$ vs $\log((\text{CaO}+\text{Na}_2\text{O})/\text{K}_2\text{O})$
- Fig. 9.5 Fields of NS and SS relative to progressively more mature pelitic rocks in the ternary diagram $\text{K}_2\text{O}+\text{Na}_2\text{O}+\text{CaO} - \text{MgO}+\text{FeO}(\text{total}) - \text{Al}_2\text{O}_3$ from Englund and Jorgensen (1973). Ternary diagram represents the full field shown in the locality figure
- Fig. 9.6 Fields of NS and SS in binary diagram of Niggli al-alk vs Al_2O_3
- Fig. 9.7 Fields of NS and SS in binary diagrams of trace elements vs Niggli al-alk: (a) Zr; (b) Ba; (c) Zn; (d) Ni; (e) Co
- Fig. 9.8 Fields of NS and SS in binary diagrams of major elements vs Niggli al-alk: (a) MnO ; (b) CaO ; (c) Fe_2O_3 ; (d) MgO ; (e) TiO_2 ; (f) Na_2O ; (g) K_2O
- Fig. 9.9 Fields of NS and SS in binary diagram of P_2O_5 vs C
- Fig. 9.10 Histograms of S/C ratios: (a) USS; (b) LSS; (c) NS
- Fig. 9.11 S vs C plots relating to SS: (a) SS S vs C raw data; (b) Graphic representation of the conditions bounding the pre-metamorphic S and C concentrations in SS (see Appendix H for details); (c) SS S vs C curves relative to sediments deposited below various water types. Black Sea sediments from Levinthal (1983); sediments from below normal oxidizing sea water taken from Levinthal (1983) and Berner (1984); modern fresh water lake sediments from Berner (1984)

- Fig. 9.12 Stability relations in Eh-pH space between some Fe and Mn compounds in water at 25°C and 1 atmosphere total pressure. Dark and light lines mark the Mn and Fe fields, respectively. The Fe^{2+} , Fe^{3+} and Mn^{2+} fields are aqueous, of which the Mn^{2+} field is by far the largest. Activity of total dissolved S = $10^{-4}m$. At lower S concentrations the fields of sulphides shrink markedly. Activity for total dissolved CO_2 = $10^{-4}m$ for Mn, and 0 for Fe. The field of siderite virtually disappears for total dissolved CO_2 < $10^{-3}m$. Modified after Garrels and Christ (1965, pp221, 243 and 381). Also plotted are fields of various naturally occurring waters taken from Baas Becking et al. (1960). The arrow from A to B marks the change in conditions when fresh water mixes with sea water
- Fig. 9.13 Profiles of total Mn in Laurentian Trough sediments (from Sundby et al., 1981)
- Fig. 9.14 Co-precipitation of Mo by Mn and Fe oxides under varying pH conditions, after Evans et al. (1974-1978). Curves as follows: a. from Chan and Riley (1966); b. and d. Ishibashi et al. (1962); c. Kim and Zeitlin (1968)
- Fig. 9.15 Fields of NS and SS in binary diagram of Cr versus various elements: (a) Cr vs C; (b) Cr vs Al_2O_3 ; (c) Cr vs SiO_2 ; (d) Cr vs Zr
- Fig. 9.16 Fields of NS and SS in binary diagram of Ni versus various elements: (a) Ni vs P_2O_5 ; (b) Ni vs Zr
- Fig. 9.17 Stability relations for Ce in Eh-pH space, at 25°C and 1 bar pressure. Activities of ions are M^{2+} , M^{3+} and M^{4+} = 10^{-6} ; total CO_2 = 10^{-3} (after Brookins, 1983). Water fields after Baas Becking et al. (1960). The line joining A to B represents the approximate redox change encountered when particles pass from river water into the sea.
- Fig. 9.18 Variations in rare earth concentrations during weathering of granodiorite (after Nesbitt, 1979).
- Fig. 9.19 Fields of NS and SS in binary diagram of Cr/(Cr+V) versus various elements: (a) C; (b) S; (c) Ni
- Fig. 9.20 Fields of NS and SS in binary diagram of Cu/(Cu+(MnO/20)) versus Cu/(Cu+(Fe_2O_3 /1400))
- Fig. 9.21 The dependence of Pb concentrations on a_{HS} for galena saturated solutions at 50°C and 100°C (after Giordano and Barnes, 1979)
- Fig. 9.22 Activities of the complexes $\text{Pb}(\text{HS})_2$ and $\text{Pb}(\text{HS})_3^-$: (a) 30°C; (b) 100°C. Total S activity = 1 for heavy line and 0.1 for light line. After Giordano and Barnes (1979)
- Fig. 9.23 Stability relations in Eh-pH space between various Pb compounds in water at 25°C and 1 atmosphere total pressure. Aqueous Pb covers a wide field in the absence of dissolved S, and this field shrinks to be restricted to the strongly acid range with increase in S content to $10^{-1}m$. Dark lines represent fields for conditions of P_{CO_2} = $10^{-4}m$ and P_s = $10^{-1}m$; light lines for P_{CO_2} = $10^{-4}m$ and P_s = 0m. After Garrels and Christ (1965, pp234 and 237)
- Fig. 9.24 Schematic model of basin geometry control on distribution of CSMQ lenses: (a) BGZ forms above Broken Hill orebody and beneath stable thermocline at time T_0 ; (b) after disruption of the thermocline, CSMQ precipitates (time T_1); (c) below the newly established thermocline (T_2) in the deepest part of the basin, CSMQ goes back into solution, leaving lenses of CSMQ on the flanks of the basin above the T_2 line; (d) the thermocline at time T_3 is re-established at the approximate position of the T_0 thermocline level, with deposition of SS preserving the CSMQ lenses
- Fig. 9.25 NS Zn variations for surface outcrop and borehole core samples versus distance from the Broken Hill orebody

- Fig. 9.26 Chondrite normalized WQ REE pattern (ALP067) compared with those from basalt associated deep ocean chert of Crerar et al. (1982)
- Fig. 9.27 Fields of WQ, DQ, NS and MDS relative to the sandstone fields of Pettijohn et al. (1972, p62) in the binary diagram $\log(\text{Na}_2\text{O}/\text{K}_2\text{O})$ versus $\log(\text{SiO}_2/\text{Al}_2\text{O}_3)$. c = core; s = surface
- Fig. 9.28 Fields of WQ, DQ, NS and MDS relative to fields of quartz arenite and high silica chert in the binary diagram SiO_2 versus $\text{CaO}+\text{MgO}$.
- Fig. 9.29 Fields of WQ, DQ, NS and MDS relative to the sandstone-quartzite field of Garrels and MacKenzie (1971) in the binary diagram of $\log(\text{SiO}_2/\text{Al}_2\text{O}_3)$ versus $\log((\text{CaO}+\text{Na}_2\text{O})/\text{K}_2\text{O})$. Heavy line from granite to basalt defines the igneous trend
- Fig. 9.38 Model showing paleo-geographical relationships between provenance, proximal and distal environments during sedimentation of the Aggeneys Subgroup
- Fig. 10.1 Effects of temperature on the $100*\text{Zn}/(\text{Zn} + \text{Pb})$ ratio for salinities of 0.5, 1.0 and 1.5m NaCl (after Huston and Large, 1987)
- Fig. 10.2 PbS solubility at 150°C in 3m NaCl solutions. Lines with negative slopes on the left side of the diagram are dominated by chloride complexes, and those with positive slopes by sulphide complexes (after Giordano and Barnes, 1979)
- Fig. 10.3 Concentration of metals in solution in equilibrium with various minerals: Ba with barite; Cu with chalcopyrite or bornite; Zn with sphalerite (after Ohmoto et al., 1983)
- Fig. 10.4 Effect of pH, temperature and salinity on the Zn/Cu and Pb/Cu ratios: (a) effect of pH on the $100*\text{Zn}/(\text{Zn} + \text{Cu})$ ratio at I = 1.0m; (b) effect of temperature on the $100*\text{Zn}/(\text{Zn} + \text{Cu})$ ratio at pH = 6; (c) effect of salinity on the $100*\text{Zn}/(\text{Zn} + \text{Cu})$ ratio at pH = 6; (d) effect of pH on the $100*\text{Pb}/(\text{Pb} + \text{Cu})$ ratio at I = 1.0m; (e) effect of temperature on the $100*\text{Pb}/(\text{Pb} + \text{Cu})$ ratio at pH = 6; (f) effect of salinity on the $100*\text{Pb}/(\text{Pb} + \text{Cu})$ ratio at pH = 6
- Fig. 10.5 $\delta^{34}\text{S}$ values for Aggeneys-Gamsberg ore deposits. Values are for sulphides above and barite below the line (after von Gehlen et al. (1983)
- Fig. 10.6 Relationship between potential sulphide mass producible (including Fe sulphide) and time for (a) various cross sectional areas of downflow, and (b) various geothermal gradients (after Strens et al., 1987)
- Fig. 10.7 Temperature-concentration relationships for total sulphide mass producible in hydrothermal brine (after Strens et al., 1987)
- Fig. 10.8 Changes in the saturation indices of minerals during cooling from a 300°C Kuroko fluid on mixing with sea water. Sp = sphalerite; Ba = barite; Cp = chalcopyrite; Py = pyrite; Hm = hematite. The saturation indices of minerals are dependent on fluid redox conditions in (b) but not in (a) (after Ohmoto et al., 1983)
- Fig. 10.9 Changes in the saturation indices of minerals during cooling from a 200°C Kuroko fluid. Abbreviations as for Fig. 10.8 (after Ohmoto et al., 1983)
- Fig. 10.10 Solubility of amorphous silica in water between 25 and 250°C (after Holland and Mallinin, 1979)
- Fig. 10.11 Relationship between proximal ores and exhalites shown in $f\text{O}_2$ - temperature space for pH between 5 at 350°C and 7 at 50°C with total S = 10^{-3}m and 1m NaCl. Modified after R. R. Large (1977)

Fig. 10.12 (a) Schematic positioning of Aggeneys-Gamsberg orebodies relative to each other within the prograding beach-barrier sedimentary model; (b) Schematic diagrams contrasting the ore-rock relationships and depth of convective fluid passage in generating the Gamsberg and Broken Hill orebodies. Note that diagrams are not to scale, and (a) should not be viewed as a cross section

Fig. 11.1 Schematic representation of tectonic regime envisaged before, during and after deposition of the Aggeneys orebodies: (a) Basement thinning and rift development; (b) Southerly progradation of beach-barrier setting over the the rift environment; (c) Detail of the syn-sedimentary graben and yoked basin settings for the three Aggeneys ore deposits, also showing thinning of quartzites to the south and maximum development of NS in the rifted blocks; (d) Right lateral simple shear couple which acted on the rift zone; (e) Response of rift zone sediments to earliest phase of deformation, with thrusting on the south limbs of synclines and accentuation of normal displacements on the north limbs. For the sake of clarity only three marker horizons are shown; (f) Schematic plan of Aggeneys area after open folding event, showing proposed locations of reactivated normal faults; (g) Schematic cross-section through the plan in (f) above

Fig. 11.2 Schematic representation of geotectonic model for development of the Namaqualand Metamorphic Complex as it affects the Bushmanland Group: (a) Generation of Vioolsdrif Suite and basement to the Bushmanland Group, resulting from south-directed subduction; (b) Sedimentation of Bushmanland Group above rifted passive margin against marginal basin. Simultaneous north-directed, shallow dipping subduction along SCCB, with generation of volcanic arc, and sedimentation of both mature passive margin and immature volcanic arc detritus; (c) Collision of continents causing south vergence and reactivation of normal faults in the Aggeneys area

Fig. A.1 Cross section through sampled boreholes showing sample numbers and lithologies: (a) Section through TS11 at Maanhaarkop; (b) Section through BH163 at Broken Hill; (c) Fence diagram through BH123 to BH164 at Broken Hill; (d) Section through WTL3 and 4 at Wortel; (e) Section through AC2 at Achab; (f) Section through VG1 at Namiesberg. Locations of Broken Hill and Maanhaarkop boreholes are shown in the locality plan with Fig. A.1c. while locations of the Achab and Namiesberg boreholes appear in Fig. A.2c. The locations of the Wortel boreholes appear in Fig. 5.3

Fig. A.2 Geological maps showing locations of surface samples: (a) Broken Hill - Klein Kop; (b) Tank Hill, Maanhaarkop, Froneman se Kop; (c) Namiesberg

Fig. A.3 Comparison between volatile-included and volatile-free trace element data (left hand side and right hand sides, respectively), when plotted against volatile-free Al_2O_3 . Differences between the two pairs of diagrams are negligible except where high Al_2O_3 concentrations coincide with elevated trace element values. Diamond = NS; Plus = LSS; Box = USS

Fig. A.4 Comparison between XRF-derived rare earth element analyses and INAA data for the same samples: (a) La; (b) Ce; (c) Nd

Fig. A.5 REE analyses of four samples by (a) INAA and (b) XRF analytical techniques, illustrating the applicability of the XRF-derived Ho estimate as an indication of relative HREE concentration

Fig. C.1 Photomicrograph of BGZ (ALP235) showing extensive brecciation and rounding of quartz grains in a clay and sericite matrix. Crossed nicols. (1cm = 400 micron)

- Fig. C.2 Photomicrograph of CS (ALP188) showing mineral banded nature, with garnet-dominated band below, followed by a biotite-rich band and then a quartz-rich band above. Plain polarized light. (1cm = 400 micron)
- Fig. C.3 Photomicrograph of DQ (ALP239) showing severely strained quartz grain surrounded by a mortar texture of polygonized quartz grains. Muscovite appears near the top right-hand corner. Crossed nicols. (1cm = 400 micron)
- Fig. C.4 Photomicrograph of DQ (ALP126) showing sheared, wispy muscovite in a matrix of recrystallized quartz grains. Crossed nicols. (1cm = 400 micron)
- Fig. E.1 Photograph of amphibolite xenoliths intruded by augen gneiss in quarry south of Broken Hill. Main xenolith is approximately 10cm wide
- Fig. E.2 Schematic structural borehole intersection through the contact zone between Basal Gneiss and Namies Schist
- Fig. E.3 Schematic cross section through Shaft Schist showing position of Grey Granoblastic Leucocratic Gneiss (GGLG) as well as the contact between USS and LSS
- Fig. F.1 OS "ore factor" score variations with distance from the orebody: (a) OS borehole core Factor 2; (b) OS borehole core Factor 3; (c) OS surface outcrop Factor 3
- Fig. G.1 Flow chart displaying the regional scale lithogeochemical exploration strategy for locating ore deposits of the Broken Hill-type in the north west Cape
- Fig. G.2 Flow chart displaying the local scale lithogeochemical exploration strategy for locating ore deposits of the Broken Hill-type in the north west Cape

LIST OF TABLES IN VOLUME 2

- Table 1.1 Published ore reserves for the Aggeneys-Gamsberg deposits
- Table 3.1 SACS (1980) lithostratigraphy of the Bushmanland and Okiep Groups in a generalized structural succession from north (top) to south
- Table 3.2 Chronology of the major events in the western Namaqua Province
- Table 4.1 Zircon grain sizes in Namies Schist and Shaft Schist
- Table 4.2 Zircon grain sizes in Broken Hill Quartzites and Median Schist
- Table 4.3 Stratigraphic thicknesses (m) of rock types at Broken Hill
- Table 4.4 Physical dimensions of Broken Hill Quartzites
- Table 4.5 Physical dimensions of Namies Schist and Shaft Schist
- Table 4.6 Physical dimensions of Biotite Graphite Zone (BGZ) and Calc Silicate Rock plus Manganese Quartzite (CSMQ)
- Table 4.7 Physical dimensions of the Broken Hill orebody and Ore Schists
- Table 6.1 Percentage pegmatite in zones of homogeneous schist
- Table 6.2 Host rock element enrichments and depletions resulting from pegmatites extraction
- Table 6.3 Ratios between surface outcrop (s) and borehole core (c) element mean concentrations of NS, USS and OS as an indication of effect of surface weathering on element distribution
- Table 6.4 NS and SS average element concentrations and coefficients of variation (S.D./Mean)
- Table 6.5 SS element concentrations relative to NS
- Table 6.6 Tests for normality and tests for equality of means for the rock-types NS and SS
- Table 6.7 NS correlation matrix
- Table 6.8 SS correlation matrix
- Table 6.9 Average coefficients of variation for NS and SS
- Table 6.10 NS and SS factor analysis parameters: (a) variances explained by each factor, and cumulative variances; (b) communalities for each element.
- Table 6.11 CS and MnQ average element concentrations for core and surface samples combined
- Table 6.12 CS element concentrations relative to USS
- Table 6.13 MnQ element concentrations relative to USS
- Table 6.14 BGZ average element concentrations and standard deviations
- Table 6.15 BGZ element concentrations relative to USS: (a) ratios of BGZ/USS on a per element basis; (b) Ca/Sr C/S and K/Na ratios of BGZ and USS
- Table 6.16 Tank Hill Schist (THS) and Green Quartzite (GrQ) element concentrations
- Table 6.17 Tests for Normality and tests for the equality of means for the rock-types NS, SS and OS
- Table 6.18 OEH average element concentrations and coefficients of variation (S.D./Mean)
- Table 6.19 OS correlation matrix
- Table 6.20 OS factor analysis parameters; (a) OS variances explained by each Factor, and cumulative variances; (b) communalities for each element
- Table 6.21 Some orebody average element concentrations
- Table 6.22 Broken Hill Quartzite (BQ) average element concentrations and standard deviations
- Table 6.23 BQ correlation matrix
- Table 6.24 BQ factor analysis parameters: (a) variances explained by each factor, and cumulative variances; (b) communalities for each element

- Table 6.25 Relative element abundances and variations in specific zones of SS
- Table 7.1 NTS and STS average element concentrations and coefficients of variation (S.D./Mean)
- Table 7.2 NTS correlation matrix
- Table 7.3 STS correlation matrix
- Table 7.4 Wortel CTSMQ element concentrations and comparative rock-types from Broken Hill
- Table 7.5 Regional Quartzite element concentrations
- Table 7.6 Regional Quartzite correlation matrix
- Table 8.1 BS CIA values relative to various rock-types and clays
- Table 9.1 Average Shale composition and comparison with average NS and SS: (a) Average Shale, average NS and SS; (b) Ratio between average element concentration of NS and average shale; (c) Ratio between average element concentrations of SS and average shale
- Table 9.2 Analyses of NS and SS and various shales for comparison
- Table 9.3 Ratios of BGZ to various black shales
- Table 9.4 Estimated SS original clay composition compared with illite and montmorillonite
- Table 9.5 MnO/(MnO+Fe₂O₃) ratios for NS and SS compared with various shales
- Table 9.6 CS average composition, comparative rocks and ratios
- Table 9.7 MnQ average composition, comparative cherts and ratios
- Table 10.1 Average base metal contents of some common crustal rocks
- Table 10.2 Equilibrium constants used in the Cu-Pb-Zn ratio calculations
- Table 10.3 Zinc/copper and lead/copper ratios of saturated solutions at varying temperatures, salinities and pH's as calculated from thermochemical data
- Table 10.4 Zinc/lead, zinc/copper and lead/copper ratios of the Aggeneys-Gamsberg orebodies
- Table 10.5 $\delta^{34}\text{S}$ values for sulphide and sulphate (barite) from the Aggeneys-Gamsberg area
- Table 10.6 Summary of conditions which obtained to produce the Aggeneys-Gamsberg orebodies
- Table A.1 Instrumental conditions adopted for major and trace element analyses using XRF spectrometers in the laboratories of the University of Cape Town Geochemistry Department
- Table A.2 Typical lower limits of detection (LLD) and absolute errors (1 standard deviation) for Bushmanland schists from this study analysed by the XRF technique. Since quartzite samples have lower mass absorption coefficients, their LLD and error values are approximately 1/3 lower than for schist
- Table A.3 Analytical data including volatiles
- Table A.4 Additional analyses: INAA and fire assay analytical data
- Table A.5 Analytical data recalculated volatile-free
- Table A.6 Analyses of three aliquots of one sample for C, H and N using gas chromatography
- Table A.7 Three duplicate INAA REE analyses (ppm) of sample ALP190
- Table C.1 List of mineralogical abbreviations used
- Table C.2 Estimated Namies Schist modal percentages
- Table C.3 Estimated Shaft Schist modal percentages
- Table C.4 Estimated Biotite Graphite Zone modal percentages
- Table C.5 Estimated Calc Silicate Rock plus Manganese Quartzite modal percentages
- Table C.6 Estimated Hangingwall Schist modal percentages
- Table C.7 Estimated Ore Equivalent Schist modal percentages
- Table C.8 Estimated Ore Equivalent Schist plus Garnet Quartzite modal percentages
- Table C.9 Estimated Upper Footwall Schist modal percentages
- Table C.10 Estimated Orebody silicate assemblage modal percentages

- Table C.11 Estimated Garnet Quartzite modal percentages
Table C.12 Estimated Broken Hill Quartzite modal percentages
Table C.13 Estimated Namies-type Schist modal percentages
Table C.14 Estimated Shaft-type Schist modal percentages
Table C.15 Estimated Calc-type Silicate plus Manganese Quartzite modal percentages
Table C.16 Estimated Regional Quartzite modal percentages
Table F.1 Factor loadings for OS "ore factors"
Table K.1 Comparison between Namies Schist at Gamsberg and at Broken Hill
Table K.2 Comparison between Quartzite descriptions at Gamsberg and at Broken Hill
Table K.3 Broken Hill oxygen isotope data (permil) from Reid et al. (1987)
Table K.4 U, Th and Pb ion microprobe analyses on zircons from White Quartzite at Froneman se Kop. (Analyst: R. A. Armstrong)

DEDICATION

To Eddie, my dear father-in-law,
who would have loved to peruse
this completed work

ACKNOWLEDGEMENTS

Completion of so large a part-time thesis over a period of 8 years would have proved impossible without the aid of numerous people, to whom I am indebted. This is particularly true considering that the University of Cape Town is separated from Krugersdorp by 1 500km.

In suggesting the project, Ben Weilers and Hennie Blignault rekindled my zest for earth sciences. My thanks are extended to Gold Fields of South Africa who, guided by Ben Weilers, Richard Viljoen and Erhart Kostlin, provided finances for transport, Cape Town accomodation, analytical- and publication- fees.

Both Dave Reid and Andy Duncan painstakingly introduced me to the world of computers and the workings of computer-controlled XRF spectrometers. As my supervisors, their patience at the early stages of the thesis will remain to their credit and my benefit. Informative discussions held with them, as well as their continuous, incisive guidance, helped mold the thesis. I also benefited from technical discussions with Bob Winter, Mike Watkeys, Julian Hobbs, Pete Smith, Tony Erlank, James Willis and John Moore. James Willis and Anton le Roux rendered backup assistance with analytical work and data reduction.

Thanks go to Graham Kletz, Mark Clarke and Dave Richardson for their aid in using the BMDP statistical package, while Christine Stock and Fatima Ferraz guided me out of problem areas encountered in PC software. Richard Johnson is thanked for giving of his valuable time translating a data file from mainframe to PC. Computers played so central a role in data- and word- processing of this thesis, that I

would like to place on record my gratitude to the developers of PC's and the writers of user-friendly software!

The late Hans Welke readily undertook the separation of quartzite-hosted zircons. Ion microprobe analyses of these were later supplied by Richard Armstrong, with whom informative discussions were held on the topic of isotope systematics. Garth Eagle made an invaluable contribution by assisting with the acquisition of carbon analyses on CSIR gas chromatographs. In providing INAA analyses of rare earth elements for a number of ALP samples, Dave Reid again injected stimulation and a more rigorous foundation to the thesis. I am most appreciative of this and his willing sharing of data pertinent to the current study. The section on thermochemistry was only possible after discussions with Mike Meyer and Dave Richardson, and a written communication from Dave Huston in Australia.

Logistical support was cheerfully provided at Aggeneys by Ivo Chunnnett and later by Dave Mourant. Joseph Afrikaner rendered much appreciated physical help in the field, while Shereen Abrams did a sterling job with sample preparation at UCT. The draughting services rendered by Les Hill, Lesley Kemmish and staff at Gold Fields have enhanced the quality of the diagrams, and all the above are thanked for their assistance, as is Gavin Martin for his photomicrographic aid.

My parents are thanked for making it possible for me to pursue a career in earth sciences. My appreciation is extended to the late Sophie and Eddie Walder for accomodation, sustenance and encouragement during numerous sojourns in Cape Town.

My wife, Lorraine, maintained her unswerving confidence, encouragement and love during this study, which proved so supportive. Her willing sacrifice of holidays and time together, for the sake of the thesis, is appreciated. Tashi and Elan showed understanding beyond their years in not having ready access to their father.

ABBREVIATIONS

Rock - types

AM	Amphibole Magnetite rock
BGZ	Biotite Graphite Zone
BQ	Broken Hill Quartzite (= WQ + DQ +- MDS)
BS	Broken Hill Schists (= NS + SS + OS)
CS	Calc Silicate Rock
CSMQ	Calc Silicate Rock plus Manganese Quartzite
CTS	Calc-type Silicate Rock
CTSMQ	Calc-type Silicate Rock plus Manganese Quartzite
DQ	Dark Quartzite
DTQ	Dark-type Quartzite
GGLG	Grey Granoblastic Leucocratic Gneiss
GQ	Garnet Quartzite
GRQ	Green Quartzite (from Tank Hill)
GTQ	Garnet-type Quartzite
HS	Hangingwall Schist
HS+GQ	Hangingwall Schist plus Garnet Quartzite
IS	Intermediate Schist
IS+GQ	Intermediate Schist plus Garnet Quartzite
LGQ	Lower Orebody Garnet Quartzite
LMA+GQ	Lower Orebody Amphibole Magnetite rock
LOB	Lower orebody
LOES+GQ	Lower Ore Equivalent Schist plus Garnet Quartzite
LSS	Lower Shaft Schist
MDS	Median Schist
MDTS	Median-type Schist
MNQ	Manganese Quartzite
MQ	Quartz Magnetite Rock (= QM)
MS	Massive Sulfide
NS	Namies Schist
NTS	Namies-type Schist
OEGQ	Ore Equivalent Garnet Quartzite
OES	Ore Equivalent Schist
OESP	Pegmatite in Ore Equivalent Schist
OESP+GQ	Pegmatite in Ore Equivalent Schist + GQ
OES+GQ	Ore Equivalent Schist plus Garnet Quartzite
OS	Ore Schist (= OES + HS + IS + UFS)
P	Pegmatite (massive)
PHS	Pegmatite in Hangingwall Schist
PNS	Pegmatite in Namies Schist
PSS	Pegmatite in Shaft Schist
PSTS	Pegmatite in Shaft-type Schist
PUFS	Pegmatite in Upper Footwall Schist
Q	Quartzite (undefined)
QM	Quartz Magnetite rock (= MQ)
RQ	Regional Quartzite (= WTQ + DTQ)
S	Schist (undefined)
SS	Shaft Schist
STS	Shaft-type Schist
STS+Q	Shaft-type Schist + Quartzite
S(ACH)	Schist at Achab (= NTS)
UFS	Upper Footwall Schist

Inselbergs

AC	Achab
BH	Broken Hill
BM	Black Mountain
FK	Froneman se Kop
KK	Klein Kop
MX	Maanhaarkop
NB	Namiesberg
PH	Plant Hill
TH	Tank Hill
WTL	Wortel

Measures

a	activity
Å	angstrom
cm	centimetres
g	activity coefficient
km	kilometres
m	metres
mm	millimetres
mt	million tonnes
m(<i>italics</i>)	molality

Other

ALP	Aggeney's Lithochemical Project
ASG	Aggeney's Subgroup
BG	Bushmanland Group
BIF	Banded Iron Formation
BSP	Bushmanland Subprovince
GFSA	Gold Fields of South Africa Ltd
HREE	Heavy rare earth elements
INAA	Instrumental neutron activation analysis
LREE	Light rare earth elements
NP	Namaqua Province
OG	Okiep Group
ORG	Orange River Group
PD	Phelps Dodge Corporation
REE	Rare earth elements
RSP	Richtersveld Subprovince
SCCB	Southern Cape Conductive Belt
XRF	X-ray fluorescence spectrometry

Rock - types (continued)

UMQ	Upper Orebody Quartz Magnetite rock
UOB	Upper orebody
UOES+GQ	Upper Ore Equivalent Schist + GQ
USS	Upper Shaft Schist
WQ	White Quartzite
WTQ	White-type Quartzite

PART A.
INTRODUCTION

PART A. INTRODUCTION

1. HISTORY AND LOCATION

The distinctive, black, malachite-stained banded iron formation of the Swartberg inselberg (now Black Mountain), drew the attention of many prospectors and geologists to the Aggeneys area in Bushmanland (Figs. 1.1 and 1.2). In 1929 a 25m deep shaft sunk into the footwall siliceous zone of the Black Mountain orebody, narrowly missed high grade mineralization. Since that time options to mineral rights over the farms Zuurwater and Aggeneys in the magisterial district of Namaqualand had been held and allowed to lapse by numerous companies. In mid-1971 Phelps Dodge Corporation (PD) sank the first borehole on the properties, and intersected the Black Mountain orebody below the gossan capping. Immediately following this discovery, gossans were recognised at Noeniepoort se Kop (now Broken Hill), Big Syncline and Gamsberg, lying some 6km south-east, 3km east and 24km east of Black Mountain, respectively (Fig. 1.2, 1.3 and 1.4). An aggressive program of base metal exploration by multi-national corporations commenced in the north-west Cape Province of South Africa. The techniques of field mapping, ground and airborne geophysics and soil and stream sediment geochemical sampling were employed, yet no additional significant base metal deposits have since been discovered. The need for more sophisticated exploration techniques became obvious in order to discover buried deposits, and in 1982 Mr B. F. Weilers and Dr. H. J. Blignault of Gold Fields of South Africa Ltd (GFSA) suggested that the author research the effectiveness of whole rock sampling as a means of locating Aggeneys-type orebodies, which stimulated the current investigation.

In 1977 PD entered into a joint venture with GFSA, and 1979 saw the opening of the Broken Hill mine (Fig. 1.2). Today the town of Aggeneys, situated 60km west of Pofadder and 100km north-east of

Springbok, serves the mine and any further development which may take place on these world class sized deposits measuring 10^7 - 10^8 million tonnes (Table 1.1). Feasibility studies continue to test the viability of the Black Mountain and Gamsberg orebodies, however, the Big Syncline deposit with its low grade Zn-Pb mineralization does not warrant further investigation at present. All four ore deposits now fall under the management control of GFSA.

2. STUDY CONTEXT, OBJECTIVES AND METHODOLOGY

2.1 Study context

Previous geological investigations in the Bushmanland area of the Namaqua Province (Fig. 1.1) have tended to be either of a regional nature (Gevers, 1937; Joubert, 1974; Paizes, 1975; Blignault et al., 1983; Moore, 1986), or localized to a specific inselberg of the semi-desert environment (Moore, 1977; Lipson, 1978; Rozendaal, 1978; Stedman, 1980). The present study lies part-way between these two extremes, examining in detail metasediments from the Broken Hill, Maanhaarkop and Froneman se Kop chain of inselbergs (Fig. 1.4), and then extending the investigation to similar rocks in outlying inselbergs up to 35km from Broken Hill. The study is restricted to the clearly metasedimentary rocks, leaving well alone the controversial quartzo-feldspathic gneisses, or so-called "floor" rocks, components of which are basement, intrusives and supracrustal rocks (Watkeys, 1986).

2.2 Objectives

In approximately decreasing order of priority, this thesis has the following objectives:

- (a) Determine the likely precursor rocks and the depositional environments to the metasediments hosting the Broken Hill orebody at Aggeneys.
- (b) Characterize lithotypes as an aid to lithostratigraphic mapping in the Aggeneys area.
- (c) Define the type of provenance which on weathering gave rise to the sediments which were subsequently metamorphosed.
- (d) Assess the genesis of the orebody and ore-associated rocks in the light of sedimentological analysis and thermochemical modelling.
- (e) Identify the likely sources for the metals and sulphur which comprise the Aggeneys-Gamsberg orebodies.

(f) Assess the existence of geochemical haloes surrounding the orebody at both local and regional scales, since haloes enlarge the exploration target size (Fig. 2.1).

2.3 Methodology

At an early stage of the thesis, constraints are placed on element mobility due to weathering, and to both prograde and retrograde metamorphism. Thereafter, surface and borehole core samples are treated separately, where practical.

Rocks at Broken Hill are characterized by making use of stratigraphy, petrography and the application of statistical techniques on the geochemistry of these units in the Broken Hill area. The structural or stratigraphic nature of the succession at Broken Hill is assessed prior to attempting genetic modelling. Reference is made to the literature in order to examine possible pre-metamorphic precursor rock-types and their depositional environments. The likely provenance and state of provenance weathering is also assessed in terms of the characteristics deduced for the Broken Hill lithotypes. Correlation between Broken Hill rocks with those from the outlying areas of Achab, Vogelstruishoek (Namiesberg) and Wortel (Fig. 1.4), are made on the basis of sequence repetition, texture and petrography. The geochemical changes between correlated lithotypes then provide a basis for regional sedimentological modelling.

Few samples from the orebody are analysed. Thermochemical modelling founded upon base metal contents of the four orebodies in the Aggeneys-Gamsberg area, is used together with conclusions drawn from detailed work on the metasediments, to derive constraints on the genesis of the ore deposits and their source of metals and sulphur.

Plotting of elements and element ratios against distance from the Broken Hill orebody is used to investigate the presence of a local ore halo. The emphasis is placed on rocks lying at the same stratigraphic horizon as the orebody. The correlative Bushmanland rocks which were unaffected by base metal mineralization provide regional background element and element ratio levels for comparison with units near the orebody.

PART B.
GEOLOGY AND PETROGRAPHY

PART B. GEOLOGY AND PETROGRAPHY

3. REGIONAL GEOLOGICAL SETTING

The schist and quartzite successions and lesser amphibolites in the Aggeneys area of Namaqualand form a part of the gneiss- and granite-dominated Bushmanland Subprovince (BSP) of the mid-Proterozoic Namaqua Province (NP) (Fig. 1.1). The metasedimentary schists and quartzites lie close to the south eastern boundary of the early- to mid-Proterozoic meta-igneous Richtersveld Subprovince (RSP). The Gordonia Subprovince to the north and east of Aggeneys is largely metapelitic in the north west, giving way to Ca-dominated metasediments and metavolcanics immediately east of Aggeneys. A distinctive Bouguer gravity anomaly which coincides with the surface expression of the Namaqua Front and Tugela Thrust Zone, marks the northern limit of the NP. The late-Proterozoic Gariep and Saldania Subprovinces, respectively, bound the BSP to the west and south. The latter boundary is taken at the Southern Cape Conductive Belt (SCCB) and coincident Beattie magnetic anomaly (Fig. 1.1). These subcontinental wide geophysical features, buried below Paleozoic Karoo cover, were interpreted by de Beer and Meyer (1983) as resulting from oceanic serpentized basalt above a north-dipping subduction zone.

The clearly metasedimentary and lesser metavolcanic rocks preserved in the north west corner of the BSP (Fig. 1.1), and collectively termed "supracrustal" rocks, have been divided by SACS (1980) into the Okiep Group (OG) to the west, and the Bushmanland Group (BG) in the east (Fig. 3.1). The schists, quartzites, banded iron formations (BIF) and amphibolites of the Aggeneys area, collectively form the Aggeneys Subgroup (ASG) within the BG. The thinness of the ASG was noted by Rozendaal (1982) who measured a 1 500m thick succession at Gamsberg. In contrast, the tectonically overlying felsic metavolcanic Hom Subgroup measures at least 2 000m in thickness (Blignault et al.,

1983), and is structurally overlain by the Guadom Subgroup of biotite-hornblende gneisses and schist. The Pella Subgroup of schist and quartzite which bears a strong similarity to rocks at Aggeneys, lies directly above the Guadom Subgroup (Table 3.1). Within the OG, schists and quartzites of the Khurisberg, Aardvark and Eenriet Subgroups (Fig. 3.1) also bear a striking resemblance to the ASG. Blignault et al. (1983) therefore correlated these similar-looking schist and quartzite Subgroups, but suggested that the Hom and Guadom Subgroups form an eastern extension of the metavolcanic Orange River Group (ORG) component of the Richtersveld Subprovince.

The ASG age is bracketed by the uppermost amphibolites at Gamsberg which yield a Sm-Nd whole-rock isochron age of $1\ 649_{-90}^{+90}$ Ma (Reid et al., 1987), and the basement of Achab Gneiss in the Aggeneys (Watkeys, 1986) and Namiesberg (Moore, 1977) areas which yield whole rock Pb-Pb ages of $2\ 020_{-150}^{+150}$ Ma (Welke and Smith, 1984). The stratiform Aggeneys-Gamsberg orebodies within the ASG, return anomalously younger ages of between 1 200 - 1 500Ma (Koeppel, 1980).

Previous workers agree that the ASG formed in shallow water, but whereas Rozendaal (1982) and Blignault et al. (1983) envisaged a continental edge or shoreline environment, Moore (1986) proposed a marginal, continental basin environment having had little access to the sea. Rozendaal (1982) concluded that a transgression caused deposition of fluvial feldspathic sandstones (now feldspathic quartzites) in the Wortel area which graded upwards through shale (now Namies Schist as defined later in section 5.1) into marine sandstones (now quartzites). Development of the ore-associated iron formation which overlies the quartzites, was related to fluids exhaled up growth faults, and derived from basaltic magma. After a regression and transgression which lead to deposition of conglomerates and shales,

the sequence at Gamsberg was capped by basaltic, shallow water extrusions (now amphibolites) (Rozendaal, 1982). The role played by lithospheric rifting in controlling sedimentology in the BG, was stressed by both Rozendaal (1982) and Moore (1986). Moore (1986) envisaged that many gneisses belong to the supracrustal suite and were derived from K-rich rhyolitic and rhyodacitic caldera ejecta. Water reworking of this volcanic debris resulted in siliclastic sedimentation, with the quartzites representing metacherts derived from subaerial acid volcanism. Metals leached from the volcanic pile precipitated as iron formation and massive sulphide in restricted anaerobic sub-basins (Moore, 1986).

The Ca-rich supracrustal rocks in the Gordonia Subprovince east of Aggeneys were called the Korannaland Sequence by SACS (1980), and comprise aluminous schists, quartzo-feldspathic gneisses, calc-silicate rock, marble, leucogneiss, amphibolite, quartzite and conglomerate. The Jannelsepan Formation of amphibolitic gneisses, schists and calc-silicate rock occur in a belt near the eastern edge of the NP, and yield a maximum Rb/Sr age of 1,5Ga at the Copperton volcanogenic Cu-Zn deposit (Cornell, 1978) (Table 3.2) (Fig. 3.2).

The OG extends as far south as Bitterfontein, where, as the supracrustal rocks in closest proximity to the SCCB, they comprise feldspathic quartzite, schists and aluminous gneisses. Moore (1986) recognised a series of east-west trending belts of meta-volcano-sedimentary rocks between Bitterfontein and Okiep (Fig. 3.2). The only available radiometric dates on the OG come from cordierite-orthopyroxene rocks in the Springbok-Komaggas area which yield U-Pb zircon dates of older than 1 700Ma for the inherited age, and a 1 200Ma age for the high-grade metamorphic event (Clifford et al., 1981).

Rocks which may be near- or actual- age equivalents of the ASG are therefore sporadically developed over a vast tract of the NP (Fig. 3.2). The SACS (1980) separation of similar packages of rock suites into different Groups based purely on geographic grounds, is probably not warranted.

The ± 2.0 Ga old mafic and ultramafic bodies which define the Groothoek Thrust and the boundary between the BSP and RSP in the Wortel area (Fig. 1.4), are the oldest known intrusives in these subprovinces, and are roughly contemporaneous with the Aggeneys basement. The Vioolsdrif Suite (VS) of granodiorite and diorite, represent new crustal material derived from mantle differentiation, and they intruded their co-magmatic 2.0Ga calc-alkali ORG volcanic rocks at about 1.9Ga (Reid and Barton, 1983). The RSP was reintruded by more acidic phases of VS some 1.73Ga ago. The Little Namaqualand Suite (1.0 - 1.2Ga) of siliceous augen granite-gneisses (Blignault et al., 1983) (Table 3.2), is the most regionally developed of the later phases intrusive into the BSP, with extensive occurrences in both the Springbok and Pella-Aggeneys areas (Fig. 3.2). The Aroams Gneiss, which is located between Aggeneys and Pella, is the largest locally developed member of the Little Namaqualand Suite.

Blignault et al. (1983) recognised two major structural episodes which deformed the BSP and RSP. The earlier Eburnian (2.0Ga) orogeny which deformed the ORG, was limited to the RSP. The younger Kibaran orogeny, pervasive in the BSP, caused the dominant east west fabric and isoclinal folds, and their related prograde metamorphic event, dated at 1.2Ga (Clifford et al., 1981). Blignault et al. (1983) interpreted the Groothoek Thrust (Fig. 1.4) as one of two late Kibaran SSW-verging thrusts in and immediately south of the RSP, along which

over 75km movement occurred. Moore (1986) suggested rather that the Groothoek Thrust marked the suture zone between the microcontinent on which the BG formed, and a super continent to the north. He cited as evidence the different basement types on either side of the Groothoek Thrust, and the ophiolite-like nature of the intrusive bodies along the Thrust. Joubert (1986) proposed rather that the Tantalite Valley Line (Fig. 3.2) of mafic intrusives and amphibolites (1.73Ga maximum age) marks the suture along which the RSP and BSP microcontinent in the south was accreted to the Gordonia Subprovince in the north (Fig. 1.1). This was followed at 1.3Ga with the accretion of the entire NP against the Kaapvaal Province.

From the greenschist facies, actinolite-hornblende dominated center of the RSP, the metamorphic grade increases both to the south and north. South of the RSP metamorphic isograds of the NP display the east-west elongation of the metasedimentary belts, the major thrust zones and the SCCB, with the highest grade metamorphic parageneses found around Garies-Kliprand (hercynite + quartz assemblage). Both the Springbok-Nababeep and Bitterfontein areas fall in the slightly lower grade garnet + cordierite + K-feldspar assemblage zones (Waters, 1986). To the north the isograds parallel the Namaqua Front where Blignault et al. (1983) showed a belt of granulite facies metamorphism extending through Grunau and Warmbad in Namibia and on to a point east of Kenhardt in South Africa. Symmetrically placed south of Bitterfontein and north of Springbok is the amphibolite facies grade assemblage of biotite + sillimanite + quartz into which the Aggeneys area falls (see Fig. 1 of Waters, 1986). The hercynite + quartz assemblage suggests maximum prograde conditions of $+800^{\circ}\text{C}$ at 5Kb, corresponding to the unusually high thermal gradient of $50^{\circ}\text{C}/\text{Km}$ (Waters, 1986), and corresponding well with the $45^{\circ}\text{C}/\text{Km}$ gradient calculated for the Aggeneys area (Lipson, 1978). Based on the high

thermal gradient and isobaric cooling history in western Namaqualand, Waters (1986) concluded that metamorphism resulted from convection caused by the ascension of dry, charnockitic magmas to levels above those presently exposed, and noted that such high heat flow acid magma provinces commonly occur in extensional regimes.

4. BROKEN HILL GEOLOGY AND PETROGRAPHY

The component rocks of the Aggeneys Subgroup (section 3) at each of the inselbergs stretching from Broken Hill through Maanhaarkop to Froneman se Kop are grossly similar (Fig. 4.1), hence the geology of only Broken Hill will be discussed in detail. Surface mapping of the area includes the work of J. M. Moore and K. Holliman (Broken Hill), J. D. Wilson (Maanhaarkop), and R. D. Lipson (Maanhaarkop and Froneman se Kop).

The ASG at Broken Hill is divided into the four formations, Namies Schist, Broken Hill Quartzite, Ore Schist and Shaft Schist. The name Namies Schist is retained from earlier workers, while introduction of the new names is justified in sections 4 and 5. Sediment-hosted, massive sulphide deposits commonly have associated a number of rock-types of limited lateral extent (often < 200m strike length and < 2m width), and Broken Hill is no exception. Consequently, these rocks have been given informal, descriptive names (Fig. 4.6) many of which have long been in use by mine staff. Several units, such as those equivalent to the ore time horizon, had not been recognised and were therefore un-named. In this thesis, rocks comprising a mixture of two components unfortunately bear clumsy, dualistic names, e.g.

Hangingwall Schist and Garnet Quartzite, abbreviated to HS+GQ. As will be shown (section 5), formations may be correlated over a wide areal extent, and these formation names are formally proposed for the ASG. It is unlikely, however, that within the formations, the names of individual rock-types which have limited distribution, will have application beyond the immediate Broken Hill area.

4.1 Structure, metamorphism and lithostratigraphy

At least four tectonic phases plastically deformed rocks in the Aggeneys area. F_2 folds (sensu Joubert, 1971) cause the major gneiss

and schist fabric, the prominent L_2 lineations which plunge at 25 - 30° along an east-north-east bearing, and control the plunge of the Broken Hill orebody. In the steeply north-dipping strata of Broken Hill, the prominent mineral lineations other than L_2 are sub-horizontal. The right-lateral Z-shape of the Broken Hill inselberg (Fig. 4.1) results from the F_2 deformation episode. Inselbergs stretching from Froneman se Kop in the east through Maanhaarkop to Broken Hill in the west, were referred to by the author (Lipson, 1978) as F_2 megaboudins developed along the southern limb of the Black Mountain Synclinorium. The metamorphic peak associated with F_2 folding has been estimated at 630 - 670°C and 2,8 - 4,5Kb at Gamsberg (Rozendaal, 1978), or 670 - 690°C and 3,4 - 4,5Kb in the Aggeneysberge (Lipson, 1978), i.e. upper amphibolite facies bordering on granulite facies. Various retrogressive episodes followed to produce mineral assemblages ranging to and below 350°C (Lipson, 1978).

Due to the intense deformation at Aggeneys the rocks are first described in their structural succession and inferences will be made throughout the thesis, based on geological and geochemical arguments, as to the original younging directions. In an idealized surface borehole at Broken Hill drilled perpendicular to dip (Fig. 4.2), first the gneisses of the "floor" rocks are intersected, followed by the supracrustal rocks investigated in this study. The latter comprise some 64% schist (506m) in the 793m thick structural succession with interspersed quartzite, ore, calc silicate rock and gneiss. Below the supracrustal rocks lie gneisses having minor amphibolite and quartzite developed.

The regional occurrence of leucocratic gneisses found underlying the schist-quartzite belts lead the author (Lipson, 1978) to propose that part of the succession at Broken Hill is overturned (Fig. 4.3). If

this interpretation is correct then the overturned succession youngs all the way from the gneisses north of Broken Hill, southwards to the grey granoblastic leucocratic gneiss (GGLG) (Fig. 4.4), a rock so named to distinguish it from mafic grey gneiss, and from the common Pink Gneiss found in Bushmanland. The GGLG forms the core of a south verging, isoclinal syncline, whereafter the schist and quartzite south of the fold axis define the "right-way-up" limb of the fold. The cross section through Maanhaarkop (Fig. 4.5) reveals the same gross structural succession as at Broken Hill, but lack of outcrop to the south of Maanhaarkop and insufficient borehole coverage leave a gap in the stratigraphic information available in the equivalent position of the Plant Hill quartzite shown in Fig. 4.4 . The stratigraphic column derived as a working model, and referred to hereafter as a *working stratigraphic column*, starts with Namies schist at the base and ends with GGLG at the top, thus placing the orebody stratigraphically above the quartzites (Fig. 4.6). The supracrustal succession in the working stratigraphic column at Broken Hill comprises only 459m (excluding GGLG) compared with the 793m long structural succession.

4.2 Broken Hill schists

4.2.1 Namies Schist (NS)

The rationale for naming the schist lying between gneiss and quartzite, Namies Schist, is presented in Section 5.1. The rock is afforded formation status as indicated in Fig. 4.6. Namies Schist (NS) is a strongly foliated, coarse-grained, quartzitic schist which displays textural variations from nodular to mottled (Fig. 4.7). The nodules, comprising a quartz-muscovite-sillimanite assemblage, are most common at, but not restricted to, the zone closest to the gneisses. Rarely are banded or massive varieties of NS found. The colour of fresh rock varies from grey-green to pink, although wet pieces of borehole core of both the schist and enclosed pegmatites

always display a reddish colour. In outcrop the schists weather dark-brown to grey where relatively quartz-poor, and lighter grey in the more quartz- and muscovite- rich areas. NS occasionally hosts one metre thick amphibolite bands and chlorite-rich schists, as well as quartzite and Garnet Quartzite bands of up to half a metre thick.

NS displays a wide modal variation, with essential minerals consisting of quartz, biotite, sillimanite, muscovite and opaque minerals. The subparallel arrangement of elongated quartz, sillimanite and the micas define the rock's well developed foliation. Close to the basal gneisses, quartz comprises some 40 - 50% of the rock, with biotite (15 - 25%) in excess of muscovite (5 - 10%) (Appendix C.1, Table C.2).

Nearer the quartzites not only do the number of quartzite interbands increase, but there is also an increase in quartz content (estimated 50 - 60%) and muscovite (estimated 10 - 25%), at the expense of biotite (estimated <5%). The occurrence of both plagioclase and microperthite (20 - 40%) is restricted to the zone adjacent to basal gneisses. An important feature of NS, however, is that irrespective of relative mica content, the primary (deformed) muscovite is frequently in stable contact with biotite. In both borehole core and surface samples, much coarser-grained, secondary (undeformed) muscovite occurs as an alteration product after sillimanite (Fig. 4.8) (Appendix C.1), while chlorite represents the major secondary product after biotite. This contrasts strongly with Shaft Schist discussed below in which muscovite forms the major alteration product after biotite.

Of the minor minerals, zircon is ubiquitous, while coarse-grained garnet, tourmaline and fine-grained sphene occur sporadically. Zircon displays a slightly elongated, but rounded form, and most commonly occurs as an interstitial mineral. No zircon overgrowths have been

noted, and metamict varieties are rare. Magnetite commonly comprises up to 5% of NS, with accessory chalcopyrite occurring as irregular blebs or streaks parallel to the foliation. Pyrite and pyrrhotite are more rarely developed. The opaque mineral content of NS does not vary systematically through the succession.

4.2.2 Shaft Schist (SS)

Shaft Schist (SS) forms a distinct horizon in the footwall of the Broken Hill orebody through which both the Broken Hill decline- and vertical- shafts were sunk. Although comprising approximately one fifth of the supracrustal sequence, SS rarely crops out due to its soft nature and negative weathering characteristic, thus borehole core and underground development offer the best exposure of this horizon. The rock-type is referred to by local mine geologists as Lower Footwall Schist, and by Lipson (1978) as Spring Schist, after the tentative correlation between it and the Spring Schist in the Aggeneysberge. SS may be further subdivided into structurally Upper and Lower horizons (USS and LSS) separated by GGLG near surface, and distinguishable from each other down dip when GGLG is no longer present, by the more siliceous character of LSS (Figs. 4.2 and 4.4). As with NS, SS should be afforded the rank of formation (Fig. 4.6). The Biotite Graphite Zone and Calc Silicate Rock plus Manganese Quartzite comprise two subunits of SS, and are described below in sections 4.2.2.1 and 4.2.2.2 .

SS is also a strongly foliated, coarse-grained rock, but unlike NS, hand specimens display relative homogeneity with little textural or mineralogical variation. Amongst the borehole cores examined, no amphibolite bands were noted. Fresh core specimens of SS and its enclosed pegmatites display a green-grey colour when both wet and dry (Fig. 4.9), although within a month of exposure to rain, oxidation of

the contained iron sulphides produces a distinctive yellow-coloured staining. In the rare outcrops of SS, the breakdown of iron sulphides and consequent generation of sulphuric acid produce alteration colours ranging through white, yellow, red and black.

The well foliated texture of SS is defined by oriented, strongly elongated quartz, sillimanite, micas, iron sulphides and graphite. Additional petrographic descriptions and estimated modal percentages appear in Appendix C.2 and Table C.3). In contrast to NS, the muscovite content never exceeds that of biotite, and virtually all muscovite is an alteration product of biotite (Fig. 4.10) or sillimanite. Only trace amounts of chlorite alteration after biotite are present.

Rounded zircon occurs in all thin sections examined, but appears finer-grained and more frequently enclosed in biotite in SS than in NS (Table 4.1). Minor exceptions exist to the above generalizations (Appendix C.2). The opaque minerals consist of pyrite and pyrrhotite, with minor graphite, but magnetite is absent. Samples with > 5% pyrite and pyrrhotite occur within 80m of the Broken Hill orebody.

4.2.2.1 Biotite Graphite Zone (BGZ)

Ryan et al. (1982) called this rock the *pyritic graphitic biotite schist*, while the term Weak Zone used by mine personnel aptly describes the poor support conditions which obtain where mining development proceeds through this incompetent horizon. The term Biotite Graphite Zone is suggested here since the unit forms a distinctive zone, though not a separate rock-type, of relative enrichment in biotite and graphite within SS. BGZ marks the structural top of SS, separating Ore Schist above from SS below (Fig. 4.2), and appears to be a stratigraphic horizon due to its persistent

and concordant nature. The green-grey coloured BGZ is a strongly foliated schist comprising millimetre thick, slickensided graphite layers in a matrix of clay and biotite-rich SS (Appendix C.2.1; Table C.4; Fig. C.1) suggesting a concentration of shear deformation at this stratigraphic level. The Zone frequently contains green-coloured pegmatites and lensoid bands of pyritic Garnet Quartzite.

4.2.2.2 Calc Silicate Rock plus Manganese Quartzite (CSMQ)

CSMQ occurs as lenses approximately 10m structurally below BGZ, with dimensions shown in Table 4.6, and has not previously been described in the literature. The two components of CSMQ are intimately interbanded, green to pink rocks, and exhibit fine to coarse-grained textures. Individual bands of the two rocks vary in size from 2 - 100cm. Within 200m south-east of the Broken Hill orebody the manganese quartzite predominates, and this displays yellow to orange boxworks after sulphides. While the Calc Silicate Rock comprises garnet, quartz, a pyroxene-amphibole mixture and sulphides including dominant pyrrhotite, and lesser disseminated galena and sphalerite, the Manganese Quartzite consists of quartz, garnet, biotite and sulphides (Appendix C.2.2; Table C.5; Fig. C.2).

At Maanhaarkop CSMQ thickens to nearly 2m and carries up to 7% Pb as cerrusite and galena in surface samples. No CSMQ samples from Broken Hill have returned such high Pb values. Also found in a 2m² outcrop associated with CSMQ on Maanhaarkop is the only unequivocal conglomerate (Fig. 4.11) found along the entire outcrop chain stretching from Broken Hill to Froneman se Kop.

4.2.3 Ore schists and orebody

The detailed geology in and immediately adjacent to the orebody is complicated both by lensoid development of the orebody and associated

rocks, as well as by later deformation causing high amplitude folds (Fig. 4.12) which juxtapose sequences of similar looking schists. The schist zone hosting the orebody and lying between the quartzites above and BGZ below, is therefore called Ore Schist (OS) (the nomenclature is further justified in section 5.2) and can be subdivided purely on structural positioning into Hangingwall Schist (HS) above the Upper Orebody (UOB), Intermediate Schist (IS) which separates UOB from the Lower Orebody (LOB), and Upper Footwall Schist (UFS) which lies between LOB and BGZ (Fig. 4.2). The Ore Equivalent Schist (OES) is defined as the lateral equivalent (both to the west and east) of the zone comprising UOB+IS+LOB (Fig. 4.6). Except in UFS which is noticeably feldspar rich, thin bands of Garnet Quartzite frequently occur in Ore Schist. The rock is then referred to as Hangingwall Schist plus Garnet Quartzite (HS+GQ), or Ore Equivalent Schist plus Garnet Quartzite (OES+GQ). Where these Garnet Quartzites are sufficiently thickly developed, they are referred to as Ore Equivalent Garnet Quartzite (OEGQ). HS displays strongly developed compositional banding. OES is most easily recognised where it comprises a massive biotite and garnet rock with minor quartz and muscovite. The biotite flakes vary up to 15mm in size and host garnets of up to 8mm diameter. Parts of IS have identical mineralogy to OES.

The term Garnet Quartzite as commonly used by mine staff is retained instead of the term garnet-quartz rock suggested by Spry and Wonder (1989), who pointed out that garnet quartzite implies that the rock was formed by metamorphism of a sandstone or chert. No misnomer is apparent in view of the wide definition of chert, which includes silica of organic, inorganic and replacement origin.

In general terms the two lenses comprising the Broken Hill orebody have separate lithologies. An abrupt increase in the quartz and

magnetite contents of OS marks the top of UOB which consists of a magnetite-bearing quartzite that grades downwards with increasing magnetite content into a quartz magnetite rock (QM) clearly belonging to the oxide facies of banded iron formations (BIF). QM grades downwards into an amphibole magnetite rock (AM) which hosts the well-defined, partly baritic massive sulphide lenses of UOB. The footwall to UOB comprises either QM or GQ, and both display sharp contacts with IS. LOB generally has the same form as UOB except that the quartz magnetite rock is absent, and sulphide mineralization in the amphibole magnetite rock is finer-grained and of a higher tenor than in the corresponding rock of UOB. LOB is sheathed in GQ. In places along the LOB upper contact GQ displays a conglomeratic appearance with a biotite garnet matrix wrapped around the quartzite "pebbles" (Fig. 4.13). The matrix consists of garnet, quartz, biotite, opaque minerals, muscovite and gahnite (Appendix C.3; Table C.11). Although quartz dominated, the "clast" comprises the same minerals except for muscovite.

Of all OS samples examined (Appendix C.3; Tables C.6 - C.9), only those from the intensely refoliated zone of an F_2 fold (Fig. 4.14) in BH112 (samples ALP172, 174 and 176) display such severe alteration that even quartz has participated in the reactions generating sericite. Coarse-grained biotite has retrograded to sericite around the fold axes. In ALP174, sericite occupies large areas of the thin section with muscovite having crystallized from the sericitic mass. Biotite is preserved at the terminations of elongated garnet, but passes rapidly into sericite away from the garnet.

The tenor of mineralization in both UOB and LOB increases progressively towards the central massive sulphide lenses. Although estimates of the orebody assemblages appear in Table C.10, detailed

descriptions of UOB and LOB fall outside the scope of this thesis, and the reader is referred to Ryan et al. (1982) for more information.

Zircon concentrations decrease from HS or UFS into OES and further into GQ and the orebody. In some of the OES samples zircon is preserved entirely as fine crystals in biotite, showing pleochroic haloes. Gahnite is limited to rocks of the orebody and their adjacent Garnet Quartzites, and to one sample of surface OES (ALP198) located some 20m from the orebody. The lack of heavy minerals other than magnetite in ALP075, a quartz magnetite rock from the Broken Hill orebody, contrasts strongly with the abundant apatite, sphene and coarse-grained, rounded zircon found in ALP228, a quartz magnetite lens from the south slopes of Froneman se Kop (Table C.10). Magnetite comprises in excess of 90% of the minerals listed under the column "Op" (opaque minerals) in Tables C.10 and C.11.

4.3 Broken Hill Quartzites (BQ)

The massive, white to glassy quartzites at Broken Hill, Maanhaarkop and Froneman se Kop, form the prominent ridges responsible for the inselberg landscape at Aggeneys. At all three hills the two distinct quartzites referred to by mine geologists as Upper Quartzite and Lower Quartzite according to their structural superposition, are separated by a Median Schist horizon (MDS) which frequently encloses dark quartzite lenses. The Lower Quartzite is generally darker coloured than the Upper Quartzite, particularly so in weathered outcrops, and the terms Dark Quartzite (DQ) and White Quartzite (WQ) introduced by Rozendaal (1982) are adopted (see section 5.1 below for justification of the formation name Broken Hill Quartzites). In total the two quartzites, measuring some 88m in true thickness, comprise an important component of the supracrustal succession at Broken Hill, and lie between the schist horizons NS and OS (Figs. 4.2 and 4.6).

Until Mr. J. Hobbs drew the author's attention to faint heavy mineral layering in the steeply north-dipping WQ at Froneman se Kop, no pristine sedimentary structures had been recognised in BQ. The dominant features of the layers is that they remain subparallel over the few metres of continuous outcrop in which they can be traced, with the occasional development of a low angle band linking two adjacent layers (Fig. 4.15). Radiographic stereo pairs from an oriented sample of one such occurrence reveals ripple-like features measuring up to 2cm across which display both concavity and pointed cusps to the south (Fig. 4.16). The apparent truncation of "foreset X" by "topset Y" (Fig. 4.16) also suggests southward younging, as does the possible "rain-drop" feature located at Z (Fig. 4.17). These features are, however, open to different sedimentological interpretations.

Furthermore, though suggestive of primary sedimentary structures, the cusps and truncations may have developed during the four major phases of structural deformation (Ryan et. al., 1982). Assuming that the sample collected is representative of the attitude of the entire hill and was not affected by local small-scale isoclinal folding, then the rocks at Froneman se Kop are overturned.

Although WQ and DQ generally have similar mineralogies, there is a tendency for DQ to contain more mica and accessory minerals than WQ (Table C.12), which accounts for the darker colour of DQ. In both WQ and DQ, quartz comprises in excess of 80% of the mode, with muscovite the next most important mineral. Heavy mineral layers continue through and not around quartz grains, which indicates extensive recrystallization of quartz, and prevents any genetic connotations being placed on quartz grain morphologies (Lipson et al., 1986). Additional BQ petrographic descriptions appear in Appendix C.4.

Ubiquitous zircon displays a well rounded and slightly elongated morphology (Fig. 4.18) with a long axis dimension averaging 80 - 95 microns (Table 4.2). Rounded grains of zircon measuring 30 - 50 microns dominate the mineralogy of the heavy mineral layers (Fig. 4.19) with lesser, rounded to idiomorphic grains of hematite/ilmenite intergrowths, and red rutile. In hand specimens of both WQ and DQ, sporadic pyrite and chalcopyrite grains concentrate along bands and zones slightly enriched in magnetite. Heavy mineral layer thickness is restricted to the width of one or two mineral grains (Fig. 4.19), hence no graded bedding is discernible (Lipson et al., 1986).

MDS displays wide variations in mineralogical proportions and is both foliated and banded. Major minerals comprise quartz, biotite, muscovite and sillimanite (Table C.12), while garnet and magnetite in quantities of between 3 and 10% each, characterize this rock and are frequently associated with small amounts of disseminated pyrite and chalcopyrite.

4.4 Physical dimensions

The stratigraphic thicknesses of each rock type measured in the sampled boreholes is given in Table 4.3 . Also included are average, total and range of thickness.

At Broken Hill, WQ can be traced along the entire 3 300m length of the inselberg, while DQ continues for only 900m, although it is inferred to extend over a similar strike length to WQ (Fig. A.2a). Remnants of both quartzites are recognised between the 6km separating Broken Hill and Froneman se Kop. Drilling at Broken Hill shows that the quartzites continue down-dip for over 750m, and for over 10km in the preferred structural interpretation of macroscopic isoclinal fold duplication of the entire succession (Fig. 4.3). WQ and DQ average

65m and 23m in true thickness, respectively (Fig. 4.4 and Table 4.4), while MDS averages 17m.

Both NS and SS display similar strike dimensions to those of the quartzites. Without exception, every borehole drilled into the 3 300m long Broken Hill inselberg has intersected the two schist horizons at their anticipated relative positions. From sporadic surface and borehole information between Broken Hill and Maanhaarkop, a strike extent of over 5km can be inferred for both schists. The lack of positive identification of SS at Froneman se Kop precludes the inference of its presence east of Maanhaarkop. While the preferred structural interpretation suggests a down-dip continuation of SS for well over 10km (Fig. 4.3), NS lacks a similar dip extent since it is not developed at Plant Hill. With reference to Fig. 4.3 it appears that NS was thinned as an incompetent layer along the sheared limb of the isoclinal fold.

An average thickness dimension of 96m for SS (Table 4.5) is based at Broken Hill on an average between the thickness from BGZ to GGLG, and from GGLG to the Plant Hill quartzite (PQ) (Fig. 4.4). No other complete borehole intersections exist on which to base this calculation. The average of 104m for NS thickness includes the thin Maanhaarkop intersection in borehole TS11 (Fig. 4.5).

The 1 - 10m wide BGZ (Table 4.6) occurs both structurally below the Broken Hill orebody, and also in percussion boreholes drilled for water near Klein Kop (Fig. 4.1). Whether BGZ exists on Maanhaarkop remains unknown as no boreholes have penetrated its anticipated stratigraphic level in that area. In contrast, folded, 1 - 7m wide lenses of CSMQ (Table 4.6) lie at a constant stratigraphic level both at Broken Hill and at Maanhaarkop. These lenses seldom occur in the

immediate structural footwall of the Broken Hill orebody, but rather structurally below, and peripherally to the orebody.

OS may be traced for the entire length of both Broken Hill and Maanhaarkop, and down dip for > 800m to the deepest borehole intersections at these hills, maintaining a width of approximately 110m (Table 4.7). Where the orebody is present, HS averages some 21m in thickness, IS 11m and UFS some 21m. Away from the orebody, OES measures up to 40m in thickness with the massive biotite garnet rock component of OES not exceeding 10m in width. The lensoid UOB and LOB measure 40 - 60m and 30 - 40m, respectively, over the bulk of their lengths. Ryan et al. (1982) quote a strike extent to the orebody of 600m and down plunge extent of over 1 200m. The relationships between major lithologies are described in Appendix E.

4.5 Conclusions

The general setting of a schist and quartzite succession with associated conglomerates and calc silicate rocks clearly suggests that the package of rocks which host the Broken Hill orebody, is metasedimentary. The likely precursors to the major schist (metapelite) and quartzite (metapsammite or metachert) units will be examined in section 9. The particularly well developed metatholeites (now amphibolites), near the top of the succession at Gamsberg and Aggeneysberge, in which amygdales are preserved (Rozendaal, 1978; Ryan et al., 1982; Reid et al., 1987) reflect volcanic input at specific times during development of the basin (see also Fig. 5.3).

5. LITHOSTRATIGRAPHIC CORRELATIONS

5.1 Broken Hill area

In an environment as structurally deformed as the NP, the possibility exists that large-scale dislocations have occurred, fortuitously juxtaposing on individual inselbergs, similar-looking but stratigraphically unrelated rock successions. Therefore in studying spatial distribution of lithogeochemical signatures in the Broken Hill area, the structural succession must be examined for the presence of large-scale, low angle (thrust) and high angle faults. If individual metasediments and their order of occurrence are correlatable between, for example, Broken Hill and Maanhaarkop (Fig. 4.1), then continuity probably existed at sometime between these two inselbergs.

The structural successions at Broken Hill and Maanhaarkop are grossly similar with the nodular to mottled, magnetite-bearing, quartz- and zircon- rich NS on the north side of both hills structurally overlying the whiter, thicker WQ, and then the darker, thinner DQ. Between the two quartzites is sandwiched the magnetite-bearing MDS that in places at both localities exhibits traces of Cu mineralization in the form of malachite staining on outcrops and chalcopyrite in borehole core. At Broken Hill MDS also hosts a stratabound and stratiform gossan lying directly structurally above the orebody. The strike extent of the gossan is restricted to the general region of the Broken Hill orebody.

The schists immediately below DQ contain 5 - 15cm wide bands of Garnet Quartzite. In borehole BH123 the two distinct Garnet Quartzite-rich zones within these schists reflect the down-plunge extremities of the Broken Hill UOB (ALP047) and LOB (ALP049), and may be correlated with two Garnet Quartzite-rich zones in borehole TS11 at Maanhaarkop (ALP130 and 132). In both boreholes BH123 and TS11, Garnet Quartzite layers are rarely found in the schist below the lower of the two major

Garnet Quartzite zones. Surface outcrops at Maanhaarkop show CSMQ and occasional outcrops of SS in the same relative structural positions as at Broken Hill. Even the percussion boreholes drilled for water between Klein Kop and Maanhaarkop intersected graphite at the depth expected for BGZ, confirming the continuity of many of the supracrustal rock-types below surface cover. Although BH123 continued through schist to intersect BGZ, CSMQ and SS, TS11 stopped short in schist below the lower Garnet Quartzite, but before testing either BGZ or CSMQ horizons (Fig. 4.5). On simple petrographic grounds, therefore, rocks at Broken Hill and Maanhaarkop may be correlated with a high degree of certainty.

Schists occupying a position between gneiss and quartzite at Gamsberg (Rozendaal, 1978) and Namiesberg are referred to by SACS (1980) as Namies Schist, with the rank of formation. In gross appearance, included lithologies and mineralogy, NS at Broken Hill is similar to that described by Rozendaal (1982) at Gamsberg (Table K.1), thus justifying the correlation between these schist horizons from the two inselbergs.

In detail, good correlation also exists between the quartzite members at Broken Hill and those described at Gamsberg by Rozendaal (1978) (Table K.2), with White Quartzite at Broken Hill the equivalent of the White Quartzite Member at Gamsberg, Dark Quartzite at Broken Hill the equivalent of the Dark Quartzite Member at Gamsberg, and MDS at Broken Hill the equivalent of the Pelitic Schist Member at Gamsberg. Although Rozendaal's (1982) quartzite nomenclature is adopted, the specific name Median Schist is preferred to his general term Pelitic Schist. Both SACS (1980) and Rozendaal (1982) express doubts about correlations between the supracrustal successions at Aggeneys-Gamsberg and at Pella, hence the term Pella Quartzite Formation which

collectively includes the Aggeneys and Gamsberg units (Rozendaal, 1978) is inappropriate. Rozendaal (1982) later suggested calling the unit the Zuurwater Quartzite Formation after the farm Zuurwater at Aggeneys. Moore (1977) simply used the word Quartzite to describe this suite of rocks at Namiesberg, while SACS (1980) preferred the term Metaquartzite unit. The name White Quartzite Formation used by Ryan et al. (1982) does not accurately reflect the presence of colour variations between white and dark members. In proposing here the term Broken Hill Quartzite Formation (BQ) for WQ, MDS and DQ, cognizance is taken of the good quartzite exposures which exist on surface, in borehole cores, and in underground workings at Broken Hill.

Maanhaarkop, Klein Kop and Froneman se Kop differ from Broken Hill chiefly in the lack of an orebody and in the thinner supracrustal successions at the former locations. The succession is so thin at Froneman se Kop that no NS separates gneisses from WQ on its north slope (Fig. 4.1). Neither OES nor SS could be positively identified on the south slope of Froneman se Kop, although the presence of SS beneath the sand cover south of Froneman se Kop is considered likely. The two garnetiferous schist samples from the south slopes of Froneman se Kop (ALP229 and 230, Fig. A.2b), are correlated with OS because of their similar petrographies (Table C.6) and similar locations within the metasedimentary succession.

The conglomerate-like GQ of the Lower Orebody (section 4.2.3) is unlikely to have gained its clastic appearance in the sedimentary environment since the unusual garnet+gahnite mineralogy is preserved in both clasts and matrix. It would be fortuitous for Fe-Zn-rich quartz pebbles to be deposited in an Fe-Zn-rich pelite. The necking evident in the more continuous, quartzitic layers (Fig. 4.13) indicates that the clasts are probably boudinaged remnants of quartz-

rich layers in a meta-pelitic matrix. Such rocks are therefore referred to as pseudo-conglomerates, and there can be no justification in correlating them with the less equivocal meta-diamictites recognised by Strydom (pers.comm., 1983) from Black Mountain and the Aggeneysberge, or the meta-conglomerate in the eastern Aggeneysberge (Ryan et al., 1982).

Problems have long existed in correlating the north-west dipping Tank Hill succession with rocks at Broken Hill and Black Mountain. Although gneiss occurs on the northwestern slope of Tank Hill (Fig. 5.1), the schist lying between gneiss and quartzite in the expected position of NS, has a gossan-like appearance with black, Mn-Fe surficial staining and occasional veins which cross-cut the foliation. Dark alteration extends into the host rock for 2cm on either side of the veins. A thin (< 100cm thick), unmineralized band of massive magnetite and barite extends for approximately 100m strike length in the schist (Figs. 5.1 and 5.2). Part of the schist grades into a Garnet Quartzite, while an isolated (10m x 10m) patch of green, fuchsitic quartzite occurs close to the quartzite contact (Fig. 5.2). Estimated modal percentages appear in Table C.2 for the schist (ALP243) and Green Quartzite (ALP244X and Y). Extensive shearing in the area precludes recognition of two distinct quartzite horizons within the quartzite zone (Fig. 5.1), but a gossanous Pb-Zn mineralized schist similar in character to Spring Schist in the Aggeneysberge, structurally underlies these quartzites.

Tentative correlations between rock types at Tank Hill with Black Mountain to the northwest and Broken Hill to the southeast, are as follows:

1. The veined schist at Tank Hill is a type of NS which hosts the three unusual rock types, massive magnetite and barite, Garnet Quartzite and green quartzite.
2. The quartzite zone structurally below NS correlates with BQ and can also be traced to Black Mountain where it lies both above and below the orebody due to isoclinal fold duplication (Fig. 4.3).
3. The mineralized schist at Tank Hill has been traced into the Lower Orebody pelitic horizon at Black Mountain by integration of detailed surface mapping results with those from a line of boreholes drilled between the two inselbergs. Towards the east the mineralized schist at Tank Hill is correlated with either the Broken Hill Orebody or with SS as a mineralized portion thereof.

The direct correlation of rocks at Broken Hill with those at Klein Kop, Maanhaarkop and Froneman se Kop appears straightforward, although correlation with Tank Hill is more tenuous.

5.2 Namiesberg, Wortel and Achab

Both Namiesberg and Wortel localities have a similar-looking gneiss-schist-quartzite suite of rocks to those described at Broken Hill. In contrast, no rock-types other than schist were intersected in borehole AC2 from Achab, and no outcrops occur within 1 000m of the borehole site.

In comparing rocks outside of the immediate Aggeneys area (regional rocks) with those at Broken Hill (local rocks), the names used at Broken Hill have been favoured. To distinguish both clearly and simply between local rocks and their likely regional counterparts, the

suffix "type" is added to the Broken Hill rock name for the corresponding regional rock. Thus for example, Namies Schist (NS) at Broken Hill becomes Namies-type Schist (NTS) at Wortel.

Similarly to Broken Hill, the major quartzite and schist horizons at both Namiesberg and Wortel may be traced along strike for several kilometers, and the packages of metasediments measure tens to hundreds of metres in thickness. The Namiesberg structural succession approximates that at Gamsberg (Rozendaal, 1982), with gneiss overlain by schist and then by a quartzite zone (Fig. 5.4). At Namiesberg this schist has a variable, foliated and banded character, with interlayers of orange-coloured muscovite gneiss (confined to the northern slopes), pink-coloured pegmatites (ALP433), and occasional dark-weathering quartzites. On both the north and south sides of Namiesberg, black Fe-Mn stained vugs in places present a slightly gossanous appearance. Moore (1977) reported thin lenses of calc silicate rock, aluminous-rich rock and amphibolites within the schist. The massive sillimanite pods in the schist have been mined as a refractory product. Both at Namiesberg and Wortel, schist lying between gneiss and quartzite becomes more feldspathic away from the quartzites. Gneiss, pegmatite and gossanous parts were excluded from all samples.

Based on the nodular texture, variability, included quartzites, adjacent rock types, the pink colour of included pegmatites, and mineralogy (Appendix C.5 and Table C.13), the schists lying between gneiss and quartzite at Namiesberg are correlated with NS. Moore (1977) proposed that the quartzite zone at Namiesberg marked the top of the stratigraphic succession, implying that schists found structurally above the quartzites are a duplication of those below. Selected traverses carried out during the sample collection program at Namiesberg showed, however, that the quartzites comprise a lower white

variety separated from a darker, pyrite-bearing type, by a banded and foliated schist horizon, in exactly the same sequence as found at Gamsberg, and reversed to the structural order at Broken Hill. Quartzites along the subvertical northern limb of the Namiesberg synclinorium can be traced around the closure into the north-dipping southern limb (Figs. 5.3 - 5.5). The whiter of these quartzites is therefore termed White-type Quartzite (WTQ) and the darker, Dark-type Quartzite (DTQ), with the schist called Median-type Schist (MDTS). These quartzites contain heavy mineral layers similar to those found in BQ. At Wortel the structure is not as clearly defined, but the north side of the Wortel mountains in the vicinity of boreholes WTL3 and WLT4 (Figs. 5.3 and 5.6) have a broadly similar structural sequence to that at Broken Hill. The quartzites are overlain firstly by a thin, light grey to pink coloured, magnetite-bearing schist (NTS) which hosts pink coloured pegmatites, and then by gneiss. The textural and mineralogical descriptions of the Regional Quartzites (RQ) are presented in Appendix C.7 and Table C.16.

At both Namiesberg and Wortel, borehole samples of schist lying on the side of the quartzites opposite to that of the gneiss, display the bottle green colour, foliated pyrite, and monotonous, unbanded character of Broken Hill SS, and are termed STS. Pale green-coloured pegmatites usually comprise in excess of 10% of the rock, by volume. At Wortel this schist hosts both the massive sillimanite pods exploited as a source of refractory ore (Appendix C.6.1) as well as the thin banded iron formation/calc silicate rock/Garnet Quartzite gossans investigated by exploration companies. Comparisons between the Broken Hill and Wortel calc silicate rocks reveal petrographic similarities except for olivine found at Wortel (Appendix C.6.2; Table C.15). In that respect the Wortel CTS has an affinity with AM at Broken Hill. The recognition that massive sillimanite pods occur in

both NTS and STS is in conflict with Rozendaal's (1982) assertion that these bodies are restricted to NS, and suggests an age of formation which possibly post-dates that of NS.

The structural geology at Wortel may be interpreted as an inclined isoclinal syncline which passes outwards into gneiss in both right-way-up and overturned limbs (Fig. 5.6). Quartzites adjacent to STS are thus correlated, and named DTQ, while those nearest the gneisses are called WTQ. At Namiesberg borehole VG1 was sited inside the synclinal structure and was not drilled sufficiently deep to intersect NTS rimming the structure (Fig. 5.4). Thus only surface samples of NTS were collected from Namiesberg while both surface and core samples of quartzites were obtained from there (Figs. A.1f and A.2c). No surface samples were collected from Wortel, and the data from two boreholes there were merged to produce one composite borehole (Appendix A.1.2; Fig. A.1d).

The light grey schists in borehole AC2 from Achab frequently display a nodular to blotchy texture. Interbands of feldspathic quartzite in the ratio of six schist to one quartzite occur for over 150m of the borehole core. Small, pink coloured pegmatites commonly invade the schist. Well rounded zircons of variable sizes are common (Appendix C.5.2) and schist mineralogy (Table C.13) is similar to that of NS. The opaque minerals consist mainly of magnetite, with pyrite and pyrrhotite being present in trace quantities only. All these attributes suggest a correlation between the Achab schist and NS, hence these rocks are also called NTS.

If the northernmost half of the Wortel structural succession is inverted to produce a working stratigraphic column as constructed at Broken Hill, then comparison between Broken Hill, Namiesberg and

Wortel reveal gross similarities, with basal gneisses overlain by NS and NTS, followed by the quartzite zone, and capped by SS and STS (Fig. 5.7). The major differences between the above areas and Gamsberg is that no Shaft-type Schist is found towards the top of the succession at Gamsberg unless the pelitic parts of the Gamsberg orebody represent mineralized STS. A conglomerate-muscovite schist and amphibolite suite (Nousees Mafic Gneiss, Rozendaal, 1982; Koeris Formation, Reid et al., 1987) cap the succession at Gamsberg. Rozendaal (1982) did suggest that part of the stratigraphy above the Gamsberg orebody was removed during the hiatus which existed prior to deposition of the unconformably overlying conglomerates. This could account for the lack of unmineralized STS at Gamsberg. In summary, it is clear that from the gneisses to DQ, good lithological correlations exist between Broken Hill, Namiesberg, Wortel and Gamsberg, while above DQ the correlation applies in the first three areas only.

Schists lying between DTQ and STS at both Namiesberg and Wortel, but not clearly looking like STS, have been designated Schist (S) and treated separately (Figs. 5.4, A.1d and A.1f). Their stratigraphic position suggests a possible correlation with OS at Broken Hill.

Praekelt et al. (1983) correlated the rocks at Gamsberg with those in the Namiesberg, calling the package from Namies Schist at the base through Dark Quartzite at the top, the Achab Formation; the schist and Banded Iron Formation directly above the quartzites, the Gams Formation; and the amphibolite, schist and conglomerate previously called Nousees Mafic Gneiss, the Bloemhoek Formation. Distinctive marker units in the ASG are so infrequently developed that the grouping of schist and quartzite by Praekelt et al. (1983) into the Achab Formation tends to blur the fundamental geology recognised by SACS (1980), to whose definition of Namies Schist, it is therefore

reverted. On the basis of their paper it is not possible to ascertain whether Praekelt et al. (1983) correlated the banded iron formation at Gamsberg with that at Broken Hill. Also, in defining the Aggeneys Ore Formation, Ryan et al. (1982) did not separate OS from SS. For these reasons the new term Ore Schist has been introduced for the package of rocks constrained between BQ and SS, which host the Broken Hill orebody. The term Koeris Formation proposed by Reid et al. (1987) is preferred to Bloemhoek Formation for the muscovite schist, amphibolite and metaconglomerate horizons which overlie the Gamsberg orebody and probably form the stratigraphic capping to SS, since Koeris is one of the type areas for this suite of rocks.

Praekelt et al. (1983) correlated a zone of muscovite enrichment at the base of their Achab Formation (i.e. base of NS) with the top of the succession at Wortel such that virtually all the quartzites and schists at Wortel would lie stratigraphically below NS. Thus in the Aggeneys area, Praekelt et al. (1983) deduce a supracrustal succession exceeding 3 000m in thickness. None of the other workers in the area (e.g. Moore, 1977, 1986; Rozendaal, 1978, 1982; Lipson, 1978, and this thesis) have, however, found evidence for stratigraphic successions exceeding 1 500m in thickness at any one locality.

5.3 Conclusions

The similar stratigraphic successions at Broken Hill, Gamsberg, Namiesberg and Wortel (Fig. 5.7) clearly suggest that correlation of the major lithostratigraphic units is both realistic and desirable, and that the use of small variations such as muscovite enrichment cannot be used as a foundation for correlation purposes. The major features of the broad correlations between these inselbergs include nodular, magnetite-bearing quartz-muscovite schists lying between basal gneisses and quartzites; a whiter quartzite overlain by a darker

quartzite; and then a monotonous bottle-green pyritic schist above the quartzites. The name Pella Quartzite Formation is replaced by Broken Hill Quartzite Formation as explained above (section 5.1), while the Aggeneys Ore Formation of Ryan et al. (1982) is here separated into Ore Schist and Shaft Schist Formations. Within the ASG the following formation names are therefore proposed (Fig. 4.6), of which the top three are new, viz.:

Shaft Schist

Ore Schist

Broken Hill Quartzite

Namies Schist

(Base)

The association of Shaft-type Schist with feldspar-free quartzites has been observed at many places in Bushmanland, including borehole cores from Annakoppies near Pella, at Hartebeestvlei south east of Pofadder and from Koeris north of Aggeneys. The suggested stratigraphic succession therefore assumes regional significance.

PART C.
GEOCHEMISTRY

PART C. GEOCHEMISTRY

Sampling techniques and analytical methods employed are reviewed in Appendix A. Sample locations appear in Figs. A1 and A2. Instrumental conditions, detection limits and error values are presented in Tables A1 and A2, and Figs. A3 - A5, while the analytical data may be found in Tables A3 - A5.

6. BROKEN HILL GEOCHEMISTRY

6.1 Element redistributions

6.1.1 Introduction

Metamorphism can significantly change the pre-metamorphic rock composition (e.g. MacRae and Nesbitt, 1980; Barby and Cuney, 1982), and the presence of pegmatites in the Broken Hill succession suggests that a degree of partial melting may have occurred. Along the boundary of amphibolite facies transition to granulite facies in southern Namaqualand, Waters and Whales (1984) showed that such melting need not necessarily result in the complete loss of elements from the rocks, since all three of the components which participated in the melting process, viz. paleosome, restite and neosome, are present within a few centimetres of each other.

The existence of later retrogressive metamorphic fluids which may have also introduced or removed elements in the Broken Hill rocks, is inferred from sericite in borehole core, and low temperature, water-rich fluid inclusions from quartz grains in gneisses throughout the Namaqualand-Bushmanland area (Schoch, 1983, pers.comm.). Such water may have been locally derived since Lipson (1978) showed an example of probable rehydration of sillimanite by the water originally produced during the transformation of muscovite + quartz to K-feldspar + sillimanite. Leaching of surface outcrops, particularly in rocks

containing sulphides, is a further process which may have changed the original composition of the metasediments. In studying element redistributions, the Broken Hill schists (BS) are the rocks chosen because they contain quartz-feldspar assemblages which would have facilitated melting; their fissility offered possible avenues for movement of retrogressive fluids; and schists are among the most susceptible of the local rock-types to weathering.

6.1.2 Constraints on rigorous modelling of element mobility during metamorphism

The geographic distribution of samples collected during the current investigation is too restricted to attempt analyzing the same rock at progressively higher metamorphic grades along strike (e.g. Evans, 1964), which would give an empirical estimate of element mobility due to prograde metamorphism. The rigorous theoretical approach requires identification of each component in the general reaction

$$\text{original rock} = \text{melt} + \text{restite} + \text{vapour},$$

and the mineral assemblages present in each of the participating solid phases. The values of partition coefficients (D_i) for elements (i) are needed between the mineral phases in the original rock and the melt. Further, the bulk composition of the original rock is required since D_i varies for different rock-types (Shaw, 1977). The likely non-modal melting steps should be known because the minerals participating in the melting process will change as individual phases are exhausted (Hertogen and Gijbels, 1976). The generalized equation

for determining the behaviour of an element during the melting process (Shaw, 1977), would have the form

$$P_i^{s-1} = p^c D_i^{c-1} + p^b D_i^{b-1} + \dots = \sum p^c D_i^{c-1}$$

where

P_i^{s-1} = non-modal melting bulk distribution coefficient for element (i) between solid (s) and liquid (l)

p^c = proportion of mineral (c) which melts

D_i^{c-1} = distribution coefficient between mineral (c) and liquid (l)

Clements and Wall (1981) showed that the liquid produced from melting of biotite-bearing metapelites does not usually have a minimum melt composition. Shaw (1977) demonstrated that in the case of granodiorite the water content of the melt will determine whether biotite or K-feldspar melts first. These are important considerations because, for example, in rhyolitic rocks $D_{Rb}^{Kf-1} = 0.34$, while $D_{Rb}^{Bt-1} = 2.24$ (Arth, 1976), showing that Rb preferentially partitions into the first-formed liquid if K-feldspar remains in the restite and biotite melts first. Since D_i^{s-1} values do not exist for a number of the minerals, such as sillimanite and muscovite, in the BS metamorphic assemblages, and the composition of the vapour, if present, is not known, it would be impossible to rigorously assess the partitioning of any element during the melting process. The methods employed to assess element mobility during metamorphism are therefore not well constrained.

6.1.3 Non-rigorous modelling of element mobility during metamorphism

6.1.3.1 Major elements

During prograde metamorphism of BS, the quantity of major elements lost to the melt is loosely constrained by Nesbitt's (1980) work which showed that even when metapelites are metamorphosed to granulite

facies and produce 30% melt, K_2O and SiO_2 in the residue decrease by 29% and 6.7% respectively, while MgO content increases by 42%, TiO_2 by 37%, CaO by 33% and total Fe as Fe_2O_3 by 32% (percentage changes calculated by the present author from the data of Nesbitt, 1980). In the case of the upper amphibolite facies metamorphism present at Broken Hill (section 4.1), major element changes are permissible only at levels somewhat below these figures.

6.1.3.2 K/Rb ratios

The K/Rb ratios of metamorphic rocks during melting is primarily controlled by the K and Rb partition coefficients of K-feldspar and biotite, relative to the liquid (Barbey and Cuney, 1982). The high D_{Rb}^{B1-1} values in rhyolitic (2.24) and dacitic (3.26) rocks (Arth, 1976) suggests that only when large volumes of biotite participate in the melting process during the transformation from amphibolite to granulite facies, will significant amounts of Rb be lost from the residue. The abundance of biotite and the high Rb concentrations of BS relative to various average shale and metapelite analyses (Fig. 6.1) confirm that no significant *losses* of Rb occurred. In absolute terms, the K content of BS overlaps that of the shale averages, whereas the Rb concentrations extend to relatively higher levels than their shale counterparts. Consequently the relatively low BS K/Rb ratio of < 200 compared with values equal to or exceeding 200 for pelitic rocks (Fig. 6.1) shows that BS is relatively richer in Rb, with NS (lower K/Rb ratio) more so than SS (higher K/Rb ratio).

Introduction of Rb would be taken up by existing minerals according to the mineral-fluid partition coefficients (D_{Rb}^{c-f}), with biotite (and muscovite) being the likely recipients of most Rb. In NS, the constant K/Rb ratio over a wide range of Rb (Fig. 6.1) could therefore

reflect Rb addition. Rb enrichment of SS is unlikely because the more Rb-rich USS has a higher K/Rb ratio than LSS.

6.1.3.3 Pegmatite and host schist

6.1.3.3.1 Physical evidence

The mineralogy of pegmatites (particularly those of less than one metre in thickness) tends to mimic that of the host rock. Pegmatites in garnet-, tourmaline- or sulphide-bearing BS contain garnet, tourmaline or sulphide, respectively; and pegmatites in galena-bearing pelitic rocks frequently contain the Pb-bearing feldspar, amazonite.

Lipson (1978) showed evidence for in-situ pegmatite generation in the Aggeneysberge, where a fracture contained within schist (i.e. not extending outside of the schist) opens up into a zone filled by pegmatite. Fig. 4.12 provides a similar example of local pegmatite derivation. If the pegmatites have a local origin, as opposed to having had some extraneous, deeper source, then a constant proportion of pegmatite to host rock would be anticipated, provided that the host was homogeneous, including volatiles, and that there are no indications of nearby shear zones which could have introduced water into the system. Such lengths of borehole core schist, homogeneous except for sporadic pegmatites, were selected and the cumulative pegmatite length within any one sample was measured and expressed in Table 6.1 as a percentage of the total sample interval. This method provides an approximate volumetric proportion of pegmatite in schist. Measurements taken along the length of core from a single borehole display small absolute variation relative to each other. In particular, Zone 1 from borehole BH123, predominantly consisting of homogeneous SS (Table 6.1), displays a virtually constant pegmatite content of 14% for all seven intervals assessed. From the foregoing,

it appears that partial melting did not lead to significant removal of liquid from its source.

6.1.3.3.2 Geochemical evidence

Within each core sample of NS, SS and OS, the corresponding pegmatites were removed and bulked to provide matching pairs of schist and pegmatite. The indications that thin pegmatites are locally derived permits an exercise of adding back to the host schist, the component of contained pegmatite in the volumetric proportion measured, and then comparing the recalculated host composition with that of the host rock, and expressing this difference as a percentage, viz.

$$\%VARN = (\text{RECALC HOST} - \text{HOST}) * 100 / \text{HOST}$$

where

$$\text{RECALC HOST} = (1 - \%PEG/100) * \text{HOST} + \%PEG/100 * \text{PEG};$$

$\%PEG$ = the measured volumetric pegmatite content of the rock;

and

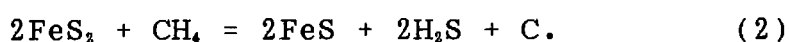
HOST and PEG are respectively the concentrations per element of the schist and pegmatite pair.

Negative values of "%VARN" indicate that the host rock (restite) has higher concentrations of the particular element, while positive values reflect host rock depletion at the expense of pegmatite. A summary of these variations in Table 6.2 shows three distinct categories i.e. elements partitioned into the pegmatites of both NS and SS (Na, Sr, Ca(?)); elements restricted to SS which show large values of "%VARN" (U and Y); and those elements in OS displaying large "%VARN" which may reflect the nearby presence of an orebody (K, Ba, Pb(?)). Only the behavior of Na, Sr and Ca will be examined here, while elements of importance to SS and OS are reviewed later in sections 9 and 10.

For all three pegmatite-SS pairs, the higher Na content of pegmatite is excessive, with "%VARN" values of between 28 and 184. Only one of these pairs has much higher Sr in the pegmatite (ALP 141; "%VARN" = 62), while higher Ca values in SS pegmatites is not consistent. Both K and Rb display small "%VARN" values, and in respect of Rb, this confirms that little biotite participated in the melting process.

6.1.3.4 Pyrite to pyrrhotite transitions

In the iron sulphide-bearing, carbonaceous SS, the pyrite-pyrrhotite transition may be used to assess the role of fluid movement through BS in general, during its metamorphic evolution. Ferry (1981) showed that few sulphide-rich schists which have been metamorphosed to sillimanite grades, still contain pyrite, due to the reactions



The passage of water through C-bearing rocks, or of methane, thus leads to the conversion of pyrite to pyrrhotite. Elevated temperatures up to sillimanite grades of metamorphism will be insufficient to convert all pyrite to pyrrhotite without large fluid/rock ratios. In fact the reaction proceeds to completion at chlorite grades of metamorphism if fluid/rock ratios are of the order of two to five (Ferry, 1981).

Pyrite is the dominant SS sulphide, although pyrrhotite has been positively identified in hand specimen, thus the inferred low fluid/rock ratio in SS limits the element mobility which could have resulted from fluid movement. Ferry (1981) postulated that the fluids driving the reactions are derived from an unknown source external to the black shales undergoing metamorphism. In the Broken Hill area there are no known C-bearing rocks either structurally above or below SS which were capable of generating a CH₄-rich fluid, thus only

equation (1) appears likely in which free carbon in the form of graphite, is readily available in SS. This reaction relies on the presence of an H₂O-rich fluid phase, which might have been derived from metamorphic dehydration of NS and quartzites (making use of the working stratigraphic column); to the low temperature water soaking phase recognised in fluid inclusions (Schoch, 1983, pers.comm.); or merely to local water generated during the transformation of muscovite + quartz to sillimanite + K-feldspar (section 6.1.1).

6.1.3.5 Oxygen isotopes

Although oxygen isotope analytical data from quartz grains will be fully presented in section 6.5, certain results are relevant to the present discussion. $\delta^{18}\text{O}$ values range from as low as 5.7‰ in NS, through ratios of the order of 9‰ in BQ to values of 14.1‰ in SS. As pointed out by Reid et al. (1987), the lack of isotopic homogenization across lithological boundaries, severely limits the quantity of pervasive metamorphic fluid which may have passed through the Broken Hill sequence.

6.1.4 Element mobility during weathering

The effects that surface weathering have on schist geochemistry are particularly important for establishing whether surface outcrop and borehole core sample data may be combined, or must be treated separately. In the two approaches adopted, firstly a specific orientation study was designed to test the effects on element mobility due to surface weathering, and secondly in a more general way, the mean element concentrations of surface outcrop samples are compared with those of their borehole core counterparts.

6.1.4.1 Comparison between specific selected samples (orientation study)

The geochemistry of distinctively banded hangingwall schist (ALP165) from a depth of 46m in borehole BH112 situated 300m east of the Broken Hill orebody, was compared with that of a similar rock-type situated near the surface position of the borehole (ALP163) (Fig. 6.2).

Calculations based on the hill slope and core foliation angles confirmed the approximate location of the correlative rock-type on surface. A second surface sample (ALP164), less banded than the first, was selected from 1m higher up the hill slope to test chemical variability over a short distance, and a second core sample (ALP166) was similarly selected from a depth of 61m in the borehole.

In Fig. 6.3 where ALP163 is used as the standard of comparison, schist geochemistry varies greatly even between two virtually contiguous surface outcrop samples, with major element chemistry differences of up to 65% for MgO, and up to 100% in the case of the trace element Cu. The two borehole core samples display slightly less element variation. Only where complete separation occurs between element values from surface outcrop and borehole core samples (Fig. 6.3) may definitive conclusions be drawn. The elements Fe_2O_3 , MnO, S and possibly C display slightly higher values on surface, but the opposite applies to K_2O , Rb, Pb, Zn, Nb and Zr. Cu displays too wide a variation to allow definitive conclusions. It is impossible to assert with 100% certainty that the core and surface sample element variations are merely a function of surface weathering, particularly since the concentrations of Zr, a relatively immobile element, differ between the two environments. These inherent variations are exemplified by the differences between the two surface samples and the two samples of borehole core.

6.1.4.2 Comparison between sample groups

When the ratios of surface outcrop samples to borehole core samples are taken for mean element concentrations of NS, USS and OS (Table 6.3), the lower values displayed by K_2O , Rb, Zn and Pb in surface samples are confirmed. Although NS and OS surface samples have relatively lower Nb and Zr values as seen in the orientation study, the two USS surface samples display slightly higher Nb and Zr concentrations than the average for USS borehole core. The relatively higher Fe_2O_3 and MnO contents of surface samples deduced from the specific orientation study cannot be substantiated by comparing their mean values in surface and core samples. The extremely low concentrations of S in surface samples (Table 6.3) disagrees with the evidence from the orientation study. The sulphuric acid created during weathering of the pyritic SS is the likely cause of the far lower concentrations of CaO, Na_2O , K_2O , S, Cu, Zn, Pb, V and Sr, and probable residual enrichment in Zr and Nb, in outcrop samples of SS.

6.1.5 Discussions and conclusions

Although a non-rigorous approach was adopted for determining the effects which metamorphism had on element distribution, constraints have nevertheless been established. NS and SS have lower K/Rb ratios than comparative pelites with similar K concentrations, with NS showing relatively higher values of Rb than SS. While Rb enrichment of NS appears likely, the same cannot be deduced for SS. Rb- and biotite- rich schists in which pegmatites occur suggest that biotite probably did not participate in the melting process. It may be speculated that the higher maximum Rb content of NS relative to SS was a result of either Rb-bearing fluids being blocked by an impervious layer e.g. the quartzites, or to the timing of Rb addition predating deposition of SS. Evidence of fluid damming should be preserved in the rock record as a zone of Rb enrichment along the base of the

impervious layer, yet no such zone has been identified, since the highest Rb content of 398 ppm occurs in schist spatially associated with the orebody. The alternative option is therefore favoured i.e. that NS predates SS, and was to some extent enriched in Rb prior to SS deposition.

The presence of pegmatites in discrete tension zones and the constant proportion of pegmatites in homogeneous schist suggest the local derivation of melts. Recalculation of original rock composition by adding back to schist the appropriate pegmatite component in the correct proportion, shows that Na in particular, and Sr to a lesser extent, were lost to the pegmatite. Ferry (1981) showed that Na is the only major element which suffers significant losses in Fe-sulphide- and C- rich metamorphic rocks (originally black shales) at the boundary between chlorite and sillimanite grades of metamorphism. In the case of SS, adding back the Na and Sr contents of pegmatites to the schist increases the host rock concentration from an average of 0.181% to 0.321% Na, and 33 ppm to 39 ppm Sr, representing increases of 77% and 18%, respectively. For NS the respective increases in Na and Sr are 19% and 12% . Care will therefore be exercised with these elements when comparing BS geochemistry with that of other pelitic rocks.

The lack of ubiquitous transition of pyrite to pyrrhotite in SS severely constrains the amount of pervasive fluid which passed through these rocks, and is corroborated by the lack of oxygen isotope homogenization between different schists. Intense retrogression associated with the F_2 refoliation zone around the eastern end of the Broken Hill orebody (section 4.2.3) suggests that the passage of non-pervasive, low-temperature fluid was restricted to tectonically prepared zones.

The study on the effects of weathering shows that significant changes probably occur in the element concentrations of outcropping schists. Separate treatment of surface outcrop and core samples is therefore necessary.

6.2 Namies Schist and Shaft Schist

Throughout this section the compositional characteristics of NS and SS are compared with each other, while comparisons with published pelite data are made in section 9. The discussion is restricted to borehole core unless surface samples are specifically mentioned. The effects of weathering on element mobility show that the two data sets must where possible be treated separately (section 6.1.4).

6.2.1 Direct geochemical contrast between NS and SS

Mineralogical differences between NS and SS (section 4.2) are reflected in certain key elements. Whereas the carbon (C) content of the more siliceous NS never exceeds 500ppm, SS consistently comprises $> 1\ 000$ ppm C (excluding one sample), and has a higher LOI (Table 6.4). Ratios of average SS/NS on a per element basis reveal major dissimilarities where this ratio has values much greater than or less than 1 (Table 6.5). SS has more S ($> 1\ 000$ ppm) but less MnO ($< 1\ 000$ ppm) and P_2O_5 (< 800 ppm) than NS. The Ba content of SS is less than half that of NS, while V and Ni contents of SS are double those of average NS (Table 6.5). Chi-squared and t-Tests performed on the data show that most elements follow a log-normal distribution, and most element means in NS and SS may be considered different at the 95% confidence limits of the one tailed Chi-squared and Student's t distributions (Table 6.6).

An obvious difference between NS and SS geochemistry is the far higher degree of inter-element correlation in SS (compare Tables 6.7 and 6.8). For example, the elements Cu, Zn, Ba, Fe₂O₃, K₂O, Rb, Al₂O₃, TiO₂, Sc, Ni, MgO, V, Co and Cr correlate strongly with each other, whereas for NS, only the elements K₂O, Rb, Al₂O₃, TiO₂, Nb, Sc, Ni, MgO and V do so. In both NS and SS, SiO₂ and Zr are strongly correlated, with SS defining the lower SiO₂ and Zr end of the spectrum (Fig. 6.4), but these elements correlate negatively with most other elements.

6.2.2 Element variability

When compared with SS, NS displays a more variable geochemical composition shown by the relatively large coefficients of variation for each element (Table 6.4). The contrast is accentuated when USS and LSS are treated separately (Table 6.9). The greater element variability in many elements of NS compared to SS is illustrated in Fig. 6.5a-h. The highest Zn (391ppm) and Ni (45ppm) values in SS, both from ALP183 (Fig. 6.5c and e), can be attributed to the corrosive weathering of pyritic SS causing contamination from the galvanized iron core holding tray left exposed to wind and rain for an unusually long period of time. Of the remaining SS samples, only ALP054, lying structurally above CSMQ, displays distinctively higher concentrations in any elements (i.e. MnO, Pb, and Co; Fig. 6.5f-h). Special significance is attached to the chemistry of ALP054, which is discussed in sections 6.2.7.3 and 9.1.5.

6.2.3 R-mode factor analysis

R-mode factor analysis is used as a convenient way of highlighting interrelationships between variables (such as geochemical elements), whereas Q-mode factor analysis addresses the correlatedness between samples. Due to problems of closure and to certain philosophical objections to the application of the varimax rotation to geochemical

data (Appendix B.2), element relatedness as shown by factor analysis will be continually assessed in terms of geological feasibility.

Both NS and SS factor analysis reveal the dichotomy between the detritally-related elements, SiO_2 and Zr, versus a suite of elements related to Al_2O_3 and K_2O . This emerges from the high negative loadings on SiO_2 and Zr and positive loadings on Al_2O_3 and K_2O in Factor 1 of both rock types (Figs. 6.6a and 6.7a), as noted previously from the correlation matrices. The high communalities for these elements (Table 6.10) indicate reliable results. The first factor accounts for approximately 40% of the total group variances (Table 6.10), and the antipodal geometric representation of silica versus alumina suggest a closure-related interdependence (Figs. 6.6 and 6.7). The separation of the rare earth elements (REE) into Factor 2 of both schists reflects the similar chemical behaviour of the REE's as a result of the addition of electrons to the inner 4f orbitals rather than the outer shells (Herrman, 1970). Factor 2 is therefore omitted from Figs. 6.6b and 6.7b in preference to Factor 4. Y serves as an indication of heavy rare earth elements (HREE) (Herrmann, 1970). In SS there exists a strong relationship between the light rare earth elements (LREE) and Y, whereas in NS, Y shows only a subdued connection with the LREE's (Figs. 6.6 and 6.7; Tables 6.7 and 6.8). In NS, Y is grouped with Pb, Zn and Ba in Factor 4, and with MnO in Factor 6. Factor 3 may be considered an alkali and alkali earth element group, except that in SS K_2O and Rb do not contribute to Factor 3. This separation of K_2O and Rb from CaO, Na_2O and Sr in SS is inherent in the correlation matrix (Table 6.8).

The major difference between NS and SS, as emphasized by factor analysis, is the NS Factors 4 and 5 which comprise the ore elements Ba, Pb, Zn, S and Cu (Fig. 6.6). In SS all these elements, excluding

Pb, have high loadings in Factor 1, related to Al_2O_3 and K_2O , and display positive correlation at the 99% confidence level (Table 6.8). SS Pb has an enigmatic association with MnO , P_2O_5 and possibly Y (Fig. 6.7). The major features and differences between NS and SS factor analysis calculations are conceptually depicted in Figs. 6.6c and 6.7c. The low communalities shown by Th in both schists and Cu in SS, indicates that care should generally be taken in interpreting Th and Cu behaviour. The unpredictable nature of Cu is a problem common to pelites (e.g. Senior and Leake, 1978).

6.2.4 Discriminant function analysis (DFA)

Reliable classification of schist and quartzite successions within the Bushmanland Group is essential to successful structural-stratigraphic mapping, and forms a prerequisite to exploration geology. In the Broken Hill area, NS and SS comprise the two most voluminous stratigraphic members, yet hand specimen distinction between these rock-types sometimes proves difficult. Discriminating petrographic features above (section 4.2) are now augmented by the more rigorous lithogeochemical characterization technique of DFA (Appendix B.3). A suite of six "immobile" elements (Al_2O_3 , Zr, Nb, TiO_2 , Th and Sc) are used for discrimination purposes (Appendix B.3). Discrimination between NS and SS on the basis of REE's is discussed below (section 6.2.5).

The BMDP DFA output for borehole core samples of NS and SS in the Broken Hill area provides moderate separation between the two populations, with one SS sample (ALP141) and two NS samples (ALP028 and ALP029) being misclassified. The elements Nb and Sc provide 91.7% correct classification (U-statistic = 0.3244; see Appendix B.3) when combined in the linear functions:

NS $539.5 \cdot \text{Nb} - 139.5 \cdot \text{Sc} - 250.2$

SS $478.1 \cdot \text{Nb} - 102.3 \cdot \text{Sc} - 219.1$.

These functions may be used by inserting for any unknown sample, the two variables and classifying the sample as NS or SS depending upon which linear function gives the greater score. The relatively poor "immobile" element DFA distinction between NS and SS indicates that additional criteria, such as petrography (section 4.2) and possibly rare earth elements (examined below in section 6.2.5) must be used in conjunction with DFA.

6.2.5 Rare earth elements (REE)

Both XRF and INAA techniques have been used to determine REE concentrations in the schists and other rocks, and although absolute concentrations for the two techniques are at different levels, the shapes of the REE patterns should retain their integrity irrespective of the technique used (Appendix A.2.5). Only three NS and four SS samples have been analysed by the INAA technique (Fig. 6.8) while a selection of NS and SS XRF-derived REE analyses are presented in Fig. 6.9. The Y concentration provides an estimate of the Ho content of the rock (Appendix A.2.5). It is common practice to plot on a per element basis, normalized instead of absolute REE data, and the standard used most frequently in this thesis is Piper's (1974) average shale, instead of chondrite. Key features of the shale-normalized REE patterns depicted in Fig. 6.8 and 6.9 are:

- (a) their relatively elevated light REE (LREE) nature;
- (b) the distinctive positive Ce and negative Nd anomalies of LSS, relative to most USS and NS samples;
- (c) the relative Nd peak in NS; and
- (d) the higher concentration of REE in NS than in SS (Fig. 6.10).

6.2.6 Contrasted behaviour of base metals in NS and SS

In contrast to SS, NS displays variable Ba, Zn and Cu concentrations (section 6.2.1). Also, NS contains more Ba, Pb, Zn and Cu than SS (Table 6.5). Lastly, NS has Ba, Pb, Zn, Cu and S separated from Factor 1, and Y separated from the LREE's (section 6.2.3), unlike the behaviour of these elements in the factor analysis of SS.

6.2.7 Minor lithologies and special samples

6.2.7.1 Calc Silicate Rock plus Manganese Quartzite (CSMQ)

Three Calc Silicate Rock (CS) and four Manganese Quartzite (MnQ) samples were analysed from this distinctive horizon within USS in the Broken Hill - Maanhaarkop area. Of these, one MnQ and two CS samples represent fresh borehole core. Due to the inherent heterogeneity of these rocks, the surface and borehole core samples were combined for averaging purposes (Table 6.11). Relative to the enclosing USS, CS shows significantly higher concentrations in the elements CaO, MnO, P₂O₅, Pb and Zn, and in the Ca/Sr ratio (i.e. 485 vs 28), and to a lesser extent in MgO, Ba and Sr. The CS elements showing slightly lower concentrations than USS include K₂O, Rb and V (Table 6.12). MnQ also shows far higher concentrations in MnO, P₂O₅, Pb and Zn, as well as in Cu, with less marked concentrations of CaO, when compared with USS. Relative to USS, MnQ has far lower concentrations in most other elements (Table 6.13). Though the base metal content of CS and MnQ are much higher than those of USS, their S concentrations are of similar magnitude. A notable feature of MnQ is the sporadically high concentration of U, As and Sb (29, 279 and 9ppm respectively) in ALP213 as determined by INAA. Although Ag-bearing (28ppm), ALP213 carries no Au (< 50ppb).

The three shale-normalized CS REE patterns are fairly variable, but in contrast to SS they display a negative Ce anomaly most distinctly

developed in sample ALP055 (Fig. 6.11a). The shale-normalized REE patterns for MnQ show no consistent trends between samples. Of the four MnQ samples analysed, two display positive slopes towards the estimated Ho position, while ALP213, a strongly weathered surface sample with boxworks after pyrite, shows very low concentrations in estimated Ho (Y <LLD) (Fig. 6.11b). Depletion in HREE is a feature common to rocks undergoing extreme surface weathering (Nesbitt, 1979), as would result from the generation of sulphuric acid from pyrite. Only one CSMQ sample, the same ALP213, was analysed for REE by the INAA method, and the negative slope towards the heavy REE (HREE) side of the diagram is still apparent, with Lu <LLD (Fig. 6.12).

6.2.7.2 Biotite Graphite Zone (BGZ)

Mean BGZ chemical composition is so similar to that of USS (Table 6.14) that only three elements, viz. MnO, Pb and Zn show more than twice the USS concentration, while CaO, P₂O₅, C and Cu have slightly lower contents (Table 6.15a). Only Na₂O, Sr and S show significantly lower concentrations, as highlighted by comparing the Ca/Sr, C/S and K/Na ratios in the two rock types (Table 6.15b). The Zr-SiO₂ relationship of BGZ accords well with USS (Fig. 6.13).

The BGZ REE patterns have similar shapes to those of USS, although showing a greater range in total REE (compare Figs. 6.14a with 6.9b and 6.8c, and Fig. 6.14b with 6.8b). The INAA data suggests that BGZ has the well developed positive Ce anomaly of LSS.

6.2.7.3 Geochemistry of ALP054

In borehole BH123, ALP054 is the schist sample lying between BGZ structurally above and CSMQ below. Classification of this sample as SS follows from its physical appearance, position in the sequence, and C concentration in excess of 0.1% (C = 0.12%). Attention has been

drawn in sections 6.2.1 and 6.2.2 to the unusual geochemistry of this sample. Relative to SS, ALP054 displays higher values of Mn, Pb, Co (Fig. 6.5f-h) and Fe, and lower concentrations of C, V, Mo and S. The high Co value of 41ppm is nearly double the figure in both SS and in schists lying immediately adjacent to the Broken Hill orebody.

6.2.7.4 Tank Hill samples

The hypothesis that the gossanous schist on the northern flank of Tank Hill may correlate with NS (section 5.1) is examined in the light of available geochemical data. The excessively high Ba, Pb, Zn and S content of Tank Hill Schist (THS) (Table 6.16) reflects the gossan producing mineralization, and cannot be used for discriminating purposes. THS and Green Quartzite (GrQ) are tested against NS and SS, these being the two thickest schist horizons at Broken Hill.

The discriminant function derived for differentiating between borehole core samples of NS and SS (section 6.2.4) was used on THS, and returns a higher score for NS than for SS (6429 vs 5998), also indicating classification as NS. The REE patterns of both THS and GrQ have the general shape of the NS surface samples, and lack the slightly positive Ce anomaly of surface SS samples (Fig. 6.15). The steep fall of THS to the estimated Ho composition is probably caused by HREE leaching in this sulphide-rich rock as explained for ALP213 (section 6.2.7.1). Compared with NS and SS surface samples, THS has MgO, Ni and Th abundances more similar to NS than to SS (Table 6.16). It is only the high TiO₂ content of THS that suggests an SS classification, but correlation with NS cannot be excluded since the average TiO₂ content of surface NS is almost half that of cored NS, and TiO₂ should be one of the least mobile elements in the weathering environment (Fig. 6.3).

Despite the large SiO₂ content of GrQ (97%, Table 6.16), the rock contains excessive amounts of Ba, Pb and Cr (561ppm, 57ppm and 64ppm, respectively). The high Cr content suggests fuchsite as the green mica responsible for the rock's colour, while Pb and Ba reflect the mineralizing event seen in the adjacent schist. As with THS, the REE pattern of GrQ accords more closely with NS than with SS (Fig. 6.15), though at low concentrations.

6.3 Ore Equivalent Horizon and Orebody

The Ore Equivalent Horizon (OEH) comprises the variety of schists and quartzites, Hangingwall Schist (HS), Intermediate Schist (IS), Upper Footwall Schist (UFS), Ore Schist plus Garnet Quartzite (OS+GQ), Ore Equivalent Garnet Quartzite (OEGQ), Garnet Quartzite (GQ) and the two separate data sets of surface and borehole core Ore Equivalent Schist (OES). The limited orebody samples taken include Upper Orebody Quartz Magnetite Rock (QM), Lower Orebody Garnet Quartzite (LGQ), Lower Orebody Amphibole Magnetite Rock (AM) and Massive Sulphide (MS).

6.3.1 Schists

Most of the statistical work performed on Ore Schists (OS) applies to the 31 sample borehole core data set comprising HS + IS + UFS + OES. XRF-derived La, Ce and Nd analyses were only performed on 19 of these samples. As done previously, the geochemistry of OS will be examined in comparison with NS and SS, whereafter comparisons will be made with various published mineralized sequences.

6.3.1.1 Geochemical characteristics

Most of the OS elements follow a log-normal distribution as revealed by Chi-squared tests (Table 6.17). Of the key elements C and S, both have concentrations more closely allied to the low levels of NS than to SS. OS has less SiO₂ and more Al₂O₃ than NS, but with

concentrations similar to those of SS, as shown by t-Tests (Table 6.17). Use of the t-Test on the other elements fails to show consistently whether OS correlates with NS or with SS. Whereas the REE's of OS have similar concentrations to those of NS and not SS, the Zr, Cr, V, Sc and Ni contents are similar to those of SS (Table 6.17). The coefficients of variation for each element tend to lie between those of NS and SS, although variations in the elements Pb, Cu and S greatly exceed those of NS (compare Table 6.18 with 6.4). It is only the correlation matrices which suggest a closer affinity of OS with NS than with SS, since SS shows far greater inter-element correlation than either NS or OS (compare Table 6.19 with 6.7 and 6.8). In particular, those elements directly or indirectly related to the ore-forming event, such as Y, P, Cu, Pb, Zn, S, Ba, Fe and Mn show poor correlation with elements outside of that group, contrasting markedly with SS. In the correlation matrix (Table 6.19), only Cr suggests an affinity of OS for SS since OS Cr is strongly correlated with a series of elements such as Al and K whereas NS Cr is not. A noteworthy feature of OS is the sporadically developed high concentrations of Mo (see footnote to Table 6.18).

6.3.1.2 R-mode factor analysis

Two sets of factor analysis were performed on OS borehole core, viz. all 31 samples but excluding La, Ce and Nd, and the 19 samples which contain the light REE's (Figs. 6.16a and b). The first analysis is used for most evaluations, while the second aids the examination of the relationship between the light REE's and other elements. The high communalities for each element (Table 6.20) indicate reliable results. Because La, Ce and Nd tend to form a grouping on their own (Fig. 6.16) they are omitted from Figs. 6.16c and d in the interests of clarity. A separate factor analysis computation was performed on OS surface

data excluding REE's, with the object of using scores for plotting ore-related factor(s) (section 6.3.1.6 and Appendix F).

As with NS and SS (section 6.2.3), Factor 1 of OS shows the strong separation of SiO_2 and Zr from a suite of elements including Al_2O_3 and K_2O . The lower loadings on Factor 1 (when compared with NS or SS) suggests the presence of additional influences. With reference to Figs. 6.16a and b it appears that Factors 2 and 3 largely comprise the ore related elements Cu, S, Fe_2O_3 , Pb, Zn, Ba, MnO and Y. In Fig. 6.16b, CaO also falls into Factor 3, and the relatively close association of CaO and P_2O_5 with Pb, Y and MnO in Fig. 6.16c suggests that they too may be incorporated with the ore-related elements, even though only CaO correlates with Pb, Cu and Y in Table 6.19. The factor analysis grouping of CaO and P_2O_5 may reflect the presence of apatite.

In common with NS (section 6.2.3) the HREE indicator element Y is completely divorced from the LREE's, and falls within the ore-related Factors. Factor 4 represents the Na_2O , CaO and Sr grouping which is separated from K_2O . The poor individual loadings, particularly on Factors 5, 6 and 7, and the lack of simple geological explanation for these element groupings, precludes further interpretation of the OS factor analysis. As summarized in Fig. 6.16d, factor analysis of OS highlights the separate grouping of ore related elements (including Y), much as seen in NS, and in contrast to SS.

6.3.1.3 Discriminant function analysis (DFA)

Though the mineralogical characteristics of OS, NS and SS have been discussed (section 4.2.3), DFA is now applied to the geochemistry of these three rock-types to aid distinction between them. In addition, the success with which OS is discriminated from NS and from SS may

indicate with which rock type OS more closely correlates. Ultimately, the combined use of petrography, DFA and REE patterns should be made in order to effect classification.

For the computation of DFA, the same six "immobile" elements used in the earlier DFA (section 6.2.4) are applied. In all, four separate analyses were performed, viz. NS vs OS, SS vs OS, NS + SS vs OS and NS vs SS vs OS. The discrimination between SS and OS is far better than between NS and OS, as revealed by the lower U-statistic in the former (0.2738 vs 0.5257). The SS vs OS DFA provides 94.6% correct classification with two SS samples (ALP056 and ALP057) and one OS sample (ALP119) being misclassified. In contrast, the NS vs OS DFA results in only an 83.3% correct classification with five NS (ALP028, ALP029, ALP061, ALP062 and ALP063) and two OS samples (ALP103 and ALP127) being misclassified. For SS, the three elements Al_2O_3 , Zr and Nb help define the classification function, whereas for NS only Zr and Nb are incorporated as shown below:

OS $5234.1 Al_2O_3 + 3078.9 Zr - 2734.0 Nb - 15720.2$

SS $5306.3 Al_2O_3 + 3121.0 Zr - 2811.6 Nb - 16106.2$

and

OS $321.2 Zr + 346.8 Nb - 615.8$

NS $335.3 Zr + 331.2 Nb - 631.9$.

The distinction between NS + SS vs OS at 85.1% correct classification is also poor (U-statistic = 0.5119), whereas the discrimination between all three rock-types provides a 92.5% separation (U-statistic = 0.1723). Only Nb goes into the classification function of the former, viz.:

OS $301.8 Nb - 197.6$

NS + SS $272.4 Nb - 161.2$,

whereas four elements contribute to separating all three rock-types:

OS -3758.7 TiO₂ + 7639.4 Al₂O₃ + 3353.3 Zr - 1409.8 Nb - 15881.4
SS -3794.9 TiO₂ + 7742.6 Al₂O₃ + 3395.6 Zr - 1476.6 Nb - 16303.8
NS -3841.1 TiO₂ + 7723.9 Al₂O₃ + 3394.6 Zr - 1417.3 Nb - 16097.7 .

Classifications are effected as described in section 6.2.3.

The low percentage correct classification evident in DFA computations including OS and NS is a reflection of close chemical similarity between these two rock-types. In contrast, the much better separation between OS and SS shows that OS is chemically distinct from SS.

6.3.1.4 Rare earth elements

The OS samples display REE patterns intermediate between NS and SS, with less strongly defined positive Ce anomalies than SS (compare Fig. 6.17 with Fig. 6.8b). In addition, a number of OS surface and core samples from both BH and MK display a marked positive HREE anomaly (Fig. 6.17).

6.3.1.5 OS correlations

The weight of evidence suggests a closer affinity of OS with NS than with SS. The sporadically high concentrations and groupings of the ore-related elements (and Y) in both rock-types contrasts strongly with SS where most ore-related elements correlate with K₂O and Al₂O₃, and Y with REE. The total REE concentrations of OS are more similar to NS than to SS, though the shapes of the OS REE patterns appear intermediate between NS and SS. It is noteworthy, however, that certain elements which distinguish SS from NS, viz. Cr, Ni and V, have concentrations in OS similar to those in SS, possibly suggesting that OS represents a transition from NS chemistry, with which it is more closely allied, to that of SS.

6.3.1.6 OS geochemical variations at Broken Hill

Key element and inter-element ratios of OS are examined to determine their three-dimensional spatial abundances with respect to the Broken Hill orebody. These include the elements exploited at Broken Hill, such as Pb, Zn and Cu, as well as associated elements found at relatively high concentrations, such as Ba, Mn and Fe. Si has also been included in the investigation because of the siliceous nature of some parts of OS. Both manganese and iron are sensitive to redox changes, hence the Mn/Mn+Fe ratio has been selected to enhance the signature of metasediments which may have formed under oxidizing conditions (high ratio). In all binary diagrams the logarithmic distance from the orebody is plotted along the X-axis in order to better define element concentrations near the orebody, while the element or ratio appears along a linear or logarithmic Y-axis. Surface outcrop and borehole core samples are treated separately. Core samples of OS only come from the east side of the orebody, whereas samples of outcropping OS comprise rocks from both west and east of the orebody (Fig. A.2a). To the east, samples were taken as far afield as Froneman se Kop (nearly 10km away from the orebody), while the presence of Tank Hill mineralization and the Black Mountain orebody west of Broken Hill necessitated that sampling not extend west beyond the Broken Hill inselberg, a distance of some 200m. Geochemical trends deduced for surface samples initially apply to data sets both west and east of the orebody combined, whereafter results from the two localities are contrasted.

In borehole core samples, the elements Zn, Mn, Ba (Figs. 6.18a-c) and to a lesser extent Cu and the Mn/Mn+Fe ratio, show wide zones of scatter about broadly defined increases in concentration towards the orebody. Outcrop samples similarly display broadly increasing concentrations of Zn, Ba and Pb towards the orebody (Figs. 6.19a-c),

but no meaningful trend is evident for Cu. The complicated Mn and Mn/Mn+Fe trends (Figs. 6.19d and e) are discussed later (section 10.7). When the "ore factor" scores from R-mode factor analysis of OS are plotted against distance from the orebody, broadly defined increasing trends towards the orebody are evident (Appendix F).

In contrasting elements and inter-element ratios of OS surface samples from west of the orebody with those located east of the deposit, different absolute values and trends are evident (Fig. 6.19a-e). The general pattern is that OS within 200m of the orebody contains higher base metal and silica concentrations to the west of the orebody than to the east. Mn and the Mn/Mn+Fe ratio attain similar concentrations on both sides of the orebody, but whereas the maximum values are obtained at approximately 60m distance from the western extremity of the orebody, the maximum to the east of the deposit is reached at a distance of 300m.

6.3.2 Ore Schist plus Garnet Quartzite (OS+GQ), Ore Equivalent Garnet Quartzite (OEGQ), Garnet Quartzite (GQ) and Orebody

The small number of samples within these individual rock types precludes a rigorous statistical assessment of their geochemistry. Only the salient features will therefore be highlighted.

6.3.2.1 Geochemical characteristics

Chemically, the orebody iron formations Quartz Magnetite (QM) and Amphibole Magnetite (AM) consist mainly of SiO₂ and Fe₂O₃, and in the case of AM, the elevated Al₂O₃ (5.4%) and MnO (7.8%) contents (Table 6.21) reflect the presence of manganiferous grunerite/cummingtonite and spessartitic garnet (Ryan et al., 1982). The iron formations also contain detectable Mo (up to 9ppm). Being part of the orebody, the elements Pb, Zn, Cu, S and in the case of AM, Ba as well, are

elevated. QM is Ba deficient (60ppm) relative to all other ore-related rocks, as discussed later in section 10.7.2.

A comparison between the ore-associated QM at Broken Hill and QM at Froneman se Kop, which although lying at the same stratigraphic level, bears no spatial relationship to ore, reveals that although both have similar SiO₂ and Fe₂O₃ concentrations, the latter has distinctly higher TiO₂, Al₂O₃ and Na₂O, and lower MgO concentrations than the former (Table 6.21). Of the base metals and related elements, the Froneman se Kop QM contains little Pb, Zn, Cu or S, but has more than double the Ba content of Broken Hill QM. The Froneman se Kop Sr concentration of 266ppm is excessive compared with its low CaO content of only 0.225%. These differences will be interpreted in section 10.7.2.

The siliceous (87% SiO₂) Lower Orebody GQ (Table 6.21) has Fe₂O₃ and Al₂O₃ as additional important major elements, and high levels of MnO (0.35%). The base metal and related elements Pb, Zn, Cu, S and Ba all occur at elevated concentrations despite their high silica content.

OS+GQ represents a rock type gradational between OS and GQ, as evidenced by its intermediate concentrations of all major elements (Table 6.18). Although OEGQ is expected to be rich in SiO₂ (by definition), the major elements Fe₂O₃, MnO, CaO and P₂O₅ are also at levels higher than in OS. In contrast, NS and SS display strong antipathetic relationships between SiO₂ on the one hand, and Fe₂O₃ and P₂O₅ on the other (Tables 6.7 and 6.8). For MnO and CaO, NS also shows a strongly negative correlation with SiO₂.

As expected, most trace elements decrease from OS through OS+GQ to OEGQ. Ore-related elements are among the notable exceptions. The Ba

and Zn contents attain maximum concentrations in OS+GQ, with average values of 813ppm and 591ppm respectively, while Pb, Cu, S and Y reach their maxima in OEGQ with average values of 203, 121, 1622 and 73ppm, respectively. Following CaO, Sr is also most concentrated in OEGQ (18ppm), yet the increase in average Zr from OS to OEGQ (267ppm to 355ppm) is an unexpected (and unexplained) result. Mo attains sporadically high values in OS+GQ and OEGQ, with a maximum concentration of 64ppm coming from one Maanhaarkop sample of OEGQ.

The relatively elevated levels of CaO (or depressed Sr concentrations) associated with the orebody, as noted above, is depicted in a plot of the Ca/Sr ratio from rocks bearing various geographical and possible genetic relationships to the orebody. Fig. 6.20 shows that while SS has the lowest ratio of all rocks, AM, OEGQ, OS+GQ and Broken Hill QM have the highest. In contrast, the K/Rb ratio remains relatively constant, with only Froneman se Kop QM having an unusually high ratio.

6.3.2.2 Rare earth elements

Of the suite of rocks comprising the orebody, orebody GQ, OEGQ and OS+GQ, INAA analyses are only available for the orebody. REE data for the additional rock-types will be taken from XRF analyses.

A strongly positive Eu anomaly characterizes the massive sulphide (MS) samples (Fig. 6.21a), in contrast to all other REE patterns seen from the Aggeneys area. MS also displays a negative Nd anomaly, particularly in the most sulphide rich sample (ALP110). Although the QM sample shows a slightly positive HREE anomaly, MS samples do not. The absolute concentrations of REE's in the orebody samples are somewhat less than in average shale. A comparison between the ore-enclosing magnetite-rich rocks and QM from Froneman se Kop show not only the higher total REE concentrations in the latter, but also that

the REE pattern peaks at Nd and not at the HREE's (Fig. 6.21b). The Nd peak is a characteristic established previously for NS.

No consistent shapes can be established for the REE patterns from orebody GQ samples. While ALP077 shows relatively high La concentrations, ALP149 has a slightly positive HREE signature (Fig. 6.21c). Both show small negative Ce anomalies. In contrast the OEGQ samples from both surface and core show a consistent and strongly developed positive slope towards the HREE's (Fig. 6.21d). The 1:1 correspondence between the REE compositions of ALP172G at Broken Hill and ALP130 at Maanhaarkop underscores the correlation between OEGQ from the two areas. OS+GQ samples show REE patterns with shapes which mainly peak at Nd, similarly to OS and NS, and the occasional sample which displays a relatively high estimated Ho composition (Fig. 6.21e).

6.3.2.3 Garnet Quartzite (GQ), Ore Equivalent Garnet Quartzite (OEGQ) and Ore Schist plus Garnet Quartzite (OS+GQ) geochemical variations at Broken Hill

The rocks included in this section are GQ which sheaths the LOB, OEGQ at tens to thousands of metres from the orebody, as well as the mixed rock OS+GQ located at variable distances from the deposit. For the sake of graphical simplicity these rocks are divided into the two categories GQ and OS+GQ. In so small and heterogeneous a data set, ratios are of more significance than individual element variations, nevertheless it is worth noting the general increase in Zn and Pb concentrations towards the orebody (Fig. 6.22a and b).

The similar ionic radii of K^+ and Pb^{2+} results in the substitution of the former by the latter in K-feldspar and in potassic mica (Sahl et al., 1974). Plotting of the calculated $Pb/Pb+K$ ratio is therefore

employed to trace possible precipitates from Pb-rich hydrothermal fluids. Zn resides primarily in biotite in sulphide- and oxide- poor metapelites (Brehler and Wedepohl, 1972). In order to determine anomalously high concentrations of Zn beyond those caused by an increase in Al-bearing minerals such as biotite, Zn is normalized to Al in the ratio $Zn/Zn+Al$. Plotting of the ratios $Pb/Pb+K$ and $Zn/Zn+Al$ reveals well defined increases towards the orebody, especially when the two rock categories are viewed independently (Figs. 6.22c and d).

6.3.3 Comparison with mineralized sequences

With reference to Fig. 6.23, Bostrom (1973) showed that oceanic sediments lie on a mixing line between the two end members of Fe-Mn-rich active ridge sediments (A), and terrigenous average continental crust (C). Both Bostrom (1973) and Marchig et al. (1982) used the Fe/Ti vs $Al/(Al+Fe+Mn)$ plot to demonstrate that as the hydrothermal metalliferous component increases, so the rock falls progressively nearer the Al and Ti deficient, Fe and Mn enriched, left hand part of the graph. The hydrothermal sediments of Marchig et al. (1982) correspond well with "Ore" samples from Broken Hill (comprising QM, AM, Lower Orebody GQ, and the OS+GQ extensions of LOB and UOB), and lie on a continuum through OS and NS into SS. OS and NS clearly show the closest resemblance to the ore samples, while SS lies even further removed from an ore signature than average continental crust (C).

The REE's of Broken Hill ore-related rocks are compared with four Recent ore sediments taken from the literature (Fig. 6.24). The two Broken Hill massive sulphide samples have total REE concentrations in excess of basalt-related Galapagos and Atlantis II hydrothermal sediments, but of a similar order of magnitude to that of the Santorini calc-alkaline (Smith and Cronen, 1983) caldera-related hydrothermal ores (Fig. 6.24a). Whereas the metalliferous sediments

from the literature all display positive HREE anomalies, the Broken Hill ores maintain a relatively flat profile. The strongly developed positive La and Eu anomalies of the basalt-related hydrothermal ores are present in weaker form in the Broken Hill ores. Only the Santorini sample displays a negative Eu anomaly (Fig. 6.24a). Broken Hill schists show higher REE concentrations than the basalt-related ores, and selected OS samples (e.g. ALP225) do display a positive HREE anomaly (Fig. 6.24b).

6.4 Broken Hill Quartzites (BQ)

Differing quartzite sampling techniques have generated two geochemically distinct data sets since core samples comprise a composite of the entire quartzite intersection including slightly more micaceous parts, while surface samples consist of a limited composite of the exposure biased towards the more siliceous parts of the horizon which form prominent outcrops. This, and minor surface leaching, result in the more representative core samples having higher values in virtually all elements other than SiO_2 (Table 6.22), thus core samples are used for comparative purposes. Of the MDS samples, only one surface and three borehole core analyses are available, and other than a lower Zn concentration in the surface sample (Table A.3), there are no obvious weathering effects. An average of all four MDS samples is therefore used.

6.4.1 Geochemical characteristics

The most notable geochemical features of BQ is its highly siliceous character (96.2% SiO_2); the high Zr content of 129ppm, considering the silica purity of these rocks; and the lack of detectable carbon (Table 6.22). Many elements are present at levels below XRF detection limits (Th, U, Mo, Ni, Sc, Co, S, C and Sr), and for the purposes of statistical treatment, samples with major element concentrations below

detection limits are given a value of 0.001%, and 1ppm for trace elements below detection limits. Of interest are the elevated concentrations at Maanhaarkop of Zn in ALP124 (WQ), and Cu and S in ALP126 (DQ), together with the presence of chalcopyrite in adjacent MDS (ALP125). BQ cannot be correlated with MnQ since in comparison the latter has relatively high concentrations of many elements (particularly MnO, CaO, P₂O₅, Sr, V, S and the base metals), but low abundances of Zr and K₂O (Table 6.11).

The BQ correlation matrix reveals only a few well defined correlations (Table 6.23). SiO₂ displays the expected antipathetic relationship with Al₂O₃, while Zn, MnO and Fe₂O₃ are positively correlated with each other. The ore-related elements Cu, Pb, Zn, Ba and Fe₂O₃ fail to form a definable group of positively correlated elements, but their concentrations do generally increase with increasing Al₂O₃ (e.g. Fig. 6.25).

Compared with WQ, the slightly higher content of minerals other than quartz in DQ (section 4.3), is also evident in the marginally increased concentrations of Al₂O₃, Fe₂O₃, Zr and particularly in REE (Table 6.22). The mineralogy and geochemistry of MDS and NS are similar. Both schists have high Fe₂O₃ contents considering their elevated SiO₂ composition. The feature of high MnO coupled with low MgO, which aids in distinguishing NS from SS, is repeated in MDS. As with NS, MDS displays sporadically high Zr concentrations (419ppm in ALP041; Table A.3), and elevated Zn averaging 209ppm (vs 194ppm Zn in NS). Only the Ba content of MDS (313ppm) differs markedly from that of NS (1253ppm), while average Cu concentrations of MDS (90ppm) exceed those of NS (37ppm).

6.4.2 R-mode factor analysis

The R-mode factor analysis is based on 8 samples (for the data set excluding REE), and five samples for the set which includes REE, thus Fig. 6.26b is used only when assessing elements in relation to REE. Notwithstanding the high communalities (Table 6.24), the analysis fails to define many easily interpretable factors. Factor 1 shows the closure-dominated relationship between SiO_2 on the one hand, and CaO , Rb , Al_2O_3 , MgO , Fe_2O_3 , K_2O and MnO , as well as the ore-related elements Pb and Zn , on the other. The well defined positive correlation between SiO_2 and Zr in schists (sections 6.2 and 6.3), does not apply to BQ (Fig. 6.26), and Zr has a high loading in Factor 2 together with Cr , Nb , TiO_2 and REE. Y displays a strongly antipathetic relationship with REE in Factor 2 (Fig. 6.26b), and with Cu in Factor 4, but Factor 4 also reveals a sympathetic relationship between Y , MnO and Fe_2O_3 .

6.4.3 Discriminant function analysis (DFA)

Of the six "immobile" elements used in the schist DFA analyses, Th and Sc fall mainly below detection limits so the analysis may only be performed using the remaining four elements, Al_2O_3 , Zr , Nb and TiO_2 . The differences between "immobile" element concentrations in WQ and DQ are so slight that no element has an F-statistic which exceeds the F-to-enter level of 1.5 (specially reduced from the value of 4.0 used in the schist analyses).

6.4.4 Rare earth elements

The single INAA analysis performed on a quartzite sample (WQ) reveals concentrations substantially lower than in schists, and a pattern having closer affinity to SS than to NS, as deduced from the positive Ce anomaly (compare Fig. 6.27 with Figs. 6.8a and b). This feature, though more common to SS, is occasionally found in NS (ALP122, Fig. 6.8a). The negative Eu anomaly is more strongly defined than in either NS or SS. REE XRF results from WQ (ALP040) and DQ (ALP042)

show slightly positive Nd anomalies similar to those displayed by NS. The difference in REE concentrations and pattern shapes for WQ and DQ (Fig. 6.27b) suggest a non-equivalence of the two rock-types unless a substantial facies change had been structurally juxtaposed. The MDS sample which contains traces of chalcopyrite (ALP125) bears a strongly positive slope towards the HREE's (Fig. 6.27b), while the second MDS sample (ALP041) has a pattern very similar to that of NS (Fig. 6.9a). MDS has too high absolute REE concentrations and lacks the fall-off to the estimated Ho position, to be equated with SS (Figs. 9b and c).

6.5 Oxygen isotopes

Analyses of oxygen isotopes were performed mainly on quartz grains at the University of Cape Town by Reid et al. (1987), in order to augment the major and trace element data of the ALP collection. The common representation is applied i.e. comparing the $^{18}\text{O}/^{16}\text{O}$ ratio of the sample with that of Standard Mean Ocean Water (SMOW) to produce the $\delta^{18}\text{O}$ ratio (Faure, 1986). The samples come from both borehole core and the surface outcrops (Table K.3), and the data are plotted along the horizontal depth scale applicable in borehole BH123, from which most of the samples were selected (Fig. 6.28). A number of features emerge whose possible significance will be interpreted in appropriate sections later on in the thesis.

With reference to Fig. 6.28, there is a marked variation in $\delta^{18}\text{O}$ values in quartz grains from different rock types. As noted with the major and trace elements, the variation between $\delta^{18}\text{O}$ in quartz grains from NS appears far greater than in SS (ranges of 0.66 vs 0.20‰, respectively). The $\delta^{18}\text{O}$ values of BQ quartz (8.9 - 9.7‰) lie between those of NS (5.7 - 6.4‰) and SS (13.9 - 14.1‰), while the orebody and ore-related rocks display quartz grain $\delta^{18}\text{O}$ values ranging between 6.6 and 9.7 (with a single sample of UFS having a value of 12.9‰).

Therefore a progression exists through the structural sequence from low $\delta^{18}\text{O}$ values above to high values below.

6.6 Geochemical relationships between adjacent lithologies

Geochemical variations perpendicular to strike are assessed by plotting the concentration of each element separately for each sample down the surface boreholes. Gradational, yet consistent geochemical patterns are then sought between comparable lithological intersections from appropriate boreholes. Since the schists immediately hosting the Broken Hill orebody (i.e. within 10-20m) are of variable composition and display elevated concentrations of ore-related elements such as Cu, Pb, Zn and Ba, only the ^{18}O information from OS will be used.

For the three boreholes sampled continuously from NS to DQ, a single composite of MDS for each borehole was taken, thus the sampling technique prevents a rigorous assessment of elemental variations from WQ through MDS to DQ. In the case of SS, core from four boreholes is used to define trends.

6.6.1 NS to BQ transition

When considering geochemical variations through NS to WQ, clearly defined examples from borehole BH123 are illustrated in Figs. 6.29a-c.

The elements may be divided into four categories:

(a) Elements which increase through NS into WQ. SiO_2 is the only member of this class;

(b) Elements which decrease through NS into WQ. All the major elements excluding SiO_2 , fall into this category, examples of which are shown in Figs. 6.29b. The trace elements Sc, Th, Nb, Co, V, Ni, Sr, Rb and Ba also decrease into WQ, examples of which are shown in Fig. 6.29c;

(c) Elements which increase along with SiO_2 up to the WQ boundary, but then decrease in WQ. Only Zr and Cr display these spatial relationships (Fig. 6.29a); and

(d) Elements which do not display consistent behaviour progressively closer to WQ, or for which insufficient data is available. The elements Y, S, Cu, Pb, Zn, U, Mo and C fall into this class.

XRF-derived REE data from BH166 reveals transitional REE patterns across NS. Except for the sample furthest from WQ (curve 1 in Fig. 6.30), NS REE patterns are all similar to each other, showing slightly positive Nd anomalies, but a systematic decrease in shale-normalized total REE values towards WQ (curve 6). Although total REE concentrations in WQ are substantially lower than in NS, a similar shape of the REE pattern is still preserved (Fig. 6.30).

The systematic increase in SiO_2 through NS into WQ (Fig. 6.29a) provides quantitative confirmation of the mineralogical gradations noted in section 4.2.1. The remarkable decrease in all other major elements and many trace elements, towards and across the NS/WQ boundary (Fig. 6.29b and c), probably reflect the effect of "closure" (Butler, 1982) resulting from the progressive SiO_2 increase. The behaviour of these elements nevertheless confirm the gradational nature of the transition through NS to WQ. The progressive increase in Zr and Cr contents of NS together with SiO_2 (Figs. 6.29a and 6.31), but lack of continuation of these trends across the boundary with WQ, probably result from specific sedimentological controls, to be discussed in section 9.3.4, and do not detract from the evidence for a continuum existing between NS and WQ.

Due to the sampling constraint mentioned, a different technique is required to examine whether the geochemical gradations continue

through to DQ. For comparative purposes, the mean element concentrations of NS for each borehole are plotted along the abscissa against the ordinate representing the element concentration of MDS and DQ in the same borehole. The three boreholes BH123, BH166 and TS11, separated by 800m and 4 800m, respectively, provide sufficient spread between profiles to test whether the geochemistry of NS in one borehole has any bearing on the geochemistry of MDS and DQ in the same borehole. For the elements SiO_2 , Al_2O_3 and REE considered as relatively "immobile", MDS and DQ display a marked dependence on the corresponding element concentrations in NS results for SiO_2 and Ce shown in (Fig. 6.32a and b). Th and V in MDS and DQ show a similar dependency on their NS concentrations. All three of the elements TiO_2 , Zr and Cr display non-positive but nevertheless similar shapes for their plots of NS versus both MDS and DQ (results for Zr plotted in Fig. 6.32c), showing that although apparently independent of NS concentrations for these three elements, the DQ concentrations of TiO_2 , Zr and Cr are mutually dependent with those of MDS. DQ but not MDS displays positive correlation with the corresponding Nb and Sc concentrations of NS. As would be anticipated of both the more mobile and the "ore-related" elements, including MnO, Rb, Pb, Fe, P_2O_5 , Co, Y, Ni, Zn, Cu, S, MgO, CaO, Na_2O , Sr, K_2O and Ba, they show no clear-cut dependence between element concentrations in NS and in the corresponding DQ and MDS samples. The evidence presented above is consistent with the existence of a continuous stratigraphic succession between NS and DQ.

6.6.2 OS $\delta^{18}\text{O}$ transitions

With reference to Fig. 6.28 it is evident that quartz grain $\delta^{18}\text{O}$ values from OS are of comparable levels with those of WQ and DQ. A substantial increase in $\delta^{18}\text{O}$ values occurs at the base of OES, with the UFS $\delta^{18}\text{O}$ ratio of 12.9‰ lying close to that of SS (-14‰).

Significantly, the break in increasing $\delta^{18}\text{O}$ values does not occur at BGZ, along which shear deformation is evident (section 4.2.2.1), hence a degree of geochemical continuity may be inferred between UFS and SS.

6.6.3 SS transitions

Unlike NS, five individual transitions in SS must be taken into account. These comprise element variations (a) directly below BGZ; (b) in the structural hanging wall of CSMQ; (c) in the footwall of CSMQ; (d) across the USS-LSS boundary; and (e) towards the quartzite at Plant Hill (PQ) (Fig. 6.33). Plots of the most significant elements from borehole cores which traverse SS are presented in Fig. 6.34.

Below BGZ the elements Th, Pb, Nb, and REE increase; while LOI, Mo, Cu, Rb and particularly CaO, P_2O_5 , C, Ba, V, Cr, Zn, Ni and MgO decrease (Figs. 6.34a and c; Table 6.25). Only one sample of SS (ALP054) is available from between BGZ and CSMQ and relative to SS in the remainder of borehole BH123, this sample in the hanging wall to CSMQ displays notable concentrations of Pb, Fe_2O_3 , MnO, Co and CaO, and low MgO, P_2O_5 , C, S, V, Ni, Ba and Zn contents (Fig. 6.34a).

Structurally below CSMQ, MnO, Zr, Cr, Th, Pb and Zn decrease strongly, while SiO_2 , P_2O_5 , Fe_2O_3 and Co increase (Fig. 6.34a). On moving from USS to LSS, a consistent increase in SiO_2 and Zr is accompanied by a marked decrease in V and Ni (Figs. 6.34a and c). Less severe decreases occur for Al_2O_3 , Fe_2O_3 , MgO, K_2O , LOI, C, Rb, Ba, (Mo), Zn, Cu and Cr. Towards PQ, LSS displays weak increases in CaO, Na_2O , Ba and Sr. The elements Al_2O_3 , TiO_2 , MnO, MgO, Ni, Zn and Cu, decrease towards PQ, except for the one or two samples immediately adjacent to PQ in which these elements increase slightly (Fig. 6.34b).

6.6.4 Ratio transitions through the succession

The wide variation in SiO₂ content of rocks through the stratigraphy at Broken Hill, suggests that it may be useful to monitor key element changes across strike with proximity to the orebody, by using inter-element ratios. Adoption of this method follows a study by Plimer and Elliott (1979) of such variations associated with the Broken Hill (Australia) deposit. Plimer and Elliott (1979) outlined the atomic properties of the element pairs K-Rb and Ca-Sr, which respectively have similar ionic radii, electronegativities and ionization potentials, causing Rb⁺ to substitute for K⁺ in minerals and Sr²⁺ for Ca²⁺. Since Rb⁺ has a slightly larger ionic radius than K⁺, Rb concentrates in hydrothermal phases relative to K, whereas Sr²⁺ being slightly smaller than Ca²⁺, is preferentially incorporated in minerals. The ratios Ca/Sr and Rb/K tend to increase progressively as hydrothermal fluids rise in the crust. Precipitates from these fluids at or near the surface of the earth should therefore retain some of the fluid's chemical composition, and the indicator used to monitor these elements in hydrothermal precipitates is the ratio Rb/(Rb+Sr) (or Rb/Sr ratio; Plimer and Elliott, 1979).

Sr substitutes for the important ore-related element Ba, particularly in barite precipitated directly from sea water, due to the inherently high Sr content of the oceans (Hanor, 1969). In cases where hydrothermal Ba is introduced into sea water, the resulting Ba/Sr ratio of barite and of the bulk rock, increases (Hanor, 1969). In addition, hydrothermal solutions become progressively depleted in Sr as discussed above, thus high Ba/(Ba+Sr) rock ratios should indicate the presence of precipitates from Ba-bearing hydrothermal fluids.

Borehole BH123 covers the succession from NS in the structural hanging wall, through OEH (OS+GQ and OEGQ in Fig. 6.35) into the SS footwall,

while BH156 only reflects the transition from OS and LGQ into SS (Fig. 6.36). It is evident from Figs. 6.35 and 6.36 that there is a general increase towards OEH in the ratios $Ba/Ba+Sr$ and $Rb/Rb+Sr$ in both boreholes, from both the structural hangingwall and footwall sides. The ratio values in the structural hangingwall exceed those in the footwall, and the increases in the ratio towards OEH in the hangingwall is better defined than in SS.

7. REGIONAL GEOCHEMISTRY AND COMPARISON WITH BROKEN HILL

Samples collected from the farms Achab, Vogelstruishoek (Namiesberg) and Wortel are used to determine geochemical background levels for various rock-types lying well removed from known mineralization and if possible to provide the compositional data required for regional sedimentological modelling. In this section the lithogeochemistry of the regional rock-types is described, and compared with appropriate units at Broken Hill. Since the schist and quartzite data sets are small, rigorous statistical testing of element distribution type is inappropriate, and the log transformations applied to the Broken Hill data are used as a matter of course.

A series of elements are plotted for boreholes BH123 (Broken Hill) and WTL3&4 (Wortel), to provide an indication of the degree of geochemical similarity between the correlated rock-types plotted along the X-axis of Figs. 7.1a-d. Zr, as one of the least-mobile elements, shows remarkably similar behaviour from the two localities, with the NS (and NTS) samples having elevated Zr concentrations relative to the SS (and STS) samples, and the quartzite and CSMQ Zr values being depressed (Fig. 7.1a). SiO₂ also shows general similarity between correlated rocks from the 2 areas, although Wortel STS is slightly elevated in silica relative to SS (Fig. 7.1b). In contrast, the Zn concentrations of BH123 rocks exceed those in comparative rock-types from WTL3&4 (Fig. 7.1c), as does the MnO concentration of all rocks excepting SS (Fig. 7.1d).

7.1 Regional schists

7.1.1 Geochemical characteristics

As with NS and SS, NTS is more silica-rich than STS, but both have less SiO₂ than their counterparts at Broken Hill, and thus contain more alumina (Table 7.1). NTS contains more CaO (0.52%) and Na₂O

(0.72%) than NS (0.17% and 0.16%, respectively). The C, V and S contents of STS exceed those of NTS, but are substantially less than in SS. Base metal concentrations of NS tend to be distinctly higher than in NTS as discussed later (section 7.3.3), but this does not hold true when comparing SS with STS. In common with SS, many STS samples have U and Mo concentrations in excess of the lower limit of detection, while NTS, like NS, does not. In general, and in keeping with the SS versus NS relationships, STS displays less major element variability than NTS, as measured by the coefficient of variation (Table 7.1), but the trace elements generally display more variability.

In contrast with NS, NTS displays far greater inter-element correlation, particularly so for the ore-related elements (compare Tables 7.2 and 6.7). There exists an enigmatic positive Pb correlation with Zr and negative Pb correlation with K_2O , Ba and Rb, but as with NS, Cu remains uncorrelated with virtually all elements in NTS. Both STS and SS show Cu positively correlated with most elements (Tables 7.3 and 6.8), and the STS correlation matrix is similar to that of SS except that Ba and Th are uncorrelated with most elements.

The Wortel CTS has the distinctive geochemical composition of low SiO_2 (39%) coupled with high Fe_2O_3 (45%), MnO (3.7%) and P_2O_5 (0.8%) which characterizes the Amphibole Magnetite rock of Broken Hill, and distinguishes it from CS (Table 7.4). Additional distinctive features of CTS include elevated Mo, Co, S and Y, and these considerations suggest that CTS correlates far more closely with AM than with CS.

The distinctive geochemical characteristics of GTQ include a relatively low SiO_2 content (66%) coupled with high concentrations of TiO_2 (0.4%), Al_2O_3 (9.5%), Fe_2O_3 (19.6%), MgO (3.0%) and Co (42 ppm) (Table 7.4). Comparisons between GTQ with both LGQ and MnQ from

Broken Hill reveal so wide a discrepancy in the above elements as to preclude correlation. GTQ cannot be called a calc silicate rock since it has more than double the iron and less than one tenth the calcium of CS (Table 7.4), and therefore emerges as an uncorrelated iron-silicate rock.

7.1.2 R-mode factor analysis

Factor analysis computations for both NTS and STS failed to reveal any specific ore-related factors. Few geologically interpretable factors emerged, and the study was not pursued.

7.1.3 Rare earth elements

NTS sample REE patterns display similar shapes and concentrations to those of NS, but with Achab NTS showing a relatively low estimated Ho concentrations (Fig. 7.2a). The shapes of STS REE patterns vary from having the positive Ce anomaly common to LSS, to having negative Ce anomalies and REE concentrations well in excess of those in SS (Fig. 7.2b). In comparing calc silicate rocks from Wortel and Broken Hill, the notable REE difference is the positive and negative Ce anomalies, respectively, and positive estimated Ho concentration of CTS (Fig. 7.2c). The Wortel GTQ also displays the positive Ce anomaly of CTS, but without the dramatic increase towards the estimated Ho values shown by both Wortel CTS and Broken Hill MnQ. Although AM at Broken Hill has a relatively elevated estimated Ho concentration, the positive Ce anomaly of CTS is not reflected in AM.

7.2 Regional Quartzites (RQ)

7.2.1 Geochemical characteristics

Similar sampling and detection limit constraints apply to RQ as they do to BQ (section 6.4), hence again the borehole core samples are used for comparisons, while in the case of MDTS a single surface sample is

included with the Broken Hill core samples. As with BQ, WTQ contains more SiO_2 and less Al_2O_3 , K_2O , Fe_2O_3 and REE than DTQ (Table 7.5), while the elevated S content of DTQ (783 ppm) reflects the pyrite frequently seen in hand specimens (Appendix C.7 and Table C.16). In comparison with BQ (Table 6.22), RQ has a far higher Na_2O content, but the two rock suites have Zr concentrations of similar magnitude. Whereas the Ba concentration of MDTs is slightly higher than in MDS, the MnO, Cu, Pb and Zn contents are substantially lower.

The RQ correlation matrix displays far more inter-element correlations than does the BQ matrix (compare Tables 7.6 and 6.23). Ba, Fe_2O_3 , K_2O , Rb, Al_2O_3 , TiO_2 and Nb are all mutually correlated, and these display a far stronger negative correlation with SiO_2 than in BQ.

7.2.2 Rare earth elements

Variation in RQ REE patterns is wide with no consistent shapes apparent. Positive estimated Ho anomalies are not confined to BQ, and both positive and negative Ce anomalies are observed (Fig. 7.2d). MDTs displays similar shapes to the REE patterns of MDS, with one of the Wortel samples (ALP449) also displaying a positive anomaly for estimated Ho (Fig. 7.2e).

7.3 Geochemical comparisons between data sets

Only correlated rock-types from Broken Hill and the regional areas are compared. OEH and the orebody therefore cannot be included in the investigation below, except when comparing AM at Broken Hill with CTS at Wortel.

7.3.1 Methods of comparison

In Figs. 7.3a-g, grouping of the elements partly follows results from the correlation matrices (Table 7.2 and 7.3), with SiO_2 and Zr on the

one hand, contrasted with the elements with which they are negatively correlated (Al_2O_3 , TiO_2 , K_2O , Na_2O , Sc, Rb and Sr). The results of Table 6.5 showed that at Broken Hill the elements Fe_2O_3 , MnO, S and V display moderate to strong concentration differences between NS and SS, and this grouping is therefore also adopted for comparing Broken Hill with regional rocks. In section 7.3.3, the elements most likely to be related to the presence of the Broken Hill orebody are grouped, and the relative behaviour of SiO_2 , Al_2O_3 and K_2O are also plotted in order to monitor the effects of closure.

Delta diagrams compare the mean element concentrations for NS, SS, WQ and DQ at Broken Hill against the appropriate mean element concentrations from the three regional areas Achab, Wortel and Namiesberg, by taking their log ratio (Figs. 7.3 and 7.6). Where the corresponding Broken Hill and regional rocks have an element of equal concentration, the log ratio is zero, but the ratio plots above the zero line when the Broken Hill rocks have a relative excess of that element, and vice versa. For the purposes of comparing non-ore-related elements, only core samples are used, whereas in section 7.3.3, certain surface sample suites will also be examined since practical applications of these techniques cannot be restricted to borehole core.

The ratio vs ratio diagram (Figs. 7.4) documents the change in the ratio of one element in Broken Hill rocks relative to their regional counterparts, as a function of the change in the ratio of another element. For example, as the Si content of Broken Hill rocks (bh) decrease relative to the equivalent regional rocks (reg), the relative Al content increases as a result of closure. In the quartzite/schist ratio part of Fig. 7.4a, the Si variation in BQ is so small that it may effectively be considered constant, thus as Si in the regional

schists increases, the $\log[\text{Si}(\text{bh})/\text{Si}(\text{reg})]$ ratio decreases, moving to the left, and the $\log[\text{Al}(\text{bh})/\text{Al}(\text{reg})]$ ratio increases. Fig. 7.5 confirms that the Al ratio variation is just a function of the regional schist SiO_2 content. At relatively high regional rock SiO_2 concentrations (i.e. in the BQ/RQ field), a small increase in RQ SiO_2 content drastically increases the BQ/RQ Al ratio, causing the curve to become virtually asymptotic.

7.3.2 Comparisons for elements unrelated to the Broken Hill orebody
The two data sets comprising the ratios Broken Hill Quartzite/Regional Schist (BQ/RS) and Broken Hill Quartzite/Regional Quartzite (BQ/RQ) appear to form a continuum when the ratios of the major elements Al, K and Fe are plotted against the Si ratio (Fig. 7.4). The SiO_2 concentration of the regional rocks is the single most important variable controlling the ratios $\text{Al}(\text{bh})/\text{Al}(\text{reg})$, $\text{K}(\text{bh})/\text{K}(\text{reg})$ and $\text{Fe}(\text{bh})/\text{Fe}(\text{reg})$ ratios for BQ/RQ and BQ/RS, as explained above, and with reference to Fig. 7.5). The BS/RS Al ratios form a well defined curve passing through the origin, but in the case of K and Fe, the curves pass just above the origin, indicating relatively higher levels of these elements at Broken Hill.

Figs. 7.3a and b reveal that Broken Hill has NS with intermediate concentrations of Si and Zr, with relatively higher Si and Zr than Achab NTS, and lower Si and Zr than Wortel NTS. Consequently, Achab NTS has higher concentrations in the elements Al, Ti, K, Na, Sc, Rb, Sr, S and V than their Broken Hill counterparts, and Wortel NTS has lower concentrations in these elements, excepting for Na and Sr. It is noteworthy that Na and Sr are the elements displaying the lowest NS/NTS ratios, suggesting that Na and Sr in NS at Broken Hill have unusually low concentrations. Mn shows significantly higher

concentrations in NS relative to both Achab and Wortel NTS, as to a lesser extent does Fe.

In the case of SS (Figs. 7.6c and d), Broken Hill is again intermediate in Si and Al composition with Namiesberg STS having relatively higher Si and lower Al than Broken Hill SS, in agreement with findings for the NS/NTS ratios. Broken Hill SS is also intermediate in concentration for the elements Na, Sr, Fe and Mn. Only S and V are consistently higher in Broken Hill SS.

For the quartzites, the Wortel and Namiesberg relative Si and Al concentrations are opposite to those in the schists, with Wortel quartzites having more Al and less Si than BQ, and Namiesberg quartzites having less Al and more Si than BQ (Fig. 7.3e-g). BQ shows conspicuously lower Sr concentrations and relatively more Fe and Mn than Wortel and Namiesberg quartzites, irrespective of the corresponding Al behaviour.

7.3.3 Comparisons for ore-related elements

The average concentrations of both core and surface NS samples from Broken Hill are relatively elevated in the elements Pb, Zn, Ba, (Mn), Fe, P and Y compared with the average regional NTS samples (from Achab and Wortel), notwithstanding the higher Si and lower Al contents of NS (Figs. 7.6a and b). In strong contrast to NS, Broken Hill SS ore-related elements with the exception of Pb, are at relatively lower concentrations when compared with regional STS (Namiesberg and Wortel) (Figs. 7.6c and d). The average Pb content of SS at 42ppm is higher than the maximum STS Pb value of 32ppm, and the highest SS Pb value of 128ppm occurs 150m into the structural footwall of the orebody. Even though average MDS and MDTS have equal Si concentrations, the ore-related elements with the exception of Ba display considerably higher

values in MDS than in MDTS, and lower Na and Sr (Fig. 7.6d), similar to the pattern seen in NS. The two Wortel MDTS samples with Ba in excess of 600ppm are responsible for the Ba anomaly.

Delta diagrams comparing element concentrations of borehole core samples of BQ to those of RQ, display relatively higher base metal and associated elements in the case of BQ (Figs. 7.6e and f). The lower Na and Sr content of BQ relative to RQ is again evident. These features are not well defined in the ratios of the surface samples of BQ relative to RQ.

7.3.4 Conclusions

There is a progressively clearer separation of SiO_2 in quartzite from Al_2O_3 in schist, moving from Wortel through Broken Hill to Namiesberg. An additional geochemical difference is that NS and BQ at Broken Hill relative to NTS and RQ, have higher levels of base metal and related elements, while Na and Sr concentrations are lower. No simple distinction can be drawn between SS and STS, however, the elevated concentrations of Pb in SS appears to be a useful indication of the nearby orebody. The existence of regional and local indicators of mineralization forms the basis of the lithogeochemical exploration strategy for locating Broken Hill-type deposits in the North West Cape (Appendix G, Figs. G.1 and G.2). This strategy would be ineffective unless combined with geological and geophysical techniques in the search for more ore.

PART D.

GEOLOGICAL AND GEOCHEMICAL MODELLING

PART D. GEOLOGICAL AND GEOCHEMICAL MODELLING

8. PROVENANCE

The chemical and mineralogical signatures of sediments are to some extent derived from the provenance area (e.g. Taylor, 1979; McLennan et al., 1983). Relative to BQ, the schists with their higher element concentrations other than SiO_2 , provide better information for the purposes of provenance modelling. U-Pb age patterns from detrital zircon grains in the quartzites (which are conformable with NS; section 6.6.1) will be assessed for provenance geochronological constraints.

8.1 Provenance age

8.1.1 Rare earth elements

BS chondrite-normalized REE patterns display the strongly negative Eu anomaly definitive of sediments derived from a post-Archaean provenance since, as shown in Fig. 8.1, the Archaean rocks have no Eu depletion. Taylor (1979) and McLennan et al. (1980) argued that the major batholith generation event which marked the close of the Archaean at +2.5Ga, fractionated Eu into early formed calcic-plagioclase, leaving the voluminous felsic fraction Eu deficient. Sediments derived from the more felsic, post-Archaean crust therefore have a negative Eu anomaly.

La and Th contents vary dramatically with the degree of igneous differentiation, thus in general terms sediments derived from more mafic Archaean crust may be distinguished from those having a relatively felsic post-Archaean provenance. From basalt to granite, La concentration varies between 16.7 and 101ppm, while Th varies from 1.12 to 50ppm. The La/Th ratio decreases from 8.8 in basalt to 2.0 in granite, hence sediments derived from the more mafic average Archaean crust have La/Th ratios of 3.6, while sediments from a younger, more

felsic provenance have ratios of approximately 2.7 (McLennan et al., 1980). The very low BS La/Th ratio of 1.8 (Fig. 8.2) suggests a strongly fractionated and hence felsic provenance of post-Archaean character. Comparing La/Th ratios of metapelites with pelites is justifiable since both La and Th are relatively insoluble, and also immobile during metamorphism (McLennan and Taylor, 1980; Cullers et al., 1974). The relatively high Th content of BS is responsible for producing a low Co/Th ratio, causing BS to plot well below the mixing curve between Archaean mafic (M) and felsic (F) volcanic rocks along which most Archaean sediments lie (McLennan et al., 1983) (Fig. 8.3).

8.1.2 Uranium/lead age dating of zircons

Individual zircons separated from the WQ outcrop at Froneman se Kop in which cross-bedded heavy mineral layers are located (section 4.3), were individually analysed on the ion microprobe at the Australian National University by Dr R. A. Armstrong. All analysed zircons display the characteristic detrital rounding described earlier (section 4.3), with two analyses being performed on zircon rims.

Plotting of the results on a conventional concordia diagram (Fig. 8.4) reveals a range of discordant age patterns but with an upper age intercept of 1 800 - 2 000Ma which approximates the calculated $^{207}\text{Pb}/^{206}\text{Pb}$ ages (Table K.4). The scatter of results below the concordia fail to define any obvious discordia, indicating episodic Pb-loss (Faure, 1986). Almost total Pb-loss in the most U-rich zircons (Table K.4) occurred between 1 000 - 1 200Ma which is a metamorphic age common in the 2 000Ma Achab Gneiss, and which corresponds with the age of intrusion of the granite precursor to the Aroams Gneiss (Armstrong et al., 1988). The zircon rims plot furthest removed from concordia, suggesting that these zircons suffered the most recent and the greatest total loss of Pb.

The data clearly suggest that the age of the provenance area for BQ does not exceed 2 000Ma, which corresponds to the interpreted age of the Achab Gneiss. As suggested by Moore (1977), Watkeys (1986) and Armstrong et al. (1988), the Achab Gneiss acted as a basement and in part possibly also as a provenance area to the Bushmanland Sequence.

8.2 State of provenance weathering

8.2.1 Major and trace elements

Relative to the average of average shale compositions given by Vinogradov (1962), Krauskopf (1979) and Turekian (1972), the most notable major element characteristics of BS are their higher K_2O content (higher by +1.25 times); and lower Na_2O , CaO and MgO composition (by +0.21, 0.04 and 0.48 times, respectively). The CaO deficiency can in part be attributed to the lack of Precambrian crustacea remains, when compared with shale averages which include post-Proterozoic lithologies. The relative intensities of the Na_2O , CaO and MgO deficiencies juxtaposed with the high K_2O contents is, however, similar to the weathering scheme proposed by Nesbitt et al. (1980). Continental weathering is characterised by losses to the oceans of the elements Na_2O , CaO , MgO and under extreme conditions of weathering, by K_2O (Nesbitt and Young, 1984; Bjorlykke, 1974). Four tests utilizing major and trace elements are employed to assess the provenance state of weathering. The first three ratios were used by Dypvik (1979), while CIA was devised by Nesbitt and Young (1982).

a. K_2O/Na_2O . Relative to average shale ratios of between 2.5 - 3.0, BS have high K_2O/Na_2O ratios ($mean_{SS} = 15$; $mean_{NS} = 28$). The high BS K_2O/Na_2O ratio is emphasized when compared with a ratio of 8.2 for Andoya (Norway), Ramsa Formation shales, which directly overlie their deeply weathered granite provenance. The relatively low Na_2O content

of BS is the main reason for their high K_2O/Na_2O values. Adding back the 77% and 19% Na_2O lost to pegmatites from SS and NS, respectively (section 6.1.5), decreases the K_2O/Na_2O ratio of SS to 8.7, i.e. broadly agreeing with Dypvik's (1979) values for pelites derived from granite, while the NS ratio decreases to 23.6, which is still high, thus emphasizing the suggestion of unusual processes which generated NS.

b. Rb/K_2O . The BS average Rb/K_2O ratio of 55 - 57 falls well within the average shale compositions listed by Vinogradov (1962) and Krauskopf (1979) of between 47 - 73. The Broken Hill values are considerably lower than the average of 172 for Dypvik's (1979) Ramsa Formation. The Norwegian granite provenance has proceeded to the kaolinite stage of weathering (Dypvik, 1979). Nesbitt et al. (1980) confirmed that although Rb/K_2O ratios decrease during initial stages of weathering of granitic rocks, the ultimate product of weathering, i.e. kaolinite, displays a marked increase of Rb/K_2O (relative to parent rock). Such behaviour of the Rb/K_2O ratio results from the preferential hydration and removal of the smaller K^+ cation and retention of Rb^+ on developing clays (Nesbitt et al., 1980) which are later physically removed to the depository to form shales.

c. Maturity Index $(Al_2O_3 + K_2O)/(MgO + Na_2O)$. Bjorlykke (1974) derived this ratio as an index of sediment maturity, based on the relatively immobile low temperature behavior of Al and K, compared with Mg and Na which are rapidly removed to the oceans. The Maturity Index for average shale varies between 5.8 - 7.2 which is considerably less than the range of 13.0 - 21.6 for BS. Even adding back the 77% and 19% Na_2O lost to pegmatites from SS and NS respectively, causes a negligible decrease in the Index (from 21.6 to 20.9 for NS and 13.0 to 11.6 for SS) since the Na_2O contribution is substantially smaller than

that of MgO. Bjorlykke (1974) found that the most mature Lower Paleozoic sediments of Norway attain a maximum ratio of 12, and suggested that the Index reflects both the type and degree of provenance weathering. In a separate study on the Mesozoic sediments of Andoya, Dypvik (1979) ascertained that the Maturity Index for the Ramsa Formation averages 57. Higher up in the succession (i.e. further removed from the provenance), the Maturity Index does not exceed a value of 10.

d. Chemical Index of Alteration - CIA.

$[(Al_2O_3 * 100)/(Al_2O_3 + CaO + Na_2O + K_2O)]$ (expressed in molecular proportions)

The CIA appears less dependent on provenance type than do the other three indices, as Nesbitt and Young (1982) have shown that both granite and basalt yield similar CIA values for their weathered end products. Comparison between CIA ranges (Table 8.1) for BS and various rocks and minerals given by Nesbitt and Young (1982), reveal that BS have slightly higher CIA values than average shale, and fall in the range of montmorillonite and illite, without attaining the kaolinite/chlorite degree of maturity. As shown for the Maturity Index above, adding back the proportion of Na₂O lost to pegmatites will not materially affect the CIA because of the small Na₂O contribution to the denominator.

8.2.2 Rare earth elements

Nesbitt (1979) showed that weathering of rocks can drastically affect their total REE concentrations by factors of 2.5 for moderately weathered granodiorite and of 0.4 for residual products i.e. kaolinite and illite, which form in fractures between less weathered parts of the granodiorite. The latter degree of alteration is restricted to rocks attacked by humic acids resulting from organic decay (Burkov and

Podporina, 1967; Nesbitt et al., 1980), a factor of little consequence during the Precambrian. Thus the likely bulk product of Precambrian weathering would be the "disintegrated zone" (Burkov and Podporina, 1967), and "altered rock" (Nesbitt, 1979), which are REE enriched. Compared with Post Archaean Australian Shales (PAAS), BS display higher REE patterns (Fig. 8.5), which probably reflect such intermediate stages of weathering. Calculations by the present author on Nesbitt's (1979) data reveal that the Eu/Eu* ratio remains virtually unaffected by the weathering process (Eu/Eu* of parent rock = 0.74; of moderately weathered rock = 0.73; of residual products = 0.76), hence the ratio in pelites should reflect the provenance composition.

8.3 Provenance composition

An assessment of provenance would be considerably simplified if a single source to Broken Hill schists (BS) could be established. Reid et al. (1987) argued that the variation in oxygen isotope ratios across stratigraphic boundaries (section 6.5) precluded a simple and single provenance for clastic quartz, however, it will be shown later (section 9.4.3) that the isotopic signature of quartz from a single source may be modified in the depository by interaction with both pore and hydrothermal fluids. The gradational relationship between NS and WQ (section 6.6.1) suggests that the chemical and mineralogical differences between these two rock-types reflect sedimentological differentiation (discussed more fully in section 9.4 below) rather than from erosion of different provenances. The fundamental chemical and mineralogical differences between NS and SS may have resulted from erosion of different provenances, and/or from depositional environment factors. The REE evidence is examined to provide clarity on this point.

8.3.1 Rare Earth Elements

Cullers et al. (1975) argued that the REE signature of clays and particularly of illite, is retained during transportation of clays from the provenance to the depository. The similar shapes to WQ and BS REE patterns, but far lower total REE concentration in WQ (Fig. 8.5) indicate that the bulk of the REE's are not contained in quartz, but in the mica, sillimanite and feldspar components of the schists. These aluminium silicates will therefore largely reflect the REE characteristics of the inherited clays since metamorphism does not significantly change the total REE content, pattern shape or Eu/Eu* ratios of shales during metamorphism (Cullers et al., 1974). BS displays a pattern of strong total REE enrichment compared with siliceous to intermediate igneous rock data from Haskin et al. (1968) (Fig. 8.5). The increase in total REE with increasing SiO₂ content of igneous rocks is apparent from Fig. 8.5, suggesting a highly felsic provenance to BS. In view of the weathered nature of the provenance (section 8.2) the total REE concentration and patterns of BS may over-estimate the siliceous nature of provenance rock composition.

The Eu/Eu* ratio, which is unaffected by weathering (section 8.2.2), can provide an idea of provenance composition. With reference to data by Haskin et al. (1968), Cullers et al. (1975) pointed out that Eu/Eu* becomes progressively smaller (i.e. increasingly large negative Eu anomaly) with increase in SiO₂ content (Fig. 8.5). Granite with SiO₂ = 60 - 70% has Eu/Eu* = 0.79, and 0.42 for granite with SiO₂ > 70%. The three NS samples average Eu/Eu* = 0.59, the single WQ sample has a value of 0.58, while the four SS samples average 0.52. The small range in Eu/Eu* ratios between NS, WQ and SS which display such a wide silica variation (68.7 - 96.3% SiO₂) do not support a contention of recognizably different provenances, but are indicative of detrital contribution to all three rock-types from similar or a single

provenance. Furthermore, the Eu/Eu* ratio of the metasediments provides an estimate of the provenance silica composition of approximately 70% SiO₂. The low La/Th ratio of BS (section 8.1.1) supports the indications of a relatively felsic provenance.

Cullers et al. (1975) identified six factors which could affect the REE patterns of shales, viz. source rock inheritance; weathering of source rock; exchange reactions during transport and deposition; diagenesis; contamination with allanite/monazite-type heavy minerals; and metamorphic changes. They suggested that source rock inheritance is the major factor controlling pelite REE patterns, which becomes modified by the intensity of provenance weathering. In the foregoing discussion, source rock composition and the effects of provenance weathering have been assessed, while metamorphic changes to REE patterns seem unlikely (Cullers et al., 1974). Neither monazite nor allanite were identified in samples of BS. Fleet (1984) indicated that diagenesis probably has little effect on the REE content of sediments, and there is no reason to suspect that exchange reactions during transport and deposition would be any different during the formation of North American Shales, and BS.

8.3.2 Major and trace elements

The original chlorite content of shales may provide an estimate of the mafic component of the provenance. The Maturity Index ($(Al_2O_3 + K_2O)/(MgO + Na_2O)$) derived by Bjorlykke (1974) varies inversely with detrital chlorite content, largely because of MgO in the denominator. The most chlorite deficient Lower Paleozoic sediments of Norway analysed by Bjorlykke (1974) have a maximum Maturity Index of 12, while the BS Index varies between 11.8 and 21.6, suggesting that chlorite, and hence mafic rock, was not an important component of the provenance.

Plotting of NS (n) and SS (s) relative to the fields of granitic to intermediate rocks, and to mafic rocks (Fig. 8.6), shows that BS falls far closer to the former than to the latter. The transformation from average crust cited by one author to average shale of the same author may provide an indication of the gross relationship which ties a specific shale to its provenance. Using the formula

$$P = S * (C_a/S_a), \text{ where}$$

P = Provenance composition;

S = Known shale composition;

C_a = Average crust composition from one author; and

S_a = Average shale composition from the same author, shows that the calculated provenance (Fig. 8.6, letters in boxes) lies closer to the field defined by granitic to intermediate rocks than to that of mafic rocks.

The relationships between the elements K, Rb, Si, Al, Ti, Zr and Cr have been chosen as they include the major and trace elements which display the least mobility during weathering (Nesbitt et al., 1980; Minarik et al., 1983; Kronberg et al., 1979). A major proportion of these elements will be transferred in detrital form from provenance to sediment. Only the data of Krauskopf (1979) and Vinogradov (1962) is used for calculating the ratio C_a/S_a, although various averages from Taylor (1964) and Turekian (1972) appear in Fig. 8.6 for reference.

The transformation of average crust to average shale (C_v and C_k to S_v and S_k, respectively; Fig. 8.6) causes a consistent pattern of K/Rb depletion in the residual crust as explained in section 8.2. The calculated K/Rb ratios for the provenance to NS and SS are 213 and 222 respectively, using the data of Vinogradov (1962); and 191 and 199

using Krauskopf's (1979) values, which both correspond fairly closely to average granite and intermediate rocks (Fig. 8.6a).

As crust is reworked and transformed to produce sedimentary rocks, the separation of quartz on the one hand from clays and micas in the other leads to the development of quartzites and shales, respectively. The Al content of the developing shale increases (Garrels and Mackenzie, 1971), thus the strongly decreasing Si/Al ratio seen in Fig. 8.6b is anticipated. Whereas granitic and mafic rocks have similar Al compositions (Fig. 8.6b), their Si contents differ sufficiently to conclude that the SS provenance had a granitic nature. The high Si content of NS and resultant low Al concentration, cause the NS provenance to plot in the extremely siliceous part of Fig. 8.6b.

The behaviour of Ti and Zr in BS is assessed since mafic rocks are richer in Zr and poorer in Ti than granites (Fig. 8.6c); and Zr- and Ti-bearing minerals tend to move together during sedimentary processes (e.g. Chandler, 1988). NS and SS both have relatively high Zr compared with average shale, but the vectors towards their precursors point in the direction of the granitic field, rather than towards that of mafic rock (Fig. 8.6c). The Cr content of the estimated NS and SS provenance also tends towards that of an intermediate rock composition (Fig. 8.6d). In pointing towards a granitic to intermediate provenance for BS rather than to a mafic one, the major and trace element data are compatible with the REE indications of a provenance having a composition of approximately 70% SiO₂.

8.3.3 Heavy mineral separates

A study of heavy mineral separates and heavy mineral layers in quartzites (section 4.3) failed to reveal any detritally rounded

garnet, kyanite, pyroxene, hornblende or staurolite. Such indicator metamorphic minerals form common detrital components of sediments derived from denudation of metamorphic rocks (e.g. Flores and Shideler, 1982; Trimonis et al., 1978), and some trace of these minerals should survive the weathering and transportation process had the quartzites been derived from a metamorphic provenance.

8.4 Discussion and conclusions

NS and SS were most likely derived from a common provenance, which the well defined negative Eu anomaly of BS suggests was felsic and hence of post-Archaean age, a result supported by the relatively high Th content of BS. The strongly negative Eu anomaly of BS also suggests that the provenance had relatively low concentrations of Ca-plagioclase. The provenance age is well constrained since the basement to BS has been dated at 2.0Ga (Armstrong, et al., 1988), and zircons inherited from the provenance give the same age. The lack of inherited metamorphic heavy minerals in the Aggeneys quartzites suggests that the provenance area was not metamorphosed.

The low Eu/Eu^* ratio of BS strongly favours a felsic provenance of ca. 70% SiO_2 composition, and this conclusion is supported by the relatively elevated total REE content of both NS and SS; by La/Th ratios of ~ 2 ; and by a variety of major and trace indicator elements suggestive of a granitic precursor. The maturity index clearly shows that chlorite, and hence basalt, was not a major component of the provenance. The well rounded zircons preserved in WQ could not have originally crystallized in a mafic rock since Poldervaart (1956) showed that in high temperature rocks, zircon is one of the last minerals to form, occupying and adopting the irregular shapes remaining just before solidification. Such zircons have little

preservation potential during detrital transport. The provenance to BS was therefore a felsic- igneous or -sedimentary rock.

It was suggested previously (Lipson, 1980) that basal gneisses in the Aggeneys area were metamorphosed rapakivi granites. Pristine rocks of this type are characterized by concentrations in the elements SiO_2 and K_2O , corresponding to some of the features of BS. REE data from the Laitila rapakivi granite (Vorma, 1976) reveals a ratio of $\text{Eu}/\text{Eu}^* = 0.08$ which is far lower than the ratio of 0.52 - 0.59 of BS. The known preservation of the Eu/Eu^* ratio from provenance to sediment discounts the likelihood of a rapakivi granite provenance. Similarly, although the Laitila massif contains high concentrations of LREE (La = 100ppm vs BS average = 55ppm), the HREE are also present at high levels (Lu = 1.17ppm) relative to BS (average Lu = 0.55ppm). A provenance of rapakivi granite would therefore not lead to the development of the observed shapes of BS REE patterns.

The high degree of sediment maturity was largely inherited from in-situ provenance weathering, as revealed by total REE contents; by Eu/Eu^* ratios; by the Maturity Index; and by the Chemical Index of Alteration. The latter two Indices suggest that the degree of weathering did not proceed to the kaolin stage, as exemplified by the thick lateritic profiles of Brazil where most K_2O contents are < 0.15 (Kronberg et al., 1979). Similarly, although the $\text{Rb}/\text{K}_2\text{O}$ ratio of BS exceeds that of average shale, it is not as high as in kaolinite.

9. GENESIS OF THE METASEDIMENTS AND STRUCTURAL IMPLICATIONS

9.1 Schists: NS and SS depositional environments

The extensive areal development of both NS and SS is a constraint in that neither schist is likely to have formed in a fluvial environment, particularly during the Precambrian when there was insufficient plant life available to trap large quantities of clay and mica before they reached either a lake or the coast (Prof. N. Smith, pers.comm., 1989). Comparisons with analyses from the literature, as well as indications of sediment maturity and likely redox conditions, are assessed together with the behavior of key elements, in order to establish possible marine or lacustrine environments in which these rocks formed.

9.1.1 Geochemical comparisons with shales

A comparison between NS and SS on the one hand, and average shale on the other reveals considerable gross geochemical similarities, with only the elements CaO, Na₂O, Sr, Ni and S occurring at considerably lower concentrations in NS, and CaO and Sr at considerably lower levels in SS (Table 9.1). The elements MgO, P₂O₅ and V are present at not quite such low levels in NS, and similarly for MnO, Na₂O, P₂O₅ and Ni in SS. Relative to average shale, NS shows twice the Zr, Pb and Zn concentrations, and SS twice the Pb and S content.

The common feature of low CaO, Sr and P₂O₅ in both NS and SS probably reflects a lack of metazoan remains prior to approximately 680Ma (Cloud, 1981). The low Ca-plagioclase content of the provenance (section 8.4) may also have contributed to a CaO deficiency of BS. Taking into account the NS and SS Na losses due to metamorphism (section 6.1) results in recalculated, average shale normalized ratios ($Na_{NS}/Na_{Av.Shale}$ and $Na_{SS}/Na_{Av.Shale}$) of 0.17 and 0.28 respectively, suggesting that low Na concentrations are an inherent characteristic

of the Broken Hill schists. The high Zr content (particularly in NS) can be related to the abundant zircon identified (section 4.2.1). The elevated Pb concentrations in both rock-types, and high Zn in NS, reflect the presence of the nearby orebody. The low Ni content of both NS and SS is not readily explained.

A comparison between both NS and SS with pelagic sediments of similar SiO₂ content shows wide element concentration differences in the key elements MnO, MgO, Na₂O, Zr, Mo, V, Ni, Co and REE (Table 9.2). Since no correlation with such pelagic sediments could be entertained, shales from the near-shore environment are therefore examined.

The unusually high SiO₂ content of NS limits the number of pelite analyses available for comparison. In a suite of shales and sandstones from the Mesozoic sediments of Andoya, northern Norway, the Upper Jurassic Dragneset Formation has been singled out for comparison since, similarly to NS, it contains a high proportion of both SiO₂ and muscovite (Dalland, 1975, p.280). Specifically, sample A103 (Breisanden Member), with SiO₂ = 77.4% (LOI < 5%) (Dypvik, 1979) bears the closest geochemical similarity to average NS (Table 9.2). The most notable differences between NS and sample A103 are the far higher Ca, P, and C in the latter (due to fossil remains); higher Na₂O, Cr, V, Ni and S; and significantly lower MnO and Ba. The elements SiO₂, TiO₂, Al₂O₃, K₂O, Sc, Co, and Zn have similar concentrations in sample A103 and in NS, and the first five elements represent some of the generally accepted least mobile elements, while Zr is not substantially higher in NS than in sample A103. Both Dalland (1975) and Dypvik (1979) concluded that the Breisanden Member formed under oxidizing conditions in an open marine environment, whereas much of the enclosing sediment formed in a reducing environment under conditions of restricted water circulation.

Since MnO is known to be a sensitive redox indicator (e.g. Krauskopf, 1979, p216), the literature was scanned to try and match the elevated MnO content of NS with rocks of similarly elevated SiO₂ concentrations. The Recent sands and muds from the Gulf of Paria off the Venezuelan coast (Hirst, 1962a,b) offer two samples (BV592 and 525) which may be compared with ALP028 which has a similar SiO₂ content, and sample S152 for comparison with ALP030 (Table 9.2). Hirst (1962a) showed that the Paria sediments have the bulk of their iron in the ferric state. Most elements in the ALP028 comparison show remarkably similar concentration levels, with the exception of the elevated Paria CaO, Sr and Na₂O, and lower K₂O and Rb. While the CaO and Sr content probably reflect the presence of organic remains (see above), the elevated Na₂O, and depressed K₂O and Rb nature of the Paria sediments is explained by Hirst (1962a) as resulting from a condition not present during the Precambrian, that is, excessive vegetation along the Orinoco River system, which absorbs K₂O (and presumably Rb as well), and therefore creates a K₂O deficiency in developing illites in the depository. The illites then degrade and absorb seawater Na₂O instead of K₂O.

In the case of SS there is a gross similarity to those black shales which have relatively low S and C concentrations. Ferry (1981) concluded that pre-metamorphic protoliths of graphitic sulphur-rich schists were almost certainly black shales, thus SS may be compared with the Jurassic Kullgrofta Member black shales of the Ramsa Formation (Dypvik, 1979); Recent Black Sea sediment (Calvert and Batchelor, 1978); and average Black Shale (Vine and Tourtelot, 1970) (Table 9.2). Noteworthy similarities include the low MnO content of black shales and SS, the high K₂O and V contents, and similar ranges of Ba. The Kullgrofta Member (KM) in particular bears a remarkable

geochemical similarity to SS, and is described by Dypvik (1979) as a non-marine bituminous shale having formed under reducing conditions. Attention is drawn to the low Na₂O contents of KM and USS (0.30%). BGZ, as part of SS, is also compared with black shale, and shows good agreement (Table 9.3), with only MnO, Pb and Zn displaying consistently higher values in BGZ. An explanation for these enrichments will be discussed in section 9.1.8.

In summary, it is shown that Phanerozoic geochemical analogues exist for NS, as exemplified by the Dragneset and Paria sediments; and for SS as indicated by black shales from Norway and the Black Sea, and by average black shale. Whereas the Dragneset and Paria sediments formed under oxidizing conditions in an open sea shelf environment, the black shales formed under reducing conditions. A detailed examination of the environments in which NS and SS developed follows.

9.1.2 Maturity and ore relatedness

In order to broadly define the processes which produced the Broken Hill Schists (BS), their geochemistry is plotted on a series of appropriate diagrams. The ternary diagram (Fe₂O₃ (total) + TiO₂ + CaO) - (SiO₂ * 0.73) - (Al₂O₃) of de la Roche (1966) (Fig. 9.1) explores the geochemical trends resulting from the erosion and reworking of various igneous rocks to sediments. SS data points lie well removed from the igneous trend, and close to, but at somewhat higher Al₂O₃ concentrations than shale, whereas NS samples plot within both igneous and sedimentary rock fields. A companion ternary diagram (MgO - K₂O - Na₂O), however, shows notably less Na₂O and a slightly higher K₂O content in BS relative to igneous rocks (especially) and to shales (Fig. 9.2). In Fig. 9.1 BS overlap the compositional field of beidillite (a Na-Ca-rich, Mg-Fe-poor montmorillonite), and lie adjacent to the illite field, whereas the high K - low Na content of

the rocks reveals in Fig. 9.2 that illitic clays were a probable component of these rocks. In neither diagram do the schists plot near the montmorillonite field. More recently de la Roche (1978) used the element combinations displayed in Fig. 9.3, which also portray the chemical effects of igneous rocks being progressively reworked by sedimentary processes to form a variety of end-member sediments such as evaporites and laterites. SS samples fall within the peraluminous field (argillaceous rocks), and lie along a trend of increasing Al enrichment and Na + Ca depletion, which occurs well removed from, and orthogonal to, the igneous trend. NS data points lie partially within the shale field, somewhat closer to, but wholly outside of, the igneous field. The trends defined by both schists indicate mature aluminous shales which formed along a continental margin environment. The clustering of a series of elements together with Al_2O_3 in the factor analyses of SS, NS and OS (sections 6.2.3 and 6.3.1.2; Figs. 6.6, 6.7 and 6.16) may therefore be interpreted as reflecting the contribution of clays, micas and possibly some feldspar.

The antipodal distributions of SiO_2 and Zr from the Al_2O_3 component in factor analysis Figs. 6.6, 6.7 and 6.16 indicate that quartz sand and zircon were moving together in the sedimentary environment as detrital minerals. The increase in Zr concentration in NS up to the boundary with, but not into WQ (section 6.6.1), while all major and many trace elements show gradational changes through NS into WQ, suggests that the NS contact with WQ marks the sedimentological horizon at which heavy mineral concentrations reached a maximum. Additional water winnowing of the sediment lead to the development of mature, quartz-rich sediment with zircon preserved mainly along single-grain-thick heavy mineral layers (section 4.3). The similar distribution that Cr shows to Zr in the transition from NS to WQ (section 6.6), suggests

the likely presence of detrital chromite or chrome-bearing magnetite, particularly in NS.

The binary plot of Garrels and MacKenzie (1971) (Fig. 9.4) also shows chemical changes which accompany the transformation of igneous rocks to sediment. NS and SS plot even further removed from the igneous trend than Precambrian slate, a feature governed by the higher K_2O and lower Na_2O and CaO contents of BS, which suggests maturity of sediment. Contrary to Fig. 9.1, BS plot well removed from either illite or montmorillonite fields.

In the ternary diagram of Englund and Jorgensen (1973) SS and NS fall between the fields defined by black shale and pelagic pelites on the one hand, and flint clay on the other (Fig. 9.5). Englund and Jorgensen (1973) concluded that of the pelites considered, flint clay represents the most mature sediment, while the greywacke-associated pelites are the least mature. Conclusions drawn from Fig. 9.5 therefore corroborate earlier evidence suggesting that NS and SS represent mature, Al-rich metapelites.

Both detrital feldspar and platy minerals (micas and clay) will have contributed to the Al and alkali concentration of the BS precursors. The Niggli al-alk parameter remains close to zero for Na- and K-feldspar (Senior and Leake, 1978), while the low Ca concentrations of both NS and SS indicate that the detrital anorthite contribution must have been negligible. If Al_2O_3 variation was predominantly due to detrital feldspar addition, the al-alk parameter would remain virtually constant. In Fig. 9.6 SS displays a clear decrease in al-alk values with increasing Al_2O_3 , hence the alumina concentration of SS is controlled by varying mica content (mainly biotite; section 4.2.2). Using MgO as an indication of the biotite content of SS, it is

apparent that while the al-alk parameter decreases with an increase in biotite content, the Al_2O_3 content increases (compare Figs. 9.6 and 9.8a). Unlike SS, NS displays virtually its full al-alk range at both 9% and 17% Al_2O_3 (Fig. 9.6). Effectively, the al-alk variation in NS may be viewed as varying between constant limits over the wide NS Al_2O_3 range, suggesting that NS alumina content is to some extent controlled by detrital feldspar, in contrast to the exclusive control of alumina in SS by platy minerals. It is apparent from Fig. 9.7a that the al-alk parameter and Zr in SS behave sympathetically, and taking cognizance of the relationships established in Figs. 9.6 and 9.8a, these suggest that the bulk of the Zr in SS is inversely related to biotite concentration and is therefore likely to be controlled by detrital zircon grains.

The well defined antipathetic relationship between al-alk and Ba, Zn, Ni and Co in SS (Figs. 9.7b-e) as well as the dependence of base metals, excluding Pb, on the major elements such as K, Al, Mg and Fe (Table 6.8), clearly indicates that the micas (mainly biotite) control these elements with positive correlation, and that the Zn-Ba-Cu concentration decrease with distance from the orebody (Fig. 6.34a) is not primarily related to the presence of the orebody. In contrast, MnO behaviour in SS is unrelated to the al-alk, and hence the mica content (Fig. 9.8a). The Pb scatter in SS (Fig. 6.5g) is unlikely to be pristine because of a lack of correlation with any other base metals, and the elevated Pb concentrations in SS pegmatites (196, 121 and 72ppm for ALP087P, ALP141P and ALP059P, respectively), suggest that Pb migration may have taken place from the orebody during formation of pegmatite .

A technique developed by Senior and Leake (1978) is applied to establishing rough estimates of the original clay composition of SS by

noting the major element concentration of the most Al_2O_3 -rich SS end-member, i.e. at the lowest al-alk values (Figs. 9.8c-g). Data in Figs. 9.1 and 9.2 showed that the two clays having analyses most similar to the resulting BS clay component are illite and montmorillonite. The estimated clay precursor to SS is shown in Table 9.4 to compare far more closely with illite than with montmorillonite, based particularly on the higher Fe_2O_3 , Na_2O and K_2O components of illite, and lower MgO .

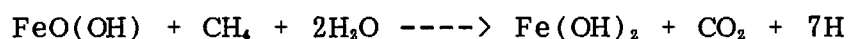
The evidence presented suggests that Broken Hill schists originally had a significant illite component, and their geochemical displacement from igneous rocks is too great to classify them as either distally reworked intrusive or extrusive rocks. Further, there are indications that these schists formed in a continental margin environment. The possibility that their high degree of maturity i.e. elevated Al_2O_3 and K_2O contents, and lower concentrations of CaO and Na_2O , could result from massive element leaching (of Ca , Na_2O and MgO), and addition (of K_2O) due to the ore-forming process, is unlikely since schists lying both structurally above and below the Broken Hill orebody generally display similar levels of concentrations in these elements.

9.1.3 Redox conditions

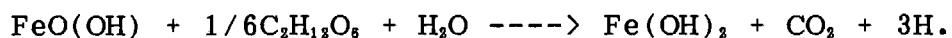
The preservation of prograde muscovite in equilibrium with biotite (section 4.2.1) suggests an oxidizing environment at some point in time during the pre-metamorphic history of NS since Dapples (1967) showed that muscovite forms (from an illitic parent) in preference to biotite, at high Eh during both early diagenesis and later burial. This oxidizing environment must have been restricted to NS through upper amphibolite facies metamorphism since the stable muscovite-biotite paragenesis occurs in NS but not in SS. Retrograde production of chlorite and muscovite from biotite in both schists indicates that

higher oxygen fugacities were widespread (Dapples, 1967) during the later metamorphic history of BS. Petrographic indicators suggesting originally reducing conditions under which SS formed, include the presence of biotite as the dominant mica, and the ubiquitous presence of Fe sulphide but absence of magnetite. Canfield and Berner (1987) showed that magnetite is dissolved in anoxic sediments. The formation of biotite at the expense of muscovite and hematite (or muscovite and chlorite) is empirically observed to be an indication of reducing conditions (Dapples, 1967).

The generally red colour of NS and the common occurrence of magnetite (Fe_3O_4) (section 4.2.1) suggest that oxidizing conditions dominated some stage of NS development. Dapples (1967) stated that the bulk colour of a rock is determined by the oxidation state of Fe, and once Fe^{2+} has been oxidized to Fe^{3+} , "there is much less tendency to reverse the equilibrium during the later history of the rock" (p.97). This oxidation of Fe is partly controlled by pH, with the slightly acidic stream environment maintaining iron as Fe^{2+} . The slightly alkaline conditions of playa lakes or the sea promote Fe^{3+} formation. The monotonous, bottle-green to grey colour of SS (section 4.2.2) is a well substantiated characteristic of anoxic sediments and results from the reduced state of Fe. As long as C is available, the generation of CO_2 provides electrons to drive Fe^{3+} to Fe^{2+} (Dapples, 1967) which leads to the production of pyrite and/or pyrrhotite instead of hematite and/or magnetite. Fairbridge (1967) showed the equations governing the reduction of Fe as



or



The paucity of C in NS but its presence in SS (section 6.2.1) shows that the reduced state of SS Fe cannot be solely attributed to metamorphism, but must have existed during deposition and/or diagenesis. During the period 1.6 to 2.0Ga which brackets the BS depositional age (Reid and Welke, 1988), the atmosphere was already oxidizing (Cloud, 1976). Oxidizing marine conditions are largely restricted to either nearshore, agitated environments in which there exists mixing with atmospheric oxygen (Hirst, 1962a), or to pelagic environments (Gundlach and Marchig, 1982; El Wakeel and Riley, 1961). The variability of NS geochemistry (section 6.2.2) suggests formation in an agitated, relatively energetic environment of the shoreface type, which has fluctuations in sedimentary input and chemical gradients (Skei, 1983, p.141) unlike conditions obtaining in the pelagic or estuarine regime. This NS inhomogeneity is also reflected in Figs. 9.3 and 9.5 where NS plots between igneous rocks and/or immature sediments on the one hand, and the more mature SS on the other. Comparison of NS whole rock geochemistry with a variety of Phanerozoic pelites reveals analogous sediments which formed in an open sea, oxidizing, continental shelf environment and not under pelagic conditions (section 9.1.1). The frequent occurrence of large detrital zircon grains in NS also suggests a proximal rather than a pelagic depository.

The evenly distributed non-carbonate C in SS ($0.1\% < C < 1.0\%$) far exceeds the maximum of 0.05% C in NS (section 6.2.1), but falls short of the black shale average organic C content of 3% (versus 0.65% for average shale; Vine and Tourtelot, 1970, p 257). Good agreement exists, however, between the chemistry of SS and those black shales with relatively low S and C contents (section 9.1.1). Furthermore, minor losses of CO_2 , and S as SO_2 or H_2S during metamorphism (section 6.1; and see below) might have lowered the C and S contents of SS.

Additional chemical parameters which distinguish black shales from non-black shales include higher concentrations in Mo, Ni, V, U, Cu, Zn (Holland, 1979) and Cr (Matzat and Shiraki, 1972-1978); and lower MnO contents (Vine and Tourtelot, 1970). Relative to NS, SS contains more Mo, Ni and Cr and far less MnO (Tables 6.4 and 6.5), while Cu and Zn concentrations in NS exceed those in SS. SS displays V and Cr concentrations comparable to average black shale, but has relatively lower Mo, Ni and Cu contents (Table 9.2). The low MnO concentrations of SS relative to black shale and average shale is marked. Many of the available indicator trace elements therefore suggest some form of black shale precursor to SS.

Extensive research on C-rich shales has established that the chemical and physical parameters of the basinal waters determine what type of black shale forms (e.g. Vine and Tourtelot, 1970; Tourtelot, 1979). The post-depositional chemistry of these sediments is preserved relatively efficiently because their erodibility decreases with increasing organic C content. The high electrostatic attraction of the commonly associated clays can prevent transportation by currents sufficiently energetic to move fine sands (Hatcher and Segar, 1976).

Black shale was defined by Tourtelot (1979) as a dark coloured mudrock containing organic matter. Black shales have formed throughout the Earth's history and result when enough organic matter is present to exhaust the environmental oxygen supply. A restricted water circulation, in which oxygen content of water is not renewed, promotes the development of black shale (Tourtelot, 1979).

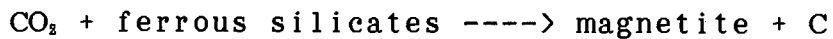
9.1.4 Behaviour of key elements and ratios during the formation of black shales

In this section, those critical elements are examined which characterize black shales. SS geochemistry is again contrasted with that of NS and inferences drawn will contribute towards constructing a basin depositional model.

9.1.4.1 Carbon, phosphorus, sulphur and copper

Individual assessments follow of the three primary sources of C in shales, viz. C component of carbonates (mineral C); hydrothermally introduced C; and biogenically produced C (organic C). A petrographic study of 12 SS samples failed to reveal the presence of any carbonate. Had carbonate existed, it must have disappeared during either diagenesis or metamorphism. Though solution of Ca into pore waters occurs during diagenesis (Sharma, 1971, p 171, quoting Friedman et al., 1968), Mg is at the same time removed from the pore waters and incorporated into the developing sediment, thus dolomite and/or magnesite would form at low temperatures, while at metamorphic grades at the boundary of granulite facies metamorphism to which the Aggeneys area was subjected (Lipson, 1978), minerals such as wollastonite (from calcite and quartz), or diopside and fosterite (from a dolomite precursor; Winkler, 1976), would be preserved in SS. The lack of any of the above indicator minerals shows that C in SS was unlikely to have formed from mineral carbonate.

C can form as one of the exhaled components from sub-sea floor convective systems during water movement and heating of CO₂, viz.



(Hutchinson et al., 1980). Were the C in SS generated in this manner, then the maximum C content should be associated with periods of maximum exhalation, i.e. with the Broken Hill orebody (discussed in detail in section 10). All check analyses for C in the Broken Hill orebody and its Ore Equivalent Horizon have failed to detect concentrations in excess of 0.05%. CO₂ could have been lost during diageneses and metamorphism, yet the Ore Equivalent Horizon lying 95m from the orebody, which contains no magnetite (but some pyrite, e.g. ALP 174 and 175), comprises a maximum of 0.02% C. An exhalative source for the C is therefore also unlikely.

If the graphite of SS were biogenically derived then the concentrations of some of the additional nutrient elements viz. O₂, N₂ and P (Turekian, 1968) should covary with C. Only the variation of P with respect to C is examined since O₂ and N₂ are gases. The fairly good positive correlation between P and C ($r = 0.61$; $n = 16$; Fig. 9.9) is consistent with a common origin for both elements. A strong correlation between C and any elements is unlikely because during diagenesis, a certain percentage of organic C is hydrolyzed and lost to the sea water, e.g. Hatcher and Segar (1976, p471) quote an absolute loss of 0.3% C from a silt-clay in Recent Bearing Sea sediments, which contained 1.38% organic C.

Since particulate phosphate rapidly dissolves on entering strongly reducing waters (Skei and Melsom, 1982), the gently increasing P₂O₅ content of SS with increasing C (Fig. 9.9) confirms that waters

immediately overlying SS were probably anoxic. The corollary holds that if oxygenated water extended down to the sea floor, i.e. no halocline existed, then most of the P_2O_5 would accumulate in the sediment. Assuming similar diagenetic losses of P_2O_5 in accumulating sediments irrespective of whether the overlying waters are oxidizing or reducing (probably less loss if oxidizing), and a loss of most of the C as CO_2 because of the oxidizing water, then P_2O_5 vs C plots for sediments formed beneath oxidized waters should be steep. In NS, the low C content ensures that this slope is almost vertical.

An organic C precursor to SS graphite has important genetic implications. Phytoplanktonic blue-green algae were the most highly developed photosynthesising organisms alive during the period 1 600 - 2 000Ma (Cloud, 1981; Plumstead, 1969) in which the Aggeneys sediments formed (Armstrong et al., 1988). Plumstead (1969) suggests that the lack of a protective ozone layer shielding ultra-violet radiation on the Earth's surface during Transvaal dolomite times of ca. 2.2Ga, restricted the blue-green algae to living subaqueously. These algae required light for photosyntheses, and Klein et al. (1987) have estimated that the maximum water depths under which the Transvaal Supergroup Campbell Rand carbonaceous shales formed was between 40 - 45m. Photosynthetic accumulation of O_2 in the atmosphere was so slow that by the start of the Phanerozoic, O_2 comprised only 1% of the atmosphere (Plumstead, 1969). Environmental constraints applicable during Transvaal times, in which algae developed on either the near-shore slope or in the intertidal zones, would therefore not have changed radically by the time SS started developing. Even today phytoplanktonic activity is greater nearer the coasts of continents than in the open ocean (Strickland, 1965).

Observations from a number of partly silled basins e.g. Lake McKerrow, New Zealand (Pickrill et al., 1981) and Elliot Bay, Seattle (Baker et al., 1983), show that most river water and its load has a short residence time in estuaries, and that the major source of sedimentation is from the sea. Proterozoic phytoplankton which grew and died in shallow water on the seaward side of a sill, could have been swept into the deeper estuary by the entering sea water, and fallen to the floor. Therefore, as long as Proterozoic organic C was produced in a nearby shallow water environment, the site of the C accumulation could have been in slightly deeper reducing water. A shallow water sedimentary environment is confirmed by the SS Ba content of 350 - 530ppm which compares with the empirically determined near shore shelf environment black shale Ba concentrations of 200 - 500ppm (Vine, 1966). This contrasts with deep water black shales which contain approximately 1 000ppm Ba (Vine, 1966).

S in SS may have been derived from either a hydrothermal source or by local evaporative and/or biogenic processes. The lack of any base metal concentrations (other than in CSMQ) in SS at Broken Hill, suggests no hydrothermal input to SS. (The mineralized CSMQ is examined in detail in section 9.1.7). Williams (1978) suggested that anoxic sediments associated with mineralization have positively skewed S/C ratios, owing to additionally derived hydrothermal S. The frequency distribution plots of S/C (Fig. 9.10), show a normal distribution for USS, and strong positive skewness for both LSS and NS. The skewness in all cases results from extremely low C concentrations, rather than S excesses. The lack of skewness in USS, the most C-rich of the three schists, coupled with its relative proximity to the Broken Hill orebody, again suggests that no significant hydrothermal S contributed to SS. No S isotope data is available from SS.

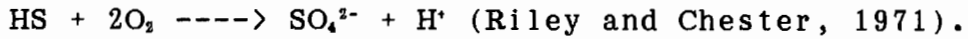
The positively correlated S-C relationship in SS (Fig. 9.11a) is typical of black shales which have formed world-wide since the late Archaean (Tourtelot, 1979), and sulphate reducing organisms, as the generator of S, have existed since the middle Archaean (Monster et al., 1979). Sulphate reduction by anaerobic bacteria is a characteristic feature of most anoxic basins (Trudinger, 1981, p.280). The model of in-situ S production requires that SO_4^{2-} is reduced either in the water column and in the sediment (under anoxic water conditions), or in the sediment alone (Leventhal, 1983). Oxygen deficient conditions cause first nitrate, and then sulphate to be turned to by bacteria as sources of O_2 for catabolism (destructive metabolism) of organic C (Richards, 1971, p.203). In all cases, the S and C contents of the sedimentary rock record will increase linearly. The reduced S first forms HS^- by the reaction



where R represents the organic residue not metabolised. *Desulfovibrio desulfuricans* is the micro-organism which accomplishes the SO_4^{2-} reduction (Leventhal, 1983). The HS^- combines with available Fe in minerals (Berner, 1971, p.202) to form FeS (mackinawite), which converts during diagenesis through greigite (Fe_3S_4) and/or pyrrhotite ($\text{Fe}_n\text{S}_{n-1}$) to pyrite (FeS_2), the stable iron sulphide (Berner, 1971, p205).

Some of the HS^- which does not form iron sulphide, can eventually be lost from the rock record due to its conversion back to SO_4^{2-} (Berner,

1972). This only occurs if the environment becomes more oxidizing
i.e.



Thus in a basin which remains anoxic over a long period of time, little S will be lost to basin waters, and the same argument will hold for organic C. According to Leventhal (1983) a positive intercept on the S axis of a S vs C plot, as in Fig. 9.11a confirms that the waters were stratified into anoxic water below and oxic water above. He explained that in addition to sulphide formation in the sediments, some insoluble sulphide forms within the reducing waters and precipitates to the sea floor, "but the usual complement of associated organic matter (R, in the equation) does not necessarily reach, and therefore is not preserved in, the sediment" (Leventhal, 1983, p134). In strongly reduced waters such as in deep fjords having a sill depth of only 2m, H₂S concentrations attain levels of up to 175 ml/l (Skei, 1983).

On oxidation during metamorphism both S and C may be lost as gases. Ferry (1981) found that the pyrite/pyrite + pyrrhotite ratio of black shales decreases along stringent lines with increased metamorphic grade (p919). Of the two reactions suggested by Ferry (1981), the one in which H₂O fluxing drives the reaction is preferred (section 6.1.3.4), viz.:



pyrite pyrrhotite

Note that although both S and C are lost as a fluid phase, the rate of loss is in the proportion of 2*S to 1*C. Not until all pyrite is

shown for reference purposes, represents the maximum possible premetamorphic S and C concentrations in SS.

Cu, similarly to S, remains soluble in the oxygenated environment, but precipitates as a sulphide under anoxic conditions (Goldberg, 1965; Heggie and Lewis, 1984). The good correlations exhibited between Cu and most other elements in SS and STS (Tables 6.8 and 7.3), but lack of correlation in either NS or NTS (Tables 6.7 and 7.2) also confirms the oxidizing and reducing nature, respectively, of NS-NTS, and SS-STS.

9.1.4.2 Manganese and iron

SS is characterized by both constant and low MnO concentrations (section 6.2.2; Table 6.4). Though constant, the Fe_2O_3 content of SS tends to be higher than average shale (section 9.1.1; Table 9.1c). The theoretical behaviours of MnO and Fe_2O_3 in a variety of aqueous and diagenetic environments are therefore examined to explain these features.

The interface between fresh and saline water represents a zone where significant chemical change takes place. In the superimposed Eh-pH diagrams for Mn and Fe, the field of soluble Mn^{2+} is far more extensive than that of Fe^{2+} . The mixing of fresh and sea water would follow a path approximating that from A to B in Fig. 9.12. Whereas Fe precipitates rapidly, Mn remains largely in solution. When river water enters the estuarine environment the ionic sea water (with cations of Na^+ , Ca^{2+} and Mg^{2+}) oxidizes the introduced, negatively charged Fe-bearing colloids (Boyle et al., 1977), which also contain lesser amounts of Mn, Al and P, and the increasingly saline water extends the flocculation process. In addition to such inorganic colloids, Sholkovitz (1976) showed that flocculation of dissolved

organic matter represents an effective mechanism for removing Fe, Mn, Al and P from river water when it mixes with sea water. Massive flocculation of colloids on encountering sea water is the major process of Fe removal in estuaries. Bowers and Yeats (1977) calculated that 89% of the river-introduced Fe remains in the St. Lawrence estuary, while under laboratory conditions, the comparable figures produced by Sholkovitz (1978) and Salamons (1980) are 95% and 90% respectively. The comparative values for Mn are 47%, 25 - 45% and 50%, respectively. Colloidally held elements will accumulate at the sediment-water interface provided that no major physico-chemical boundaries in the water are encountered. If the oxidized colloids pass through a thermocline below which anoxic conditions prevail, then Mn^{4+} is reduced to the soluble form of Mn^{2+} (Goldberg, 1965, p183), thus limiting the amount of Mn which reaches the sediment. Far more acidic and anoxic conditions are required for the reduction of insoluble Fe^{3+} compounds to soluble Fe^{2+} , than for the reduction of Mn^{4+} compounds to Mn^{2+} (Fig. 9.12). Only extreme variations in fugacities of S (from $10^{-6}m$ to $10^{-1}m$) would materially change the gross Eh-pH stability fields for Mn and Fe shown in Fig. 9.12. Thus under constant conditions of anoxia, less Mn than Fe reaches the sediment-water interface. The formation of insoluble FeS particles within anoxic waters (e.g. Skei and Melsom, 1981) further accentuates the separation of Fe from Mn in the developing sediment.

During the diagenesis of sediments, reducing conditions also result in the formation of Mn^{2+} which diffuses upwards (Hatcher and Segar, 1976, p471), as confirmed by Riley and Chester (1971, p408) who showed that the enrichment of Mn in pore waters occurs at the expense of the host sediment. The presence of organic matter in the sediment further aids solution of Mn as an organic chelate (amino acid complex) (Riley and Chester, 1971, p405). The anticipated concentration of Mn just above

reducing sediments is found in the St. Lawrence estuary (Bewers and Yeats, 1979). Sundby et al. (1981) showed that Mn is enriched to between 1 000 - 5 000ppm within only the top 20mm of oxidized pelitic sediments forming in the Gulf of St. Lawrence. Below this level the reduced nature of the sediment causes the Mn content to drop to between 450 - 1 000ppm (i.e. MnO = 580 - 1 290ppm). Individual profiles to depths of 30cm in the sediments show that below the zone of surface sediment oxidation, Mn contents remain virtually constant (Fig. 9.13). This profile may be compared with the constant Mn content of SS (Fig. 6.34a).

Redissolution experiments by Boyle et al. (1977) showed that little Fe goes back into solution in the estuarine environment, which confirms observations by Bewers and Yeats (1979) and by Duinker and Nolting (1978) that in waters directly overlying the bottoms of estuaries, only Mn (and not Fe) concentrations are increased. The ratio $\text{MnO}/(\text{MnO}+\text{Fe}_2\text{O}_3)$ of sediment should therefore provide a sensitive redox indicator. The SS average ratio of 0.006 agrees well with world black shale averages of 0.007 (Table 9.5), suggesting development of SS under the reducing conditions necessary for the development of black shales. The ratio is approximately quarter the NS average of 0.023 which falls between the two world average shale values of 0.016 and 0.123. SS MnO concentrations averaging 500ppm are so low compared with the St. Lawrence sediments as to suggest that not only was SS formed as a reduced sediment, but that the waters overlying SS were also anoxic.

9.1.4.3 Vanadium and molybdenum

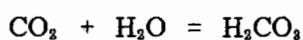
The V content of USS, averaging 183ppm, is much higher than that of average shale (V = 130ppm) or NS (V = 46ppm), and it compares favourably with the average black shale V concentration of 150ppm

quoted by Vine and Tourtelot (1970). USS, with Mo = 3.4ppm, displays slightly higher Mo concentrations than the average shale values of 2.0 - 2.6. The Mo concentration of USS nevertheless lies well below the black shale average of 10ppm. LSS averages 78ppm V which is somewhat less than the average shale value of 130ppm V (Vine and Tourtelot, 1970). Few LSS and NS samples analysed contain Mo in concentrations in excess of the lower limit of detection (~ 1.5ppm), therefore the higher Mo and V contents of USS only, will be examined in the three environments of oxidizing and reducing waters, and reducing sediments.

Under oxidizing, aqueous, low temperature and neutral pH conditions, the major mechanism of Mo removal from solution is by coprecipitation with MnO_2 and $Fe(OH)_3$. Similarly, virtually all non-detrally bound V coprecipitates with $Fe(OH)_3$ between a pH range of 8.5 to < 4.0 (Fig. 9.14). Flocculation of Fe and Mn colloids associated with the mixing of fresh and sea water (section 9.1.4.2) will therefore remove large proportions of the available Mo and V from surface waters in the nearshore environment.

When Mo which is bound with $Fe(OH)_3$ passes downwards into reducing waters, the entire colloid continues to fall to the sediment-water interface. Mo and V also precipitate with fine-grained iron sulphides (Bertine, 1972), which are common in the stagnant water layer of stratified water bodies (e.g. Lake Kivu, Degens et al., 1972).

Reducing waters are slightly acidic due to the reaction



(Turekian, 1968), and at pH = 6 - 7, a series of thiomolybdates form ($[MoO_2S_2]^{2-}$ ----> $[MoOS_3]^{2-}$ ----> $[MoS_4]^{2-}$) which in the presence of Fe cause the precipitation of the trisulphide MoS_3 (Evans et al., 1974-

1978). By contrast, the orthomolybdate $[\text{MoO}_4]^{2-}$ is very soluble in alkaline solutions. Acidity also enhances the fixation of Mo and V on organic matter (Coveny and Martin, 1983). Contreras et al. (1978) speculated that the diagenetic conversion of mackinawite/greigite to pyrite (i.e. $\text{FeS} \rightarrow \text{FeS}_2$) leads to the expulsion of Mo due to the large difference in ionic radii between Mo^{6+} and Fe^{2+} , and the loss of Mo to interstitial pore water was empirically confirmed by Holland (1979). Mo and V enrichment nevertheless represents a characteristic of black shales (Krauskopf, 1967).

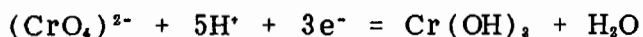
Bertine and Turekian (1973) suggested that oceanic sediments which form under oxidizing conditions are Fe-Mn oxide rich with a Mo/U ratio = 3, while reducing sediments have Mo/U = 1, this feature being largely governed by U solubility in the oxidizing environment. Only four SS samples have both Mo and U in excess of the lower limits of detection (~ 1.5ppm and 3.5ppm, respectively), and these average Mo/U = 0.8 (s.d. = 0.2).

In summary it is suggested that in the case of USS, the soluble $[\text{MoO}_4]^{2-}$ anion available in surficial, oxygenated waters, coprecipitated with MnO_2 and $\text{Fe}(\text{OH})_3$. On passing downwards into reducing, acidic waters, only that Mo bound with the Fe floccules continued to fall to the sea floor and formed insoluble MoS_3 . Soluble $(\text{MoS}_4)^{2-}$ coprecipitated with either organic C or with fine-grained sulphides. During diagenetic transformation of Fe sulphide to pyrite, some of the originally precipitated Mo, but not V, was probably lost. The direct proportionality of Mo solubility to temperature (Evans et al., 1974-1978), will have resulted in further Mo escaping during metamorphic losses of water or volatiles from SS.

9.1.4.4 Chromium

Average black shale tends to be slightly richer in Cr than average shale (100ppm vs 90 - 100ppm) (Vine and Tourtelot, 1970; Vinogradov, 1962; Turekian, 1972; Krauskopf, 1979). USS, with 109ppm Cr, has a higher Cr content than both black shale and NS (72ppm). The behavior of Cr in the sedimentary environment is, however, complicated by its presence both in detrital minerals such as chromite and magnetite, as well as in clay minerals which derive a component of their metals from overlying and interstitial water (called the hydrogenous component by Goldberg (1954) and Piper (1971) due to derivation of material from the hydrosphere, and in contrast to biogenous, lithogenous and cosmogenous components). The clays later convert to micas where Cr substitutes extensively for Al (Matzat and Shiraki, 1972-1978). This dual mode of occurrence has lead Holland (1979, p.1679) to attribute the relative enrichment of Cr over the elements Cu, Ni, V and Zn in some black shales, to addition of detrital chromite.

The low temperature aqueous behavior of Cr has not received extensive attention in the literature, leading to inconsistent conclusions. Matzat and Shiraki (1972-1978) claim that progressive oxidation causes the insoluble Cr^{3+} cation to be oxidized to Cr^{6+} (in the form of the soluble anion $(\text{CrO}_4)^{2-}$). In evidence they quote the depleted Cr content of oxidized, deep sea Fe-Mn nodules. Although the equation governing this behavior of Cr, as given by Piper (1971), viz.



shows that acidic (H^+), reducing (e^-) environments lead to the precipitation of Cr (as $\text{Cr}(\text{OH})_3$), yet Piper's (1971) data from the Framvaren fjord in Norway reveals that in the extremely anoxic waters

developed below the well defined pycnocline, suspended Cr goes into solution.

In SS, the good positive correlation between Cr and both C and Al_2O_3 (Table 6.8; Figs. 9.15a and b) suggests Cr fixation in SS by both biogenic and hydrogenous processes, while the antipathetic relationship of Cr with SiO_2 and Zr (Table 6.8; Figs. 9.15c and d) suggests non-detritally derived Cr. The behaviour of Cr in SS supports a model of a reducing environment fixing Cr on developing clays, and also suggests that the waters overlying SS, never attained the degree of extreme anoxia present in the Framvaren fjord. In contrast, NS Cr displays negative correlation with C and Al_2O_3 , and positive correlation with SiO_2 (Figs. 9.15a-c). Notwithstanding the approximately constant Cr concentration over a wide range of Zr concentrations (Fig. 9.15d), the opposite behaviour of Cr in NS relative to SS suggests a component of detritally contained Cr as chromite or chrome-bearing magnetite in NS (see also section 9.1.2).

9.1.4.5 Nickel and cobalt

The Ni content of SS averaging 22 - 34ppm, by far exceeds the 12ppm average of NS. These values are, however, lower than average shale (68 - 95ppm; Vinogradov, 1962; Turekian, 1972; Krauskopf, 1979), average black shale (50ppm, Vine and Turekian, 1970), and world averages of 80 - 320ppm Ni quoted by Turekian (1968-1978) for deep sea pelagic sediments. Fresh water pelites and nearshore clays average between 25 - 52ppm Ni (Turekian, 1968-1978), thus absolute Ni concentrations also discount the possibility that either SS or NS formed in the pelagic environment.

During continental weathering, Ni and Co are rapidly adsorbed onto suspended particulate matter (mainly illite and montmorillonite) and

remain in suspension until reaching sea water at the interface with the estuarine environment (Turekian, 1971). Here, Co in particular goes into solution, with Sholkovitz (1978) showing that Co forms extremely stable complexes with the Cl^- anion of sea water. Therefore whereas 40% of the Ni in river water is flocculated on encountering sea water at salinities of 0 - 18‰, only 10% of the Co is. The efficient removal of Ni and Co by organic material reaches a maximum under alkaline conditions, but as the pH drops to between 7 and 4, lesser Ni and Co remain adhered to organic C (Coveney and Martin, 1983). An additional method of Ni and Co removal from aerated solutions is by co-precipitation with Fe and Mn oxides (Turekian, 1968-1978; Murray and Brewer, 1977), while under anoxic conditions, anions of sulphide cause the precipitation of Ni (Turekian, 1968-1978) and Co (Piper, 1971). The sulphide-rich bottom waters of the Black Sea contain more Ni than the overlying aerated waters (Burns et al., 1973-1978) thus reflecting the sulphide influence on Ni. Measurements by Bowers and Yeats (1977) showed that some 12% of the Ni entering the St. Lawrence estuary from the continent, fails to escape to the ocean. These considerations have lead Turekian (1971) and Vine (1966) to the conclusion that the reducing environment represents a major site for Ni accumulation.

In reducing sediments, Heggie and Lewis (1984) found that Co behaves almost identically to Mn i.e. Co, and to a lesser extent Ni, go into the pore waters, leaving the sediments Co depleted. The Ni/Co ratio may therefore act as a redox indicator, with high ratios indicating anoxic conditions of deposition. The Ni/Co ratio in SS far exceeds that in NS ($\text{Ni/Co}_{\text{SS}} = 2.1$; $\text{Ni/Co}_{\text{LSS}} = 1.8$; $\text{Ni/Co}_{\text{NS}} = 1.1$), suggesting a more oxidizing environment for NS than for SS. The Ni/Co ratio of both SS and NS is, however, far less than the ratios in both average black shale and average shale (5.0 and > 3.4 , respectively).

The positive correlation of P_2O_5 , one of the nutrient elements, with Ni in both SS and NS (Fig. 9.16a), suggests that Ni could not have been of detrital origin as might be anticipated for nickeliferous, detrital chromite (Holland, 1979, p.1678). This conclusion is supported by the lack of positive correlation between Ni and Zr in either of the schists (Fig. 9.16b).

It may be concluded that Ni and Co adsorbed onto suspended particle matter entered an estuarine environment via rivers, and during the mixing of fresh and sea water, more Ni was flocculated than Co. Available organic matter and precipitating Fe-Mn oxides adsorbed both Ni and Co and facilitated their removal from the oxidizing zone. Within reducing waters, adsorption of Ni and Co onto precipitating sulphides further depleted the waters of these elements, yet during the diagenetic stages, more Co than Ni went back into solution under the reducing conditions obtaining in SS. Relative to NS, SS has the higher Ni/Co ratio. That this ratio is still considerably less than that of average black shale might be the result of a slightly less reducing environment for SS than for average black shale, as supported by the lower C content of SS. No significant detrital contribution of Ni was made to either SS or NS.

9.1.4.6 Zinc and uranium

According to Wedepohl (1972), the major mechanism for both transport and deposition of Zn is along with the detrital minerals chromite, magnetite, colloidal iron oxide, and iron oxide coatings on other minerals. Of the adsorbing minerals, only montmorillonite, peat moss and precipitated Fe oxides are significant Zn retainers (up to 2% Zn; Wedepohl, 1972) while illite, the predominant clay precursor to both SS and NS (section 9.1.2), and kaolinite adsorb an order of magnitude

less Zn from a sea water solution. The most important characteristic of the low temperature aqueous behavior of Zn is that extremely little Zn is trapped in the estuarine environment, as long as the sill level is not unusually high. Of the Zn entering the St. Lawrence estuary from the continent, only 0.1% is trapped in the estuarine sediment (Bewers and Yeats, 1977). In contrast, the Framvaren Fjord anoxic waters of Norway, which are dammed by a sill lying only two metres below water level, have suspended Zn particles and framboidal pyrite forming, and the sediments contain 1 000ppm Zn (Skei, 1983). In the St. Lawrence estuary, Zn behaves similarly to Mn in that the bulk of the Zn which does precipitate and reaches the sediment, goes back into solution, thus greatly increasing the Zn content of bottom waters (Bewers and Yeats, 1979). The relative Zn deficiency of SS (106ppm; excluding ALP183 with Zn = 391ppm; section 6.2.2) confirms the reducing, estuarine environment of SS formation, when compared with the relatively Zn rich NS (194ppm).

The solubility of U is largely controlled by its oxidation state, with reducing conditions favouring U fixation in developing sediment (Pertlik et al., 1978). Insufficient U analyses above XRF detection limits of approximately 4.5ppm are available from SS and NS for a comprehensive assessment of U distribution in these schists.

Partial melting of BS has produced pegmatites in SS (section 6.1.5) with marked enrichments of U (\leq 65ppm), while NS pegmatites are not uraniferous. Dostal and Capedri (1978) showed that at the upper limits of medium grade metamorphism, U is lost from the fractures and cleavage planes of ferromagnesian minerals, especially from biotite. Metamorphism does not mobilize U from the major U-bearing accessory minerals such as zircon, magnetite-ilmenite, sphene, rutile and apatite. Dostal and Capedri (1978) calculated that 60 - 70% of U in

metapelites at medium grade metamorphism occurs along cleavage and fracture planes, while the remainder is locked up in accessory minerals. Though absolute U contents of both NS and SS are very low, the marked U concentration of SS-related pegmatites suggests that U was more readily accessible to metamorphic fluids in SS than in NS. Whereas most U in NS is probably tied up in the accessory minerals zircon, sphene and magnetite, and was therefore detritally introduced, a proportion of the U in SS is held in biotite and might have been adsorbed from the waters onto the reducing C and clay surfaces of the developing SS sediment. Such a hydrogenous origin for U is common to fine-grained carbonaceous sediments (Pertlik et al., 1978).

9.1.4.7 Rare earth elements

The lower total REE content of SS relative to NS, and the small but frequently developed positive Ce anomaly in SS may result from one or both of two controlling factors. Firstly the lowered total REE concentrations of coal-hosting rocks is attributed by Herrman (1970) to the low pH conditions known to promote the solution and removal of REE. Soluble Ce^{3+} is oxidized to insoluble Ce^{4+} when river water first encounters sea water (e.g. Piper, 1974), hence Ce has quarter the residence time in sea water of the other light REE's, i.e. 50 years versus 200 years (Wildeman and Haskin, 1965). Theoretically, Ce, being the only REE with a different solubility distribution in Eh-pH space, may be fractionated from the other REE's when subjected to increasing pH and/or Eh (Fig. 9.17), whereas the remaining REE's and Y start to precipitate only when the pH exceeds approximately 7.5 (Brookins, 1983). Ce tends to become strongly bound with clays measuring between 0.02 - 0.1 micron in diameter (Carpenter and Grant, 1967).

Secondly, the clay-rich residual products of a weathered granodiorite are strongly and preferentially enriched in Ce relative to La and Nd when normalized to the parent rock REE composition (Fig. 9.18), and the total REE concentrations of such clays are also depleted (Nesbitt, 1979). Relative to NS, the more Al-rich SS may therefore have inherited its positive Ce anomaly directly from the weathered provenance. Similarly, the lower total REE concentration of SS relative to NS, may also have been inherited from the weathered source.

9.1.4.8 Additional ratios

The fixing of V by organic C, as promoted by increased acidity (e.g. Coveney and Martin, 1983) has lead both Dypvik (1979) and Large (1981a) to use the Cr/V ratio as a measure of reducing conditions, with the lowest ratio signifying the most reducing and acidic environments. Furthermore C, S and Ni are all fixed in sediments formed in reducing environments (sections 9.1.4.1 and 9.1.4.5) thus, combining these elements in plots of Cr/(Cr+V) vs C, S and Ni produces sensitive redox indicators. When applied to NS and SS there is a clear progression from NS through LSS to USS at the high C, Ni and S ends of the plots which coincides with the low Cr/(Cr+V) ends of the spectrum, thus showing that USS was formed in the most reducing and acidic environment of the three rock types, while NS formed under the most oxidizing conditions (Figs. 9.19a-c).

As outlined in section 9.1.4.2, oxidizing waters promote the fixing of both Mn and Fe in developing sediments, while reducing conditions lead to Mn, only, returning to solution. In contrast, Cu precipitates in reducing waters (Heggie and Lewis, 1984) but remains in solution under oxidizing conditions (section 9.1.4.1). The Cu/Mn ratio is therefore expected to be higher than that of Cu/Fe, in reducing sediments, and

vice versa in oxidizing sediments. Combining both parameters in one plot (Fig. 9.20) clearly shows the separation of NS from SS as expected of sediments formed in oxidizing and reducing environments respectively. As in Figs. 6.5f-h, sample ALP054 again plots as an outlier.

9.1.5 Significance of ALP054 geochemistry

Although easily classified as SS, sample ALP054, lying in the immediate structural hanging wall of CSMQ in borehole BH123, has a series of unusual geochemical characteristics outlined in section 6.2.7.3 and in Figs. 6.34a and 9.20. The elements MnO, Co and Fe₂O₃ have all been shown to concentrate in sediments which form under oxidizing conditions (sections 9.1.4.1 and 9.1.4.5), while in a similar environment, C, V, Mo and S are lost as gases or go into solution (sections 9.1.4.1 and 9.1.4.3). The geochemical composition of ALP054 suggests that although the schist was originally deposited in reducing waters to form SS, waters overlying the developing sediment changed from strongly reducing to strongly oxidizing for a relatively brief period of time. Additional sampling would be required to support this conclusion.

9.1.6 SS depositional rates

Formation of the homogeneous SS must have occurred in an environment of prolonged quiescence, as with other black shales. This may be contrasted with near shore (shoreface) marine environments which are normally unstable, with fluctuations in circulation, sediment input and chemical gradient (Skei, 1983). Using a rate of 3mm per year for sedimentation of Framvaren fjord black shales (Skei, 1983, p141), it would take approximately 80Ma of persistent, quiet, stratified water conditions for the 100m of SS to form. This figure is calculated as follows:

Framvaren sediments comprise 96% H₂O and 4% solid matter; SS consists of 6% H₂O and 94% solid matter. Therefore in one year, the amount of SS produced is

$$\begin{array}{ccc} & [4/100 + (6/100 * 4/100)] * 3\text{mm/y} & \\ & \downarrow & \downarrow \\ \text{sediment contribution} & & \text{water contribution} \end{array}$$

i.e. 0.13mm/y of SS.

At this rate it would take 79Ma (say 80Ma) for the 100m of SS to form. Jefferson et al. (1983) accurately calculated accumulation rates of between 0.5 and 4.0m per million years for grey shales associated with the Cirque Pb-Zn-Ag-Ba deposit of British Columbia. These rates translate to between 25 and 200Ma per 100m of shale developed, thus bracketing the 80Ma estimate derived from Skei's (1983) data. These sedimentation rates would fit well within the c.a. 400Ma time span between the 2 000Ma old basement to the Bushmanland Sequence (Armstrong, et al., 1988), and the 1 600Ma old amphibolites (Reid, et al., 1987) which post-date SS.

9.1.7 Calc Silicate Rock plus Manganese Quartzite (CSMQ)

Any model proposed for the formation of Calc Silicate Rock (CS) must account for the negative Ce anomaly and the high MnO, P₂O₅ and base metal contents of this unit (section 6.2.7.1). The mineralization displayed by CSMQ might simply be explained as another pulse of hydrothermal activity similar to that responsible for the two Broken Hill ore lenses. Alternative methods of forming CSMQ will also be examined.

9.1.7.1 Geochemical comparisons

No calcic rock analyses could be found in the literature which approximate CS. Because the Scandanavian shales used above (section 9.1.1) host calcic rocks, analyses of the latter rocks are used for comparison with CS. Also chosen are the calc silicate rocks found in the Broken Hill Australia area as a Proterozoic analogue associated with an orebody. Compared with the Scandanavian shallow marine calc silicate rocks, CS displays extremely high MnO and base metal values, and lower alkali metals and Zr contents (Table 9.6). The MnO-rich nature of CS is confirmed when compared to the Australian calc silicate rocks. CS also contains consistently more P_2O_5 than the other comparative calcic rocks.

The general appearance of Manganese Quartzite (MnQ), its association with CS, and its low Zr content suggest some form of chert precursor to these rocks, and since MnQ cannot be correlated with BQ (section 6.4.1), chert analyses from the literature are used for comparison purposes. As with CS, no obvious analogues could be found. Compared with massive chert overlying volcanogenic manganese ores in Japan, MnQ contains significantly more MnO, in addition to Al_2O_3 , Fe_2O_3 , CaO, K_2O and P_2O_5 , and shows a relative deficiency in only MgO (Table 9.7). The MnO- and P_2O_5 - rich nature of MnQ also preclude simple comparisons with cherts derived from organic or volcanic processes (Table 9.7).

9.1.7.2 Possible hydrothermal derivation

The chemical compositions of CS and of MnQ differ markedly from those of possible correlatives within the Broken Hill (Aggeneys) deposit. Compared with Amphibole Magnetite Rock, CS has an order of magnitude more CaO and less than a quarter the MnO and Fe_2O_3 contents (compare Table 6.11 with Table 6.21). MnQ has an order of magnitude more P_2O_5 than Garnet Quartzite, five times its CaO and double its MnO contents.

It could be argued that the chemistry of the hydrothermal solutions responsible for generating the Broken Hill deposit changed in CSMQ-times to approximate that responsible for causing parts of the Australian Broken Hill deposit, in which the base metal sulphides display a direct relationship with CaO, MnO and P₂O₅ (Stanton et al., 1978). In this model, the negative Ce anomaly displayed by CS would have been inherited from sea water, either in its recirculated, hydrothermal form, or from sea water in the depository.

9.1.7.3 Possible authochthonous derivation

The formation of SS beneath a shallow, stratified, sea water column which was strongly reducing and slightly acidic just above the sediment-water interface (section 9.1.3), may have contributed to the unusual geochemistry of CSMQ. An examination of conditions which exist in stratified water columns shows that the interface between overlying oxidizing and underlying reducing waters frequently also marks a rapid change in temperature, from warm above to cold below (thermocline) (Riley and Chester, 1971; Piper, 1971); in salinity to more saline below (halocline, Pickrill et al., 1981) and thus more dense (pycnocline, Piper, 1971); and frequently from alkaline above to acidic below (Degens and Stoffers, 1976; Riley and Chester, 1971). Because of the rapid variation in physical conditions across a thermocline, a number of elements behave differently on either side of the boundary. Mn²⁺ and Fe³⁺ concentrate in solution just below thermoclines, due to an equilibrium established by the process of their upward diffusion through the thermocline, oxidation, and subsequent precipitation and downward return through the thermocline (Degens and Stoffers, 1976). These authors further suggested that during the Precambrian, water below the thermoclines was nearly saturated with silica since no silica-secreting organisms had yet evolved, and due to the lower pH in anoxic basins, carbonates did not

precipitate. The concentration of soluble P_2O_5 reaches a maximum just below the thermocline (Piper, 1971; Skei and Melsom, 1982), while Al_2O_3 concentrations are far greater above than below the thermocline (Skei, 1983). As mentioned earlier (section 9.1.4.6), the anoxic H_2S -rich water lying below the thermocline in the Framvaren Fjord contains suspended framboidal pyrite and sphalerite (Skei, 1983).

Some form of thermocline disruption must have occurred for a short period during SS times to have allowed the formation of the carbonate precursors to the calcic pyroxenes and amphiboles of CSMQ (Table C.5). Degens and Stoffers (1976) suggested that a drop or break-up of a thermocline causes the destabilization and precipitation of the elements Mn ($Mn^{2+} \rightarrow Mn^{4+} + 2e^-$), Fe ($Fe^{2+} \rightarrow Fe^{3+} + e^-$), Mg, carbonates, P, Si, and the minerals pyrite and sphalerite. At Lake Kivu, $(FeMn)CO_3$ and $MgCO_3$ rapidly precipitate when the thermocline drops, such that stacked layers of manganosiderite reflect an oscillating thermocline. The dissociation of soluble phosphoric acid (HPO_4^{2-}) to insoluble PO_4^{3-} requires an increase in pH (Sheu and Burkart, 1982). The rapid decrease in Al content below the thermocline (Skei, 1983) suggests that a drop or breakup of the thermocline would increase the amount of Al in solution and therefore decrease the quantity of hydrogenous Al reaching the sea bed.

Thermodynamic modelling by Giordano and Barnes (1979) of Pb behaviour in aqueous solutions at low temperatures has shown a strongly positive increase in Pb solubility as a function of a_{H_2S} (Fig. 9.21). At 30°C and total sulphur activity < 0.1 , the Pb concentrations are maximized and constant at $pH < 6$, while at higher sulphur activities a Pb maximum is achieved at $pH = 7$ (Fig. 9.22a). With an increase in temperature to 100°C, the soluble Pb maximum increases by an order of magnitude and occurs at $pH < 6$ (Fig. 9.22b). At 30°C (Fig. 9.22a) a

decrease in the S activity and/or increase in pH due to a disrupted thermocline would lead to Pb precipitation as cerussite or anglesite (Fig. 9.23).

A strongly negative Ce anomaly such as that developed in CS (section 6.2.7.1) may be directly inherited from sea water (Tlig and M'Rabat, 1985) and these authors showed that such depletions are common to Tunisian Cretaceous carbonates formed beneath sea water in a variety of environments, thus if CSMQ precipitated rapidly, it is likely that the water signature would be reflected in the rock. In addition to the positive Ce anomaly inherited by some SS samples from the weathered provenance (section 8), the developing SS may have preferentially accumulated the Ce lost from sea water. Reid et al. (1987) found that the Big Syncline marbles at Aggeneys have ^{13}C ratios compatible with sea water derivation, and they suggested that certain low ^{18}O values usually indicative of a non-marine origin may have resulted from metamorphic exchange. Most of the geochemical characteristics of CSMQ viz. unusually high concentrations in P_2O_5 , MnO, Pb, MgO, CaO, SiO_2 , Zn and S; depletions in Al_2O_3 ; and a negative Ce anomaly, are therefore accounted for in the model of a dropped or disrupted thermocline.

The control which physical properties had on the basin water chemistry provides an explanation to the factor grouping of P_2O_5 , MnO and Pb in SS (Factor 5; Fig. 6.7). During times of basin stagnation, these elements remained largely in solution but concentrated at the thermocline boundary, while during the period of thermocline disruption, the complexes of P, Mn and Pb precipitated to be incorporated into CSMQ.

In seeking mechanisms to explain the thermocline destabilization, it is noteworthy that the only unequivocal conglomerate recognised by the author in the Broken Hill-Maanhaarkop area occurs as a 2m² outcrop adjacent to CSMQ (section 4.2.2.2). An inrush of pebbles into a stratified, partially enclosed, stagnant basin must have been triggered by a storm or earthquake. The net effect of such violent changes would be to temporarily destroy any water stratification, particularly around the edges of a micro-basin, and to increase the pH due to an inrush of fresh water together with pebbles. Concentrations in the elements U, As, Sb and Ag are not, however, accounted for in such a model.

The distribution of SS and CSMQ shows that the postulated thermocline extended from at least Broken Hill to Maanhaarkop, a strike distance of 5km. Reasons for the lensoid nature of CSMQ might reflect basin geometry. Initial disruption of the thermocline would have led to CSMQ precipitation over the entire basin, but re-establishment of the thermocline initially in the deepest parts of the basin would have caused rapid re-dissolution, leaving lenses of CSMQ preserved peripherally to the basin depocentre. By the time the thermocline was established back to its original level, these lenses may have been partially buried by sedimentation and hence rendered less prone to acid attack, analogous to the manganosiderite lenses in Lake Kivu (Degens and Stoffers, 1976).

9.1.7.4 Preferred model for CSMQ origin

Neither of the suggested models for CSMQ derivation completely satisfy all the relevant facts. Whereas the geochemical differences between CS and MnQ on the one hand, with rocks of the Broken Hill (Aggeneys) deposit on the other, suggest different modes of formation for CSMQ relative to the orebody, the elevated concentrations of U, Sb, As and

Ag in MnQ favour derivation from some hydrothermal source. Both processes may well have operated simultaneously. The thinness of CSMQ and its location within the reduced SS indicate that irrespective of whether the hydrothermal or disrupted thermocline process was dominant, the basin geometry and chemical conditions of basin waters both above and below the thermocline would still have caused precipitation of most of the elements comprising CSMQ, and would have constrained preservation of that rock. It is suggested that fault-related, hydrothermal activity which produced the elements U, As, Sb and Ag, as well as a possible component of the MnQ silica, much like the volcanogenic or exhalative source of the massive Japanese cherts (Watanabe et al., 1970), was associated with earthquakes which triggered the discharge of conglomerate into the basin. In general, it is likely that the more violent discharges of metalliferous hydrothermal fluid into a meromictic basin, will trigger the precipitation of the elements Mn, Fe, P and Si as a result of disruption of the thermocline, and these elements will accumulate as gangue components of ores formed on the sea floor in developing black shale environments.

9.1.8 Biotite Graphite Zone (BGZ)

The similarity between BGZ and USS established in section 6.2.7.2 indicates that the former is also a type of black shale. The lower SiO₂ and Zr content of BGZ (Fig. 6.13) suggests that BGZ is comprised of more hydrogenous/biogenous, and less lithogenous (or clastic) material than USS. BGZ compares even more favourably with black shales than does SS in view of its higher concentrations of Mo, V, Ni and C (Table 9.3). With regard to the relatively elevated concentrations of MnO, Pb, Zn and Cu, and depressed Na₂O, S and Sr in BGZ (section 9.1.1), a likely cause is the passageway created by BGZ

for Recent oxidizing and acidic meteoric waters, as revealed in underground exposures, from the structurally overlying strata which include the Broken Hill orebody. Such Recent contamination may also account for the decreasing Zn concentrations found in SS progressively further from the orebody (Fig. 6.34a).

The high clay content of BGZ is the likely reason for its elevated C concentration since C adsorption increases with decreasing clay grain size (Sharma, 1971). In order for the clay- and C- rich BGZ to have formed, less detritus contributed to BGZ development than to that of SS. The formation of BGZ and SS under such quiet conditions effectively capped and preserved the Broken Hill orebody.

9.2 Structural geology summary

On the basis of physical evidence it was shown that the rock-types at Broken Hill may be correlated directly with those at Maanhaarkop (section 5.1), hence continuity of strata along strike exists for over 5km. It is also necessary to establish to what extent the structural superposition of rocks across strike at Broken Hill may be considered a stratigraphic succession, and what their facing direction is. Conclusions will be drawn from evidence presented earlier.

At Broken Hill the interfaces between lithologies of contrasting competency, such as between schist and quartzite, and along BGZ, would be the planes most likely to act as zones of structural dislocation. NS and WQ form a single continuous succession (sections 4.2.1 and 6.6.1), while continuity exists between NS, MDS and DQ without much lateral movement having occurred (section 6.6.1). Localization of the MDS gossan to the immediate vicinity of the Broken Hill orebody in a tectonic environment in which subhorizontal lineations and slickensides predominate (section 5.1), also militates against the

gossan forming part of a thrust slice off the Broken Hill orebody since sub-vertical slickensides would have resulted. The unusually high Y concentrations in MDS (74ppm) and OEGQ (103ppm) from a borehole through the succession at Maanhaarkop confirm that little structural dislocation exists between these two rock-types. The regional recurrence of the WQ-MDS-DQ succession from Broken Hill to Namiesberg to Wortel, and the different shapes of the WQ and DQ REE patterns (section 6.4.4) indicate that these quartzites could not originally have formed a single horizon duplicated by thrusting or folding. The Zn concentrations of both surface outcrop and borehole core samples of NS, which is separated from the orebody and OEH by BQ, increase progressively nearer the orebody, from as far away as 5km (Fig. 9.25). It is unlikely that the Broken Hill deposit could fortuitously have been structurally juxtaposed with the maximum Zn concentration in NS.

The anomalously high Pb content of SS (Fig. 7.6c) strongly suggests that if any major dislocation occurred along the slickensided BGZ, then this post-dated the pegmatite-forming event to which the SS Pb anomaly was probably causally related (section 9.1.2). The geometric location of CSMQ peripherally to, but seldom lying directly structurally below the orebody, is suggestive of the orebody occupying the deepest part of the basin (section 9.1.7), and renders improbable the likelihood that significant displacement occurred along BGZ. Whether the entire metasedimentary succession is allochthonous with respect to the gneisses, as proposed by Watkeys (1986), lies outside the scope of this thesis.

Regionally, the gneisses occur below the metasediments, while at Broken Hill gneiss overlies the schist-quartzite-orebody succession (section 4.1). Additional physical evidence which suggests overturning of the succession along the Broken Hill line of outcrops

is inversion of the cross-bedding in X-Ray radiographs of orientated quartzite from Froneman se Kop (section 4.3). Examination of many more samples would be required before placing much reliance on this single observation. The geochemical data has, however, shown that in contrast to SS, NS bears the signature of the Broken Hill orebody in respect of base metals, Ba and REE concentrations (section 6.2.6). This NS characteristic does not persist away from the Broken Hill area since both NTS and STS fail to show the ore-related signatures. The oxidizing environment to which the SS sample ALP054 was clearly subjected (section 9.1.5), must have immediately predated deposition of CSMQ as explained in section 9.1.7.3, thus supporting the interpretation of the Broken Hill succession as overturned.

9.3 Quartzites: Genesis and depositional environment

9.3.1 Geochemical comparisons with chert and sandstone

Comparisons of geochemical analyses from Broken Hill Quartzites (BQ) with those of highly siliceous cherts and clastic quartzites, reveals that of the analysed elements, only the Zr content of BQ is significantly higher than that of chert. The oxides and elements MnO, MgO, CaO, Na₂O, Ba, Sr, Mo, Cr, Ni and Co in BQ are all at lower levels of concentration than in chert (Table 9.8). No trace element analyses for quartz arenites were located, but their major element contents are of similar magnitude to those of BQ. In chert, the higher content of a number of the above oxides and elements such as MgO, CaO, Sr, Cr, Ni and Co probably reflect the influence of the genetically related mafic and felsic volcanics. A comparison between the shapes of REE patterns from deep oceanic chert associated with basaltic volcanism, and a sample of WQ (ALP067) reveal a clear distinction based on the marked negative Eu anomaly of the BQ sample, and its relatively higher LREE content (Fig. 9.26). Such features

typify felsic rocks (section 8), whereas the chert REE patterns shown are inherited from their mafic source rock (Crerar et al., 1982).

The extremely high SiO_2 content of BQ results in most samples plotting in the quartz arenite field of Pettijohn et al. (1972) (Fig. 9.27). BQ lie within the high SiO_2 range of quartz arenites, and importantly, MgO , CaO , Na_2O and K_2O levels are generally as low as those of quartz arenites, in contrast to the relative alkali- and alkali earth- rich cherts. In a binary plot of SiO_2 vs $\text{CaO} + \text{MgO}$, BQ fall within and close to the field defined by four of the five quartz arenite analyses, and all except one analysis (ALP124) fall well outside of the high-silica chert field. Rather, BQ lies along a mixing line between NS and pure SiO_2 (Fig. 9.28) as also defined in Figs. 9.27 and 9.29 where the orientations of the four BQ subsets all extend towards NS. Attention is drawn to the Maanhaarkop samples of WQ and MDS (ALP124 and ALP125, respectively) in Figs. 9.28 and 9.29 since they frequently fall outside of the fields defined by the remaining WQ and MDS analyses. These two samples have elevated base metal contents as discussed later (section 9.3.5), which may have a bearing on their unusual geochemistry.

BQ displays a $(\text{CaO} + \text{Na}_2\text{O})/\text{K}_2\text{O}$ ratio even lower than that of average sandstone and quartzite (Fig. 9.29), and geochemical comparison with quartz arenites (Table 9.8) indicates that this may be attributed to BQ having a higher K_2O and lower CaO content than quartz arenite. The high $\text{SiO}_2/\text{Al}_2\text{O}_3$ ratio of BQ borehole core compares well with the average quartzite $\text{SiO}_2/\text{Al}_2\text{O}_3$ ratio of Garrels and McKenzie (1971) (Fig. 9.29), while the BQ surface samples fall higher up on the plot due to the previously mentioned surface sampling bias towards the most quartz-rich rocks. The entire linear trend from NS to BQ lies parallel to, but displaced towards a lower $(\text{CaO} + \text{Na}_2\text{O})/\text{K}_2\text{O}$ value, than

the sandstone to quartzite trend shown by Garrels and McKenzie (1971) (Fig. 9.29).

Erlank et al. (1978) suggested an average of 19ppm Zr for flint and chert from various locations, while Maxwell (1953) failed to even detect Zr in 24 samples of chert flint, ranging in age from Precambrian to Recent, and having a wide geographic distribution. The higher Zr content of BQ (108 - 149ppm; Table 9.8) therefore suggests a detrital, terrigenous, rather than a chert origin, and the morphology of heavy minerals (section 4.3) corroborates this interpretation. Since NS formed from detritus deposited in an agitated environment, and strong genetic links exist between NS and WQ, MDS and DQ (sections 4.2.1 and 6.6.1), placer processes apparently led to the formation of BQ. Notwithstanding this evidence, the possibility of a chert precursor to BQ as proposed by Moore (1986), will still be examined prior to comparing BQ with various sandstones.

9.3.2 Chert as a precursor

Krauskopf (1959) suggested that some form of subaqueous volcanic or exhalative Si input is necessary to produce the vast quantity of Si contained in chert. This Si later accumulates by inorganic or organically-assisted processes in a series of environments which include deep water siliceous ooze both associated and not associated with pillow lavas and serpentinites (Thurston, 1972; Grunau, 1965; Crerar et al., 1982; Gundlach and Marchig, 1982), and the shallow to intermediate water cherts of Bramlette (1946) and Hughes (1976). Various chert-types are examined below, and their characteristics then compared with those of BQ. The organically derived cherts are of no further consequence to this study since silica-secreting organisms had not developed prior to 1.3Ga (Cloud, 1981, p13).

The Caballos Formation of western Texas has similar geometric dimensions to BQ, extending for over 30km with a 45m thick lower novaculite (massive, milky white chert) and upper 120m thick novaculite being underlain, overlain and separated by interbedded chert and shale (Folk and McBride, 1976). McBride and Folk (1977) found numerous shallow water- to subareal- indicating structures including sand pockets within novaculite, petrified logs, evaporite pseudomorphs and paleosoil features. The accessory minerals and inclusions comprise illite, carbonate minerals, radiolaria, spores, organic matter and pyrite.

The Strelley Pool chert of the Archaean Pilbara block, Western Australia (Lowe, 1983), formed in a large (120km diameter), restricted, hypersaline basin. The chert is 25m thick, continuous over tens of kilometers and lies near the top of a volcanic greenstone belt. Evidence of abundant biogenic activity includes organic laminite, stromatolites, carbonaceous mats and oncoliths, and the lack of shale suggests low detrital input. One-to-fifteen centimetre thick layers of laminated and cross-laminated "wind-blown" sand, containing up to 5% zircon plus opaque minerals, fill cavities in underlying dessicated quartzite. The preservation of silicified evaporites is widespread.

The shallow water cherts from marine and lacustrine environments outlined above display the important common parameters of widespread evaporites and carbonates, both of which are lacking in BQ. Since pyritic quartzites on the adjacent farm of Koeris still contain visible graphite, the argument could not be used that all C in quartzite at Broken Hill may have been lost under diagenesis and/or metamorphism. The lack of volcanoclastic rock fragments or feldspar phenocrysts further preclude comparison of BQ with Conception Group

cherts, while the Strelley Pool chert has no greenstone counterpart in the shale- and felsic gneiss- dominated environment of Aggeneys. With regard to the development of subparallel, single-grain-thick heavy mineral layers of BQ, such concentrations are either lacking in shallow to intermediate water cherts, or are present together with sand in pockets or as fillings in dessicated chert surfaces.

The 128 million tonne Beowawe siliceous sinter in Nevada (Rimstidt and Cole, 1983) comprises a delta shaped mound (65m thick; 1,6km long) which formed from geothermal solutions that welled up the Malpais graben-bounding fault. Though silica composition of this deposit is not available, elements of interest include Na (0,28 - 0,49%), Ca (0,23 - 0,25%) and Sr (82 - 181ppm). The limited lateral extent of the mound shaped siliceous sinter contrasts with the tabular habit of BQ. Additionally, the elements Na, Ca and Sr in which sinter is enriched, are strongly depleted in BQ.

9.3.3 Sandstone as a precursor

Horne (1979) suggested that there exist only three ways of producing clean quartz arenites viz. by diagenetic overgrowths on sand grains; by erosion of a pure quartz provenance; and where sands have been winnowed of finer-grained and less stable minerals. Silicified soils are rarely developed (Horne, 1979), and the regular geochemical gradations from NS into WQ effectively discount either silicified soils or a pure quartz provenance as precursors to BQ. Beach-barrier shorelines, as well as additional environments in which quartz-rich clastic sediments form, are now examined for their applicability to BQ genesis.

9.3.3.1 Beach-barrier shoreline sands

A beach-barrier island system has three components which are a subaerial, sandy barrier island chain; an enclosed body of water (lagoon or estuary) lying behind it on the landward side; and tidal inlets which join the estuary to the sea (Reinson, 1979). Barrier islands form along continental margins where an abundant sediment supply is fed to a low gradient, continental shelf lying adjacent to a low relief coastal plain. Tidal ranges must also be as low as 4m otherwise barrier islands cannot form. Tidal ranges of between 2 - 4m produce short, stunted barrier islands whereas areas of microtidal variation (< 2m) produce long, linear barrier islands with insignificant tidal inlets or deltas. The shoreface (seaward side) acts as a major source of sediment for the barrier island. The lower shoreface (most seaward side) comprises fine to very fine-grained sands interlayered with silty mud, while the middle shoreface contains sandbars comprising clean sands with minor silt. The cleanest sands lie in the intertidal zone i.e. the foreshore. Laminations are mainly planar (sub-parallel). Backshore dunes are wind generated while further landward, washover deposits comprising back-barrier sand flats, are formed. The lagoonal facies of interbedded sandstone, shale, siltstone and organic matter, reflect the most landward of the barrier island components. According to Reinson (1979, p70), regressive, or prograding beach-barrier sequences coarsen upwards whereas transgressive sequences show neither upward-coarsening nor upward-fining features. The transgressive sequences are well preserved only if there is a rapid rise in sea level. In contrast, regressive sequences have much greater preservation potential.

The Late Miocene Cohansey quartz arenite of Southern Jersey (Carter, 1978), displays all the features of a barrier island system as described above. The quartz arenite attains a maximum thickness of

30m, although Carter (1978) suggested that a slow regression or a number of regressive-transgressive phases would cause thicker sand deposits. Heavy mineral layers of between < 1cm to 30cm thick occur in various laminated sand facies, with the well sorted foreshore sands containing laminations continuous for over 10m, with bases sometimes defined by heavy minerals. In the Cohansey sandstones the carbonaceous remains of abundant burrowing animals are still preserved.

The beach-barrier shoreline sand model could adequately account for all the physical and chemical features of BQ. Though the thickness of BQ is somewhat greater than, for example, the Cohansey quartzites, it is feasible that a persistent regression, effected by a constant rate of basin subsidence or a constant rate of provenance uplift, possibly with minor transgressive phases, could lead to development of the 80m thick WQ. Jurassic barrier sandstones up to 47m thick have been documented in southern England by Davies et al. (1971). The strike extent of over 50km for the Carter Caves sandstone of Kentucky (Reinson, 1979), testifies to the extreme lateral continuity of microtidal beach-barriers, while the down-dip extent is a function of the time span over which progradation continued. In BQ the presence of heavy mineral layers having a predominantly planar habit is consistent with intertidal foreshore sedimentation. The extensive carbon remains in the Miocene Cohansey sandstone which are attributed to burrowing animals (Carter, 1978), had not yet evolved during the mid-Proterozoic, thus the lack of carbon in BQ does not detract from the beach-barrier model.

The only components of the beach-barrier system missing from BQ are the tidal inlets, washover deposits and backshore dunes. Tidal inlets would be poorly developed in conditions of microtidal variation, which

would also promote the development of persistent barrier islands. At Broken Hill the pelitic and psammitic rock types MDS, DQ, HS and UFS could conceivably represent washover deposits and backshore dunes (although no specific evidence is led to support the possibility), since they lie between the postulated beach-barrier, WQ, to the north, and the estuarinal SS (section 9.1.4) to the south.

9.3.3.2 Shallow marine siliclastic sandstones

Shallow marine siliclastic sandstones consist of sand blankets and minor shelf sand bars. Sand blankets comprising enormous volumes of silica, extend for hundreds of kilometres. The Jura quartzite sequence of Scotland is some 5 000m thick, with individual sandstones up to 350m thick. Off the Oregon coast (on the continental shelf) the sand facies occurs at depths of 50 - 100m and comprises sands, gravels, quartz, feldspar and rock fragments (Johnson, 1978, p223). Blanket sandstones are typically cross-bedded. Winnowing of light material (Johnson, 1978, p232) could conceivably lead to heavy mineral concentrations.

Minor shelf sand bars range in size from 3 - 10m in height, 1 000 - 2 000m in width and tens of kilometres in length. They display sharp contacts with their underlying muddy sediments (Johnson, 1978, p226).

Blanket sandstones are far too thick, and too immature to be compared with BQ. The cross-bedded nature of blanket sandstones is not reflected in the planar to low angle bedding found in WQ. By contrast, the 80m thick WQ is too thick and extensively developed to be compared with the 10m high shelf sand bars, which are only 1 - 2km wide. Similarly, their sharp contact with muddy sediments differs markedly from the gradational contact of WQ with NS.

9.3.3.3 Deltaic sandstones

Deltas are composed of a number of different rock types, but three factors tell forcefully against BQ having originated as deltaic deposits. These are that deltas as a whole form discrete shoreline protruberances, although wave-dominated deltas may have linear fronts (Miall, 1984); deltas tend to form exceptionally thick sedimentary successions (Elliot, 1978, p97); and the active river courses in a delta produce distinctive bar finger sands which have a linear, rather than planar geometry (Pettijohn et al., 1972, p467). BQ have a tabular form, and the entire Aggeneys supracrustal succession is less than 1 000m in thickness. Furthermore, deltaic sandstones have high angle cross-beds (Miall, 1979, p48), versus planar bedded to low angle cross-beds in the Aggeneys heavy mineral layers. The planar bedding which is the dominant bedform of the quartzites, in no way resembles the typical convolute bedding produced in deltas due to rapid loading of sand onto unconsolidated mud.

9.3.3.4 Massive sandstone facies of turbidites

The massive sandstone facies of deep water turbidites comprise a series of thick, graded beds which are rapidly deposited (Walker, 1979, p92). Besides the graded beds and concave-up fluid escape features, these rocks contain no sedimentary structures. It is doubtful whether such rapid dumping could lead to the SiO₂ purity of BQ.

9.3.3.5 Fluvial sandstones

The extensive nature of BQ, lack of channels and lag deposits (Walker and Cant, 1979), and their extreme silica purity, are not consistent with fluvial sandstones. Fluvial conditions are unlikely to produce quartz arenites, no matter how prolonged the river transport (Pettijohn et al., 1972, p224).

9.3.3.6 Lacustrinal siliclastic sandstones

Although in general, sediment types in lakes differ little from their marine counterparts, the lower wave energy and common fluctuation of water level result in compositionally less mature sediments than are produced in the marine environment (Collinson, 1978, p65). The extreme silica purity of BQ is therefore unlikely to have been produced by lacustrinal conditions.

9.3.3.7 Aeolian dunes

Although aeolian sandstones are characterised by a lack of clays, micas or gravels (Collinson, 1978, p92), their large scale cross-bedding at relatively high angles (Walker & Middleton, 1979, p33), differs from the frequency and attitude of heavy mineral laminations in WQ. Furthermore the strongly developed geochemical gradation from NS into WQ could not be explained by aeolian processes, as no preferred vertical variation has been documented from dunes (Walker and Middleton, 1979, p40), however, as long as the BQ-NS contact was developed subaqueously, a component of BQ could have developed subareally as dunes. The average maximum thickness of aeolian dunes of >> 100m, greatly exceeds average BQ thicknesses. Beach foreshores have a higher mica content than dunes (Shepard and Young, 1961) since wind winnowing deflation processes effectively remove all the micas (Krynine, 1942). The presence of muscovite as the next most abundant mineral after quartz in BQ (section 4.3) tells against an aeolian origin for the major portion of BQ.

9.3.4 Genesis of heavy mineral layers

The common methods of producing heavy mineral layers in sandstones are water winnowed residues and aeolian deflation residues. Authigenic and metamorphic generation of zircon is also possible.

The most common current environment for the development of heavy mineral layers is along submerged beaches (Mitchell and Reading, 1978, p453). Carter (1978) attributed the heavy mineral layers of the Cohansey barrier sand deposit to water winnowing of low density grains from fine, high density ones. Aeolian deflation residues can concentrate heavy minerals when windstorms remove silt and less dense material from bedloads (Collinson, 1978), and this process may have been responsible for generating a small proportion of the heavy mineral layers in BQ, i.e. in that part of BQ which is of possible aeolian origin. In addition to the heavy mineral layers, the common dissemination of heavy minerals throughout BQ, however, suggests that little of the heavy mineral concentrations are of aeolian origin. Water as opposed to wind winnowing was therefore probably responsible for generating most of the BQ heavy mineral layers.

Having already demonstrated the gradational nature of NS into BQ and MDS, it can be seen in Fig. 9.30 that heavy minerals, as indicated by Zr content, were optimally concentrated at a whole rock composition of approximately 82% SiO₂. At higher SiO₂ levels, the sheer silica purity of the rock caused the Zr content to decrease markedly.

Saxena (1966) showed that zircons are neither as resistant to chemical and physical breakdown as commonly thought, nor are zircons solely a high temperature, igneous mineral. Authigenic zircons frequently comprise up to 90% of the zircons contained in a sediment, having formed from a fine-grained "brown mass" comprising rutile, ilmenite and zircon. Metamorphic zircons formed in this manner tend towards euhedralism. Saxena (1966) stressed that little if any authigenic zircon will form around zircons hosted by clean sediments which lack the "brown mass". The rounded zircons located in the clean BQ matrix

suggests that except for rare idiomorphic zircon overgrowths on rounded zircon grains, no authigenic or metamorphic zircon growth occurred in BQ. Rounded rims on zircon which return 2,0Ga old ages (section 8.1.2) attest to overgrowths having been produced in the provenance. Rounding is the frequently observed morphology of zircons in beach sand environments (e.g. Shepard and Young, 1961), and must have resulted from abrasion during clastic travel, as suggested by Pettijohn et al. (1972).

9.3.5 Conclusions

Examination of the physical and geochemical attributes of silica-rich rocks reveals that no chert could have acted as a precursor to BQ. Moore (1986) argued that the presence in Namaqualand quartzites, of (a) minor ferruginous units; (b) widespread S enrichment; (c) local B, Zn and Pb rich units; and (d) Ca- and Mg- rich bands, indicate that the quartzites themselves were cherts. While it is agreed that iron- and base metal- rich units within the quartzites are probably of chemogenic origin, the lenticular shape of these units and their mineralogy resemble, at a smaller scale, those of the Aggeneys-Gamsberg orebodies. These thin units were probably formed by processes which gave rise to the orebodies (discussed later in section 10), and therefore do not reflect on the genesis of their enclosing quartz host rocks. The widespread S referred to by Moore (1986) is preferentially concentrated as pyrite in the stratigraphically higher DQ at Broken Hill, Namiesberg and Wortel, and is interpreted as reflecting the change from oxidizing conditions under which NS and WQ formed, to the reducing environment in which SS developed. The Ca- and Mg- rich bands referred to by Moore (1986), are not found in the current study area, and cannot be commented upon here.

The evidence presented suggests that BQ represents a metamorphosed, highly mature detrital sandstone or quartz arenite which, due to the lack of carbonate cement, can be further classified as alkaline-earth-poor quartz arenite (Pettijohn et al., 1972, p62). Quartz arenites form at craton margins (Pettijohn et al., 1972, pp224 and 547; Potter, 1984). The microtidal, partially submerged beach-barrier along a continental margin is suggested as the most likely environment in which BQ formed, and the relatively thick development of quartzite suggests a constant rate of subsidence and/or provenance uplift. Following from the beach-barrier model and the gradational link with NS is the assertion that the shoreline prograded. Furthermore, the upward coarsening successions typical of beach-barrier facies agrees with the interpretation that NS lies stratigraphically below BQ (section 9.2).

The majority of the BQ zircon grains are of detrital origin, as are the rounded rutile grains and hematite-ilmenite intergrowths, testifying to the high preservation potential of zircon up to the border of granulite facies metamorphism. A percentage of the muscovite contained in BQ may also be of direct detrital origin, however, the quartz grain morphologies do not reveal any information regarding their detrital history due to extensive recrystallization. The presence in DQ of gahnite on Klein Kop, and vein-bounded tourmaline on Maanhaarkop possibly testify to the presence of mineralizing processes, as does the Pb value of 47ppm in the Klein Kop sample and 67ppm Zn in a DQ sample on Broken Hill. Highly anomalous values of Cu, Zn, S and Y from borehole intersections of WQ, MDS and DQ (ALP124, 125 and 126) on Maanhaarkop deserve exploration follow-up work.

9.4 Local sedimentary genetic model

9.4.1 Physical environments

Of the four metasedimentary formations defined at Broken Hill, OS is not directly used for modelling purposes because of geochemical complications resulting from the presence of the orebody. It was shown that NS developed in an oxidizing, agitated environment of the shoreface type from detrital, terrigenous sediment, whereas SS is a metamorphosed black shale partly of hydrogenous origin, having formed in a quiet, meromictic, reducing, estuarinal or lagoonal basin which prevailed for some 80Ma (section 9.1.6). The thermocline was disrupted once, leading to precipitation of CSMQ and to oxidation of SS in the immediate stratigraphic footwall of CSMQ. Structurally sandwiched between NS and SS the metamorphosed quartz arenitic BQ formed as a beach-barrier along a continental margin in a microtidal environment (section 9.3). Although now complicated by structural disturbances, strong indications exist that the three units NS, BQ and SS were spatially related in the depository, since NS grades into WQ, and both of these rock-types display physical and geochemical links with MDS and DQ (section 6.6.1). NS and the detrital component of SS were probably derived from a similar provenance (section 8). The geometric positioning of the orebody with respect to CSMQ (section 9.1.5) suggests little movement along BGZ. Justification therefore exists for seeking a simple, unifying sedimentary model for the genesis of NS, BQ and SS.

It was shown that SS and BQ were generated in sea water and under the influence of coastal processes (sections 9.1 and 9.3.5). The estuarinal, beach-barrier and shoreface environments were shown in sections 9.1.2, 9.1.4 and 9.3 to accord well with the physical and geochemical constraints imposed by SS, BQ and NS respectively, whereas pelagic sedimentation can be discounted on the grounds that, *inter*

alia, an agitated shoreline environment was necessary for the development of BQ (section 9.3).

Only at the interface of continental and oceanic environments are the divergent parameters of shallow, agitated and quiet sea water conditions fulfilled. The beach-barrier model offers the three major components sought i.e. foreshore (NS), beach-barrier sands (BQ) and estuary/lagoon (SS). It follows from the evidence for an inverted stratigraphic succession (section 9.1.5 and 9.2) that NS stratigraphically underlies and coarsens upwards to WQ, which accords well with the high preservation potential of a prograding beach-barrier system (section 9.3.3.1). Reinson (1979) showed that in this progradational environment, the beach-barrier sandstone is then overlain by the reducing beds (Fig. 9.31) with which SS may be equated. These factors suggest that SS prograded over BQ which in turn prograded seawards over NS. Discriminant function analysis indicates that NS and OS, as opposed to SS, were probably very similar rock types, suggesting that NS-type sedimentation persisted landwards beyond the quartzites. In the beach-barrier model this implies that OS was largely a washover deposit comprising redistributed NS shoreface sediments. The major change in sedimentary conditions therefore occurred somewhere near BGZ, and not at the quartzites.

The paleogeography and sedimentology of the Mississippi River coastal area offers an analogy with the Broken Hill metasediments. A Late Jurassic shoreline straddled the Arkansas-Louisiana State boundary, with sediments of the Cotton Valley Group being deposited as terrestrial coastal plain red beds to the north, followed progressively southwards by lagoonal black pelites (Hico Shale), barrier island psammite (Terryville Sandstone), and open marine pelites (Bossier Formation) (Thomas and Mann, 1966). As the shoreline

prograded southwards, and the basin deepened in that direction, the marine shales were sequentially overlain by the beach-barrier sandstone and the lagoonal pelites (Fig. 9.32). All contacts between different lithologies are gradational. Maximum documented thicknesses for the units are 610m (Hico Shale), 426m (Terryville Sandstone) and 200m (Bossier Formation). The entire sequence extends laterally for well over 160km, and continues down dip for in excess of 10km. Knowles Limestone overlies the complete succession, and thickens towards the south. The lithological analogies drawn are that SS equates with Hico Shale, BQ with Terryville Sandstone and NS with Bossier Formation. In this dynamic model any one stratigraphic horizon is diachronous (Figs. 9.32 and 9.33), thus all three rock-types formed synchronously, with BQ and then SS progressively building out seawards over earlier formed NS. Deeper parts of the basin, as defined by sea floor topography, would then have preserved thicker successions of NS.

There are certain fundamental similarities between the host rocks to the Broken Hill (Aggeneys) deposit, and to the Broken Hill (Australia) orebody in an environment at somewhat higher metamorphic grades. Although the nature of premetamorphic rocks at the stratigraphic base of the sequence in Australia (Suites 1 to 3) are still hotly debated (e.g. Wright et al. (1987) claim these are metasediments while Stevens and Stroud (1983), Plimer and Lottermoser (1988) and Willis et al. (1988) interpret these as metavolcanic rocks), Suite 4, the Mine Sequence, and younger rocks, are interpreted as predominantly of metasedimentary origin by all workers. The Broken Hill (Australia) orebody lies within a 1 500m-thick pelitic-to-psammitic suite of rocks (Suite 4) which are in turn overlain by 700m of graphite-bearing, pelitic and psammitic rock which hosts lenses of calc silicate rock (Stevens and Stroud, 1983).

The Broken Hill Quartzites (BQ), as metamorphosed quartz arenites, offer valuable information regarding the tectonic setting of the depository. Due to the extreme maturity of quartz arenites, they must have formed along a cratonic margin (Pettijohn et al., 1972, pp.224 and 547) where sedimentary working and reworking is most effective. Dickenson et al. (1983) showed that the most quartz-rich sands are derived from stable craton interiors having low relief (p223), with progressively less mature sediments being derived from more tectonically active areas such as magmatic arcs. Potter (1984) tested the Dickenson et al. (1983) hypothesis by sampling beach sands around the entire South American continent, and found that the most mature beach sands, corresponding to quartz arenite, are forming along the tectonically passive or trailing east coast, having derived their sediment from the Guyana and Brazilian shields. A plot of both Broken Hill and Regional Quartzites on the discriminant diagram of Bhatia (1983) clearly classifies all quartzites as having formed along a passive margin (Fig. 9.34). The extreme purity of BQ and their likely derivation along a craton margin strongly suggest a cratonic interior provenance. In addition, the maturity of BS (section 9.1.2) and the lack of a basaltic to andesitic provenance (section 8) militate against a fore arc basin setting since these tend to accumulate immature greywacke-type sediments (Bhatia and Taylor, 1981).

9.4.2 Geochemical differentiation

It is proposed that a provenance of granodioritic composition (section 8.3) represents the starting point for the geochemical sedimentary differentiation process which led to the Broken Hill metasediments. According to various weathering schemes (e.g. Garrels and McKenzie, 1971) Ca, along with Na would rapidly be removed from the provenance to the sea. Though Na remains largely soluble, Ca is precipitated as

carbonate minerals at some distance well removed from the provenance. Except for CSMQ, the entire suite of Broken Hill metasediments is Ca-poor, thus the calc silicate metasediments found both to the south and east of Aggeneys (Paizes, 1975) might represent the missing Ca which accumulated in a more distally removed, stable shelf environment. It is suggested that the granodioritic source first underwent residual Al enrichment towards an SS type composition (Fig. 9.35) before the process of sedimentary differentiation took place. This is represented in Fig. 9.36 by the granodioritic composition shifting first to the left in the direction of SS and the base of NS, solely due to in-situ weathering. This residuum would then have been transported to the depository. During shoreface deposition and reworking of such detritus, the NS chemical composition was then enriched in silica and depleted in alumina, reflecting progressive removal of micaceous minerals and clays from disintegrated feldspars. The physical and geochemical differentiation reached a boundary condition with the development of BQ (Figs. 9.35 and 9.36). The entire process may be schematically represented by granodiorite first undergoing residual Al enrichment due to weathering, whereafter these residual products were subjected to different depositional histories, with SS formation being more dominated by clay deposition, as opposed to the largely quartz and heavy mineral concentrating processes which led to the development of NS and BQ (Fig. 9.37).

9.4.3 Oxygen isotopes

The wide variation in quartz oxygen isotopes between NS and SS (section 6.5), yet their likely common provenance (section 8) indicates retention of a complex historical record in these rocks. The sedimentological model outlined above is thus tested against the oxygen isotope data.

Seeing that BQ is comprised almost entirely of quartz, it is reasonable to assume that little isotopic shift as a result of either diagenesis or metamorphism could occur in this rock and it should therefore most closely preserve the provenance $\delta^{18}\text{O}$ ratio. As shown by Reid et al. (1987), the oxygen isotope signature of BQ is similar to that of Vioolsdrif granite, a nearby composite batholithic body predominantly composed of tonalite and granodiorite (Reid, 1979), which acted as a possible contributor of detritus to the Bushmanland Group. NS and OS oxygen isotopic ratios are depleted in ^{18}O relative to BQ, while the SS ratios are relatively heavy (Fig. 6.28). With reference to the latter, it was asserted in sections 9.1.4 and 9.1.6 that SS formed slowly within a partly closed basin, with significant hydrogenous input. Although such basins preferentially lose ^{18}O to evaporation, leaving the basin waters ^{18}O enriched (Faure, 1986, pp 432 - 435), the $\delta^{18}\text{O}$ shift is only of the order of 2‰ and would hardly affect the developing sediment. Berner (1971) showed that although most quartz is of detrital origin, "a considerable proportion is also formed in sediments during diagenesis as chert and silica cement" (p158). Both quartz and opaline silica (a predecessor to quartz) form authigenically. In sea water the electrolytes and the relatively high pH range of 7.5 to 8.3 result in rapid precipitation of amorphous silica into a gel which in hardening into opaline silica, encloses some sea water (Berner, 1971, pp 158 - 161). Blatt (1987) estimated that up to 15% of the quartz in shales may be of such origin. ^{18}O is strongly fractionated into silica relative to water with which it equilibrates, such that at 0°C the $\delta^{18}\text{O}$ difference is +42, and this decreases linearly with temperature to +36 at 20°C (Faure, 1986, Fig. 24.12). In addition, the $\delta^{18}\text{O}$ composition of clays is determined by the water and temperature conditions obtaining at the time of clay formation, with higher temperature waters in warm climates resulting in clays with $\delta^{18}\text{O}$ values in excess of +20‰ (Faure, 1986, Fig. 25.8).

The $\delta^{18}\text{O}$ ratio also increases with decrease in grain size (Blatt, 1987). Compared with the agitated and detrital dominated environment in which NS formed, the restricted SS basin environment would have promoted both a higher clay content as well as a significant hydrogenous silica component which may have resulted in the positive $\delta^{18}\text{O}$ shift from that of BQ (+8,9 to +9,7) to that of SS (+13,9‰ to +14,1‰). A simple weighting calculation shows that only a 10% quartz contribution with $\delta^{18}\text{O}$ of +40‰, and 90% quartz with $\delta^{18}\text{O}$ of +10‰ produces average quartz with $\delta^{18}\text{O}$ of +13‰. The high $\delta^{18}\text{O}$ ratio of hydrogenous clays may have also contributed to the "heavy" $\delta^{18}\text{O}$ signature of SS quartz due to re-equilibration of detrital quartz with clay during metamorphism.

Standard Mean Ocean Water (SMOW) has a $\delta^{18}\text{O}$ ratio of zero, hence sedimentary and metamorphic rocks with positive $\delta^{18}\text{O}$ values which interact with large quantities of sea water during convection in the earth's crust, experience a depletion in their ^{18}O composition. Higher temperatures promote water-rock interaction and isotopic exchange, as does a vein networking (Faure, 1986), and the country rock effectively suffers a form of contact metamorphism. The low $\delta^{18}\text{O}$ values of NS are therefore entirely compatible with the indication that NS was affected by the ore-forming process (section 9.2), and suggests that hydrothermal fluid passed through NS on its passage towards deposition of the orebody and related rocks. As noted in section 6.5, the most dramatic jump in $\delta^{18}\text{O}$ ratios occurs not at any obvious structural boundary, but in the immediate structural footwall of the orebody. Since the Broken Hill succession is overturned (section 9.2) and the low $\delta^{18}\text{O}$ signature of the orebody is attributed to the ore forming process, it appears that the younger successions unaffected by any hydrothermal event were able to retain their pristine $\delta^{18}\text{O}$ signatures.

9.5 Facies variations and regional sedimentary genetic model

In the ratio-ratio diagrams (Figs. 7.4a-c) the continuum seen between the BQ/RQ and BQ/RS data sets when Al, K and Fe ratios are plotted against their respective Si ratios, and the fact that Si is the most important single element controlling the ratios, suggests that the schists were variably swamped by silica sand, producing progressively more silica-rich rocks up to the sandstone (now quartzite) end-member. The decrease in Al, K, and Fe results from the effects of closure, since each element ratio plots on a continuum through the X-Y origins.

The variations in Si and Al content of Broken Hill core samples and of Regional rocks (Fig. 7.4a and Table 9.9) shows that schists at Achab and Namiesberg (NTS and STS) are both more Al-rich and Si-deficient than their Broken Hill counterparts, while Namiesberg quartzites (WTQ and DTQ) are more Si-rich and Al-deficient than at Broken Hill. This relationship indicates a cleaner separation at Namiesberg and Achab areas between Si and Al, than found at Broken Hill. It is therefore interpreted that maturity of sedimentation at Achab-Namiesberg had reached a more advanced stage than at Broken Hill. In contrast, Wortel displays poorer separation between Al and Si than at Broken Hill. Prolonged water working of sediment in the Namiesberg-Achab area should have resulted in maximum release to the sea water of the Na, Ca and Sr components of the detritus. Namiesberg SS does show the maximum deficiency in Na and Sr (and Ca) relative to Broken Hill and Wortel (Figs. 7.3c and d) in a relationship antipathetic to that of Al and K. A reason for Broken Hill NS, rather than NTS and RQ at Achab and Namiesberg having the lowest Na and Sr concentrations, will be examined in section 10.7.2. The implication is that although all three components of the beach-barrier environment are found at Wortel, Broken Hill and Achab-Namiesberg, Wortel is the most proximal and Achab-Namiesberg the most distal of the three areas, suggesting a

south-easterly progradation of the shoreline from a provenance lying somewhat to the north-west in the direction of the most prominently developed part of the Vioolsdrif batholith (Fig. 9.38). As pointed out by D. A. Richardson (pers.comm., 1989) these variations could also be interpreted as a slowing down in the rate of progradation, with deposition in the Namiesberg-Achab area occurring over a longer period of time than in the Wortel area. Notwithstanding the more Al-rich nature of STS at Namiesberg, the Broken Hill V, C and S SS concentrations far exceed those at Namiesberg (section 7.1.1), suggesting possible quieter and a slightly deeper water lagoonal environment at Broken Hill than at Namiesberg.

Of the minor rock-types from the Regional areas, the well defined geochemical correlation between CTS and AM, but not with CS (section 7.1.1), suggests possible ore association characteristics of the Wortel CTS, as does its relatively elevated estimated Ho content (section 7.1.3). The relatively high estimated Ho concentrations of Wortel WTQ and MDTs (Figs. 7.2d and e) may also reflect some hydrothermal component. The pod-like form of massive sillimanite bodies as well as their occurrence in different parts of the succession (in STS at Wortel and in NTS at Namiesberg, section 5.2) indicates that their time of formation post-dated the depositional age of their host rocks.

It was suggested by the author (Lipson, 1981a) that the massive white quartzites of the Bushmanland Group generally thin from Pella through Aggeneys, some 45km to the south, until thin, metre-wide remnants only are covered by the younger Karoo sediments and Kalahari sands some 10 - 30km to the south of Aggeneys. Along the same traverse, the calc silicate horizons become more prominent. In equating Bushmanland calc silicate horizons with Knowles Limestone, in the analogy of the Cotton

Valley Group (Fig. 9.33), then a northerly provenance to the Bushmanland Group at Aggeneys is also suggested, with a shoreline which prograded in a southerly direction (Fig. 9.38). It is noteworthy that Colliston (1983, p110) similarly proposed mature linear shoreline sands as opposed to deltaic distributary sands in the Pella-Dabenoris area, on the basis of a transitional lower contact into immature sandstones.

From Fig. 9.33 it is clear that although red beds are developed closest to the provenance, only during transgressive cycles will they be preserved at the base of the succession. Shoreline progradation results in red beds overlying the black shale. Laminated feldspathic quartzites have been mapped by the author (unpub. work) below NS near the gneiss contact at Wortel, and interpreted as arkosic sediments by Rozendaal (1982, Table 90, p282) who refers to these rocks as the Beenbreek Formation. These feldspathic quartzites are not found at the base of the supracrustal succession in the Aggeneys area suggesting that during progradation, the red beds were either not locally developed or were deposited at the top of the succession, and have subsequently been eroded in most places. Only in the Eastern Aggeneysberge, preserved in a synclinal structure, are numerous quartzo-feldspathic gneisses found which may represent such feldspathic quartzites.

10. GENESIS OF THE OREBODY AND ORE EQUIVALENT HORIZON

The problems caused by dynamothermal metamorphism apply equally to establishing the genesis of the Broken Hill orebody as they do to the origin of the host rocks. The interpretations made regarding the latter will now be used as a framework to help solve questions about the former. In general terms the Broken Hill orebody lies within similar rock-types and at approximately the same stratigraphic level as the Gamsberg, Black Mountain and Big Syncline orebodies (Figs. 4.3 and 5.7). The four deposits display so many physical similarities (Ryan et al., 1982; Rozendaal, 1982), that their geneses can reasonably be assumed to be linked. Consequent modelling and discussion, using data from all four orebodies as well as from similar deposits found elsewhere, will explore boundary conditions limiting the possible source of the metals, S and Ba, the likely mineralizing fluid physical properties, and the ore depositional environments.

10.1 Distinctive physical characteristics of the Broken Hill orebody, its host rocks, and implications

The upper amphibolite facies grade of both host rocks and ore bodies in the Aggeneys-Gamsberg area (Ryan et al., 1982; Rozendaal, 1982), indicate that the orebodies were already emplaced at the time of metamorphic onset, hence the mineralizing fluids could not have been derived by metamorphic fluid expulsion at a greater depth. The Broken Hill orebody is unlikely to be of replacement origin since the stratigraphic column taken through the deposit is increased by the thickness ($\leq 40\text{m}$) of the deposit.

At Black Mountain it has been personally observed that gradationally cross-cutting, large-scale silicification of schist, coincident with the development of garnets, chalcopyrite and pyrite to form a Garnet Quartzite, is geographically limited to an area adjacent to the

maximum development of Pb-Cu-Zn ore in banded iron formation. The ore and Garnet Quartzite occur along the axis of an isoclinal fold which plunges for well over 2km, and in which significant refoliation has occurred. The well constrained location of silicification suggests that development of the Black Mountain Garnet Quartzite is likely to have formed as part of the mineralizing process. These factors are therefore consistent with the view of Ryan et al. (1982) that the Black Mountain Garnet Quartzite represents a footwall alteration zone. Broken Hill lacks these epigenetic characteristics. While the Black Mountain orebody probably overlies its feeder zone much like the Sullivan deposit (Ethier et al., 1976), Broken Hill thus appears more distal in nature.

The only direct indications of possible syn-sedimentary volcanic activity are the thin (< 5m wide) amphibolites at the base of the Black Mountain succession, and the amygdaloidal amphibolites which occur at the top of the metasedimentary successions at Gamsberg (Rozendaal, 1982) and in the eastern Aggeneysberge (Ryan et al., 1982). Otherwise the orebodies lie within a continental to continental margin sediment package of metamorphosed shales and sandstones (section 9.4), and are unrelated to any lava domes or local subvolcanic intrusives which characterize volcanogenic deposits (Sato, 1972; Campbell et al., 1981). The local syngenetic, shale- or clastic- hosted massive sulphide orebodies may be classified as sedimentary exhalative (sedex) deposits, along with the Mt Isa Pb-Zn lenses and the Sullivan deposit.

In contrast to the Mississippi Valley type (MVT) deposits which form in carbonates by a process of subsurface cavity filling and replacement (Rhodes et al., 1984) over an extended period of time of up to 50Ma (Cathles and Smith, 1983), the sedex orebodies develop at

the sea water-sediment interface, thus any cessations of sulphide generation will result in dilution of the orebody by the OS sedimentary gangue. NS and OS, as clastic sediments, probably formed far more quickly than the SS rate of 1.2m per million years (section 9.1.6), thus the Broken Hill massive sulphide must have developed rapidly, and Finlow-Bates (1979) estimated that for the Mount Isa sulphide lenses, up to 1cm of ore carrying 25% Pb would form in approximately five weeks.

10.2 Distinctive chemical characteristics of the Broken Hill orebody, its host rocks, and implications

10.2.1 Redox conditions of host rocks

It was shown that during deposition of SS, the sediments formed beneath a water column open to the sea (sections 9.1.4.1 and 9.1.7), and that BQ probably formed in a coastal setting (section 9.3.5), hence it is likely that OS also formed beneath sea water. Total dissolved S concentrations in sea water fall between $10^{-1}m$ to $10^{-2}m$ (Krauskopf, 1979), thus Fig. 9.12 is appropriate. Though iron sulphides are stable over a wide range in pH conditions, in sea water the Eh needs to drop from +0.3 volts to -0.2 volts at a constant pH of 8 (Fig. 9.12) in order for sulphides to form, otherwise hematite is the likely stable iron mineral. Magnetite occupies a very restricted field in Eh-pH space, and would form in the depository only if the dual unusual conditions were met of high pH (> 9) and low Eh (< -0.4) (Fig. 9.12). Away from the orebody where precipitation rates were probably much slower, such strongly reducing conditions would be manifest by the preservation of carbon (C). The predominance of Fe oxide, as opposed to Fe sulphide, along the orebody time horizon in OS (section 4.2.3) is therefore consistent with the low C content of OS. Berner (1971, p203) considered a lack of C the most important limiting factor in the reduction of SO_4^{2-} to H_2S , which is necessary for the

production of sedimentary Fe sulphide. The inference is that Fe incorporated into the developing OS outside of the orebody, precipitated as hematite under oxidizing conditions, and was later converted to magnetite during metamorphic recrystallization. The unusually high Mo content of 19ppm in ALP212, a sample of OES situated 740m east of the orebody, coincides with the elevated MnO concentration of 0.8%, and independently emphasizes the strongly oxidizing environment under which OES formed, since the aqueous behaviour of Mo is Eh dependent, and Mo only coprecipitates with manganese oxide under oxidizing conditions (Contreras et al., 1978).

In contrast to the Broken Hill environment, the iron formation immediately associated with the Sullivan deposit predominantly consists of pyrrhotite, and classifies as sulphide facies, while the host rocks comprise grey-green, thinly bedded quartzites, siltstones and argillite with ubiquitous pyrrhotite and very minor magnetite (Sangster, 1972). The Sullivan iron formation clearly developed in an environment which was already reducing, whereas it is proposed that the Broken Hill orebody created a reducing sub-environment (massive sulphide) within an oxidizing environment, similar to the model suggested by Stanton (1972) for the Australian Broken Hill deposit.

Had the Broken Hill Quartzites acted as a sandstone aquifer for introduction of epigenetic, oxidizing waters into reducing shales, it is unlikely that the oxidation of Fe would have taken place in rocks both above and below the aquifer (OS and NS). In the case of OS, the sharp and consistent cut-off in oxide Fe at BGZ could not readily be explained by this model, and neither could the massive, and individually restricted nature of the UOB and LOB lenses.

10.2.2 Low Zn/Pb ratio and source rocks

The unusually low Zn/Pb ratios at Black Mountain and Broken Hill relative to other sedex deposits were highlighted by Lydon (1983). When considering a possible source of Pb, only felsic rocks display relatively elevated Pb and Ba contents (Table 10.1), while Cu and Zn concentrations are highest in basalts. Graf (1977, p544) sketched the general empirical variation in orebody metal content as a function of the likely source rock chemical composition, from the Cu-Zn Cyprus deposits which overlie basalt, through the Cu-Pb-Zn Kuroko deposits formed in a mixed felsic to mafic volcanic suite, to the K-feldspar-rich New Brunswick deposits which are Pb-rich relative to the Kuroko deposits. As far as the source of Fe is concerned, Graf (1977) pointed out that even in felsic rocks, the Fe content is over 100 times that of their base metals, so there is no lack of Fe availability for producing the iron sulphides (or oxides) of the orebody.

A Rb rich ore-forming fluid may be deduced at Broken Hill from the increase in the Rb/Rb+Sr ratio progressively nearer the orebody (section 6.6.4; Fig. 6.35b). Ellis (1979, p648) showed that in order to enrich geothermal waters in the rarer alkalies such as Rb, the rocks being leached are likely to have had a composition varying from andesitic to rhyolitic. The sporadically high base metal content of NS (sections 4.2.1 and 6.2.6) suggests that the mineralizing fluid originated at greater depth below the orebody than at the stratigraphic level of NS. The felsic (K-feldspar-rich) basal gneisses which underlie the orebodies, and constitute by far the most abundant rock type of the Namaqua Province (Lipson, 1980; Watkeys, 1986) are thus a possible source of metals for the Aggeneys-Gamsberg deposits.

10.3 Ore fluid chemistry

10.3.1 Zn/Pb ratio of fluid

In order to evaluate the causes of unusually low Zn/Pb ratios in ore, it is necessary to examine the behaviour of this ratio in the fluid which generates a deposit. The Zn/Pb ratio of the eventual precipitate will equal that of the causative hydrothermal fluid, provided that $m_{\text{H}_2\text{S}} > m_{\text{Total metal}}$ in the fluid (Ohmoto et al., 1983). A sulphur deficient fluid ($m_{\text{H}_2\text{S}} < m_{\text{Total metal}}$) at 200°C tends to deposit one metal only, while a S-rich fluid at 250°C will produce polymetallic deposits (Ohmoto et al., 1983). In thermochemical modelling of the Zn/Pb ratio in fluids at moderate temperatures, Huston and Large (1987) showed that provided all metals in solution are transported as chloride complexes, and that either $m_{\text{H}_2\text{S}} > m_{\text{Total metal}}$ or that the metals are close to saturation, then only temperature and NaCl content of the hydrothermal solutions significantly affect the ratio. Under these circumstances, the hotter solutions are more Pb-rich while the more saline ones are relatively Zn-rich (Fig. 10.1). Huston and Large (1987) expected that bedrock composition influences the Zn/Pb ratio of ore forming fluids only in the extreme cases such as where the Pb-deficient basaltic source to Archaean deposits or to black smokers results in total undersaturation of the fluid with respect to Pb.

The applicability of Huston and Large's (1987) work and subsequent thermochemical modelling (section 10.3.2) depends on whether the conditions outlined are fulfilled. The activities of the ligands Cl^- , HS^- , H_2S and OH^- in solution, rather than the concentrations of metals in rocks, control the ore-carrying capacity of fluids (Barnes, 1979). Cl^- represents by far the most important ligand which complexes with the saline, slightly acid solutions typically responsible for generating massive sulphide deposits (Large, 1977). At 200°C, Cl^- complexing of Zn and of Pb is eight orders of magnitude greater than S

complexing (Barnes, 1979). At lower temperatures the transport of Zn by bisulphide complexes becomes important in neutral to alkaline solutions with unusually high S contents ($> 0.1m \approx 32\ 000\text{ppm}$) (Large, 1977; Bourcier and Barnes, 1987). Pb transportation by S complexes over a variety of temperatures is extremely poor below reduced S concentrations of approximately $2.5m$ (Fig. 10.2) (Giordano and Barnes, 1979). It is therefore evident that at temperatures of less than -200°C the S-ligand transport of Zn (but not Pb) becomes important in solutions rich in reduced S. Sulphate plays very little part in transporting ore metals since barite is much less soluble in hydrothermal sulphate-rich waters than in sulphide waters yet barium is carried in the ore solutions (Barnes, 1979). The Ba concentration of hydrothermal fluids varies as a function of $a_{\text{SO}_4^{2-}}$ and is independent of both $a_{\text{H}_2\text{S}}$ (Fig. 10.3) and of temperature (Ohmoto et al., 1983) such that at $a_{\text{SO}_4^{2-}} = 10^{-4}m$, the Ba concentration is $\sim 10^{-6}m$. At similar levels of $a_{\text{H}_2\text{S}}$, the Zn concentration is $\sim 10^{-2}m$, and is independent of $a_{\text{SO}_4^{2-}}$.

From the foregoing it therefore appears likely that Cl^- complexes were the major ligands responsible for metal transport in the Aggeneys-Gamsberg deposits. As regards the S content of the ore fluid relative to its contained metal, the great volume of iron sulphide in the Aggeneys-Gamsberg deposits (Ryan et al., 1982; Rozendaal, 1982), much of which is pyrite, suggests that the ore-forming solutions were S-rich ($m_{\text{H}_2\text{S}} > m_{\text{Total metal}}$).

10.3.2 Solubility modelling of Cu-Pb-Zn ratios

Although many similarities exist between the four deposits in the Aggeneys area, the two major differences are

(a) their wide variation in Cu-Pb-Zn ratios, from the Cu-rich and Zn-deficient Black Mountain orebody to the Zn-rich and Cu-deficient Gamsberg orebody, and

(b) the local depositional environments as deduced from the rocks directly hosting the orebodies.

Examination of theoretical factors controlling the Cu-Pb-Zn ratios are a prerequisite for evaluating whether the depositional environments in any way influenced the metal ratios of the enclosed deposits. In order to apply the models of Ohmoto et al. (1983) and Huston and Large (1987), the requirement of $m_{H_2S} > m_{Total\ metal}$ in ore forming fluids responsible for ore generation is reasonable in the Aggeneys-Gamsberg deposits (section 10.3.1). For the purposes of metal element ratio modelling which includes Cu, the simplest Cu sulphide for which data is available, i.e. chalcocite (Cu_2S) is used as a first approximation of insoluble Cu minerals. The equations for the $100*Pb/(Pb+Cu)$ and $100*Zn/(Zn+Cu)$ ratios are based on Huston and Large (1987) for the $100*Zn/(Zn+Pb)$ ratio (hereafter referred to as the Pb/Cu, Zn/Cu and Zn/Pb ratios respectively). Unlike the Zn/Pb ratio, however, the derived equations for the Pb/Cu and Zn/Cu ratios, viz:

$$\begin{aligned}
 [m_{Tot\ Cu}] / [m_{Tot\ Pb}] = & \\
 & \{ \{ (a_{Cl^-}) / ((g_{(CuCl_2)^-}) * (K_1)^{0.5} * a_{H^+}) \} + \{ (a^2_{Cl^-}) / (g_{(CuCl_2)^{2-}}) \\
 & * (K_2)^{0.5} * a_{H^+} \} + \\
 & \{ 1 / (g_{(CuCl)^+}) * (K_3)^{0.5} \} + \{ (a_{Cl^-}) / (K_4)^{0.5} \} + \{ (a^2_{Cl^-}) / (g_{(CuCl_2)^-}) * (K_5)^{0.5} + \\
 & \{ (a^3_{Cl^-}) / (g_{(CuCl_4)^{2-}} * (K_6)^{0.5} \} / \\
 & [\{ 1 / ((g_{PbCl^+}) * (K_{PbCl^+})) \} + \{ (a_{Cl^-}) / (K_{PbCl_2^0}) \} \\
 & + \{ (a^2_{Cl^-}) / (g_{(PbCl_2)^-} * K_{PbCl_2^-}) \} + \{ (a^3_{Cl^-}) / ((g_{PbCl_4^{2-}}) * (K_{PbCl_4^{2-}})) \}]
 \end{aligned}$$

and

$$\begin{aligned}
 [m_{Tot\ Cu}] / [m_{Tot\ Zn}] = & \\
 & \{ \{ (a_{Cl^-}) / ((g_{(CuCl_2)^-}) * (K_1)^{0.5} * a_{H^+}) \} + \{ (a^2_{Cl^-}) / (g_{(CuCl_2)^{2-}} * (K_2)^{0.5} * a_{H^+}) \} + \\
 & \{ 1 / (g_{(CuCl)^+}) * (K_3)^{0.5} \} + \{ (a_{Cl^-}) / (K_4)^{0.5} \} + \{ (a^2_{Cl^-}) / (g_{(CuCl_2)^-} * (K_5)^{0.5} + \\
 & \{ (a^3_{Cl^-}) / (g_{(CuCl_4)^{2-}} * (K_6)^{0.5} \} / \\
 & [\{ 1 / ((g_{ZnCl^+}) * (K_{ZnCl^+})) \} + \{ (a_{Cl^-}) / (K_{ZnCl_2^0}) \} \\
 & + \{ (a^2_{Cl^-}) / (g_{(ZnCl_2)^-} * K_{ZnCl_2^-}) \} + \{ (a^3_{Cl^-}) / ((g_{ZnCl_4^{2-}}) * (K_{ZnCl_4^{2-}})) \}]
 \end{aligned}$$

are pH dependent with the relative Cu concentration increasing with pH (Appendix I). The ratios are still independent of fO_2 and activity of dissolved S. From sets of simultaneous equations the equilibrium constants (K) were calculated between 25 and 300°C (Table 10.2) while the activity coefficients for the various Cu complexes were calculated over salinities ranging between 0.25 and 3.0m NaCl (Appendix I), from the modified Debye-Huckel equation (Helgeson, 1969). K_{NaCl} values were taken from Huston and Large (1987), while a value of one was used for the activity coefficients of uncharged species (Helgeson et al., 1981). A subset of values in the matrices for the Pb/Cu and Zn/Cu ratios over varying temperatures, salinities and pH's (Table 10.3) are graphically plotted in Figs. 10.4a-f.

By far the most important parameter influencing the Pb/Cu and Zn/Cu ratios is the variation in pH, with the ratios stretching between 100% (at pH = 4) and 0% (at pH = 8) for both ratios over virtually all temperature and salinity ranges (Figs. 10.4a and d). As noted from the equations for the ratios, the relative Cu content of the ore fluid increases (ratio decrease) with pH, with the most dramatic ratio changes occurring over the pH range of 5 - 6.5 for the Pb/Cu ratio, and 5.5 - 7 for the Zn/Cu ratio.

As far as temperature is concerned, the Pb/Cu ratios display maximum relative Cu enrichment between temperatures of 100 - 180°C over all pH and salinity ranges (Fig. 10.4d). The Zn/Cu ratio shows greater complexity, with the relative Zn content decreasing up to 200°C whereafter at higher temperatures the ratio increases and then decreases (Fig. 10.4b). The common assumption that with a decrease in temperature Cu precipitates first is thus not always true. For the Pb/Cu ratio, relative Cu solubility first increases with decreasing temperature, and only decreases at temperatures below -140°C.

Salinity has little effect on the Pb/Cu ratio except at molalities below 1, where a further decrease in ionic strength of the solution results in a rapid rise in the relative Pb concentration, and applies over all pH ranges (Fig. 10.4f). The Zn/Cu ratio also shows a rapid relative Zn increase below $m_{\text{NaCl}} = 1$, but contrary to the Pb/Cu ratio the Zn/Cu ratio increases as the molality increases above a value of 1. Clearly, ore fluids with $m_{\text{NaCl}} = 1$ are those most relatively enriched in Cu, and most relatively depleted in Zn (Fig. 10.4c).

10.3.3 Cu-Pb-Zn ratios at Aggeneys-Gamsberg

Use of the metal contents published in Ryan et al. (1982) for calculation of metal ratios, results in simplifications since each orebody comprises a number of physically and chemically distinct layers or lenses. Only gross ore fluid chemistry may thus be inferred for each deposit.

The metal ratios of the four orebodies vary widely (Table 10.4). Reading off the data of Huston and Large (1987) shown in Fig. 10.1, the approximate mineralizing temperatures for the various deposits are:

	Gamsberg	Big Syncline	Broken Hill	Black Mountain
Temperature (°C)	100 - 150	180 for all m_{NaCl} 220 or 260 for $1.5m_{\text{NaCl}}$	280	300

Approximate salinity boundaries of $0.5 - 2.0m_{\text{NaCl}}$ may be inferred from the literature based on measured fluid inclusion salinities in Kuroko fluids with $0.6 - 1.37m_{\text{NaCl}}$ (Ohmoto et al., 1983); general estimates of approximately $1.6m_{\text{NaCl}}$ (Barnes, 1979); $1.5m_{\text{NaCl}}$ for the elastic-hosted Jason deposit (Gardner and Hutcheon, 1985); and $1.4 - 2.6m_{\text{NaCl}}$ for the

high temperature fluid inclusions at the carbonate-hosted Silvermines deposit (Samson and Russell, 1987).

Utilizing the data in Figs. 10.4a-f, Table 10.3, and the temperature and salinity constraints above, estimates may be made of the ore solution pH variations for the individual Aggeneys-Gamsberg ore deposits from the Zn/Cu and Pb/Cu ratios, viz:

	Gamsberg	Big Syncline	Broken Hill	Black Mountain
pH (Zn/Cu)	4.0 - 4.5	4.1 - 4.3	4.9 - 5.4	5.9 - 6.2
pH (Pb/Cu)	4.0 - 4.3	4.2 - 4.6	4.7 - 5.2	5.6 - 5.8

The two sets of estimates independently read off the Zn/Cu and Pb/Cu plots produce remarkably similar pH values which show a consistent increase in estimated ore fluid pH from Gamsberg through Big Syncline and Broken Hill to Black Mountain.

By re-applying the pH and temperature constraints gained above and reading off from Figs. 10.4a-f and Table 10.4, it is possible to estimate the salinities (m_{NaCl}) for the ore fluids responsible for the four orebodies, viz:

	Gamsberg	Big Syncline	Broken Hill	Black Mountain
m_{NaCl} (Zn/Cu)	0.25 - 0.3	0.5 - 1.5	0.4 - 1.2	0.8 - 1.2
m_{NaCl} (Pb/Cu)	0.4	0.3 - 0.8	0.5 - 0.7	1.0 - 2

10.4 Sulphur isotopes and source of sulphur

The S isotope compositions in the Aggeneys-Gamsberg area cover a wide range, with the lowest $\delta^{34}S$ from sulphide and sulphate found at Black Mountain and the most positive at Gamsberg (von Gehlen et al., 1983) (Table 10.5; Fig. 10.5). The systematic variation through time of sea

water and ore sulphide isotopic compositions led Sangster (1976) to conclude that sea water sulphate is the ultimate source of most S in ore deposits, hence organic and inorganic mechanisms of SO_4^{2-} reduction are examined.

The metabolic activity of oceanic anaerobic bacteria, notably *Desulphovibrio desulphuricans*, act as a catalyst for the reduction of sulphate to sulphide. In the process the lighter ^{32}S isotope is more commonly reduced (Sangster, 1976), hence the $\delta^{34}\text{S}$ values in such biogenically derived sulphides which are incorporated into sedimentary rocks, range from -5 to -30‰ (Ohmoto and Rye, 1979). The residual sulphate in the water becomes enriched in ^{34}S , and as long as the system remains closed to sulphur such as in a lagoon, then any evaporites formed from this water will bear the signature of isotopically heavy S (Sangster, 1976).

Analytical data from various geothermal fields reveal that at temperatures around 250°C the H_2S and HS^- contents of the solutions increase at the expense of SO_4^{2-} (Ellis, 1979), and Nielsen (1979) and Ohmoto and Rye (1979) agree that inorganic reduction of SO_4^{2-} only begins above -250°C. Under these conditions the sea water $\delta^{34}\text{S}$ value of 20‰ is lowered to produce sulphides with $\delta^{34}\text{S}$ of +5 to +20‰ (Ohmoto and Rye, 1979). In contrast, igneous rocks have $\delta^{34}\text{S}$ values of -0‰, hence ore deposits having sulphides with 0‰ $\delta^{34}\text{S}$ values are interpreted as having been derived from fluids of magmatic origin (Ohmoto and Rye, 1979).

In the Aggeneys-Gamsberg area, von Gehlen et al. (1983) viewed the strongly positive $\delta^{34}\text{S}$ of barite as indicative of a restricted basin or lagoonal environment. They interpreted the increase of sulphide and sulphate $\delta^{34}\text{S}$ values from west to east as reflecting the mixing of two

sulphur sources, viz. magmatic-exhalative S ($\delta^{34}\text{S} \approx 0\text{‰}$) from the Black Mountain area with local evaporite derived S ($\delta^{34}\text{S} \approx +30\text{‰}$) from the Gamsberg area. The positive $\delta^{34}\text{S}$ sulphide value in the Broken Hill deposit, however, is unlikely to have resulted from the mixing of two fluids above the sediment-water interface, with one having $\delta^{34}\text{S}$ values near zero and another with strongly positive $\delta^{34}\text{S}$ values, because the Broken Hill orebody formed in an environment which had little or no restricted water circulation. It is therefore suggested that the positive $\delta^{34}\text{S}$ ratio of Broken Hill sulphides was established *before* exhalation, and that reduction of SO_4^{2-} occurred in the crust at temperatures of $\geq 250^\circ\text{C}$. The same reasoning applies to the magnetite-rich and carbon-deficient Black Mountain orebody. The lowest sulphate $\delta^{34}\text{S}$ value of the Black Mountain area probably reflects the contribution of normal sea water SO_4^{2-} , since barite, in deriving its SO_4^{2-} from sea water, precipitates rapidly when Ba is exhaled, and adopts approximately the local aqueous $\delta^{34}\text{S}$ of SO_4^{2-} (Sangster, 1976). None of the Aggeneys-Gamsberg deposits could have formed in inland basins since freshwater has sulphur $\delta^{34}\text{S}$ values of zero (Sangster, 1976).

As suggested by von Gehlen et al. (1983), the highest $\delta^{34}\text{S}$ sulphate ratios in the east indicate that Gamsberg ore formed in the most restrictive of the Aggeneys-Gamsberg depositional environments. This interpretation is supported by the common presence of graphite in the Gamsberg orebody (Rozendaal, 1982). The local sea water in the Gamsberg basin therefore probably had a positive $\delta^{34}\text{S}$ signature caused by bacterial reduction of SO_4^{2-} , both prior to and during ore deposition, whereas prior to exhalation, sea water in the Black Mountain and Broken Hill depositories had relatively unmodified $\delta^{34}\text{S}$ ratios.

The layered amphibolite near the base of the Black Mountain succession along the contact between gneiss and schist possibly contributed a minor amount of magmatic S there. The decrease in $\delta^{34}\text{S}$ sulphide from Gamsberg to Black Mountain may also reflect an *increase* in $f\text{O}_2$ and/or pH since a positive shift in the $f\text{O}_2$ value by 1 log unit or in pH by 1 unit results in a $\delta^{34}\text{S}$ *decrease* in sulphides by up to 20‰ (Ohmoto, 1972).

10.5 Basin dewatering versus deep convection of fluids

The two proponents of contrasting, current models for the generation of the sedex deposits (Lydon, 1983, 1986; and Russell, 1983, 1986) find common ground in the envisaged extensional tectonic environments of 2nd and 3rd order fault-bounded basins as ore depocentres. The models differ in the explanations of the source of the metals and fluids responsible for generation of these deposits.

Lydon (1983, 1986) envisaged a finite source fluid derived from shallow depths due to the metamorphic release of connate water from sediments when clays transform to micas. The sedimentary successions with thicker source beds will generate the larger ore deposits. The source of heat required to drive the metamorphism and fluid expulsion is seen as elevated heat flow related to faulting and incipient magmatic activity (Lydon, 1986). An essential component of the model is a thick (few 100m), thermally insulating and hydraulically sealing shaley rock which allows geopressuring of an underlying aquifer where the mineral transformations take place.

In contrast, Russell (1983, 1986) proposed that the fluids which generate the ore deposits represent the infinitely rechargeable source of overlying sea water which permeates the crust via ever deepening convective cells in areas of extensional tectonics. The fluids

progress downwards into the basement to depths of as much as 15km, being limited only by the deformation change from brittle to ductile failure. Sea water becomes modified on its downward journey, increasing in acidity and attacking feldspars which release a series of elements including base metals. These fluids are focused in their upward journey along the master faults, to be exhaled on the sea floor.

Strens et al. (1987) and Samson and Russell (1987) argued that the sedex temperatures of ore fluid formation lie between the high temperatures related to a magmatic source, and the temperatures of 100 - 150°C (maximum of 200°C) associated with Mississippi Valley-type deposits (Cathles and Smith, 1983). The latter authors showed that it is only under the most exacting conditions of rapid and episodic connate water expulsion from a basin that fluid temperatures of 150°C may be brought to within 1km of the surface. Temperatures deduced for fluids responsible for generating the Aggeneys-Gamsberg deposits, ranging from 300 - 150°C (section 10.3.3), bracket the fluid inclusion homogenization temperatures of ~250°C deduced from the Jason Pb-Zn sedex deposit in Canada (Gardner and Hutcheon, 1985), and the 50 - 260°C homogenization temperatures (mode at 190°C) deduced for the carbonate-hosted Pb-Zn-barite Silvermines deposit in Ireland (Samson and Russell, 1987).

It is unlikely that the Lydon (1983, 1986) model of normal dewatering alone could produce either the volume of sulphide or the 250°C temperatures associated with the sedex deposits. Strens et al. (1987) showed by rigorous quantitative modelling of geothermal gradients of as low as 30°C/km that a single-pass, single-fluid convective cell of hypersaline seawater penetrating through basin sediments and into the basement is capable of producing sizable lead-zinc deposits. These

cells deepen with time by a process of crack propagation to the maximum temperature constraint of -250°C , representing the transition between brittle and ductile failure (White and White, 1983).

Strens et al. (1987) modeled the circulation as two phases, viz. downward recharge through a porous (fractured) rock and an upflow cycle of turbulent, focused and rapidly discharged fluids. They estimated the maximum amount of potential sulphide mass which can be transported to the depositional site, requires an optimal permeability of -10^{-16}m^2 in the recharge cycle. At higher permeability, such as would be anticipated in unconsolidated sediments or volcanoclastics, Strens et al. (1987) found that the flow is controlled by the upflow characteristics, and the potential sulphide mass drops slightly, while at lower permeability, the low flow rate limits the volume of fluid which can pass through the system.

In the absence of intrusives, the potential sulphide mass will depend on the size of the recharge cell (Fig. 10.6) thus for a geologically reasonable cross-sectional area of say 80km^2 (i.e. $10\text{km} * 8\text{km}$), some nine million tonnes (mt) of sulphide may be produced, approximately equivalent to the 40mt of ore grading say 25% total sulphide found at Broken Hill. The additional 12mt of Fe contained in magnetite is not yet accounted for. Viewing the deposit as comprising the two lenses Upper Orebody (UOB) and Lower Orebody (LOB), each with its own distinct lithology and Cu/Pb+Zn ratio (Ryan et al., 1982; Wilson, 1981), and using a UOB:LOB contained S + metal ratio of say 2:1, then some 14mt contained S + metal exist in the UOB and 7mt in the LOB. Though Strens et al. (1987) have modeled up to a maximum of only 9mt contained sulphide, Figs. 10.6a and b suggest that additional metal leaching would be promoted, possibly up to and beyond the required 14mt of contained S + metal in the UOB, if any of the following

conditions were met, viz. (a) a greater cross-sectional area of downflow (exceeding 80km²); (b) a higher geothermal gradient (exceeding 30°C/km); or (c) an increase in the time span over which the cell exists (beyond 50 000 years). Clearly the Strens et al. (1987) model produces tonnage figures of a similar order of magnitude to the Broken Hill orebody.

Once the hydrothermal cell has worked its way down to the zone of brittle-ductile transition in the crust, ore deposition will terminate as access to additional geothermal energy ceases and the fluid temperature drops due to the ingress of cool sea water (Strens et al., 1987). These authors calculated that some 10⁶ years pass before the rocks re-equilibrate to the ambient geothermal gradient and are able to once again crack at the onset of the next tectonic pulse. This sets in motion an entirely new convective cell which would be capable of producing a separate orebody having its own distinctive characteristics, much as the upper and lower lenses of the Broken Hill orebody.

Lydon's (1983, 1986) finite ore-fluid model can be tested by simple mass balance. A 40mt orebody such as Broken Hill (excluding the Fe contained in magnetite) comprising say 21mt contained S + metals or approximately 18.8mt metals, would require a pure illite source region of 10km * 10km * 1.34km (Appendix J). Using more realistic parameters of only a maximum of 50% of the source region being illite; that the thickness of the protore could not exceed 0.5km (at Broken Hill this would include the schist and Pink Gneiss stratigraphically below the orebody); and that the extraction/concentration efficiency at the point of discharge had been say 50%, then only 2mt or 11% of the required metal could have been produced. As Lydon's (1983, 1986) model stipulates that the fluid is non-renewable, the UOB and LOB

cannot be treated separately as done above for the Strens et al. (1987) model. Lydon's (1983) model is virtually incapable of producing sufficient fluid for a large sedex deposit (i.e. in excess of say 5mt contained metal in the Aggeneys area. Considering the size of the Aggeneys-Gamsberg deposits (Gamsberg is in excess of 150mt), Lydon's (1986) belief that the maximum size of the deposit will be limited by the thickness of the underlying argillaceous rocks, does not appear to be valid.

The Lydon (1983, 1986) model fails to explain the high heat flows required, since both at Aggeneys and in the case of the Irish deposits, the available cover rocks are relatively thin, and little evidence exists for nearby intrusions. The heat contributed from the thin amphibolite at the base of the Black Mountain succession (section 10.1) would be minimal. The amphibolites at the top of the Big Syncline and Gamsberg successions probably reflect later stages of rifting, and Reid et al. (1987) concluded that the mantle source to the amphibolites display subduction-related metasomatic characteristics similar to those found in active continental margins and island arcs, including those of the back arc environment. The local geothermal gradient was therefore probably increasing during the time of ore deposition, but the levels of heat flux must have been well below those required to satisfy the Lydon (1986) model.

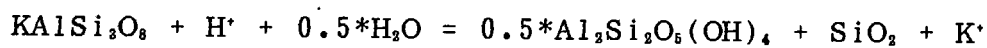
As a variation on the Lydon (1983, 1986) model, Moore (1986) also proposed that the metals were leached from the near surface environment. He suggested that weathering or hydrothermal processes acted on Pink Gneiss which stratigraphically immediately underlies NS, and which Moore (1986) interpreted to have been acid volcanics still in an unconsolidated state during the time of ore formation. The metals were then concentrated in highly restricted anaerobic sub-

basins where they precipitated as base metal sulphide deposits. Problems with this model include the calculation that unrealistically high heat flows (ca. 600°C/km) would be required to produce the low Zn/Pb ratios observed at Black Mountain, which are estimated to have formed from solutions at temperatures of ca. 300°C (section 10.3.3). Moore's (1986) leaching model cannot account for the well defined, distinct metal ratios at each of the Aggeneys-Gamsberg deposits, and it has been shown (section 10.2.1) that not all the local basins in which ore is found, were reducing when the metals were deposited. The metasediments are also shown to be so mature that it is highly unlikely that they were derived from proximal, contemporaneous, unconsolidated volcanics which are a necessary condition for Moore's (1986) model.

Due to the thin available cover rocks in the Irish midlands, Lydon (1986) was forced to conclude that dehydration of the Old Red Sandstone (ORS) produced the metal-rich ore fluids which gave rise to the Irish deposits. LeHuray et al. (1987) showed, however, that the ORS underlies only a few of the Irish deposits, and there exists a one-to-one correspondence between individual deposit Pb isotope ratios and the underlying basement of Lewisian gneisses, thus linking the origin of Pb in the orebodies directly to their basements, and supporting the models of Russell (1986) and Strens et al. (1987). In similar Pb isotope studies on Swedish Phanerozoic and Proterozoic strata-bound sulphide ore deposits, Johansson and Rickard (1984) and Johansson and Rickard (1985) also found that the Pb was derived from the well homogenized, pre-existing basements.

Lydon (1986) argued that so large a volume of water would be required to alter crystalline basement to liberate metals, that insufficient

metal concentrations could be achieved to form an orebody, based on hydrolysis reactions of the type

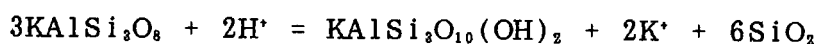


K-feldspar

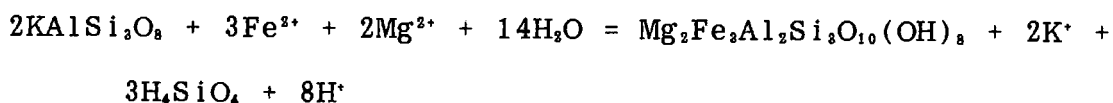
Kaolinite

Quartz

which require 10⁴kg of reactant solution at a pH = 4 to alter 1 mole of K-feldspar. Kaolinite is, however, the end stage product of acid reaction with K-feldspar. K-mica represents an intermediate stage of alteration which in fact buffers solutions passing through granitic rocks to becoming progressively more acidic at higher temperatures (Barnes, 1979), via reactions of the type

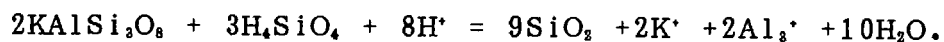


(Ellis, 1979). Large (1977) also showed that K-feldspar may be altered by reactions which do not consume H⁺, but do consume water, e.g.

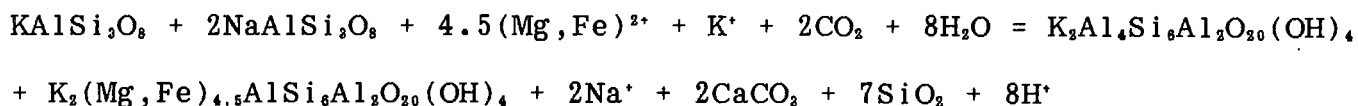


Chlorite

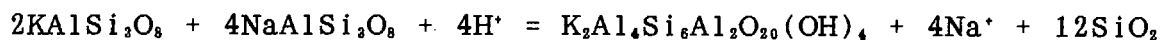
whereafter



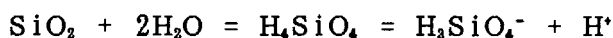
Depending on the Mg and Fe concentration of the solute, metals liberated from K-feldspar could be concentrated in a relatively limited volume of solution. Beach (1980) quoted similar reactions e.g.



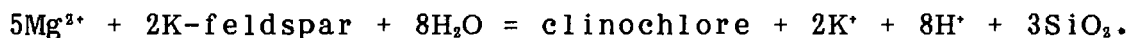
and



and suggested further that one way proton generating reactions which also consume H_2O , such as



must exist in order to remove and precipitate elsewhere the SiO_2 generated at the site of K-feldspar destruction. The rapid destruction of biotite even under conditions of surface weathering would provide the required Fe and Mg (Minarik et al., 1983; Nesbitt and Young, 1984). The critical role played by Mg in solution was emphasized in the experimental results of Bischoff et al. (1981) who reacted sea water and brine with greywacke. They found that at temperatures of 200°C and 350°C the seawater pH drops dramatically to 5.2 and 4.8 respectively, and in the case of K-feldspar, and with Mg^{2+} sourced from seawater or dolomite, they envisaged that the responsible proton generating reaction is



The reactions above involving Fe-Mg-bearing micas, show that solutions buffered by the more mafic rocks have a higher pH than fluids in contact with granitic rocks (Barnes, short course, 1990).

Berner and Holdren (1977) showed that K-feldspar breakdown occurs mainly on fracture surfaces and not by diffusion processes, therefore models involving crack propagation in basement will be conducive to K-

feldspar destruction. Infiltration of surface waters to depths of -12km have long been postulated, and Ferry (1986) argued that multipass circulation of metamorphic fluids, rather than continual recharge, could be an important feature of regional metamorphism which allows for high fluid/rock ratios. These systems would also help concentrate base metals. Russell (1986) showed from physical tests carried out at Camborne that water pumped into boreholes drilled to depths of 2km infiltrates the basement down to depths of -4.8km.

Strens et al. (1987) acknowledged that the type of fluid flow envisaged in their and Russell's (1986) model is not ideal for scavenging metals, and not as theoretically effective as connate fluids released during metamorphic dewatering, however they argued that if only 10% of the 10ppm Pb contained in a rock volume measuring 20km * 15km * 10km were stripped, a total of 5mt of Pb would be removed. If all the metal is precipitated at the point of exhalation, this could produce an orebody of 50mt grading 10% Pb i.e. roughly the same order of magnitude as Broken Hill. To emphasize the principle of metals being stripped from basement rocks, Strens et al. (1987) quoted zones of impermeable, but Cu depleted epidosite below Cyprus volcanogenic orebodies which appear to have acted in a porous manner to the fluids. While Barnes (1979) suggested that metal concentrations of at least 10ppm in solution are necessary for the generation of base metal deposits, Barrett and Anderson (1988) pointed out that the metal concentrations of fluids exhaling to produce the potential Cu-Zn orebodies at the East Pacific Rise and in the Guaymas Basin are 1 000 times lower than 10ppm. They suggested that a combination of high fluid flow rate over a prolonged period, and an excess of reduced S over metals, will cause the efficient precipitation of all transported metals on discharge. Barrett and Anderson's (1988) work therefore casts doubt on the necessity for a

connate water source of ore-forming fluid. The heat requirement is still essential since the capacity for hydrothermal brines to concentrate metals increases exponentially with temperature, as indicated by Strens et al. (1987) (Fig. 10.7) and Ohmoto et al. (1983) who showed that the Pb, Zn and Ag content increase dramatically in fluid from 200 - 300°C. Crust heated by intrusions, or areas of elevated geothermal gradient, will thus have the greatest capacity for generating fluids which may carry sufficient metals for producing large orebodies.

10.6 Ore and gangue deposition

The relatively shallow water depths of 45m (section 9.1.4.1) under which Broken Hill ore deposition probably occurred would not inhibit the development of a sedex deposit. The curves of Haas (1971) show that boiling takes place at shallow depths (low hydrostatic head), with associated precipitation of some mineral phases due both to supersaturation and to cooling. In the Red Sea Atlantis II deposit, Zierenberg and Shanks (1986) determined that below the sediment-water interface, the ore-forming brines are heated to 255°C. It is evident from high temperature (> 334°C) cubanite + chalcopyrite + pyrite assemblages found in the deposit (Pottorf and Barnes, 1983), that earlier formed crystallized solid phases are bodily transported up the focused fluid channelways, thus subsurface boiling would not prevent the formation of ore at the sediment-water interface. The sporadically high Mo values in OEH (Table 6.18) suggest that boiling may have occurred prior to exhalation, since Arnorsson and Ivarsson (1985) found in Iceland geothermal waters that boiling and mixing with cold sea water leads to molybdenite undersaturation, and these processes favour leaching of Mo from the country rock. Localized showings of molybdenum were noted by the writer in the basal gneisses at both the Aggeneys township and the quarry near the mine's reduction

plant, and these occurrences demonstrate the potential for the basement to have supplied Mo to leaching hydrothermal fluids. Hemley et al. (1986) showed that pressure release along gently decreasing temperature gradients leads to greater (and not less) fluid capacity for carrying the elements Fe, Zn and Pb, again indicating that boiling would have little effect on the capacity for the metal-bearing solution to produce a sedex deposit. Both Large (1983) and Plimer (1981) recognised that the cross-cutting, epigenetic components of stratiform orebodies may increase at shallower depths, but without preventing the formation of major, layered sedex deposits.

By far the most important parameter responsible for precipitation of sulphides is temperature drop. The Kuroko ores formed within a 50°C drop in the initial ore fluid temperature after only 10% mixing with cold sea water (Ohmoto et al., 1983, p589). These authors used plots of Saturation Index (SI) vs temperature to assess the depositional characteristics of cooling hydrothermal fluids, where

$$SI = a_{ZnCl(n)}^{2-n} \cdot [(a_{H_2S} / \{ (a_{H^+})^2 \cdot (a_{Cl^-})^n \})] \cdot 1 / K_{sphalerite},$$

and where $K_{sphalerite}$ is the equilibrium constant for the reaction

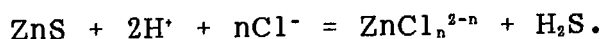


Fig. 10.8 shows that cooling from high temperature (300°C) fluids saturated in sphalerite, galena, chalcopyrite and barite will promote chalcopyrite precipitation as well as that of sphalerite, galena and barite ($SI > 1$), whereas cooling from lower temperature solutions (200°C) (Fig. 10.9) leads to precipitation of the latter three minerals, but chalcopyrite goes into solution. Virtually all the Ba will precipitate on entering seawater because SI continues to increase

with a drop in temperature, and there is more Total SO_4^{2-} in sea water than in ore fluids (Ohmoto et al., 1983). The $\text{SI} > 1$ requirement is a necessary but not sufficient condition for mineral precipitation, especially in the case of silica, as discussed in section 10.7.1 below.

10.7 Ore Equivalent Horizon (OEH)

Components of OEH which formed at the same time as the orebody, carry the signature of mineralization (section 6.3). Biotite-garnet-rich schist, or bands of garnetiferous quartz-rich rock, are features commonly associated with massive sulphide ore deposits. In the Gossan Lead district of Virginia, Gair and Slack (1984) described biotite-, chlorite- and garnet- rich rocks occurring as lenses within 10m of the hangingwall or footwall of the orebody, and interpreted these as metamorphosed alteration zones or intermixed chemical and clastic sediments, while chloritite exhalites (Bernard et al., 1982) and chlorite schist (Graf, 1977, p535) have been described from the Spanish Huelva Province and the New Brunswick area of Canada, respectively. McLeod and Stanton (1984) recognised phyllosilicate layers associated with stratiform sulphide deposits of south eastern Australia with the biotite-rich horizons representing metamorphism of hydrothermally derived nontronite which precipitated as aprons to the orebodies. The siliceous exhalite (tetsusekiei) developed over a considerable areal extent both surrounding the Kuroko orebodies and occurring in their immediate hangingwalls (Ohmoto et al., 1983; Kalogeropoulos and Scott, 1983), can probably be equated with the layers of Ore Equivalent Garnet Quartzite at Broken Hill.

Factors to be considered in this section will be the reasons for formation of OEH, and the physico-chemical controls which resulted in different element distributions east and west of the orebody. The

increase in certain elements nearer the orebody, as well as the behaviour of REE will also be examined. The general lack of metamorphic element migration in the Broken Hill area (section 6.1) suggests that the defined geochemical signatures of ore-related elements were present, at the latest, once diagenesis had ceased.

10.7.1 Origin of OEH

The paucity of zircon in OES, GQ and the orebody (section 4.2.3) suggests that these rocks were largely of chemogenic origin. The source of silica for GQ both surrounding the orebody as well as for the layers found in OEH, may be sought in the ore fluids. In solution, silica occurs in the form of monomers such as $\text{SiO}_2 \cdot n\text{H}_2\text{O}$ and is neither influenced by ionic strength of the solution nor pH near the neutral range (Holland and Malinin, 1979). Temperature is the major control on silica solubility and deposition. A saturated water solution at 250°C contains 1 000ppm amorphous silica, but a temperature drop to 25°C will cause precipitation of some 900ppm (Fig. 10.10).

The ratio A/M of surface area available for precipitation (A) to the mass of water (M) also has a pronounced effect on silica precipitation (Rimstidt and Barnes, 1980). Within fractured rocks the combined effect of slow cooling and a high A/M ratio promotes Si precipitation, producing the siliceous footwall stockworks (e.g. the Black Mountain Garnet Quartzite), whereas the A/M ratio is close to zero when hot fluid mixes with cold sea water above the sea floor, and though base metals precipitate, Si precipitation is relatively inhibited. Ohmoto et al. (1983) suggested that the relatively low Si content of many massive sulphide deposits is strong evidence that these deposits formed above the sea floor. Had Si precipitated together with precipitation of sulphides, the deposits would not be economical. The

location of GQ surrounding but not contained within the LOB, and as stringers in OES, might well reflect the continued movement in solution of Si relative to the base metals; due to the low A/M ratio in sea water.

The biotite in OES was probably derived from a combination of two sources. Terrigenous, illitic clays are thought to have provided the Al and some of the K, while K, Fe and Mg were supplied by the exhalative fluids which passed through the potassic, biotite-bearing basement rocks (Lipson, 1980) from which components of the ore-forming fluids were derived (section 10.5). Ellis (1979) stated that the most important equation governing reaction between K and Na in the hydrothermal environment is



With higher temperature, and independent of pH variation, the K/Na ratio in the fluid increases i.e. the equation moves to the left, thus any rapidly exhaled fluids will be K-enriched relative to Na. As such fluids cool on moving vertically up towards the lower temperature environment, they normally exchange some K for Na in the solid phases encountered (White, 1965). Mg^{2+} (and Fe^{2+}) may be liberated from Mg-silicate under conditions where acidic solutions attack relatively Ca-silicate-poor rocks (Ellis, 1979).

As described above, temperature drop is the major factor responsible for silica precipitation, but the oxidation state of Fe will vary. Any hydrothermal fluid starting from a point corresponding to A in Fig. 10.11 will follow a path roughly from A to B as it nears the surface and cools, with base metal sulphides precipitating (Large, 1977). In Large's (1977) terminology these form the proximal ores,

but the ratio oxidized S/reduced S (So/Sr) of the environment which the remaining hydrothermal fluid encounters will determine the form of Fe which precipitates. For $So/Sr < 1$, Fe sulphide forms whereas for $So/Sr \gg 1$, magnetite precipitates to the left of B. If during cooling and equilibration of the fluid to the sea water fO_2 value of 10^{-62} atm (Large, 1977, p562), the environment is sufficiently oxidizing, then hematite will form. The UOB, and later on the LOB, formed as minerals precipitated when hydrothermal solutions passed between points A and C as shown in Fig. 10.11. The complex redox conditions obtaining in specific subenvironments within which components of the ore lenses formed, and the order and mechanism of precipitation, lie beyond the scope of this thesis. Away from the orebody, the Ore Equivalent Garnet Quartzite and some of the elements incorporated into OS, formed as exhalites as the fluids passed from C to D (Fig. 10.11), with progressively less volume of precipitate being formed.

10.7.2 Metal haloes and assymetry

The high K_2O/Na_2O ratio of 39 for borehole core OS samples (calculated from Table 6.18) might be attributed to the K-metasomatism experienced during hydrothermal alteration associated with falling temperatures after exhalation (section 10.7.1). Plimer and Elliot (1979) listed a series of deposits for which Na and Ca losses and K gains have been documented in strata stratigraphically equivalent to orebodies, which they attributed to slight alteration associated with ore deposition. In the case of the ore equivalent tetsusekiei, Kalogeropoulos and Scott (1983) considered that similar chemical alteration resulted from a thermal event which post-dated the blanket-like deposition of tetsusekiei. In the Broken Hill area it is likely that OEH was forming over the entire life-span of the orebody, thus each new layer of depositing OEH would provide heat to the unconsolidated precipitate

on the sea floor, and allow additional alteration of the type documented by Kalogeropoulos and Scott (1983), viz. albite to chlorite to sericite. The relatively high K_2O/Na_2O value of 28 (23.6 after Na_2O recalculation) for NS, versus an average of 15 (8.7 after Na_2O recalculation) for SS, again reflects the NS association with ore-forming processes, and may be the reason for NS and BQ at Broken Hill having lower Sr contents, and in most cases lower Na as well, than in the Achab-Namiesberg area (section 7).

Reasons for the increasing Ca/Sr ratio progressively closer to the more highly mineralized parts of the orebody (Fig. 6.20) may be sought in the differential behaviour of Ca and Sr in hydrothermal solutions. Though the solubility of celestite ($SrSO_4$) is smaller by an order of magnitude than that of anhydrite ($CaSO_4$), the strontianite ($SrCO_3$) solubility is greater than that of calcite ($CaCO_3$) above 200°C. All four minerals become progressively less soluble at higher temperature (Holland and Malinin, 1979). The increasing Ca/Sr ratio closer to QM and AM may therefore indicate that once deposited, the central portions of the orebody remained above 200°C sufficiently long for preferential calcite rather than strontianite deposition, with QM (highest Ca/Sr ratio) at the base of the orebody remaining hotter for longer. Metamorphic recrystallization later led to the destruction of calcite during the development of silicates (Lipson, 1978; Rozendaal, 1982). Higher temperatures in QM were possibly also partly responsible for the lower Ba concentration there since barite solubility increases at higher temperature (Holland and Malinin, 1979).

Rocks such as Amphibole Magnetite which are part of the orebody, contain MnO contents of up to 7.8% (Table A.3). Outside of the complex redox subenvironments in which ore was forming, however, the

maximum MnO concentration lies at some distance from the orebody (section 6.3.1.6), and this is not a feature unique to Broken Hill. Smith and Cronen (1983) showed that in sediments surrounding the Santorini caldera and hydrothermal centre, Mn content actually increases away from the vent area. This phenomenon may be examined by contrasting the redox behaviours of Fe and Mn, since although Fe²⁺ and Mn²⁺ have similar ionic potentials (IP = 2.7 vs IP = 2.5) and are soluble, Mn⁴⁺ (IP = 6.7) has a far greater IP than Fe³⁺ (IP = 4.7) thus requiring considerably higher oxidizing conditions before Mn moves from the field of soluble cations to the field of insoluble hydrolysates (Mason, 1958; and section 9.1.4.2). The reducing sea water associated with the immediate environs of the Broken Hill orebody (section 10.2.1 and above) would prevent large scale Mn precipitation until the more normal redox sea water conditions were encountered, and the observed asymmetry to the location of the maximum Mn concentrations at 60m from the western closure of the orebody, but 300m from the eastern extremity (section 6.3.1.6), suggests that the packets of reduced water drifted from west to east. The lack of mixing with sea water may also be deduced from the notable difference in Ba concentration between QM (60ppm), AM (1 273ppm) and GQ (2 435ppm) which suggests that lower in the orebody stratigraphy, Ba in the ore fluid had little contact with sea water SO₄²⁻ as explained above (section 10.6), but higher up and further out, increased mixing resulted in progressively more barite precipitation.

The higher Cu-Si and Ba-Pb signature of OS immediately west relative to the signature east of the orebody (section 6.3.1.6) also indicates that the ore fluid flowed in an easterly direction with the west side of the orebody lying closest to the hydrothermal vent. At temperatures of below 50°C such as would be expected of sea water into which the hydrothermal fluid was introduced, the Zn/Pb and Zn/Cu

ratios of the solution are extremely high (Figs. 10.1 and 10.4b), suggesting that in the cool environment, temperature is the dominant parameter controlling relative Cu, Pb and Zn concentrations. Cu and Pb would preferentially precipitate near the vent, while Zn should remain in solution for a longer period of time, as suggested by the shallow drop-off in Zn concentration east of the orebody (Fig. 6.19a). The high Zn concentrations west of the orebody may be attributed to co-precipitation with the other metals. Si will also precipitate nearer the vent in response to falling temperature (Fig. 10.10), as will Ba (Figs. 10.8a and 10.9a). This evidence as well as the observation that the highest NS surface sample base metal concentrations occur in the west of Broken Hill (ALP205), clearly suggest that the vent from which the Broken Hill ores were exhaled, lies either at the western extremity of the orebody, or possibly even further west than that. Both Lydon (1983) and Large (1977) have remarked on the evidence suggesting that exhaled hydrothermal fluid is capable of flowing down a paleoslope until being trapped in a sub-basin. Seeing that aqueous sulphate and sulphide species do not readily equilibrate during rapid temperature changes below 200°C, exhaled solutions have the opportunity to move away from the vent and cool rapidly (Large, 1977).

10.8 Possible significance of Tank Hill

A number of unique features displayed by NS at Tank Hill are suggestive of proximity to a hydrothermal vent (sections 5.1 and 6.2.7.4). These include the gossan-like appearance and slight mineralization of NS there; the occasional cross-cutting veinlets; the bands of magnetite and barite; the presence and lensoid occurrence of Green Quartzite (GrQ) and Garnet Quartzite (GQ) hosted by NS; and the relatively high base metal content of samples of the latter and of NS. The fuchsitic GrQ comprises 97% SiO₂, yet it contains 561ppm Ba, 57ppm

Pb and 64ppm Cr (Table 6.16). In comparison, BQ with similar silica levels has < 10ppm Cr or Pb, and < 50ppm Ba (Table 6.22). Schreyer et al. (1981) described fuchsite corundum rocks and fuchsite quartzites, albeit in greenstone settings from the southern African Archaean, as residual end members resulting from post-volcanic exhalative alteration of komatiitic lavas. Ba substitutes for K in the lattice of fuchsite in these rocks. Surface outcrop NS samples with Cr levels of 114ppm already show a degree of Cr enrichment over their borehole core counterparts (Cr = 72ppm), thus the possibility exists at Tank Hill that the leaching of NS of most elements by hydrothermal solutions led to the relative residual enrichment of Cr there. The high Ba and Pb contents of GrQ testify to the mineralizing event, and silicification (or residual Si enrichment) to produce the restricted occurrences of GrQ and GQ, add weight to the hypothesis that Tank Hill represented a hydrothermal centre in the Aggeneys area. The localized barite and magnetite bodies could represent the near-vent, possibly subsurface, stratiform deposition of Ba and Fe in the oxidizing NS environment.

Nowhere on the Broken Hill inselberg do there exist similar features suggestive of proximity to a hydrothermal conduit. In section 10.10 below, a model will be detailed in which Tank Hill is proposed as a possible source from which emanated the ore-bearing fluids that ultimately flowed to form the Broken Hill orebody.

10.9 Rare earth elements

Aspects of REE patterns which reveal petrogenetic information include the absolute REE concentrations; the nature of the Ce and Eu anomalies since these two REE elements are more readily oxidized and reduced, respectively, than the other REE's; and the slope of the REE profile towards the HREE's. Sea water, as a common component of fluid which

interacts with solid phases to form sedimentary host rocks and orebodies, is often found to impart to these rocks its strongly negative Ce anomaly (low Ce residence time), and positive slope towards the HREE's (HREE have a higher residence time than LREE) (Herrmann, 1970). Currently forming ores to a large extent display these features (Fig. 6.24), even though sea water has absolute REE levels of the order of 10^{-7} those of shale.

A feature of the Broken Hill ores and ore related rocks is their narrow range of normalized REE concentrations which is of similar magnitude to that of the Broken Hill schists, but contrasts markedly with the wide variations displayed by the presently forming ores (Fig. 6.24). Either the Broken Hill ores contain significant proportions of their host rocks, or both rock-types ultimately originated from a common source. The two Garnet Quartzites and one of the two Massive Sulphide samples analysed, display a weakly developed negative Ce anomaly (Fig. 6.21). Only the magnetite-rich parts of the orebody and some of the ore-associated schists display relative enrichments in HREE. Accepting that rocks at Broken Hill formed below sea water (sections 9.1.4.1, 9.1.7 and 10.4), then very little time elapsed between sulphide deposition and burial since Fleet (1984) and Ruhlin and Owen (1986) convincingly showed that hydrothermal sediments adopt the sea water REE signatures given sufficient exposure time.

The high total REE content of the ores probably reflects a felsic source since granitic rock has some three times the REE content of basalt (Herrmann, 1970), and the Broken Hill ores compare far more favourably in their total REE concentrations with the intermediate caldera-related (Smith and Cronen, 1983) Santorini ores than with the basalt-related Atlantis II and Galapagos deposits (Fig. 6.24).

Michard and Albarede (1986) concluded that the fluid characteristics

determine the Eu concentration of hydrothermal sediments since acidic, reduced waters at $> 250^{\circ}\text{C}$ are required to convert Eu^{3+} to the more soluble Eu^{2+} , and both Alderton et al. (1980) and Strong (1984) found that in the case of REE's, sericitic alteration of feldspar, as envisaged for the basal gneisses at Aggeneys, leads to a selective loss of Eu. Graf (1977) noted that it is the Eu^{3+} ion which fractionates into baritic rocks to form EuSO_4 , thus explaining the most strongly defined positive Eu anomaly in Massive Sulphide sample ALP110 which contains 2% barite.

Seeing that the orebody itself fails to show HREE enrichments suggests that the positive HREE patterns seen in sporadic samples of OS, OEGQ and NS (sections 6.3.1.4 and 6.2.5) may not be a direct consequence of mineralization. Furthermore, mobilization of HREE requires strongly alkaline solutions (McLennan and Taylor, 1979; Michard and Albarede, 1986; Michard et al., 1987), conditions which were not likely to have produced the Aggeneys-Gamsberg deposits (section 10.3.3). HREE preferentially partition into chlorite (Alderton et al., 1980) and garnet (Graf, 1977), hence it is likely that the HREE signatures of some of the schists and Garnet Quartzites were inherited from the overlying sea water by the exhalative components of precursors to biotite and garnet, during periods of sufficient quiescence. The relatively elevated HREE patterns from a few NS samples may represent the preferred accommodation of the smaller HREE ions (Alderton et al., 1980) in the pre-biotite, chlorite-glaucinite lattice during passage of some mineralizing fluids through NS. The NS signature is possibly akin to that in the Kidd Creek footwall alteration zone (Campbell et al., 1984). The relative HREE enrichment of some Aggeneys samples compared with NTS samples from Achab suggest that analysis of REE's still offer exploration application, similar to the advantages suggested by Campbell et al. (1982) for distinguishing between

pregnant versus barren felsic volcanics in the Canadian greenstone belts.

Compared with the magnetite-rich rocks associated with Broken Hill mineralization, the magnetite ironstone ALP228 from Froneman se Kop has a much higher total REE content and is relatively depleted in HREE. Elevations in the elements Th, U, Zr, Y and REE together with the high Ti levels suggest that ALP228 is predominantly of detrital placer origin and is unrelated to mineralization.

The lack of an elevated HREE signature in the Tank Hill samples (all taken from Tank Hill surface outcrop) may be attributed to extreme weathering accentuated by sulphuric acid gained from sulphides in these rocks, which resulted in preferential removal of HREE (Nesbitt, 1979). A similar explanation was proposed for the low HREE content of MnQ (section 6.2.7.1).

10.10 Genetic model for Aggeneys-Gamsberg orebodies and OEH

Application of Cu-Pb-Zn ratio modelling to the Aggeneys-Gamsberg deposits (section 10.3.3) showed that the four orebodies were probably generated by independently operating convecting systems which gained their metals by circulating deep into the basement (section 10.5). The possibility that fluids migrated laterally along an aquifer and selectively deposited their metals, has already been discounted in section 10.1 and 10.2.1. An alternative hypothesis of a single convective cell which exhaled hydrothermal fluid at a point source, is highly unlikely because the fluid would have had to migrate over tens of kilometres, progressively and selectively precipitating out different elements. The deposits should then be continuous, instead of only having possible OEH linking them. If the fluid reached the surface in the Black Mountain-Tank Hill area, these being chosen

because of their hydrothermal alteration features (section 10.1 and 10.8), then the barite at Gamsberg must have had a source independent from that of the sulphide orebody since the instability of Ba in contact with sea water (sections 10.4 and 10.6) would preclude its migration beyond the limits of the reducing hydrothermal packet of solution. A dual source model for Zn and Ba at Gamsberg would be highly fortuitous. The convective system responsible for generating the Cu-rich Black Mountain orebody must have been more alkaline (Figs. 10.4a and d) than systems at the other deposits. If these fluids then migrated eastwards precipitating the bulk of the Pb in the Broken Hill area and then most of the Zn in the Big Syncline and Gamsberg areas, the fluids would have had to evolve to progressively more acidic compositions in order to preferentially retain Pb and then Zn in solution (see 50°C curves in Figs. 10.4a and d). Such a model is untenable because mixing with normal seawater (pH = 8.1 - 8.3; Krauskopf, 1979, p46) in the zones between the different basins, would have kept the solutions alkaline. Furthermore, the temperature drop encountered on exhalation (section 10.6) would have precluded migration of metal-charged fluids over the required distances.

In reviewing the genesis of the orebodies it is pertinent to summarize some of the key limiting factors present in the Aggeneys-Gamsberg area. These include the fact that the supracrustal rocks are unusually thin, in total measuring < 1 000m, of which only some 60% of the succession occurs below the orebodies, thus metal leaching of the basement is likely. The Bushmanland Subprovince is so dominated by exposures of highly siliceous and potassic gneisses and granites, including those which definitely predate the orebodies (i.e. Achab Gneiss), that even had major thrust-type dislocations taken place, all four orebodies would effectively still lie on a common felsic basement, yet each deposit has unique metal ratios. There are no

gross intrusions underlying the ore horizon which could have stimulated convection, thus geothermal energy was the most likely source of heat. The thin amphibolite layer at the boundary between gneiss and NS below the Black Mountain orebody, and the minor lenses of amphibolite within NS at Broken Hill, could have contributed only small quantities of thermal energy. The presence of rifting in the Aggeneys-Gamsberg area was likely (Lipson, 1981a; Rozendaal, 1982), as suggested by the amphibolites (tholeiitic meta-basalts; Reid et al., 1987) at Koeris, Aggeneysberge and Gamsberg, and the clastic wedges of conglomerate and diamictite at Black Mountain and Aggeneysberge (Ryan et al., 1982; Strydom, pers.comm., 1982). The higher heat flow associated with these rift faults which separated the individual basins, could therefore have set convection in motion, and helped focus fluids during exhalations.

At the time of ore deposition, the Broken Hill basin was at least partly open to the sea (sections 9.1.4.1, 9.1.7 and 10.4) and the same may be deduced for the basin at Black Mountain since similar oxygenated rocks which lack graphite, predominate there. In contrast, the Gamsberg basin was enclosed (section 10.4), and the accumulation of organic remains on the sea floor would have consumed O_2 during conversion to CO_2 , resulting in increased H^+ concentration (Grasshoff, 1975). Such falls in pH below thermoclines are recorded from Lake Kivu (Degens and Stoffers, 1976) and Framvaren Fjord (Piper, 1971) hence on a regional basis, sea water pH at the time of ore deposition must have decreased towards the east, as corroborated by the more positive $\delta^{34}S$ ratio being located in that direction (section 10.4). The lowest $\delta^{34}S$ ratios from the Black Mountain area suggest that this basin was even more open to the sea than Broken Hill. The Cu-Pb-Zn ratio modelling independently showed that ore solutions became progressively more acidic towards the east (section 10.3.3). Von

Gehlen et al. (1983) suggested that bacterial reduction of sulphate in the enclosed Gamsberg basin caused an enrichment of ^{34}S in the basin waters. This fluid thus already had the attributes of low pH (section 10.3.3) and reduced S (section 10.4), most significant for generating solutions with high Zn/Pb and Zn/Cu ratios, before being convected down into the basement to later re-emerge as the metalliferous hydrothermal solutions having positive $\delta^{34}\text{S}$ ratios. Not only Zn but also Ba concentrations would be enhanced in these solutions, while the more oxidizing, S-deficient waters would carry more Pb but far less Ba (section 10.3.1). The low temperature ($< 200^\circ\text{C}$) fluids rich in reduced S would be dominantly Zn-rich - Pb-poor (section 10.3.1), while similar fluids rich in Cl^- (and not in reduced S) would be relatively Pb enriched. Thus the Zn and Ba in the Gamsberg deposit are readily explained, while circulation of more oxidizing and higher temperature water led to the Broken Hill orebody being Pb-rich, but relatively Ba-poor. Clearly these are not the only reasons for the difference between the Gamsberg and Broken Hill deposits since Black Mountain has substantial Pb as well as an associated 8mt barite deposit. The highest temperature fluids which formed the Black Mountain deposit (section 10.3.3), had similar surface water $f\text{O}_2$ concentrations to those at Broken Hill, but would have nevertheless promoted Ba extraction in the Black Mountain hydrothermal cell because the solubility of Ba increases with temperature up to at least 300°C if the NaCl content is $> 1m$ (Holland and Malinin, 1979), conditions which were probably met at Black Mountain but not at Broken Hill (section 10.3.3).

It is therefore suggested from the discussion above that while the source and isotopic character of S for the orebody sulphides is envisaged as circulated sea water derived partly or wholly from the same local basin into which the ore fluids would ultimately be

debouched, cold sea water sulphate was the source of sulphur for barite precipitation when the hydrothermal Ba reached the basin. Inherent in the proposed model of circulating convective cells which leached the basement, is that large quantities of fluid must have been pumped through the basement (high fluid/rock ratios), as also proposed by LeHuray et al. (1987) for the formation of the Irish deposits.

The Gamsberg orebody probably formed from fluids which penetrated to relatively shallow crustal levels, as deduced from the low fluid temperatures. The felsic and potassic nature of the crust encountered enhanced the fluid's acidity (section 10.5). Exhalation back into the enclosed basin further lowered the pH so that with time, the fluid system became more efficient at leaching Zn from the crust. This resulted in the observed increasing Zn concentrations found stratigraphically higher up in the Gamsberg orebody (Martin, 1989). As fluids reached the sediment-water interface, no metals would have escaped due to the enclosed nature of the basin, hence confirming that the Gamsberg ore fluid must have contained Zn to the virtual exclusion of Cu and Pb.

Of the Aggeneys-Gamsberg deposits, Black Mountain had the highest temperature fluid as deduced from thermochemical modelling (section 10.3.3) and from the maximum temperature drop (Fig. 10.10) indicated at Black Mountain by the large quantity of silicification in the form of Garnet Quartzite replacement of schist there. Small zones containing chalcopyrite and pyrite in basal gneisses at Black Mountain have not been documented from any of the other deposits, and suggest that not only did fluids pass through the gneisses in the stratigraphic footwall of the Black Mountain deposit, but that these solutions at Black Mountain were also at higher temperatures than elsewhere. These indications of high temperature fluids suggest that

fluids penetrated to the greatest depth at Black Mountain. During the convective flow of oceanic water in the Black Mountain area through the felsic rock of the exposed crust, the fluid pH would decrease (section 10.5). The Cu-rich nature of Black Mountain indicates that the fluid composition was in fact less acidic than for any of the other deposits. It is therefore suggested that the more deeply penetrating Black Mountain convective cell reacted extensively with crust of a more mafic composition at depth in order to have buffered the fluid to the high estimated pH values. The slightly more acidic character of the Broken Hill convective cell fluids, and the lower estimated fluid temperatures, suggest that in the case of Broken Hill, the fluids did not penetrate to the same depth as those of Black Mountain, and reacted only to a limited extent with the proposed more mafic crust.

The relative positioning of the Aggeneys-Gamsberg deposits with respect to the prograding beach-barrier sedimentary system is schematically shown in Fig. 10.12a in which Black Mountain and Broken Hill formed in the more oxidizing washover deposit zone which was in communication with the open sea (probably via inlets not shown in the illustration), while Big Syncline and Gamsberg developed in what was a more restricted part of the estuarinal environment where reducing conditions predominated. The details of ore in relation to host rocks, and of convective cells, are contrasted between Gamsberg and Broken Hill in Fig. 10.12b.

It was suggested in section 10.5 that successive cycles of convecting fluid could result in the formation of ore lenses with distinct metal characteristics. If tectonic activity occurred before restoration of the rocks to the ambient geothermal gradient, then subsequent convective cells would be shorter lived, resulting in the younger ore

lens being smaller, as found at Broken Hill. The Intermediate Schist would represent sedimentation which occurred during the period between hydrothermal exhalations.

Once deposited, the orebodies would represent easily erodible soft sediments, and it is envisaged that the slow formation of the stratigraphically overlying BGZ and SS in the quiet, prograding, restricted environment (sections 9.1.6 and 9.5), ensured preservation of the Broken Hill deposit. Large (1981b) concluded similarly that quiet (graphitic) conditions are necessary for the preservation of sedex deposits.

In summary, the salient points envisaged for the genesis of the orebodies and OEH follow below. Each of the four Aggeneys-Gamsberg deposits developed from independent hydrothermal fluid convecting cells with the composition of the water in the overlying rift-bounded basin to some extent determining the physical properties of the circulating fluids (Table 10.6). The deeply circulating fluids at Black Mountain and the Cu-rich nature of that orebody, suggest that the basement is probably more mafic at depth. Both the depth of fluid circulation which controlled fluid temperature and pH, as well as the initial fluid properties prior to convective circulation, ultimately determined the proportions of metals leached from the basement. Consequent orebodies largely retained the metallic ratios of the fluid since the condition $m_{\text{Total S}} \gg m_{\text{Total metal}}$ was met. A high fluid/rock ratio obtained throughout the mineralizing events which tapped the renewable source of overlying sea water. Metals were deposited within a few kilometres of the individual conduits, mainly due to temperature loss. The driving force for convection was probably geothermal energy, which requires that the fluids propagated progressively deeper with time. In the case of Broken Hill, this process may have continued until the

brittle-ductile boundary was encountered, at which point the mineralizing process for the UOB lens ceased. Following a period of sedimentation during which time IS was deposited, generation of a shorter-lived convective cell resulted in LOB being formed.

Although focused at specific centres along faults, the exhaled fluids also leaked through the footwall rocks such as NS and basal gneisses, depositing sporadic, disseminated base metal sulphides in both, and minor Garnet Quartzite lenses in NS. Rocks stratigraphically overlying the Broken Hill orebody remained unaffected by the mineralizing event. As the Broken Hill ore fluid moved down the paleoslope in an easterly direction from its vent at Tank Hill, minor amounts of exhalative components were deposited to form OEH. The bulk of the mineralizing fluids probably came to rest in the deepest part of the Broken Hill basin, which was oxidizing except for that part affected by the highly reducing hydrothermal fluids. Small parcels of the fluid continued eastwards to produce OEH as far away as Maanhaarkop.

11. CONCLUSIONS

11.1 Stratigraphy and sedimentology

In the study of rocks around Aggeneys, use has been made of field relationships, petrography, and lithogeochemistry, with emphasis on the latter because of the degree of metamorphic alteration and structural complexity. An investigation into the degree of element mobilization due to metamorphism has revealed that care need be taken only with the elements Na and and to a lesser extent Sr, which were lost to pegmatites.

Along the line of inselbergs stretching from Broken Hill to Maanhaarkop and underlying a suite of felsic gneisses, three major litho-types exist, namely the structurally overlying Namies Schist (NS), Broken Hill Quartzite (BQ) and then Shaft Schist (SS). Both the petrography and lithogeochemistry reveal that NS and BQ are linked by gradational variations, while SS is likely to have formed a conformable part of the succession. Between BQ and SS occurs a mixed suite predominantly comprising schist (most similar in character to NS), which hosts the Broken Hill orebody as well as Ore Equivalent Schist and Garnet Quartzite. The unit as a whole is called Ore Equivalent Horizon (OEH). Geochemical evidence suggests that OEH has also maintained its continuity in the rock succession. Within SS but near the contact with OEH, are found thin lenses of Calc Silicate Rock plus Manganese Quartzite (CSMQ).

Physical characteristics as well as lithogeochemistry reveal that whereas NS formed in an agitated, oxidizing environment, with deposition of detrital quartzites as an end member, SS formed as a black shale in a shallow water lagoonal or estuarinal environment with CSMQ representing the only temporary reversion to oxidizing conditions. The high S content of SS and the negative Ce anomaly of

CSMQ indicate that these rocks formed beneath sea water. Sporadically high base metal values in NS indicate that the chemistry of NS was affected by the mineralizing event, and this interpretation is consistent with the lower $\delta^{18}\text{O}$ values in NS than in SS. The Broken Hill succession as seen today is therefore interpreted as overturned, based on the above evidence; on the inverted cross-bedding in quartzites; on the observation that SS in the immediate hangingwall of CSMQ was also oxidized; and on the regional presence of gneiss at the base of metasedimentary successions in Bushmanland.

The triad NS, BQ and SS emerge as metasediments of high chemical maturity, and together with their low Eu/Eu* ratio suggest that their deposition occurred along a passive continental margin setting. The order of occurrence from NS through BQ to SS conforms well with linear beach-barriers with NS representing the seaward shoreface sediments, BQ the quartz arenite beach and dune environment, and SS the sediments formed in the partly enclosed basin nearer the continent. Large components of OEH probably represent washover deposits sourced from NS. Such continental margin sequences are dynamic systems which commonly prograde with the shoreface sediments coarsening upwards to the quartz arenites, and in turn being overlain by the black shale.

Mapping, petrographic work and lithogeochemistry have confirmed both the presence and polarity of the triad of rocks in the Namiesberg-Achab and Wortel areas, hence it is suggested that progradation extended from well to the north of Aggeneys to some point south of the area. The Late Jurassic Cotton Valley Group straddling the Gulf of Mexico represents an analogous model in which the same triad of rocks give way closer to the provenance to arkosic red beds, which both underlie and overlie the succession. In Bushmanland, such metasediments may be present in the form of the Beenbreek Formation,

the feldspathic quartzites in places at the base of the succession at Wortel, and in the feldspathic quartzites or quartzitic gneisses at the top of the succession in the Aggeneysberge. Recognition of the regional nature of the metasedimentary triad considerably simplifies stratigraphy in the schist and quartzite belts of the Aggeneys Subgroup.

Comparisons between the chemistry of rocks from Aggeneys, Namiesberg-Achab and Wortel indicates that variable sand input was the dominant factor controlling regional facies variation. Progressively cleaner separation of Al from Si in the schists and quartzites further south suggest progradation in a southerly direction away from a northerly provenance. The thickening of quartzite to the north of Aggeneys supports this contention. The REE patterns amongst other evidence show that a weathered granodioritic parent probably contributed its detritus to forming the Aggeneys Subgroup, and both the Pb isotope and oxygen isotope data are compatible with a provenance of granodioritic rocks of the Vioolsdrif Suite. Ca removed from the provenance during early stages of weathering was probably precipitated in a distal environment to form the calcic rocks south and east of Aggeneys, while the Na remained in solution. Detrital transport of the granodioritic residuum lead to the generation of Ca- and Na- depleted shales and sandstones.

The chemistry of Calc Silicate Rock and of Manganese Quartzite differ significantly from that of possible correlative rocks in the Broken Hill orebody, yet the elevated concentrations of base metals and U, Sb, As and Ag in CSMQ certainly suggest a hydrothermal component. It is suggested that the fairly violent introduction of metal-bearing, hydrothermal fluids into the meromictic basin caused disruption of the thermocline beneath which SS was forming. The elements and oxides

P_2O_5 , MnO, Fe_2O_3 , MgO, CaO and SiO_2 at the thermocline boundary, as well as the introduced metals, then precipitated to form CSMQ, while Al_2O_3 remained soluble. As acidic conditions re-established in the deepest part of the basin, CSMQ dissolved, leaving peripheral lenses of the rock. The lack of CSMQ in the immediate stratigraphic hangingwall of the orebody therefore suggests that ore was deposited in the deepest part of the local basin.

From the foregoing, there appears to be little sedimentological control on the location of the Broken Hill orebody within the prograding shoreline, save that progradation of SS almost immediately above the deposit helped in its preservation. Possibly the regional occurrences of small sulphide deposits within NS (Rozendaal, 1982) reflect the vestiges of deposits largely destroyed by the subsequent high energy style of sedimentation.

11.2 Ore genesis and local tectonics

The higher heat flow normally associated with rift environments, as alluded to in section 10.10, would have promoted the leaching of metals by convecting fluids, and as envisaged by Rozendaal (1982), these structures would focus the flow of returning hydrothermal solutions. The germain features envisaged for localizing the orebodies are represented schematically in Figs. 11.1a-c, and depict the most likely, though unproven, tectonic controls on the mineralization process. East-north-east trending continental margin rift faults developed in the basement before or during early sedimentation of the Aggeneys Subgroup (Fig. 11.1a) over which the beach-barrier system prograded to the south, producing the thickest development of NS in the Aggeneys-Gamsberg area and a thinning of BQ towards the south (Fig. 11.1b). Tilted, fault-bounded rift blocks are envisaged as having created the sub-basins necessary for the

development and trapping of the individual ore deposits (Fig. 11.1c). Periodic mineralization in the Aggeneys area over such stationary "hot spots" is manifest by minor sulphide mineralization in NS at the western closure of the Aggeneysberge (Lipson, 1978) and in the eastern Aggeneysberge, and possibly at Tank Hill as well, while small lenses of sulphide occur at Broken Hill within MDS. The two superposed lenses comprising the Broken Hill orebody also represent a stationary source generating mineralization in successively higher layers of the stratigraphy.

The synsedimentary growth faults in the Aggeneys area produced individual yoked basins of which that at Black Mountain was the deepest and hottest and probably overlaid the master faults "a" and "b" in the rift system (Fig. 11.1c). Fault "b" fed the fluids to the proximal Black Mountain orebody, while fault "a" which had its surface expression at Tank Hill, fed the more distal Broken Hill orebody. The onset of a right-lateral simple shear couple (Fig. 11.1d) initiated synclinal formation at Black Mountain (Fig. 11.1e), being the hottest and deepest of the sub-basins, and this earliest deformation at Aggeneys caused reactivation of the normal faults into either reverse faults (thrusts) on the southern limbs of synclinal structures, or greatly exaggerated the throw on the normal faults, causing major "losses" of supracrustal rocks between the inselbergs. Measurement of lineations at Broken Hill suggest subhorizontal movement, thus instead of movement from north to south as indicated by the northerly dip in Bushmanland, the movement direction probably had a strong westerly component. The later, open folding in the Aggeneys area produced the configuration seen today, with folding of the postulated reactivated growth faults which cross-cut the strata at shallow angles (Figs. 11.1f and g). It is of note that a structure conforming to fault "a" bringing quartzite and ore progressively into contact with gneiss, has

been located in drill hole intersections between Black Mountain and Tank Hill (Stedman, 1980).

Modelling of processes responsible for the generation of deposits with such widely varying metal ratios over so thin a supracrustal succession has shown that independent cells of convecting fluid must have leached many kilometres down into the basement. Selective stripping by solutions, of radiogenic Pb from basement feldspars commonly results in syngenetic ore deposits returning Pb-Pb ages younger than their host rocks (Prof. H. Barnes, 1990, pers.comm.), and may account for the anomalous 1 200 - 1 500Ma ages determined for the Aggeneys-Gamsberg orebodies by Koepfel (1980). The combined effects of utilization by the convective systems of the physically and chemically different waters from the individual basins, and the depth of fluid penetration into a basement which probably becomes more mafic at depth, were responsible for the differential leaching of metals. In the case of Broken Hill, once the fluids were focused up the major faults and exhaled onto the sea floor, the sulphide load was deposited rapidly in the nearby Broken Hill basin, mainly in response to falling temperature. The layered Garnet Quartzite and biotite-garnet schist lying along the time horizon of the orebody represent a combination of exhalite not incorporated into the orebody and terrigenous clays. Some of this material may have emanated from subsidiary cracks in the sea floor at varying distances from the major faults, thus contaminating strata stratigraphically below the ore time horizon. Certain elements and inter-element ratios in both OEH and NS could therefore be used at local and regional scales to guide the explorationist towards a potential orebody.

11.3 Ore halo and exploration

It is shown that NS near the Broken Hill orebody has higher concentrations in the elements Pb, Zn, Ba, Fe, P and Y than in regionally developed NS unrelated to known mineralization. This observation holds notwithstanding the more Si-rich and Al-poor nature of NS samples from Broken Hill. Broken Hill Quartzites near the orebody also have elevated concentrations of the elements Cu, Pb, Zn, Mn and Fe, and lower Na and Sr, than their regional counterparts. For SS, only the element Pb is significantly higher near the orebody.

The mineralization halo along the Ore Equivalent Horizon extends for up to 10km from the Broken Hill orebody. Samples of Ore Schist from borehole core reveal increases in the elements Zn, Mn and Ba towards the orebody, while for outcrop samples of that rock, the elements Zn, Ba and Pb show a general increase nearer the orebody. When the "Ore Factor" scores from Factor Analysis of Ore Schist from both borehole core and outcrop samples are plotted against distance, there is also a general increase in scores towards the orebody. For the rock-type Garnet Quartzite, and the mixed rock Ore Schist and Garnet Quartzite, both the Zn and Pb contents increase towards the orebody, as do the Pb/Pb+K and Zn/Zn+Al ratios.

The geochemical trends described in the Ore Equivalent Horizon are defined by broad scatter about the generally increasing values of indicator elements and inter-element ratios progressively nearer the Broken Hill orebody. Numerous samples are required for confident application of the technique to the search for more ore.

11.4 Geotectonic setting

The Groothoek Thrust (Fig. 1.4) was viewed by Moore (1986) as the suture zone between the northerly subducting "Namaqualand microcontinent" on which is located the Bushmanland Group, and the Vioolsdrif Suite to the north. He stressed the role which subduction had on lithospheric evolution of the area, since not only were the calc-alkaline volcanics of the Orange River Group attributed to melting above the subduction zone, but acid volcanism which post-dated the continent-continent collision event, was also indicated just to the north of the envisaged suture zone. It is these late volcanics which Moore (1986) proposed were feeding the "Namaqualand peripheral basin" in which the Bushmanland Group was developing. Joubert (1986) has, however, called into question the likelihood that the Groothoek Thrust marks a suture since the mafic intrusives which help define the thrust zone are definitely not obducted oceanic crust, but probably represent the mafic to ultramafic base or subvolcanic complex part of the Orange River Group. The possibility that south of Vioolsdrif the Thrust cuts rocks of the Vioolsdrif Suite also suggests that the Thrust is not a cryptic suture. Blignault et al. (1983) interpreted the Groothoek Thrust as just one of a number of thrusts. Gravity profiles from de Beer and Meyer (1983) do not detect the Groothoek Thrust and show rather that the Namaqua Front Zone (Fig. 1.1) is the northern boundary to the craton. To the north and south of the Groothoek Thrust the basements of Orange River Group-Vioolsdrif Suite and Achab Gneiss, respectively, have approximately the same ages of 2.0Ga (Reid and Barton, 1983; Welke and Smith, 1984; Armstrong et al., 1988), and remarkably similar metasediments occur on both sides of the Thrust. The quartzites in the Pella and Dabenoris areas look the same as those at Aggeneys and both contain heavy mineral layers. Fresh schist borehole core examined from the Pella area has all the attributes of SS, while the quartzite-banded iron formation-muscovite

schist-conglomerate suite occurring in the Dabenoris area has the same characteristics and stratigraphic polarity as found at Gamsberg. Since both basement and cover rocks to the north and south of the Groothoek Thrust have such similar properties, there is little reason to deduce that separate continents originally existed on either side.

The dating of 2.0Ga detrital zircons from BQ renders unlikely Moore's (1986) model of 1.6Ga acid volcanics synchronously feeding detritus to the developing Bushmanland basin. The present study has also shown that weathering of a continental granodioritic provenance was required to generate the metasediments at Aggeneys, therefore rocks of the Vioolsdrif Suite, which probably formed the interior when the siliclastic Bushmanland Group was developing along the continental margin, remains a likely provenance. The Pink Gneiss which underlies the metasediments and falls outside the scope of this study, may well represent a composite felsic rock of both igneous origin (intrusive or extrusive) or reworked igneous rock, as proposed by Moore (1986). The sedimentary components thereof, which were derived from the youngest and most felsic part of the Vioolsdrif Suite, probably formed red bed deposits.

Early (2.0Ga) subduction from the north (Fig. 11.2a) probably generated the calc-alkaline Vioolsdrif Igneous Suite (Joubert, 1986), followed by deep weathering of this predominantly granodioritic terrain. The Namaqua Front represents the suture zone once continent-continent collision eventually occurred (Fig. 11.2b). Although Stowe (1986) suggested that subduction along the Southern Cape Conductivity Belt (SCCB) (Fig. 1.1) in the Vanrhynsdorp area started at only ~1.0Ga, it is suggested here that subduction may have commenced at an earlier date (1.7 - 1.8Ga) which generated a second granitoid and volcanic belt. The Bushmanland basin formed on the passive margin

adjacent to a marginal basin (Fig. 11.2b), and east-west rifting there might have been influenced by SCCB subduction. The weathered Vioolsdrif provenance contributed sediments along the passive northern margin. Immature detritus was fed into the Bitterfontein area from the volcanic arc to the immediate north and from the continent to the south, to produce the feldspathic quartzites and metapsammitic gneisses mapped by Moore (1986). "A-subduction"-type megasuture tectonics (Mitchell and Reading, 1986, p513) which followed the continent-continent collision in the south, may have caused thrusting with a south-west vergence (Fig. 11.2c) which reactivated normal faults in the Bushmanland basin. The geotectonic model favoured therefore comprises three continents and two subduction zones, with the Bushmanland and Richtersveld Subprovinces representing a single micro-continent (Fig. 11.2b).

The major zones of rifting in the Aggeneys area are probably analagous to those found along passive continental margins as shown by Falvey and Mutter (1981) over which sediments typically prograde. These Australian examples refer to continental breakup with sea floor spreading, causing basins having up to 6km of sediment. In contrast the thin (< 1km thick) Aggeneys Subgroup is here envisaged as having formed along the passive margin side of a shallow marginal basin (Fig. 11.2b) which, as shown in Fig. 11.67E of Mitchell and Reading (1986), are commonly high heat flow regimes. The increased geothermal gradients in the Aggeneys-Gamsberg area during the time of ore deposition probably heralded the transition of the Aggeneys environment from one of passive continental margin as deduced from the lowermost part of the supracrustal succession, to that of a back arc basin (Reid et al., 1987) as suggested by the amphibolites and conglomerates at the top of the succession. The combination of passive margin rifting, thick felsic basement and local areas of

elevated temperature were probably the key factors leading to generation of the Aggeneys-Gamsberg Pb-Zn-Cu sedex deposits. Progradation of SS at Broken Hill ensured preservation of the deposit.

PART E.
APPENDICES AND REFERENCES

12. APPENDICES

APPENDIX A SAMPLING AND ANALYTICAL TECHNIQUES

A.1 Sampling rationale and techniques

A.1.1 Parameters common to borehole core and surface outcrop sampling

A previous orientation study on MnO distribution surrounding the Broken Hill and Big Syncline orebodies (Lipson, 1981b) showed an exponential increase in MnO concentrations with decreasing distance from each deposit. Samples for the current study were therefore collected more frequently progressively closer to the orebody in order to detail the geochemical character of the rocks over the zone of most rapid chemical change (Figs. A.1 and A.2).

No samples were taken across major lithological contacts. Bands of < 2m (usually pegmatite or quartzite) were omitted except for interbedded OES and GQ where a combination of the two were taken, and the sample called OES+GQ. All weathered or fractured pieces of rock were omitted from samples.

A.1.2 Borehole core samples

Most sampled core taken was of BX diameter (~43mm). Five to ten centimetre pieces of homogeneous core were taken at intervals of ~1.5m, and accumulated over the sampled width of up to 90m for some quartzites.

Two Wortel boreholes were sampled because neither was adequate for sampling of complete stratigraphic successions. WTL4, which contains the most complete stratigraphic succession, is too veined and fractured at shallow depths (< 372m from surface) to be sampled for litho-geochemical purposes. The supracrustal succession in WTL3 was therefore sampled from 261m down to 470m, whereafter sampling continued from the same stratigraphic horizon at a depth of 394.9m in WTL4 to the end of the hole (Fig. A.1d).

A.1.3 Surface outcrop samples

Along the strike of specific lithologies, a bulk sample was collected from an area measuring up to 10m * 10m. All obvious weathered portions of the rock were removed in the field.

A.2 Analytical methods

A.2.1 Sample preparation

All external surfaces of borehole core were sanded down using emery paper. Where possible, any signs of weathering, veining or fracturing were separated from the main sample using a manual or hydraulic splitter. In the case of sample ALP183, selection of recently weathered borehole core from a rusted core tray could not be avoided. The standard techniques employed by the Geochemistry Department of the University of Cape Town (Duncan et al., 1984) were used for analyzing the Bushmanland rocks. The fresh chips of sample were then cleaned in

distilled water by ultrasonic agitation for 10 - 20 minutes, followed by drying at 110°C for +4 hours. A jaw crusher fitted with Mn-lined, carbon steel jaws, was used to reduce the sample to +10mm chips. All apparatus in the crusher with which the sample comes into contact was carefully cleaned and off-cuts from the splitting phase was crushed as a precontaminant, prior to crushing the next sample. The crushed sample was coned and a representative 60g aliquot extracted for pulverizing for 25 minutes in an agate Siebtechnik vessel. Cleaning and precontamination of the vessel followed the procedure outlined for the jaw crusher. Some 6g of the pulverized sample was compressed into a pellet, using 2% mowiol solution as binder, a die to shape the pellet, boric acid as a backing, and a hydraulic press which subjected the pellet to seven tonnes pressure. Trace element and Na₂O analyses were performed on these briquettes. The H₂O- and loss on ignition (LOI) were determined by weight loss on heating a 1.5gm aliquot of pulverized sample to 110°C and 1 000°C, respectively. The major rock-forming oxides excluding Na₂O were determined on duplicate glass disks fused at 1 000°C and comprising 0.28g of ashed sample, 1.5g of flux (Spectroflux 105) and 0.02g of NaNO₃ as outlined by Norrish and Hutton (1969). Fusion was performed in a Pt-Au crucible and the bead cast in a carbon mould.

A.2.2 X-ray fluorescence spectrometry (XRF)

Virtually all analyses excluding that of carbon, were performed on the Siemens SRS-1 and Phillips PW1400 wavelength dispersive XRF spectrometers, with the K-alpha line being measured for all major and most trace elements (Table A.1). Blanks and standards were measured and all the data corrected via programmes on the HP 1 000 mini-computer, for background, spectral line interference, dead-time, instrumental drift and position in the sample holder carousel. Standards utilized included rocks from the USGS and South African NIMROC collections. The lower limits of detection (LLD) and counting errors for all elements deduced by XRF are given in Table A.2. A number of quartzite samples for which the elements Na₂O, MgO, and MnO fall below the LLD, were analysed at the ppm level by Gold Fields Laboratories using the Atomic Absorption Spectroscopic (AAS) technique. All AAS analyses were run in duplicate with blanks being measured to monitor background, and pure elements diluted in 10% HCl, used as standards. Silicates were dissolved in HF and all solutions were measured at 10% HCl dilution. In order to integrate the low level AAS data with the XRF analyses, a reduced major axis linear regression was performed on duplicate AAS- and XRF- derived analyses which fall above the XRF lower limit of detection, and the AAS analyses were adjusted using the regression equations.

A.2.3 Volatile-free recalculation

In Tables A.3 and A.5 are presented the uncorrected and volatile-free data, respectively. For all statistical calculations and all graphical representations of the analytical data, the volatile-free major elements are used together with the original, uncorrected trace element data, since volatile-free recalculation of trace elements result in negligible changes. The difference between plotting

volatile-included and volatile-free trace elements against volatile-free major elements may be graphically seen in Fig. A.3, chosen as an extract from Fig. 6.5, for which there exists a wide variation in LOI and H₂O⁻ concentrations. It is only at the high Al₂O₃ end of the spectrum, where their contributions to the total major element analyses become significant, that the difference between the trace element concentrations on a volatile-included- and volatile-free-basis can actually be recognised, such as the change from 45ppm to 47ppm Ni at 20.7% Al₂O₃, and 272ppm to 281ppm Pb at 20.4% Al₂O₃.

A.2.4 Gas chromatography

Carbon analyses were conducted on 50 aliquots of pulverized sample, using a Carlo Erba Strumentazione Gas Chromatograph Element Analyzer (model 1106) housed in the National Research Institute for Oceanography in the CSIR Stellenbosch Laboratories. The instrument utilizes the thermal conduction principle of detection. Empty crimped tin boats acted as blanks, while two different standards were inserted at intervals throughout the runs and comprised acetanilide (C₈H₉NHCOCH₃) and cyclohexanone dinitrophenylhydrazone (C₁₂H₁₂N₂O₂). Lower limits of detection are approximately 0.01% C. Previous carbon analyses on McArthur River samples by Lambert and Scott (1975) had shown that at high S concentrations, S overloading of the instrument traps had resulted in S being read as C in the detection chamber. In order to test for this problem in the current study, three different weight aliquots of a pulverized C- and S- bearing sample were analysed (Table A.6) and showed that increased sample weight does not lead to an increase in the C content, thus S overloading at S concentrations of 1.4% does not constitute a problem. Furthermore, Table A.6 also shows that samples in excess of 5mg sample weight may be considered homogeneous.

A.2.5 Comparison between XRF and Instrumental Neutron Activation Analysis (INAA) results for rare earth elements

Most ALP samples were analysed for the three light REE's (LREE), La, Ce and Nd using the XRF techniques outlined above. An estimate of the chondrite-normalized Ho concentration was obtained by multiplying Y by 0.5 (Hanson, 1980), and since

$$\begin{aligned} \text{Ho}_{\text{sample}}/\text{Ho}_{\text{chondrite}} &\approx Y_{\text{sample}}/2, \\ \text{Ho}_{\text{sample}} &\approx (Y_{\text{sample}} * \text{Ho}_{\text{chondrite}})/2, \text{ therefore} \\ \text{Ho}_{\text{sample}}/\text{Ho}_{\text{shale}} &\approx (Y_{\text{sample}}/2) * (\text{Ho}_{\text{chondrite}}/\text{Ho}_{\text{shale}}) \\ &\approx Y * 0.0272 \text{ for} \end{aligned}$$

Ho_{chondrite} = 0.0730 (Taylor and Gorton, 1977) and Ho_{shale} = 1.34 (Piper, 1974). Thus the shale-normalized Ho estimate may be gained by multiplying Y by 0.0272. A total of 23 samples were analysed by kind courtesy of D. L. Reid for a range of REE's, as well as a series of additional elements using the INAA technique (Jacobs et al., 1977) and resulting data processed using the Teabags program (Lindstrom and Korotev, 1982) at the New Mexico Institute of Mining and Technology. Table A.7 shows the high precision of the INAA data. The counting errors for individual sample measurements are less than the standard

deviations of three replicate analyses, thus the latter are used for quoting two sigma errors for La, Ce and Nd of 4.9, 11.3 and 7.6, respectively. Comparisons between La, Ce and Nd analyses by the two techniques performed on the same samples reveal that the INAA values are usually higher than those obtained by XRF, with the relative deviation at a maximum in the middle XRF value range (at approximately 30ppm for La and Nd, and 65ppm for Ce; Fig. A.4). Thus although a discrepancy exists in the absolute concentrations of the LREE's, the shapes of the REE profiles should be fairly consistent and comparable between samples analysed by the two techniques.

The accuracy of the Ho estimate can only be indirectly assessed by comparing the shapes of INAA and XRF derived REE patterns, since Ho was not analysed by INAA. Fig. A.5a displays INAA data for samples with a range in heavy REE (HREE) values, while Fig. A.5b shows the corresponding XRF derived REE patterns with the Ho estimate. The shapes of both INAA and XRF REE patterns at the HREE end of the spectrum are sufficiently similar, albeit at different absolute concentrations, to justify using XRF data with recalculated Y as a Ho estimator for interpretive purposes in samples where INAA data are not available.

APPENDIX B STATISTICAL TECHNIQUES

B.1 Correlation

The Pearson correlation matrix is calculated from \log_{10} transformed data within BMDP program P4M (factor analysis). For SS the data set is 23 samples because REE data is not available for the remaining two samples. C analyses were run on 16 samples including the two for which REE are outstanding.

B.2 Factor analysis

Davis (1973, p412-413) suggests that many of the multivariate statistical methods do not have as rigorous a theoretical background as univariate data analysis. Also many of the multivariate techniques have been worked out only for the most restrictive assumptions. The more general assumptions are inadequately known for many real world problems. Temple (1978) criticized the use of factor analysis in geology on the grounds that the hypotheses are complex since they consist of believing in (i) a small number of factors, and in (ii) partitioning the variances into "uniquenesses" and "communalities", terms which have never really been defined. Temple (ibid.) asserted that the varimax rotation does not really improve the meaningfulness of the factors, thus he advocates the use of the unrotated (principal) components since in addition they do not rely on complex hypotheses. Chayes and Trochimczyk (1978), however, even questioned the use of principal component analysis (and hence factor analysis) on closed arrays. From the foregoing it is clear that problems abound in applying factor analysis to closed arrays. Davis (1973) nevertheless asserted the proved empirical usefulness of factor analysis in a geological context. In this thesis, careful application of R-mode factor analysis is ensured by using mainly high factor loadings before accepting that the elements contribute to a factor; by checking element associations back with the correlation matrix; by noting those factors for which closure is clearly operating; and by only accepting geologically reasonable associations.

All correlation matrices and hence factor analyses are performed on \log_{10} transformed data, with major elements first being converted to ppm as suggested by Le Maitre (1982, p110). The data is standardized to ensure equal means and variances before performing factor analyses. The elements C, U and Mo are omitted from all factor analysis calculations due to their levels of concentration falling below the lower detection limits.

B.3 Discriminant function analysis (DFA)

DFA is a multivariate statistical technique used to distinguish between defined groups using measured variables. The method serves to weigh and linearly combine the discriminating variables such that the statistical definition of the groups is optimized. Although a basic assumption of DFA is that the variables are normally distributed, departures from normality are not too serious (Le Maitre, 1982). All DFA computer runs are therefore performed on \log_{10} transformed data, which provides a reasonably close approximation to normality (section

6.2.1). BMDP program P7M (Dixon, 1983) offers variable selection in a stepwise manner, successively incorporating the element with the next highest "F" statistic into the discrimination function. The procedure continues with inclusion and expulsion of variables until no additional variables provide improved discrimination. The summary statistics generated by the program include a parameter known as the Wilke's Lambda or U-statistic which is an inverse measure of the effectiveness of the discriminant function. The default "F-to-enter" of four was accepted in the case of schist discrimination, but was lowered to 1.5 for quartzite due to the low "F" statistics caused by fairly similar group means.

Selection of elements to be used in discriminating between various schists and quartzites has been limited to less mobile elements because not only has the Bushmanland Group been subjected to non-isochemical metamorphism (section 6.1), but at Aggeneys the presence of four orebodies might have left some base metal-related imprint on the host rocks. In studies on hydrothermally altered rhyolite associated with the Phelps Dodge massive sulphide deposit in Quebec, Maclean and Kronidiotis (1987) found that the elements Al, Zr, Nb, Ti and Y show the least mobility. The factor analysis evidence that Y displays similarities to the base metals (section 6.2.3), precludes its use as an "immobile" element, but necessitates its inclusion as one of the ore-related elements. Th and Sc are used since Th is far less mobile than uranium, and tends to become residually enriched in resistate minerals such as zircon, or in clays, during weathering and alteration (Pertlik et al., 1978), and Floyd and Winchester (1978) found that Sc is also relatively immobile during metamorphism and hydrothermal activity. Finlow-Bates and Stumpfl (1981) showed that Sc is mobilized in the most intensely altered and sulphidized portions of rocks hosting volcanogenic massive sulphide deposits, but no samples included in the present DFA runs showed indications of intense alteration or sulphidation.

APPENDIX C ADDITIONAL PETROGRAPHIC DESCRIPTIONS

C.1 Namies Schist (NS)

In NS, sillimanite and its alteration products of muscovite and sericite comprise some 5 - 20% of the rock, with only a fraction of the sillimanite being completely fresh. Tourmaline is pleochroic from deep- to light- green. For estimated modal percentages see Table C.2.

C.2 Shaft Schist (SS)

Intense sericitization of feldspars in SS is not limited to surface samples, and gridiron twinning of coarser-grained microcline was recognised only in a few thin sections. The common presence of sericite masses pseudomorphing a finer-grained, polygonal mineral suggests the original presence of plagioclase, although no polysynthetic twinning was recognised in thin section. Much of the sillimanite has also been altered to sericite. The only discernable differences between the degree of alteration of SS on surface and in borehole core lies in the darker colour and dustier appearance of surface biotite, and the complete sericitization of surface sillimanite.

A variety of accessory minerals occur in SS. Most zircons occur as fine-grained inclusions in biotite, with occasional zircon grains included in quartz and rarely showing overgrowths. Tourmaline (pleochroic from deep yellow to pale green) is sporadically developed (found in three SS samples only). Apatite occurs in the form of medium-grained, interstitial, elongated prisms, while rare garnet occurs as fine-grained (8 micron) equant grains enclosed in quartz, or 40 micron grains showing an intergrown contact with biotite.

Oval-shaped pegmatitic neosomes within SS measuring 2cm x 1cm, comprise coarse-grained quartz and strongly sericitized feldspar. Pyrite and/or pyrrhotite rim the entire neosome. Estimated modal percentages of SS appear in Table C.3.

C.2.1 Biotite Graphite Zone (BGZ)

In certain thin sections BGZ shows evidence of severe deformation (Fig. C.1), with rounded and sometimes brecciated quartz grains in an anastomosing matrix of clay and sericite.

BGZ has a comparable mineral assemblage to SS, including high biotite to muscovite proportions (Table C.4), lack of pristine muscovite, presence of graphite and sulphides, and the absence of magnetite. In thin section the higher content of sericite and clay in BGZ distinguish it from SS. Neither tourmaline nor plagioclase are recognised, although some felted masses of sericite may pseudomorph plagioclase. As in SS, zircons appear to have a bimodal size distribution, with most being extremely fine-grained and rounded, while a significant proportion display coarse and broken habits. An associated quartzite horizon comprises some 5 - 8% garnet, K-feldspar, some sulphide, but neither magnetite nor zircon. Due to its thinness

and discontinuous nature, no geochemical analyses were performed on this rock.

C.2.2 Calc Silicate Rock plus Manganese Quartzite (CSMQ)

Individual bands comprising the Calc Silicate Rock have a decussate texture. Banding in ALP188 is defined by alternating garnet- and quartz- rich layers (Fig. C.2). Grain sizes, shape and mineralogy (Table C.5) vary considerably, with ubiquitously present garnet ranging in diameter and shape from 40 micron with xenoblastic habit (ALP055), to idiomorphically developed, 3mm porphyroblasts (ALP188). Coarse-grained (5mm) clinopyroxene which dominates ALP055, is not present in any other thin sections of Calc Silicate Rock.

Garnet displays varying degrees of alteration to chlorite, ranging from minor chloritization of garnet edges, to equant grains in a felted chloritic mass. All garnet grains contain inclusions predominantly of quartz. The diopside of ALP055 is pleochroic from pale pink to pale green, displays twinning, and contains lamellae inclusions of an amphibole which is pleochroic from colourless to pale yellow. Micro shear zones in pyroxene are retrograded to fibrous amphibole. Minor coarse-grained (2mm long) amphibole prisms lie in stable contact with pyroxene. Some of the chlorite of ALP121c probably pseudomorphs pyroxene since a faint orthogonal relic cleavage is visible.

Quartz appears as unstrained, coarse-grained (up to 3,5mm diameter) interstitial filling between the mafic minerals of pyroxene and garnet. Abundant sericite is present in only ALP188 where it is pseudomorphous, probably after plagioclase. The same rock contains biotite flakes which are partially altered to chlorite, and interstitial epidote. The rare apatite of ALP121c displays a coarse-grained (1mm diameter) xenoblastic habit, while zircon, with long axes measuring 20 micron to 1mm, mainly displays an idiomorphic shape. Positively identified opaque minerals are pyrite, pyrrhotite, sphalerite and galena, which occur both interstitially to the silicates as well as included in pyroxene.

Banding in the Manganese Quartzite is defined by layers of opaque minerals, comprising iron sulphide, sphalerite and galena. These rocks vary from being equigranular with recrystallized unstrained quartz grains measuring 20 micron in diameter, and meeting in well defined triple junctions, to showing intense undulose extinction in grains measuring 3mm. Only in ALP213 are shear zones developed within the quartzite. Garnet, which is scattered throughout the rock, varies in habit from idiomorphic to equant, and averages 15 - 50 micron in diameter. Neither biotite nor the rare tourmaline (pleochroic from colourless to deep blue, and measuring five micron on the long axis), display obvious preferred orientation. Inclusion-free gahnite displays a rounded habit and measures 15 micron in diameter. Clays develop after iron sulphides in surface samples of manganese quartzite.

C.3 Ore Schists (OS) and Orebody

The component schists of OS generally display similar mineralogies, but differ widely in their modal proportions (Tables C.6 - C.9). The common petrographic characteristics are therefore described, with reference being made to features limited to specific samples.

All OS samples display a well developed foliation defined by biotite, elongated, strained quartz, sillimanite, elongated garnet, and K-feldspar porphyroblasts. On a microscopic scale folding of biotite and muscovite flakes reflect deformation seen in outcrop. The rocks are generally coarse-grained with the individual minerals quartz, muscovite, biotite, garnet, sillimanite and feldspar commonly of the order of 1mm along the long axis. Specific porphyroblasts of garnet and K-feldspar measure up to 8mm. Many schist specimens display compositional banding at the cm scale, with more quartz-rich portions forming quartzite layers, trains of sillimanite nodules defining aluminous-rich bands, and garnet-biotite concentrations constituting the mafic layers. The latter assemblage typifies the silicate mineralogy of the immediate orebody environment and ore-related rocks. The same garnet-biotite pairing as found in ALP047 and ALP049, which are the direct down-plunge continuations of UOB and LOB, respectively, is also found in OES both close to and far removed from the orebody.

Of the two forms of garnet present, the massive variety is most common and displays alteration along cracks to chlorite plus opaque mineral dusting. The bulk of the chlorite present, however, replaces biotite. Biotite concentrically rims the skeletal and possibly younger variety of garnet which poikiloblastically encloses quartz, biotite and occasionally sillimanite. The presence of this second type of garnet seems to be restricted to rocks which have undergone a large degree of sericitic alteration.

K-feldspar appears prominently in hand specimens and thin sections of UFS, but microscope examination reveals that HS and OES may also contain up to 10% of the mineral (Tables C.6, C.7 and C.9), while OES+GQ commonly carries large (up to 8mm across) K-feldspar porphyroblasts which poikiloblastically include quartz, biotite and garnet (e.g. ALP049). K-feldspar occasionally displays perthitic intergrowths and more rarely gridiron twinning. Sillimanite and K-feldspar seldom touch, and the zone separating the two minerals frequently comprises simplectic intergrowths of undeformed muscovite and quartz. Only in ALP047, a strikingly unaltered sample, are folded trains of helicitically preserved sillimanite found in K-feldspar. The bulk of the muscovite and sericite in the schists occurs as a retrograde product after biotite, K-feldspar and sillimanite. Although the prismatic faces of biotite and muscovite appear to lie in stable contact, the basal terminations of one mineral against the other commonly reveal a reactionary boundary. In rocks displaying a large degree of folding the hinge zones of folded sillimanite are retrograded to muscovite. Only in the massive sulphide sample of the orebody (ALP081) is there no indication of a precursor to muscovite.

The presence of sericite is only documented in Tables C.6 - C.11 where the original mineral can no longer still be distinguished.

Comparing OS surface samples with borehole core does not reveal great changes due to weathering. The major alteration effects are opaque dusting of the biotites and garnets, and a greater degree of feldspar sericitization.

Zircon which occurs in quartz almost invariably displays rounded terminations similar to the detrital zircons found in the quartzites. ALP114, a GQ from BH114 represents one exception to the above general rule, with zircon being abundant and associated both with gahnite and with biotite. Unusually long zircon grains are present, also showing rounded terminations, and rounded zircon cores are overgrown by crystalline zircon.

Gahnite has a subidioblastic form, becoming prismatic in the one schist sample (ALP198). The tourmaline of ALP102 has an idioblastic, coarse-grained habit with minor fine-grained tourmaline crystals scattered throughout the rock. Apatite displays subidioblastic, hexagonal form and commonly occurs as fine-grained inclusions in quartz, but rare fine-grained sphene and rutile are xenoblastic.

The well banded OES+GQ continuation of UOB (ALP047) requires special mention as four distinct units are discernable. ALP047A consists of a quartz magnetite rock in which magnetite grades over the length of the thin section, from constituting 35% of the rock and averaging 0.5mm in grain size, to 60% of the rock and averaging 3mm. Both quartz and garnet concentrations behave antipathetically to magnetite, while gahnite content increases with that of magnetite. Only in the most magnetite-rich portion do chalcopyrite and pyrite appear. ALP047C contains the three distinct bands noted in Table C.8. The quartz- and zircon- deficient garnet-biotite band measures 2mm across. The two remaining bands each measure 10mm across, but in neither is zircon prominently developed.

Judging from the geographical location of ALP190 and the amount of contained K-feldspar, this sample would more accurately classify as UFS rather than OES. It is therefore treated as UFS throughout the thesis.

C.4 Broken Hill Quartzites (BQ)

In BQ quartz grain sizes and shapes reflect the local strain history. They vary from coarse grains showing undulose extinction measuring in excess of 1cm in diameter, and separated from other grains by mortar textured quartz (Fig. C.3), to totally polygonized, recrystallized, unstrained, fine-grained quartz. Muscovite grains are distributed evenly throughout the quartzite, with grain sizes ranging between 140 - 2 000 micron in long dimension within a single thin section (Fig. C.4). Muscovite morphology provides indications of different muscovite ages, with undeformed, simplectic intergrowths with quartz post-dating severely deformed and sheared grains. No firm

petrogenetic connotations may be attached to muscovite due to the simplicity of mineral parageneses present in quartzites.

Biotite occurs at various stages of alteration to chlorite in laths measuring between 130 and 1 100 micron in long axis. Rare garnets occur skeletally enclosed in quartz (Table C.12). Idioblastic zircon overgrowths on rounded zircon inclusions are also rare. The zircon grains occur both concentrated along the heavy mineral layers as well as scattered throughout the quartzite, and lie between various mineral grains, or enclosed in quartz or in mica. Where hosted by muscovite or biotite/chlorite, the zircons display radioactive-damage haloes.

Tourmaline is restricted to a sample of DQ on Maanhaarkop (Table C.12), which is the equivalent rock type to the tourmaline-bearing quartzite at Gamsberg (Rozendaal, 1978). The coarse-grained (300 x 2 000 micron) idioblastic tourmaline lies within or closely related to a vein which cross-cuts at low angles, the rock foliation as defined by oriented muscovite. Gahnite has only been identified in one specimen (ALP240 from DQ on Klein Kop) where it occurs as small (80 micron) rounded grains in quartz, or associated with biotite. Spinel is equally rarely developed (ALP240), and occurs in quartz unrelated to any specific bands. The opaque minerals tend to be larger (40 - 80 micron) than the associated zircon grains. Bright red rutile similarly occurs as rounded to subrounded grains measuring 75 to 100 micron.

The garnets in MDS measure up to 3 500 micron and poikiloblastically enclose quartz grains. The green spinel found in ALP125 from Maanhaarkop is probably gahnite rather than hercynite since the whole rock averages 308ppm Zn. Abundantly developed zircon grains display a well rounded habit and vary from much finer-grained (10 to 40 micron) than in the adjacent quartzites, to long dimensions similar to the quartzite zircons (i.e. 70 to 100 micron; Table C.12).

C.5 Namies-type Schist (NTS)

C.5.1 NTS at Namiesberg

Banding on the microscopic scale is reflected by 2mm wide layers of feldspathic quartzite and quartzite. Sericitization of K-feldspar is insufficient to obliterate the common gridiron twinning observed, and plagioclase grains are occasionally recognised. As with other schist samples from surface exposures, the biotite flakes from Namiesberg NTS are strongly weathered with the production of large quantities of opaque dust. None of the remaining opaque minerals comprise pyrite or pyrrhotite. The bulk of the zircons found in NTS are elongated with rounded terminations, have variable grain sizes, and occur in quartz, K-feldspar and micas.

C.5.2 NTS in Achab borehole

The coarse-grained schist (up to 8mm long porphyroblasts) comprises quartz, biotite, sillimanite, feldspar and muscovite. Gridiron

twinning, and the habit of filling gaps between quartz and plagioclase, commonly distinguishes K-feldspar. Zircons occur mainly in the leucocratic minerals as coarse- (200 micron) and fine-grained, well rounded crystals. Estimated modal percentages appear in Table C.13.

C.6 Shaft-type Schist (STS)

Under crossed nicols STS from both Namiesberg and Wortel display a distinctive "furry" appearance due to the high content of fresh and altered, coarse-grained sillimanite, measuring up to 8mm in length. Although sericitized K-feldspar is a common component of the rock, gridiron twinning can seldom be identified, and no plagioclase has been recognised (Table C.14). Muscovite always occurs in quantities subordinate to biotite and is clearly a retrograde product after sillimanite, K-feldspar and biotite.

Of all the NTS and STS samples examined, garnet occurs in the thin section of only ALP430, an STS sample from Wortel. The garnet poikiloblastically encloses fine-grained, elongated quartz trains which lie sub-parallel to the surrounding foliation. Only the immediately adjacent biotite concentrically surrounds the garnet.

The opaque minerals in STS always comprise pyrite and less commonly pyrrhotite, and no magnetite has been recognised. The sulphides adopt either a foliated form or the pyrite occurs as cubes.

Zircons occur differently in STS relative to NTS. They are always found as fine specks with large pleochroic haloes in biotite, and when coarser-grained, the frequently metamict zircons adopt irregular to angular shapes, and produce wide pleochroic halos in biotite.

C.6.1 Massive Sillimanite

While the massive sillimanite bodies which are being exploited measure tens of metres in width, borehole WTL3 intersected only 1.5m of the rock type. Contacts with the surrounding STS are sharp, although the sillimanite content of the schist does increase nearer the massive sillimanite. Essential minerals of the rock comprise sillimanite extensively altered to muscovite, lesser quartz, non-sulphide opaque minerals associated with accessory sphene and rutile, and elongated zircons with ragged terminations.

C.6.2 Calc Silicate-type Rock plus Manganese Quartzite

The above field name encompasses the two separate rock-types, Garnet-type Quartzite (GTQ) and Calc silicate-type rock (CTS). Borehole WTL4 intersected some 13m of CTS, with the GTQ mainly flanking the central CTS. The CTS is a massive to slightly foliated, dark green rock with grain sizes of individual pyroxene grains of up to 12mm. The dark pink coloured interbands of weakly foliated GTQ have maximum biotite grain sizes ranging up to only 1mm.

GTQ displays a simple mineralogical assemblage of quartz, garnet and biotite (Table C.15), with alignment of the latter mineral imparting

the weak foliation seen in hand specimen. The equant garnet contains minor quartz inclusions. Apatite commonly preserved in quartz and biotite displays a subidioblastic, hexagonal shape. Zircon grains occur only as fine specks showing pleochroic halos in biotite.

CTS is a heterogeneous rock with two thin sections displaying completely different mineralogies (Table C.15). In ALP446CY 50% of the rock comprises orthoferrosilite (biaxial positive; high relief), while 50% of ALP446CX is composed of fayalite (biaxial negative; $2V = 30 - 40^\circ$) (Table C.15). In both rocks grunerite forms the alteration product after the major components and garnet, while biotite and apatite represent prograde minerals.

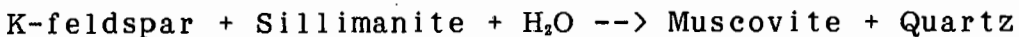
C.7 Regional Quartzites (RQ)

In thin section a clear distinction exists between the quartzites from Wortel, which comprise at least 20% feldspar, and those from Namiesberg which are feldspar-free (Table C.16). Plagioclase in Wortel WTQ has the composition of andesine, and together with K-feldspar it is slightly sericitized. Heavy mineral layers (HMLs) defined by trains of zircon grains and opaque minerals, occur in both WTQ and DTQ from Wortel, with biotite and/or chlorite forming an important related mineral. The associated garnet and epidote-group minerals in ALP437 are clearly non-detrital as they display scalloped contacts with quartz. Zircon grain sizes in the HMLs vary up to 170 micron, but in the host quartzite these range up to 300 micron. The zircons display oval to elongated shapes with rounded terminations, and slight metamorphic overgrowths on the terminations. Pyrite occurs in both cubic and rounded form of which the latter may be detrital.

MDTS is a foliated and banded rock being similar in appearance to NTS, with pink-coloured enclosed pegmatites. Magnetite comprises one of the rock forming minerals. The banded variety of MDTS (ALP426; Table C.16) has quartz-rich layers of 7mm width separated by sillimanite-biotite rich layers of 2mm width. The included, rounded, coarse-grained (180 micron) zircons in the quartz-biotite layers near the contact with the sillimanite layer may reflect the base of a graded bed.

APPENDIX D METAMORPHISM

The best available indicators of prograde metamorphism are the rare sillimanite-K-feldspar intergrowths in ALP047 and ALP438. Abundant evidence exists for the retrograde reaction



as follows:

- a. simplectic intergrowths of muscovite and quartz are common in NTS and STS from both Namiesberg and Wortel
- b. ALP415 has virtually no sillimanite but abundant K-feldspar and the simplectic intergrowth, suggesting that the retrograde reaction was arrested at the point of sillimanite consumption
- c. in ALP438 (STS from Wortel) the contact between sillimanite and K-feldspar is preserved, with some of the sillimanite dissolving into a simplectic intergrowth of muscovite + quartz.

In a single thin section of OS, non-pervasive retrograde metamorphism may be deduced from zones displaying extreme biotite sericitization occurring near areas of fresh biotite. It appears that the reaction froze when all available water had been consumed as also suggested by the partial retrogression of feldspar to sericite. The extensive and severe alteration observed in the samples from borehole BH112 is a localized phenomenon suggesting that retrogressive fluids were focused along specific zones within the schists. The prograde peak of metamorphism was attained just after F_2 deformation (Joubert, 1971; Lipson, 1978), thus such extensive retrogression associated with F_2 folding was unexpected. Perhaps the S_2 refoliation presented more open channelways for retrogressive fluid movement later in the history of these rocks. The evidence of biotite preservation at the terminations of elongated garnet suggests that the fluid flow was in the plane of the foliation. The fact that chlorite generation after biotite and opaque minerals occurs in both surface and borehole core shows that such retrogression predates the alteration due to current weathering.

Metamorphic conditions appear similar between Broken Hill, Wortel and Namiesberg, but a more intensive study would be needed to show whether or not any metamorphic gradients exist. Because of these uncertainties, it was decided to normalize all geochemical major element data to 100% before comparing the chemistry of rocks at Broken Hill with those from the other areas (see also Appendix A.2.3).

APPENDIX E RELATIONSHIPS BETWEEN MAJOR LITHOLOGIES

E.1 Gneisses through NS to WQ

From Broken Hill to Froneman se Kop the only exposed contact between NS and gneisses is found at Maanhaarkop, where the interface is sharp. Borehole cores from the vicinity of Broken Hill reveal the detailed complexity of this contact zone. Near NS the gneisses comprise components of both the granoblastic pink variety and inequigranular augen gneiss. Similar looking augen gneiss in the Aggeneys quarry is clearly of intrusive origin (intrusive into an amphibolite; Fig. E.1). As a generalization, the gneisses pass structurally downwards first through a thin (1 - 2m wide) chlorite-biotite+feldspar/quartz rock, (contact A, Fig. E.2) into a schist of up to 15m width. The schist passes back into a 6 - 30m wide gneiss, with the interface zone (contact B; Fig. E.2) sometimes being interbanded over 6m in a gradational-like relationship, while the actual contact is interpreted at a thin (< 1m wide) chlorite-amphibole rock. The contact between the interlayered gneiss and NS (contact C; Fig. E.2) varies from being interbanded (gradational?) over 2m, to sharp. The last appearance of gneiss is marked by either an associated pegmatite or a 0.5m wide layer of biotite-chlorite schist.

E.2 OS through SS to Plant Quartzite (PQ)

The contact between structurally overlying OS and the graphitic BGZ can be accurately defined by the garnet-out and graphite-in criterion. With the diminution of clay content, BGZ grades downwards into SS. SS displays sharp though interbanded contacts with lenses of CSMQ, which it hosts. The contact between silica-poor Upper Shaft Schist (USS) and siliceous Lower Shaft Schist (LSS) (contact C; Fig. E.3) is defined on chemical grounds, as it was not originally visually recognised. LSS displays a sharp contact with GGLG in borehole BH164 (contact B; Fig. E.3), while the contact between USS and GGLG is not exposed. LSS displays a sharp contact with the underlying quartzite (PQ). Minor quartz interbands and extensive pegmatites (neosomes?) are developed over the last 10m of SS.

APPENDIX F ORE SCHIST FACTOR SCORES RELATED TO THE OREBODY

R-mode factor analysis computed on borehole core samples of OS, reveal primary (lower factor number) and secondary "ore factors" (section 6.3.1.2). For surface outcrop OS samples, a single "ore factor" emerged, which incorporates strongly positive loadings on the elements Zn, Cu and Pb, and negative loadings on MgO, Ni, Y and CaO (Table F.1). Plotting of the factor scores for each sample as a function of distance from the orebody shows broadly defined increasing trends towards the orebody (Fig. F.1). West of the orebody the surface OS factor scores are higher than to the east.

APPENDIX G LITHOGEOCHEMICAL EXPLORATION STRATEGY

Both regional- and local- scale lithogeochemical exploration techniques indicating the presence of Broken Hill-type ore in the north west Cape have been examined. The former will aid in identifying areas at the scale of tens of kilometres which hold potential for mineralization, while the latter pertains to areas smaller than 10km where an ore centre is being sought.

In both flow charts which detail exploration strategies (Figs. G.1 and G.2), an attempt should be made to identify the stratigraphic succession in order to apply the appropriate lithogeochemical techniques. If distinctions, particularly between schists, cannot be made on the basis of geology and petrography (section 4.2), then the discriminating lithogeochemical statistical parameters examined in section 6.2, are suggested for this purpose. Generalized tests only, shown on the left-hand side of Figs. G.1 and G.2, may be used failing the confident separation of rock-types. Where successful separation has taken place, then in the regional flow chart, the delta diagrams (section 7.3.3) are used to distinguish fertile from barren target areas. For local exploration, monitoring of the concentrations and values of specific elements and ratios as applicable to OEH (section 6.3.1.6 and 6.3.2.3), is advocated to lead the explorationist through the ore halo to the orebody.

Irrespective of whether or not the stratigraphic succession is defined, the potential for the presence of base metal sulphides may be tested for as advocated at the base of Figs. G.1 and G.2. Whereas at the regional scale this consists of factor analysis (Appendix F), for localized exploration, two ratios are suggested which increase towards mineralization across stratigraphic boundaries (Figs. 6.35 and 6.36). The successful definition of a prospective regional area naturally leads to work at the local scale.

Broad scatter about the generally increasing trends of indicator elements and inter-element ratios progressively nearer the Broken Hill orebody, define the geochemical vectors towards ore. The practical application of these techniques should rely on trends defined by numerous samples. Misleading interpretations could result from small data sets.

Substituting the co-ordinates for point A' into equation (6) solves for c, hence the equation of the line limiting the maximum C and S concentrations of SS is:

$$y = 1.53x + 0.52 \text{ ----(7)}$$

Relatively little pyrrhotite has been identified in SS, so a maximum of 50% conversion of pyrite to pyrrhotite can safely be used to calculate maximum possible C and S concentrations of the pre-metamorphic SS. Instead of doubling the current S content of SS, as in the case of 100% pyrite conversion to pyrrhotite, only 50% of the current value is added to the current S content, giving maximum and minimum S ordinate values of 0.63 and 2.16% respectively. Corresponding C abscissa values, calculated as before, give 0.11 and 1.18% (Fig. 9.11b, pts. X and X'). The slope of the line defining the locus of points along which 50% conversion of pyrite to pyrrhotite has occurred, is calculated as before, generating the equation

$$y = 1.43x + 0.47 \text{ ----(8)}.$$

In summary, the calculated range of C and S values for pre-metamorphic SS is:

$$\begin{array}{l} 0.11\% \text{ C ; } 0.63\% \text{ S} \\ \text{and} \\ 1.18\% \text{ C ; } 2.16\% \text{ S.} \end{array}$$

APPENDIX I CALCULATION OF Pb/Cu AND Zn/Cu RATIOS IN FLUIDS

The method used for calculating the Pb/Cu and Zn/Cu ratios follows that outlined by Huston (1988, pers.comm.), for the Zn/Pb ratio i.e. first determine the ionic strength of the solution and then calculate the Pb/Cu and Zn/Cu ratios. The ionic strengths were given by Huston (1988, pers.comm.) for the temperature range 25 - 300°C and over NaCl_{total} molalities of 0.25 - 3.0, as follows:

Calculated ionic strength ($I \approx m_{Cl^-}$)

(m _{NaCl}) _{total}	25°C	50°C	100°C	150°C	200°C	250°C	300°C
.25	.246	.247	.247	.246	.241	.233	.210
.50	.486	.489	.489	.485	.470	.451	.396
1.0	.949	.959	.958	.947	.908	.859	.739
1.5	1.388	1.407	1.407	1.387	1.317	1.241	1.058
2.0	1.802	1.831	1.832	1.803	1.699	1.602	1.360
3.0	2.553	2.601	2.604	2.560	2.392	2.273	1.932

Calculation of the individual CuCl species equilibrium constants (K_{eq}) with Cu₂S as the insoluble sulphide, was performed in the standard manner by solving sets of simultaneous equations all taken from Helgeson (1969), and adding up the K_{eq} values.

Since the total molality of any species is the sum of molalities of all species containing the element (Garrels and Christ, 1965, p56), the term $m_{total\ Cu}/m_{total\ Pb}$ may be written as

$$\frac{\{m_{CuCl_2^-} + m_{CuCl_3^{2-}} + m_{CuCl^+} + m_{CuCl_2} + m_{CuCl_3^-} + m_{CuCl_4^{2-}}\}}{\{m_{PbCl^+} + m_{PbCl_2} + m_{PbCl_3^-} + m_{PbCl_4^{2-}}\}}$$

where

$$m_{CuCl_2^-} = (a_{Cl^-}^2 * a_{H^+}) / (g_{CuCl_2^-} * K_1^{0.5})$$

$$m_{CuCl_3^{2-}} = (a_{Cl^-}^3 * a_{H^+}) / (g_{CuCl_3^{2-}} * K_2^{0.5} * a_{H_2S}^{0.5})$$

$$m_{CuCl^+} = (a_{Cl^-} * a_{H^+}^2) / (g_{CuCl^+} * K_3^{0.5} * a_{H_2S}^{0.5} * a_{H_2}^{0.5})$$

$$m_{CuCl_2} = (a_{Cl^-}^2 * a_{H^+}^2) / (g_{CuCl_2} * K_4^{0.5} * a_{H_2S}^{0.5} * a_{H_2}^{0.5})$$

$$m_{CuCl_3^-} = (a_{Cl^-}^3 * a_{H^+}^2) / (g_{CuCl_3^-} * K_5^{0.5} * a_{H_2S}^{0.5} * a_{H_2}^{0.5})$$

$$m_{CuCl_4^{2-}} = (a_{Cl^-}^4 * a_{H^+}^2) / (g_{CuCl_4^{2-}} * K_6^{0.5} * a_{H_2S}^{0.5} * a_{H_2}^{0.5})$$

and where g_{CuCl^+} is the activity coefficient of the CuCl⁺ complex. Substituting activities, activity coefficients and equilibrium constants for concentrations, and simplifying, the equation may be expressed as:

$$\frac{[m_{Tot\ Cu}]}{[m_{Tot\ Pb}]} = \frac{\{ (a_{Cl^-}) / ((g_{CuCl_2^-}) * (K_1)^{0.5} * a_{H^+}) \} + \{ (a_{Cl^-}^2) / ((g_{CuCl_3^{2-}}) * (K_2)^{0.5} * a_{H^+}) \} + \{ 1 / ((g_{CuCl^+}) * (K_3)^{0.5}) \} + \{ (a_{Cl^-}) / (K_4)^{0.5} \} + \{ (a_{Cl^-}^2) / ((g_{CuCl_3^-}) * (K_5)^{0.5}) \} + \{ (a_{Cl^-}^3) / ((g_{CuCl_4^{2-}}) * (K_6)^{0.5}) \}}{\{ 1 / ((g_{PbCl^+}) * (K_{PbCl^+})) \} + \{ (a_{Cl^-}) / (K_{PbCl_2}) \} + \{ (a_{Cl^-}^2) / ((g_{PbCl_3^-}) * K_{PbCl_3^-}) \} + \{ (a_{Cl^-}^3) / ((g_{PbCl_4^{2-}}) * (K_{PbCl_4^{2-}})) \}}$$

The equation for $m_{total\ Cu}/m_{total\ Zn}$ is similarly derived.

The following constants were applied in calculating individual activity coefficients using the Debye-Huckel equation

$$a^{\circ} = 3.5 \cdot 10^{-8} \text{ cm for Cl}^{-}$$

$$a^{\circ} = 4.0 \cdot 10^{-8} \text{ cm for singly charged species}$$

$$a^{\circ} = 5.0 \cdot 10^{-8} \text{ cm for doubly charged species}$$

$$b = 0.04$$

The values for A and B at varying temperatures were taken from Helgeson et al. (1981). All Pb and Zn equilibrium constants omitted in Table 4 of Huston and Large (1987) were calculated by this author using linear extrapolation of the existing data. This assumption is reasonable as shown by fitting linear regressions to the complete data sets which all reveal correlation coefficients in excess of 0.99 .

As with the calculation of the Zn/Pb ratio, first the product $m_{\text{total Cu}}/m_{\text{total Pb}}$ and $m_{\text{total Cu}}/m_{\text{total Zn}}$ are calculated before substitution into the equations

$$100 \text{ Zn}/(\text{Zn} + \text{Cu}) = 100/[1 + (m_{\text{total Cu}}/m_{\text{total Pb}})(\text{at.wt.}_{\text{Cu}}/\text{at.wt.}_{\text{Pb}})], \text{ and}$$

$$100 \text{ Pb}/(\text{Pb} + \text{Cu}) = 100/[1 + (m_{\text{total Cu}}/m_{\text{total Zn}})(\text{at.wt.}_{\text{Cu}}/\text{at.wt.}_{\text{Zn}})].$$

The values from these final equations are used for creating the graphs showing the inter-relationships existing between temperature, pH and salinity in controlling the Cu-Pb-Zn ratios.

APPENDIX J MASS BALANCE FOR GENERATING BROKEN HILL OREBODY USING LYDON'S DEWATERING MODEL

Lydon (1986, p 565) showed that conversion of 1 mole illite to muscovite produces 11.6 g solution at a concentration of 1 638ppm trace metal, assuming an initial 50ppm metal concentration in the illite. In round terms 384g illite produces 11.6g solution i.e. 1kg illite produces say 3g solution, or 1 tonne produces say 30kg solution which carries 0.05Kg, or 5×10^{-5} tonnes metal. In order to produce 18.8×10^6 tonnes metal, then $(18.8 \times 10^6) / (5 \times 10^{-5}) = 3.76 \times 10^{11}$ tonnes illite are required. For a theoretical illite source region measuring 10km * 10km in surface area, and having an SG of 2.8, the thickness of the illite sheet can be calculated i.e.

$$10\ 000 \times 10\ 000 \times x \times 2.8 = 3.76 \times 10^{11} \text{ tonnes}$$

where x = thickness in m.

Therefore x = 1 340m, or 1.34km.

Thus in order to produce the 18.8 mt total metal contained in the Broken Hill orebody, Lydon's (1986) model would require a pure illite source region measuring 10km * 10km * 1.34km.

APPENDIX K SUNDRY TABLES REFERRED TO IN THE TEXT

Table K.1 Comparison between Namies Schist at Gamsberg and at Broken Hill

Table K.2 Comparison between Quartzite descriptions at Gamsberg and at Broken Hill

Table K.3 Broken Hill oxygen isotopes

Table K.4 U, Th and Pb ion microprobe analyses on zircons from White Quartzite at Froneman se Kop

13. REFERENCES

- Adachi, M., Yamamoto, K. and Sugisaki, R. (1986). Hydrothermal chert and associated siliceous rocks from the northern Pacific: their geological significance as indication of ocean ridge activity. *Sedim. Geol.*, **47**, 125-148.
- Alderton, D. H. M., Pearce, J. A., and Potts, P. J. (1980). Rare earth element mobility during granite alteration: evidence from southwest England. *Earth Planet. Sc. Lett.*, **49**, 149-165.
- Armstrong, R. A., Reid, D. L., Watkeys, M. K., Welke, H. J., Lipson, R. D. and Compston, W. (1988). Zircon U-Pb ages from the Aggeney's area, Central Bushmanland. *Abs., geol. Soc. S. A. Geocongress 88, Univ. Natal, Durban*, 493-496.
- Arnorsson, S. and Ivarsson, G. (1985). Molybdenum in Iceland geothermal waters. *Contr. Miner. Petrol.*, **90**, 179-189.
- Arth, J. G. (1976). Behaviour of trace elements during magmatic processes - a summary of theoretical models and their applications. *J. res. U.S. geol. Surv.*, **4**, 41-47.
- Baas Becking, L. G. M., Kaplan, I. R. and Moore, D. (1960). Limits of the natural environment in terms of pH and oxidation - reduction potentials. *J. Geol.*, **68**, 243-284.
- Baker, E. T., Cannon, G. A. and Herbert, C. C. Jnr. (1983). Particle transport processes in a small marine bay. *J. Geophys. Res.*, **88**, 9661-9669.
- Barbey, P. and Cuney, M. (1982). K, Rb, Sr, Ba, U and Th geochemistry of the Lapland granulites (Fennoscandia). LILE fractionation controlling factors. *Contr. Miner. Petrol.*, **81**, 304-316.
- Barnes, H. L. (1979). Solubilities of ore minerals, 404-460. In: Barnes, H. L., Ed., *Geochemistry of hydrothermal ore deposits*. John Wiley & Sons, New York, 798pp.
- Barrett, T. J. and Anderson, G. M. (1988). The solubility of sphalerite and galena in 1-5 m NaCl solutions to 300°C. *Geochim. Cosmochim. Acta*, **52**, 813-820.
- Beach, A. (1980). Retrogressive metamorphic processes in shear zones with special reference to the Lewisian complex. *J. struct. Geol.*, **2**, 257-263.
- Bernard, A. J., Dagallier, G., and Soler, E. (1982). The exhalative sediments linked to the volcanic exhalative massive sulphide deposits: a case study of European occurrences, 553-564. In: Amstutz, G. C., El Goresy, A., Frenzel, G., Kluth, C., Moh, G., Wauschkuhn, A. and Zimmerman, R. A. Eds., *Ore genesis: The state of the art*. Spec. Pub. Soc. Geol. appl. Miner. Deps., 2. Springer Verlag, Heidelberg, 804pp.
- Bernard, H. A., Leblanc, R. J. and Major, C. F. (1962). Recent and Pleistocene geology of southeast Texas, 175-205. In: *Geology of the Gulf Coast and central Texas and guidebook of excursions*: Houston Geol. Soc., Geol. Soc. Amer. Annual Meeting, Houston, Texas
- Berner, R. A. (1971). *Principles of chemical sedimentology*. McGraw-Hill Book Co., New York, 240pp.
- Berner, R. A. (1972). Sulfate reduction, pyrite formation, and the oceanic sulfur budget, 347-364. In: Dyrssen, D. and Jagner, D. Eds., *The changing chemistry of the oceans*, Wiley Interscience, Stockholm.
- Berner, R. A. (1984). Sedimentary pyrite formation: an update. *Geochim. Cosmochim. Acta*, **48**, 605-615.
- Berner, R. A., and Holdren, G. R. (1977). Mechanisms of feldspar weathering: some observational evidence. *Geology*, **5**, 369-372.
- Bertine, K. K. (1972). The deposition of molybdenum in anoxic waters. *Mar. Chemistry*, **1**, 43-53.

- Bertine, K. K. and Turekian, K. K. (1973). Molybdenum in marine deposits. *Geochim. Cosmochim. Acta*, **37**, 1415-1434.
- Betton, P.J., (1984). Nd and Sr isotopic evidence for the evolution of the Namaqualand Mobile Belt, Southern Africa. *Abs., Conference on Middle to Late Proterozoic lithosphere evolution, Precambr. Res. Unit, Univ. Cape Town*, p.7.
- Bewers, J. M. and Yeats, P. A. (1977). Oceanic residence times of trace metals. *Nature*, **268**, 595-598.
- Bewers, J. M. and Yeats, P. A. (1979). The behaviour of trace metals in estuaries of the St. Lawrence basin. *Naturaliste Can.*, **106**, 149-161.
- Bhatia, M. R. (1983). Plate tectonics and geochemical composition of sandstones. *J. Geol.*, **91**, 611-627.
- Bhatia, M. R. (1985). Rare earth element geochemistry of Australian Paleozoic graywackes and mudrocks: provenance and tectonic control. *Sedim. Geol.*, **45**, 97-113.
- Bhatia, M. R. and Taylor, S. R. (1981). Trace element geochemistry and sedimentary provinces: a study from the Tasman Geosyncline, Australia. *Chem. Geol.*, **33**, 115-125.
- Bischoff, J. L., Radke, A. S. and Rosenbauer, R. J. (1981). Hydrothermal alteration of greywacke by brine and seawater: roles of alteration and chloride complexing on metal solubilization at 200° and 350°C. *Econ. Geol.*, **76**, 659-676.
- Bjorlykke, K. (1974). Geochemical and mineralogical influence of Ordovician island arcs on epicontinental clastic sedimentation. A study of Lower Palaeozoic sedimentation in the Oslo region, Norway. *Sedimentology*, **21**, 251-272.
- Blatt, H. (1987). Oxygen isotopes and the origin of quartz. *J. sedim. Petrol.*, **57**, 373-377.
- Blignault, H.J., van Aswegen, G., van der Merwe, S.W., and Colliston, W.P. (1983). The Namaqualand geotraverse and environs: part of the Proterozoic Namaqua Mobile Belt. *Spec. Publ. geol. Soc. S. Afr.*, **10**, 1-29.
- Bostrom, K. (1973). The origin and fate of ferromanganoan active ridge sediments. *Stockholm Contr. Geol.*, **27**, 149-243.
- Bourcier, W. L. and Barnes, H. L. (1987). Ore solution chemistry-VII. Stabilities of chloride and bisulfide complexes of zinc to 350°C. *Econ. Geol.*, **82**, 1839-1863.
- Boyle, E. A., Edmond, J. M. and Sholkovitz, E. R. (1977). The mechanism of iron removal in estuaries. *Geochim. Cosmochim. Acta*, **41**, 1313-1324.
- Bramlette, M. N. (1946). The Monterey Formation of California and the origin of its siliceous rocks. *Prof. Pap., U. S. geol. Surv.*, **212**, 57pp.
- Brehler, B. and Wedepohl, K. H. (1972). Zinc. In: Wedepohl, K. H., Ed., *Handbook of Geochemistry*, Springer-Verlag Publishing Company, Berlin, 30-A-1 - 30-H-3.
- Brookins, D. G. (1983). Eh-pH diagrams for the rare earth elements at 25°C and one bar pressure. *Geochem. J.*, **17**, 223-229.
- Burkov, V. V. and Podporina, Y. K. (1967). Rare earths in granitoid residuum. *Dokl. Acad. Nauk. SSSR.*, **177**, 214-216.
- Burns, R. G., Burns, V. M. and Turekian, K. K. (1973-1978). Nickel. In: Wedepohl, K. H., Ed., *Handbook of Geochemistry*, Springer-Verlag Publishing Company, Berlin, 28-A-1 - 28-O-2.
- Burns, R. G., Burns, V. M. and Turekian, K. K. (1974-1978). Cobalt. In: Wedepohl, K. H., Ed., *Handbook of Geochemistry*, Springer-Verlag Publishing Company, Berlin, 27-A-1 - 27-O-1.
- Butler, J. C. (1982). The closure problem as reflected in discriminant function analysis. *Chem. Geol.*, **37**, 367-375.

- Calvert, S. E. and Batchelor, C. H. (1978). In: Ross, D. A. and Neprochnov, Y. P., Eds., *Initial reports of the deep sea drilling project*, 42, Part 2, U. S. Government printing office, Washington.
- Cameron, E. M. and Garrels, R. M. (1980). Geochemical composition of some Precambrian shales from the Canadian Shield. *Chem. Geol.*, 28, 181-197.
- Campbell, I. H., Franklin, J. M., Gorton, M. P., Hart, T. R. and Scott, S. D. (1981). The role of subvolcanic sills in the generation of massive sulfide deposits. *Econ. Geol.*, 76, 2248-2253.
- Campbell, I. H., Coad, P., Franklin, J. M., Gorton, M. P., Scott, S. D., Sowa, J., and Thurston, P. C. (1982). Rare earth elements in volcanic rocks associated with Cu-Zn massive sulphide mineralization: a preliminary report. *Can. J. Earth Sci.*, 19, 619-623.
- Campbell, I. H., Leshner, C. M., Coad, P., Franklin, J. M., Gorton, M. P., and Thurston, P. C. (1984). Rare-earth element mobility in alteration pipes below massive Cu-Zn-sulfide deposits. *Chem. Geol.*, 45, 181-202.
- Canfield, D. E. and Berner, R. A. (1987). Dissolution and pyritization of magnetite in anoxic marine sediments. *Geochim. Cosmochim. Acta*, 51, 645-659.
- Carpenter, J. H. and Grant, V. E. (1967). Concentration and state of cerium in coastal waters. *J. mar. Res.*, 25, 228-238.
- Carter, C. H. (1978). A regressive barrier and barrier-protected deposit: depositional environments and geographic setting of the Late Tertiary Cohansey sand. *J. sedim. Petrol.*, 48, 933-950.
- Cathles, L. M., and Smith, A. T. (1983). Thermal constraints on the formation of Mississippi Valley-type lead-zinc deposits and their implications for episodic basin dewatering and deposit genesis. *Econ. Geol.*, 78, 983-1002.
- Chan, K. M. and Riley, J. P. (1966). The determination of molybdenum in natural waters, silicates, and biological materials. *Analyt. Chim. Acta*, 36, 220-.
- Chandler, F. W. (1988). Quartz arenites: review and interpretation. *Sedim. Geol.*, 58, 105-126.
- Chayes, F. and Trochimczyk, J. (1978). An effect of closure on the structure of principal components. *Mathl. Geol.*, 4, 323-3337.
- Clemens, J. D. and Wall, V. J. (1981). Origin and crystallization of some peraluminous (S-Type) granitic magmas. *Can. Miner.*, 19, 111-131.
- Clifford, T.N., Stumpfl, E.S., McIver, J.R., Burger, A.J., McCarthy, T.S., and Rex, D.C. (1981). Mineral-chemical and isotopic studies of Namaqualand granulites, South Africa: a Grenville analogue. *Contr. Miner. Petrol.*, 77, 225-250.
- Cloud, P. (1976). Major features of crustal evolution. *Annex. Trans. geol. Soc. S. Afr.*, 74, *Alex du Toit Mem. Lect.*, 14, 33pp.
- Cloud, P. (1981). Evolution of ecosystems, 6-18. In: Skinner, B. J., Ed., *paleontology and paleoenvironments*. William Kaufmann, Inc., Los Altos.
- Collinson, J. D. (1978). Alluvial sediments, 15-60. In: Reading, H. G., Ed., *Sedimentary environments and facies*. Blackwell, Oxford, 569pp.
- Colliston, W. P. (1983). Stratigraphic and depositional aspects of the Proterozoic metasediments of the Aggeneys Subgroup at Pella and Dabenoris. *Spec. Publ. geol. Soc. S. Afr.*, 10, 101-110.
- Contreras, R., Fogg, T. R., Chasteen, N., Gaudette, H. E. and Lyons, W. B. (1978). Molybdenum in pore waters of anoxic marine sediments by electron paramagnetic resonance spectroscopy. *Mar. Chemistry*, 6, 365-373.

- Cornell, D.H. (1978). Age and metamorphism of the Copperton Formation, Prieska District. In: Verwoerd, W.J. (ed.). Mineralization in metamorphic terrains. *Spec. Publ. geol. Soc. S. Afr.*, 4, 223-234.
- Coveney, R. M. and Martin, S. (1983). Molybdenum and other heavy metals of the Mecca Quarry and Logan Quarry Shales. *Econ. Geol.*, 78, 132-149.
- Crerar, D. A., Namson, J., So Chyi, M., Williams, L. and Feigenson, M. D. (1982). Manganiferous cherts of the Franciscan assemblage: I. General geology, ancient and modern analogues, and implications for hydrothermal convection at oceanic spreading centers. *Econ. Geol.*, 77, 519-540.
- Cullers, R. L., Yeh, L., Chaudhuri, S. and Guidotti, C. V. (1974). Rare earth elements in Silurian pelitic schists from N. W. Maine. *Geochim. Cosmochim. Acta*, 38, 389-400.
- Cullers, R. L., Chaudhuri, S., Arnold, B., Lee, M. and Wolf, W. Jr. (1975). Rare earth distribution in clay minerals and in the clay-sized fraction of the Lower Permian Havensville and Eskridge shales of Kansas and Oklahoma. *Geochim. Cosmochim. Acta*, 39, 1691-1703.
- Dalland, A. (1975). The Mesozoic rocks of Andoy, northern Norway. *Norges geol. Unders.*, 316, 271-287.
- Dapples, E. C. (1967). Diagenesis of sandstones, 91-125. In: Larsen, G. and Chilingar, G. V. Eds., *Diagenesis in sediments*. Elsevier Publishing Company, Amsterdam.
- Davies, D. K., Ethridge, F. G. and Berg, R. R. (1971). Recognition of barrier environments. *Bull. Am. Ass. Petrol. Geol.*, 55, 550-565.
- Davis, J. C. (1973). *Statistics and data analysis in geology*. John Wiley & Sons, Inc., New York, 534pp.
- de Beer, J.H. and Meyer, R. (1983). Geoelectrical and gravitational characteristics of the Mamaqua-Natal Mobile Belt and its boundaries. *Spec. Publ. geol. Soc. S. Afr.*, 10, 91-100.
- Degens, E. T., Okada, H., Honjo, S. and Hathaway, J. C. (1972). Microcrystalline sphalerite in resin globules suspended in Lake Kivu, East Africa. *Miner. Deposita*, 7, 1-12.
- Degens, E. T., and Stoffers, P. (1976). Stratified waters as a key to the past. *Nature, Lond.*, 263, 22-27.
- de la Roche, H. (1966). Sur l'existence de plusieurs facies geochemiques dans les schistes Paleozoiques des Pyrenees Luchonnaises. *Geol. Rdsch.*, 55, 274-301.
- de la Roche, H. (1978). La chimie des roches presentee et interpretee d'apres la structure de leur facies mineral dans l'espace des variables chimiques: fonctions specifiques et diagrammes qui s'en deduisent- application aux roches ignees. *Chem. Geol.*, 21, 63-87.
- Dickinson, W. R., Beard, L. S., Brackenridge, G. R., Erjavec, J. L., Ferguson, R. C., Inman, K. F., Knepp, R. A., Lindberg, F. A. and Ryberg, P. T. (1983). Provenance to North American Phanerozoic sandstones in relation to tectonic setting. *Bull. geol. Soc. Am.*, 94, 222-235.
- Dixon, W. J. (1983). *BMDP statistical software*. University of California Press, Berkeley, 734pp.
- Dostal, J. and Capedri, S. (1978). Uranium in metamorphic rocks. *Contr. Miner. Petrol.*, 66, 409-414.
- Duinker, J. C. and Nolting, R. F. (1978). Mixing, removal and mobilization of trace metals in the Rhine estuary. *Ned. J. Sea Res.*, 12, 205-223.
- Duncan, A. R., Erlank, A. J. and Betton, P. J. (1984). Analytical techniques and database descriptions. *Spec. Publ. geol. Soc. S. Afr.*, 13, 389-395.
- Dypvik, H. (1979). Mineralogy and chemistry of the Mesozoic sediments of Andoya, northern Norway. *Sedim. Geol.*, 24, 45-67.

- Elliot, T. (1978). Deltas, 97-142. In: Reading, H. G., Ed., *Sedimentary environments and facies*. Blackwell, Oxford, 569pp.
- Ellis, A. J. (1979). Explored geothermal systems, 632-683. In: Barnes, H. L., Ed., *Geochemistry of hydrothermal ore deposits*. John Wiley & Sons, New York, 798pp.
- El Wakeel, S.K. and Riley, J. P. (1961). Chemical and mineralogical studies of deep-sea sediments. *Geochim. Cosmochim. Acta*, 25, 110-146.
- Englund, J. and Jorgensen, P. (1973). A chemical classification system for argillaceous sediments and factors affecting their composition. *Geol. Foren. Stockholm, Forh.*, 95, 87-97.
- Erlank, A. J., Smith, H. S., Marchant, J. W., Cardoso, M. P. and Ahrens, L. H. (1978). Zirconium. In: Wedepohl, K. H., Ed., *Handbook of Geochemistry*, Springer-Verlag Publishing Company, Berlin, B-O.
- Ethier, V. G., Campbell, F. A., Both, R. A. and Krouse, H. R. (1976). Geological setting of the Sullivan orebody and estimates of temperatures and pressure of metamorphism. *Econ. Geol.*, 71, 1570-1588.
- Evans, B. W. (1964). Fractionation of elements in the pelitic hornfels of the Cashel-Lough Wheelaun intrusion, Connemara, Eire. *Geochim. Cosmochim. Acta*, 28, 127-156.
- Evans, H. T., Manheim, F. T. and Landergren, S. (1974-1978). Molybdenum. In: Wedepohl, K. H., Ed., *Handbook of Geochemistry*, Springer-Verlag Publishing Company, Berlin, 42-A-1 to 42-O-2.
- Fairbridge, R. W. (1967). Phases of diagenesis and authigenesis, 19-89. In: Larsen, G. and Chilingar, G. V. Eds., *Diagenesis in sediments*. Elsevier Publishing Company, Amsterdam.
- Falvey, D. A. and Mutter, J. C. (1981). Regional plate tectonics and the evolution of Australia's passive continental margins. *Bull. Aust. Bur. Miner. Resour. Geol. Geophys.*, 6, 1-29.
- Faure, G. (1986). *Principles of isotope geology*. John Wiley and Sons, New York, 587pp.
- Ferry, J. M. (1981). Petrology of graphitic sulfide-rich schists from south-central Maine: an example of desulfidation during prograde regional metamorphism. *Am. Miner.*, 66, 908-930.
- Ferry, J. M. (1986). Infiltration of aqueous fluid and high fluid:rock ratios during greenschist facies metamorphism: a reply. *J. Petrology*, 27, 695-714.
- Finlow-Bates, T. (1979). Cyclicity in the lead-zinc-silver - bearing sediments at Mount Isa Mine, Queensland, Australia, and rates of sulfide accumulation. *Econ. Geol.*, 74, 1408-1419.
- Finlow-Bates, T. and Stumpfl, E. F. (1981). The behaviour of so-called immobile elements in hydrothermally altered rocks associated with volcanogenic submarine-exhalative ore deposits. *Miner. Deposita*, 16, 319-328.
- Fleet, A. J. (1984). Aqueous and sedimentary geochemistry of the Rare Earth Elements, 343-373. In: Henderson, P., Ed., *Rare earth element geochemistry*. Elsevier Science Publishers, Amsterdam.
- Flores, R. M. and Shideler, G. L. (1982). Discriminant analyses of heavy minerals in beach and dune sediments of the Outer Banks barrier, North Carolina. *Bull. geol. Soc. Am.*, 93, 409-413.
- Floyd, P. A., and Winchester, J. A. (1978). Identification and discrimination of altered and metamorphosed volcanic rocks using immobile elements. *Chem. Geol.*, 21, 291-306.
- Folk, R. L. and McBride, E. F. (1976). The Caballos novaculite revisited Part I: origin of novaculite members. *J. sedim. Petrol.*, 46, 659-669.
- Gair, J. E., and Slack, J. F. (1984). Deformation, geochemistry, and origin of massive sulfide deposits, Gossan Lead District, Virginia. *Econ. Geol.*, 79, 1483-1520.

- Gardner, H. D., and Hutcheon, I. (1985). Geochemistry, mineralogy, and geology of the Jason Pb-Zn deposits, Macmillan Pass, Yukon, Canada. *Econ. Geol.*, **80**, 1257-1276.
- Garrels, R. M., and Christ, C. L. (1965). *Solutions, minerals, and equilibria*. Harper and Row, and John Weatherhill, Inc., Tokyo, 450pp.
- Garrels, R. M. and MacKenzie, F. T. (1971). *Evolution of sedimentary rocks*. Norton, New York, 397pp.
- Gevers, T. W., Partridge, F. C. and Joubert, G. K. (1937). The pegmatite area south of the Orange River in Namaqualand. *Mem. geol. Surv. Un. S. Afr.*, **31**, 180pp.
- Giordano, T. H., and Barnes, H. L. (1979). Ore solution chemistry VI. PbS solubility in bisulfide solutions to 300°C. *Econ. Geol.*, **74**, 1637-1646.
- Goldberg, E. D. (1954). Marine geochemistry 1. Chemical scavengers of the sea. *J. Geol.*, **62**, 249-265.
- Goldberg, E. D. (1965). Minor elements in sea water, 163-196. In: Riley, J. P. and Skirrow, G., Eds., *Chemical oceanography*, Academic Press, London, 712pp.
- Graf, J. L. (1977). Rare earth elements as hydrothermal tracers during the formation of massive sulfide deposits in volcanic rocks. *Econ. Geol.*, **72**, 527-548.
- Grasshoff, K. (1975). The hydrochemistry of landlocked basins and fjords, 455-597. In: Riley, J. P., and Skirrow, G., Eds., *Chemical oceanography*. Academic Press, London.
- Grunau, H. R. (1965). Radiolarian cherts and associated rocks in space and time. *Eclogae Geol. Helv.*, **58**, 157-208.
- Gundlach, H. and Marchig, V. (1982). Ocean floor "metalliferous sediments" - two possibilities for genesis, 200-210. In: Amstutz, G. C., El Goresy, A., and Frenzel, G., Kluth, C., Moh, G., Wauschkuhn, A. and Zimmerman, R. A. Eds., *Ore genesis: The state of the art*. Spec. Pub. Soc. Geol. appl. Miner. Deps., 2. Springer Verlag, Heidelberg, 804pp.
- Haas, J. L. (1971). The effect of salinity on the maximum thermal gradient of a hydrothermal system at hydrostatic pressure. *Econ. Geol.*, **66**, 940-946.
- Hanor, J. S. (1969). Barite saturation in sea water. *Geochim. Cosmochim. Acta*, **33**, 894-898.
- Hanson, G. N. (1980). Rare earth elements in petrogenetic studies of igneous systems. *Ann. Rev. Earth Planet. Sc.*, **8**, 371-406.
- Hartnady, C., Joubert, P. and Stowe, C. (1985). Proterozoic crustal evolution in southwestern Africa. *Episodes*, **8**, 236-244.
- Haskin, L. A., Haskin, M. A., Frey, F. A. and Wildeman, T. R. (1968), 889-912. In: Ahrens, L. H. Ed., *Origin and distribution of the elements*. Pergamon Press.
- Hatcher, P. G. and Segar, D. A. (1976). Chemistry and continental margin sedimentation, 461-477. In: Stanley, D. J. and Swift, D. J. P. Eds., *Marine sediment transport and environmental management*. John Wiley.
- Heggie, D. and Lewis, T. (1984). Cobalt in pore waters of marine sediments. *Nature*, **311**, 453-455.
- Helgeson, H. C. (1969). Thermodynamics of hydrothermal systems at elevated temperatures and pressures. *Am. J. Sc.*, **267**, 729-804.
- Helgeson, H. C., Kirkham, D. H., and Flowers, G. C. (1981). Theoretical prediction of the thermodynamic behavior of aqueous electrolytes at high pressures and temperatures: IV. Calculation of activity coefficients, osmotic coefficients, and apparent molal and standard and relative partial molal properties to 600°C and 5 kb. *Am. J. Sc.*, **281**, 1249-1516.

- Hemley, J. J., Cygan, G. L. and d'Angelo, W. M. (1986). Effect of pressure on ore mineral solubilities under hydrothermal conditions. *Geology*, 14, 377-379.
- Herrmann, A. G. (1970). Yttrium and lanthanides. In: Wedepohl, K. H., Ed., *Handbook of Geochemistry*, Springer-Verlag Publishing Company, Berlin, 39,57-71-B - 39,57-71-O.
- Hertogen, J. and Gijbels, R. (1976). Calculation of trace element fractionation during partial melting. *Geochim. Cosmochim. Acta*, 40, 313-322.
- Hirst, D. M. (1962a). The geochemistry of modern sediments from the Gulf of Paria - I: The relationship between the mineralogy and the distribution of major elements. *Geochim. Cosmochim. Acta*, 26, 309-334.
- Hirst, D. M. (1962b). The geochemistry of modern sediments from the Gulf of Paria - II: The location and distribution of trace elements. *Geochim. Cosmochim. Acta*, 26, 1147-1187.
- Holland, H. D., (1979). Metals in black shales - a reassessment. *Econ. Geol.*, 74, 1676-1680.
- Holland, H. D., and Malinin, S. D. (1979). The solubility and occurrence of mon-ore minerals, 461-508. In: Barnes, H. L., Ed., *Geochemistry of hydrothermal ore deposits*. John Wiley & Sons, New York, 798pp.
- Horne, J. C. (1979). The orthoquartzite problem, p370. In: Ferm, J. C. and Horne, J. C., Eds., *Carboniferous depositional environments in the Appalachian region*. Univ. S. Carolina, Columbia.
- Hughes, C. J. (1976). Volcanogenic cherts in the late Precambrian Conception Group, Avalon Peninsula, Newfoundland. *Can. J. Earth Sci.*, 13, 512-519.
- Huston, D. L., and Large, R. R. (1987). Genetic and exploration significance of the Zinc Ratio ($100Zn/(Zn + Pb)$) in massive sulfide systems. *Econ. Geol.*, 82, 1521-1539.
- Hutchinson, R. W., Fyfe, W. S. and Kerrich, R. (1980). Deep fluid penetration and ore deposition. *Miner. Sci. Engng.*, 12, 107-120.
- Ishibashi, M., Fujinaga, T. and Kawamoto, T. (1962). Fundamental investigation on the dissolution and deposition of molybdenum, tungsten and vanadium in the sea. *Rec. Oceanogr. Wks. Japan, spec.* 6, 215-.
- Jacobs, J. W., Korotev, R. L., Blanchard, D. P. and Haskin, L. A. (1977). A well tested procedure for instrumental neutron activation analysis of silicate rocks and minerals. *J. Radioanalytical chem.*, 40, 93-114.
- James, H. L. (1954). Sedimentary facies of iron-formation. *Econ. Geol.*, 49, 235-285.
- Jefferson, C. W., Kilby, D. B., Pigage, L. C. and Roberts, W. J. (1983). The Cirque barite-lead-zinc deposits, northeastern British Columbia, 121-140. In: Sangster, D. F., Ed., *Short course in sediment-hosted lead-zinc deposits*. Mineralogical association of Canada, Victoria, 309 pp.
- Johansson, A., and Rickard, D. (1984). Isotopic composition of Phanerozoic ore leads from the Swedish segment of the Fennoscandian Shield. *Miner. Deposita*, 19, 249-255.
- Johansson, A., and Rickard, D. (1985). Some new lead isotope determinations from the Proterozoic sulfide ores of central Sweden. *Miner. Deposita*, 20, 1-7.
- Johnson, H. D. (1978). Shallow siliclastic seas, 207-258. In: Reading, H. G., Ed., *Sedimentary environments and facies*. Blackwell, Oxford, 569pp.
- Jones, B. F. and Bowser, C. J. (1978). The mineralogy and related chemistry of lake sediments, 179-235. In: Lerman, A. Ed., *Lakes. Chemistry, geology and physics*. Springer-Verlag, New York, 363pp.

- Joubert, P. (1971). The regional tectonism of the gneisses of part of Namaqualand. *Bull. Precamb. Res. Unit, Univ. Cape Town*, 10, 220pp.
- Joubert, P. (1974). The gneisses of Namaqualand and their deformation. *Trans. geol. Soc. S. Afr.*, 77, 339-345.
- Joubert, P. (1986). Namaqualand - a model of Proterozoic accretion? *Trans. geol. Soc. S. Afr.*, 89, 79-96.
- Kalogeropoulos, S. I. and Scott, S. D. (1983). Mineralogy and geochemistry of tuffaceous exhalites (tetsusekiei) of the Fukazawa Mine, Hokuroku District, Japan. *Econ. Geol., Monogr.* 5, 412-432.
- Kim, Y. A. and Zeitlin, H. (1968). The determination of molybdenum in seawater. *Limnol. Oceanogr.*, 13, 534-.
- Klein, C., Beukes, N. J. and Schopf, J. W. (1987). Filamentous microfossils in the Early Proterozoic Transvaal Supergroup: their morphology, significance, and paleoenvironmental setting. *Precamb. Res.*, 36, 81-94.
- Koepfel, V. (1980). Lead isotope studies of stratiform ore deposits of the Namaqualand, N. W. Cape Province, South Africa, and their implications on the age of the Bushmanland Sequence. *Proc. 5th IAGOD Symp.*, 1, 195-207.
- Krauskopf, K. B. (1959). The geochemistry of silica in sedimentary environments. *Soc. econ. palaeont. Miner. spec. Publ.*, 7, 4-19.
- Krauskopf, K. B. (1967). Source rocks for metal-bearing fluids, 1-33. In: Barnes, H. L. Ed., *Geochemistry of hydrothermal ore deposits*. Holt, Rinehart and Winston Inc., New York.
- Krauskopf, K. B. (1979). *Introduction to geochemistry*. McGraw-Hill, Inc., Tokyo, 617pp.
- Kronberg, B. I., Fyfe, W. S., Leonardos, O. H. Jr. and Santos, A. M. (1979). The chemistry of some Brazilian soils: element mobility during intense weathering. *Chem. Geol.*, 24, 211-229.
- Krynine, P. D. (1942). Differential sedimentation and its products during one complete geosynclinal cycle. *Anales 1 st Congreso Panamericano Ingenieria de Minas y Geologia*, 2, 537-561.
- Lambert, I. B. and Scott, K. M. (1975). Carbon contents of sedimentary rocks within and around the McArthur zinc-lead-silver deposit, Northern Territory. *J. geochem. Explor.*, 4, 365-369.
- Large, D. E. (1981). Sediment-hosted submarine exhalative lead-zinc deposits - review of their geological characteristics and genesis, 469-507. In: Wolf, K. H. Ed., *Handbook of strata-bound and stratiform ore deposits*, 9. Elsevier Publishing Company, Amsterdam.
- Large, D. E. (1981). The geochemistry of the sedimentary rocks in the vicinity of the Tom Pb-Zn-Ba deposit, Yukon Territory, Canada. *J. geochem. Explor.*, 15, 203-217.
- Large, D. E. (1983). Sediment-hosted massive sulphide lead-zinc deposits: an empirical model. In: Sangster, D. F., Ed., *Short course in sediment-hosted lead-zinc deposits*. Mineralogical association of Canada, Victoria, 309 pp.
- Large, R. R. (1977). Chemical evolution and zonation of massive sulfide deposits in volcanic terrains. *Econ. Geol.*, 72, 549-572.
- LeHuray, A. P., Caulfield, J. B. D., Rye, D. M., and Dixon, P. R. (1987). Basement controls on sediment-hosted Zn-Pb deposits: a Pb isotope study of carboniferous mineralization in Central Ireland. *Econ. Geol.*, 82, 1695-1709.
- Le Maitre, R. W. (1982). *Numerical petrology*. Elsevier Scientific Publishing Co., New York, 281pp.
- Leventhal, J. S. (1983). An interpretation of carbon and sulfur relationships in Black Sea sediments as indicators of environments of deposition. *Geochim. Cosmochim. Acta*, 47, 133-137.

- Lindstrom, D. J. and Korotev, R. L. (1982). TEABAGS: Computer programs for instrumental neutron activation analysis. *J. Radioanalytical chem.*, **70**, 439-458.
- Lipson, R. D. (1978). Some aspects of the geology of part of the Aggeneysberge and surrounding gneisses Namaqualand. *M.Sc. thesis (unpubl.)*, Univ. Witwatersrand, 100 pp.
- Lipson, R. D. (1980). The granitic rocks surrounding the Aggeneysberge: a metamorphosed rapakivi suite? *Trans. geol. Soc. S. Afr.*, **83**, 179-192.
- Lipson, R. D. (1981a). North west Cape aeromagnetic coverage - interpretation of linears and high - low pair anomalies. Internal GFSA Co. Rep. (unpubl.), 11pp.
- Lipson, R. D. (1981b). Manganese dispersion around the Broken Hill and Big Syncline orebodies, Aggeneys. Internal GFSA Co. Rep. (unpubl.), 7pp.
- Lipson, R. D., Martin, G. J., and Hobbs, J. B. M. (1986). Heavy mineral layers: evidence of a clastic origin for Bushmanland quartzite genesis at Aggeneys. *Trans. geol. Soc. S. Afr.*, **89**, 367-372.
- Lowe, D. R. (1983). Restricted shallow-water sedimentation of early Archean stromatolitic and evaporitic strata of the Strelley Pool Chert, Pilbara Block, Western Australia. *Precambr. Res.*, **19**, 239-283.
- Lydon, J. W. (1983). Chemical parameters controlling the origin and deposition of sediment-hosted stratiform lead-zinc deposits, 175-250. In: Sangster, D. F., Ed., *Short course in sediment-hosted lead-zinc deposits*. Mineralogical association of Canada, Victoria, 309 pp.
- Lydon, J. W. (1986). Models for the generation of metalliferous hydrothermal systems within sedimentary rocks and their applicability to the Irish Carboniferous Zn-Pb deposits, 555-577. In: Andrew, C. J., Crowe, R. W. A., Finlay, S., Pennell, W. M, and Pyne, J. F., Ed., *Geology and genesis of mineral deposits in Ireland*. Irish association for economic geology, Dublin, 711pp.
- MacLean, W. H. and Kranidiotis, P. (1987). Immobile elements as monitors of mass transfer in Hydrothermal alteration: Phelps Dodge massive sulfide deposit, Matagami, Quebec. *Econ. Geol.*, **82**, 951-962.
- MacRae, N.D. and Nesbitt, H.W. (1980). Partial melting in common sedimentary rocks: a mass balance approach. *Contr. Miner. Petrol.*, **75**, 21-26.
- Marchig, V., Gundlach, H., Moller, P. and Schley, F. (1982). Some geochemical indicators for discrimination between diagenetic and hydrothermal metalliferous sediments. *Mar. Geol.*, **50**, 241-256.
- Martin, G. J. (1989). The mineralogical investigation of borecore samples from the Gamsberg zinc deposit, north west Cape. *Gold Fields Laboratories Report (unpubl.)*, Gam/2, 15pp.
- Mason, B. (1958). *Principles of geochemistry*. John Wiley and Son, New York, 310pp.
- Matzat, E. and Shiraki, K. (1972-1978). Chrome. In: Wedepohl, K. H., Ed., *Handbook of Geochemistry*, Springer-Verlag Publishing Company, Berlin, 24-A-1 - 24-O-1.
- Maxwell, J. A. (1953). Geochemical study of chert and related deposits. *Geol. Soc. Am. Bull. Abstr.*, **64**, p1452.
- McBride, E. F. and Folk, R. L. (1977). The Caballos novaculite revisited Part II: chert and shale members and synthesis. *J. sedim. Petrol.*, **47**, 1261-1286.
- McLennan, S. M., and Taylor, S. R. (1979). Rare earth element mobility associated with uranium mineralisation. *Nature*, **282**, 247-250.

- McLennan, S. M., and Taylor, S. R. (1980). Th and U in sedimentary rocks: crustal evolution and sedimentary recycling. *Nature*, **285**, 621-624.
- McLennan, S. M., Nance, W. B. and Taylor, S. R. (1980). Rare earth element-thorium correlations in sedimentary rocks, and the composition of the continental crust. *Geochim. Cosmochim. Acta*, **44**, 1833-1839.
- McLennan, S. M., Taylor, S. R. and Eriksson, K. A. (1983). Geochemistry of Archean shales from the Pilbara Supergroup, Western Australia. *Geochim. Cosmochim. Acta*, **47**, 1211-1222.
- McLeod, R. L., and Stanton, R. L. (1984). Phyllosilicates and associated minerals in some Paleozoic stratiform sulfide deposits of southeastern Australia. *Econ. Geol.*, **79**, 1-22.
- Miall, A. D. (1979). Deltas, 43-56. In: Walker, R. G., Ed., *Facies models*. Ainsworth Press, Ontario, 211pp.
- Miall, A. D. (1984). Deltas, 105-118. In: Walker, R. G., Ed., *Facies models, second edition*. Ainsworth Press, Ontario, 317pp.
- Michard, A., and Albarede, F. (1986). The REE content of some hydrothermal fluids. *Chem. Geol.*, **55**, 51-60.
- Michard, A., Beaucaire, C., and Michard, G. (1987). Uranium and rare earth elements in CO₂-rich waters from Vals-les-Bains (France). *Geochim. Cosmochim. Acta*, **51**, 901-909.
- Minarik, L., Absalon, K., Kollnerova, Z., and Klecka, M. (1983). Chemical changes of granite during its weathering, 293-306. In: Augustithis, S. S., Ed., *Leaching and diffusion in rocks and their weathering products*. Theophrastus Publications S.A., Athens.
- Mitchell, A. H. G. and Reading, H. G. (1978). Sedimentation and tectonics, 439-476. In: Reading, H. G., Ed., *Sedimentary environments and facies*. Blackwell, Oxford.
- Mitchell, A. H. G. and Reading, H. G. (1986). Sedimentation and tectonics, 471-591. In: Reading, H. G., Ed., *Sedimentary environments and facies*. Blackwell, Oxford, 615pp.
- Monster, J., Appel, P. W. U., Thode, H. G., Schidlowski, M., Carmichael, C. M. and Bridgwater, D. (1979). Sulfur isotope studies in early Archean sediments from Isua, West Greenland: implications for the antiquity of bacterial sulfate reduction. *Geochim. Cosmochim. Acta*, **43**, 405-413.
- Moore, J.M. (1977). The geology of Namiesberg, northern Cape. *Bull. Precamb. Res. Unit, Univ. Cape Town*, **20**, 69pp.
- Moore, J.M. (1986). A comparative study of metamorphosed supracrustal rocks from the western Namaqualand Metamorphic Complex. *Ph.D. thesis (unpubl.)*, Univ. Cape Town, 370 pp.
- Murnane, R., and Clague, D. A. (1983). Nontronite from a low temperature hydrothermal system on the Juan de Fuca Ridge. *Earth Planet. Sc. Lett.*, **65**, 343-352.
- Murray, J. W. and Brewer, P. G. (1977). Mechanisms of removal of manganese, iron and other trace metals from sea water, 292-325. In: Glasby, G. P., Ed., *Marine manganese deposits*. Elsevier Publishing Company, Amsterdam.
- Nance, W. B. and Taylor, S. R. (1976). Rare earth element patterns and crustal evolution - I. Australian post-Archean sedimentary rocks. *Geochim. Cosmochim. Acta*, **40**, 1539-1552.
- Nesbitt, H. W. (1979). Mobility and fractionation of rare earth elements during weathering of a granodiorite. *Nature*, **279**, 206-210.
- Nesbitt, H. W. (1980). Genesis of the New Quebec and Adirondack granulites: evidence for their production by partial melting. *Contr. Miner. Petrol.*, **72**, 303-310.
- Nesbitt, H. W., Markovics, G. and Price, R. C. (1980). Chemical processes affecting alkalis and alkaline earths during continental weathering. *Geochim. Cosmochim. Acta*, **44**, 1659-1666.

- Nesbitt, H. W., and Young, G. M. (1982). Early Proterozoic climates and plate motions inferred from major element chemistry of lutites. *Nature*, **299**, 715-717.
- Nesbitt, H. W., and Young, G. M. (1984). Prediction of some weathering trends of plutonic and volcanic rocks based on thermodynamic and kinetic considerations. *Geochim. Cosmochim. Acta*, **48**, 1523-1534.
- Nielsen, H. (1979). Sulfur isotopes, 283-312. In: Jager, E., and Hunziker, J. C., Ed., *Lectures in isotope geology*. Springer-Verlag, Berlin.
- Norrish, K. and Hutton, J. T. (1969). An accurate X-ray fluorescence spectrographic method for the analysis of a wide range of geological samples. *Geochim. Cosmochim. Acta*, **33**, 431-453.
- Ohmoto, H. (1972). Systematics of sulfur and carbon isotopes in hydrothermal ore deposits. *Econ. Geol.*, **67**, 551-578.
- Ohmoto, H., and Rye, R. O. (1979). Isotopes of sulfur and carbon, 509-567. In: Barnes, H. L., Ed., *Geochemistry of hydrothermal ore deposits*. John Wiley & Sons, New York, 798pp.
- Ohmoto, H., Mizukami, M., Drummond, S. E., Eldridge, C. S., Pisutha-Arnond, V., and Lenagh, T. C. (1983). Chemical processes of Kuroko formation. *Econ. Geol., Monogr.* **5**, 570-604.
- Paizes, P. E. (1975). *The geology of an area between Vaalkop and Aggeneys in the vicinity of Pofadder, north-western Cape Province*. M.Sc. thesis (unpubl.) Univ. Witwatersrand, 220pp.
- Pertlik, F., Rogers, J. J. W., Adams, J. A. S., and Haack, U. K. (1978). Uranium. In: Wedepohl, K. H., Ed., *Handbook of Geochemistry*, Springer-Verlag Publishing Company, Berlin, 92-A-1 - 92-O-1.
- Pettijohn, F. J., Potter, P. E. and Siever, R. (1972). *Sand and sandstone*. Springer-Verlag, Berlin, 618pp.
- Pickrill, R. A., Irwin, J. and Shakespeare, B. S. (1981). Circulation and sedimentation in a tidal-influenced fjord lake: Lake McKerrow, New Zealand. *Est. Coastal Shelf Sci.*, **12**, 23-27.
- Piper, D. Z. (1971). The distribution of Co, Cr, Cu, Fe, Mn, Ni and Zn in Framvaren, a Norwegian anoxic fjord. *Geochim. Cosmochim. Acta*, **35**, 531-550.
- Piper, D. Z. (1974). Rare earth elements in the sedimentary cycle: a summary. *Chem. Geol.*, **14**, 285-304.
- Plimer, I. R. (1981). Water depth - a critical factor for exhalative ore deposits. *Bull. Aust. Bur. Miner. Resour. Geol. Geophys.*, **6**, 293-300.
- Plimer, I. R. and Elliott, S. M. (1979). The use of Rb/Sr ratios as a guide to mineralization. *J. geochem. Explor.*, **12**, 21-34.
- Plimer, I. R. and Lottermoser, B. G. (1988). Comments and replies on "Sedimentary model for the giant Broken Hill Pb-Zn deposit, Australia". *Geology*, **16**, 564-565.
- Plumstead, E. P. (1969). Three thousand million years of plant life in Africa. *Annex. Trans. geol. Soc. S. Afr.*, **72**, *Alex du Toit Mem. Lect.*, **11**, 72pp.
- Poldervaart, A. (1956). Zircon in rocks. 2. Igneous rocks. *Am. J. Sc.*, **254**, 521-554.
- Potter, P. E. (1984). South American modern beach sand and plate tectonics. *Nature*, **311**, 645-648.
- Pottorf, R. J., and Barnes, H. L. (1983). Mineralogy, geochemistry, and ore genesis of hydrothermal sediments from the Atlantis II Deep, Red Sea. *Econ. Geol., Monogr.* **5**, 198-223.
- Praekelt, H.E., Colliston, W.P., and Schoch, A.E. (1983). The stratigraphic interpretation of a highly deformed Proterozoic region in central Bushmanland, South Africa: first correlation of structurally separated metasediments of the Aggeneys Subgroup. *Precamb. Res.*, **23**, 177-185.

- Reid, D. L. (1979). Age relationships within the mid-Proterozoic Vioolsdrif Batholith, lower Orange River region. *Trans. geol. Soc. S. Afr.*, **82**, 305-311.
- Reid, D.L. and Barton, E.S. (1983). Geochemical characterization of granitoids in the Namaqualand geotraverse. *Spec. Publ. geol. Soc. S. Afr.*, **10**, 67-82.
- Reid, D. L., Welke, H. J., Erlank, A. J., and Betton, P. J. (1987). Composition, age and tectonic setting of amphibolites in the central Bushmanland Group, western Namaqua Province, southern Africa. *Precambr. Res.*, **36**, 99-126.
- Reid, D. L., Erlank, A. J., Waters, D. J. and Moore, J. M. (1987). *Isotopic and trace element characterisation of the Aggeneys-type metal sulphide deposits and host rocks*. C.S.I.R. N.G.P. Annual Prog. Rep. (unpubl.), 8pp.
- Reid, D. L. and Welke, H. J. (1988). Radiogenic and stable isotope characteristics of the Aggeneys-Gams ore deposits, central Bushmanland. *Abs., geol. Soc. S. A. Geocongress 88, Univ. Natal, Durban*, 497-499.
- Reinson, G. E. (1979). Barrier island systems, 57-74. In: Walker, R. G., Ed., *Facies models*. Ainsworth Press, Ontario, 211pp.
- Rhodes, D., Lantos, E. A., Lantos, H. A., Webb, R., J. and Owens, D. C. (1984). Pine Point orebodies and their relationship to the stratigraphy, structure, dolomitization, and karstification of the Middle Devonian Barrier Complex. *Econ. Geol.*, **79**, 991-1055.
- Richards, F. A. (1971). Anoxic versus oxic environments, 201-217. In: Hood, D. Ed., *Impingement of man on the oceans*. Wiley-Interscience, New York.
- Riley, J. P. and Chester, R. (1971). *Introduction to marine chemistry*. Academic Press, London, 465pp.
- Rimstidt, J. D., and Barnes, H. L. (1980). The kinetics of silica-water reactions. *Geochim. Cosmochim. Acta*, **44**, 1683-1699.
- Rimstidt, J. D. and Cole, D. R. (1983). Geothermal mineralization I: the mechanism of formation of the Beowawe, Nevada, siliceous sinter deposit. *Am. J. Sc.*, **283**, 861-875.
- Rozendaal, A. (1978). The Gamsberg zinc deposit, Namaqualand. In: Verwoerd, W.J. (ed.). *Mineralization in metamorphic terrains*. *Spec. Publ. geol. Soc. S. Afr.*, **4**, 235-265.
- Rozendaal, A. (1982). The petrology of the Gamsberg zinc deposit and the Bushmanland iron formations with special reference to their relationships and genesis. *Ph.D. thesis (unpubl.)*, Univ. Stellenbosch, 363 pp.
- Ruhlin, D. E., and Owen, R. M. (1986). The rare earth element geochemistry of hydrothermal sediments from the East Pacific Rise: examination of a seawater scavenging mechanism. *Geochim. Cosmochim. Acta*, **50**, 393-400.
- Russell, M. J. (1983). Major sediment-hosted exhalative zinc + lead deposits: formation from hydrothermal convection cells that deepen during crustal extension, 251-282. In: Sangster, D. F., Ed., *Short course in sediment-hosted lead-zinc deposits*. Mineralogical association of Canada, Victoria, 309 pp.
- Russell, M. J. (1986). Extension and convection: a genetic model for the Irish Carboniferous base metal and barite deposits, 545-554. In: Andrew, C. J., Crowe, R. W. A., Finlay, S., Pennell, W. M., and Pyne, J. F., Ed., *Geology and genesis of mineral deposits in Ireland*. Irish association for economic geology, Dublin, 711pp.
- Ryan, P.J., Lawrence, A.L., Lipson, R.D., Moore, J.M., Paterson, A., Stedman, D.P., and van Zyl, D. (1982). The Aggeneys base metal sulphide deposits, Namaqualand, South Africa. *Econ. Geol. Res. Unit, Univ. Witwatersrand, Inf. Circ.*, **160**, 33p.
- SACS (1980). (Compiler, L.E. Kent) Stratigraphy of South Africa, Part I. *Handb. geol. Soc. S. Afr.*, **8**, 690pp.

- Sahl, K., Doe, B. R. and Wedepohl, K. H. (1974). Lead. In: Wedepohl, K. H., Ed., *Handbook of Geochemistry*, Springer-Verlag Publishing Company, Berlin, 82-B-1 - 82-O-1.
- Salamons, W. (1980). Adsorption processes and hydrodynamic conditions in estuaries. *Envir. Technol. Lett.*, 1, 356-365.
- Samson, I. M., and Russell, M. J. (1987). Genesis of the Silvermines zinc-lead-barite deposit, Ireland: fluid inclusion and stable isotope evidence. *Econ. Geol.*, 82, 371-394.
- Sangster, D. F. (1972). Precambrian volcanogenic massive sulphide deposits in Canada: a review. *Can. geol. Surv. Pap.*, 72-22, 44pp.
- Sangster, D. F. (1976). Sulphur and lead isotopes in strata-bound deposits, 219-265. In: Wolf, K. H., Ed., *Handbook of strata-bound and stratiform ore deposits*, 2, Elsevier Publishing Company, Amsterdam.
- Sato, T. (1972). Behaviors of ore-forming solutions in seawater. *Min. Geol.*, 22, 31-42.
- Saxena, S. K. (1966). Evolution of zircons in sedimentary and metamorphic rocks. *Sedimentology*, 6, 1-33.
- Schreyer, W., Werding, G. and Abraham, K. (1981). Corundum-fuchsite rocks in greenstone belts of southern Africa: petrology, geochemistry, and possible origin. *J. Petrology*, 22, 191-231.
- Senior, A. and Leake, B.E. (1978). Regional metasomatism and the geochemistry of the Dalradian metasediments of Connemara, western Ireland. *J. Petrology*, 19, 585-623.
- Sharma, G. D. (1971). Sediments, 169-188. In: Hood, D. Ed., *Impingement of man on the oceans*. Wiley-Interscience, New York.
- Shaw, D. M. (1977). Trace element behaviour during anatexis. In: Proc. Chapman Conference on partial melting in the earth's upper mantle, 96, Bull. Dept. Geol. mineral. Industr. Portland, Oregon, 189-283.
- Shaw, D. M. (1979). Trace element melting models. *Phys. chem. earth*, 11, 577-586.
- Shepard, F. P. and Young, R. (1961). Distinguishing between beach and dune sands. *J. sedim. Petrol.*, 31, 196-214.
- Sheu, D. and Burkart, B. (1982). Inferred paleosalinity and phosphate content of carbonate rocks from a cyclic evaporite-carbonate rock sequence. *J. sedim. Petrol.*, 52, 897-903.
- Sholkovitz, E. R. (1976). Flocculation of dissolved organic and inorganic matter during the mixing of river water and seawater. *Geochim. Cosmochim. Acta*, 40, 831-845.
- Sholkovitz, E. R. (1978). The flocculation of dissolved Fe, Mn, Al, Cu, Ni, Co and Cd during estuarine mixing. *Earth Planet. Sc. Lett.*, 41, 77-86.
- Skei, J. (1983). Geochemical and sedimentological considerations of a permanently anoxic fjord - Framvaren, south Norway. *Sedim. Geol.*, 36, 131-145.
- Skei, J. M. and Melsom, S. (1982). Seasonal and vertical variations in the chemical composition of suspended particulate matter in an oxygen-deficient fjord. *Est. Coastal Shelf Sci.*, 14, 61-78.
- Smith, P. A., and Cronen, D. S. (1983). The geochemistry of metalliferous sediments and waters associated with shallow submarine hydrothermal activity (Santorini, Aegean Sea). *Chem. Geol.*, 39, 241-262.
- Spry, P. G. and Wonder, J. D. (1989). Manganese-rich garnet rocks associated with the Broken Hill Lead-Zinc deposit, New South Wales, Australia. *Can. Mineral.*, 27, 275-292.
- Stanton, R. L. (1972). A preliminary account of chemical relationships between sulfidated lode and "banded iron formation" at Broken Hill, New South Wales. *Econ. Geol.*, 67, 1128-1145.

- Stanton, R. L., Roberts, W. P. H. and Chant, R. A. (1978). Petrochemical studies of the ore environment at Broken Hill, New South Wales: 5 - Major element constitution of the load and its interpretation. *Proc. Australas. Inst. Min. Metall.*, **266**, 51-77.
- Stedman, D. P. (1980). The structural geology and metamorphic petrology of Black Mountain, Namaqualand. *M.Sc. thesis (unpubl.)*, Univ. Witwatersrand.
- Stevens, B. P. J. and Stroud, W. J. (1983). Rocks of the Broken Hill Block: their classification, nature, stratigraphic distribution, and origin. *Rec. geol. Surv. New South Wales*, **21**, 323pp.
- Stowe, C. W. (1986). Synthesis and interpretation of structures along the north-eastern boundary of the Namaqua Tectonic Province, South Africa. *Trans. geol. Soc. S. Afr.*, **89**, 185-198.
- Strens, M. R., Cann, D. L., and Cann, J. R. (1987). A thermal balance model of the formation of sedimentary-exhalative lead-zinc deposits. *Econ. Geol.*, **82**, 1192-1203.
- Strickland, J. D. H. (1965). Organic productivity, 478-610. In: Riley, J. P., and Skirrow, G., Eds., *Chemical oceanography*. Academic Press, London, 712pp.
- Strong, D. F. (1984). Rare earth elements in volcanic rocks of the Buchans area, Newfoundland. *Can. J. Earth Sci.*, **21**, 775-780.
- Stroud, W. J., Willis, I. L., Bradley, G. M., Brown, R. E., Stevens, B. P. J. and Barnes, R. G. (1983). Amphibole or pyroxene-bearing rocks, 227-287. In: Stevens, B. P. J. and Stroud, W. J., Eds., *Rocks of the Broken Hill block: their classification, nature, stratigraphic distribution, and origin*. *Record geol. Surv. New South Wales*, **21**.
- Sugisaki, R., Yamamoto, K. and Adachi, M. (1982). Triassic bedded cherts in central Japan are not pelagic. *Nature*, **298**, 644-647.
- Sundby, B., Silverberg, N. and Chesselet, R. (1981). *Geochim. Cosmochim. Acta*, **45**, 293-307.
- Taylor, S. R. (1964). Abundance of chemical elements in the continental crust: a new table. *Geochim. Cosmochim. Acta*, **28**, 1273-1285.
- Taylor, S. R. (1979). Chemical composition and evolution of the continental crust: the rare earth element evidence, 353-376. In: Mc Elhinny, W. M., Ed., *The earth: its origin, structure and evolution*. Academic Press, London.
- Taylor, S. R. and Gorton, M. P. (1977). Geochemical application of spark source mass spectrography - III. Element sensitivity, precision and accuracy. *Geochim. Cosmochim. Acta*, **41**, 1375-1380.
- Taylor, S. R. and McLennan, S. M. (1981). The rare earth element evidence in Precambrian sedimentary rocks: implications for crustal evolution, 527-548. In: Kroner, A. Ed., *Precambrian plate tectonics*. Elsevier Publishing Company, Amsterdam, 781pp.
- Temple, J. T. (1978). The use of factor analysis in geology. *Mathl. Geol.*, **4**, 379-387.
- Thomas, W. A. and Mann, C. J. (1966). Late Jurassic depositional environments, Louisiana and Arkansas. *Bull. Am. Ass. Petrol. Geol.*, **50**, 178-182.
- Thurston, D. R. (1972). Studies on bedded cherts. *Contr. Miner. Petrol.*, **36**, 329-334.
- Tlig, S. and M'Rabet, A. (1985). A comparative study of the rare earth element (REE) distributions within the Lower Cretaceous dolomites and limestones of Central Tunisia. *Sedimentology*, **32**, 897-907.
- Tourtelot, H. A. (1979). Black Shale - its deposition and diagenesis. *Clays Clay Miner.*, **27**, 313-321.

- Trimonis, E. S., Shimkis, P. P. and Ross, D. A. (1978). Mineral composition of coarse-silt fraction of the Black Sea Late Cenozoic sediments, 413-426. *In: Usher, J. L. and Supko, L., Eds., Initial Reports of the Deep Sea Drilling Project, 42 (2)*, Washington U. S. Govt, Printing Office.
- Trudinger, P. A. (1981). Origins of sulphide in sediments. *Bull. Aust. Bur. Miner. Resour. Geol. Geophys.*, 6, 279-285.
- Turekian, K. K. (1968). *Oceans*. Prentice Hall, New Jearsey, 120pp.
- Turekian, K. K. (1968-1978). Nickel. *In: Wedepohl, K. H., Ed., Handbook of Geochemistry*, Springer-Verlag Publishing Company, Berlin, 28-B-1 - 28-O-2.
- Turekian, K. K. (1971). Rivers, tributaries and estuaries, 9-73. *In: Hood, D. Ed., Impingement of man on the oceans*. Wiley-Interscience, New York.
- Turekian, K. K. (1972). *Chemistry of the earth*. Holt, Rinehart and Winston, Inc., New York, 131pp.
- van de Kamp, P. C., Leake, B. E. and Senior, A. (1976). The petrography and geochemistry of some Californian arkoses with application to identifying gneisses of metasedimentary origin. *J. Geol.*, 84, 195-212.
- Vine, J. D. (1966). Element distribution in some shelf and eugeosynclinal black shales. *Bull. U.S. geol. Surv.*, 1214E, E1-E31.
- Vine, J. D. and Tourtelot, E. B. (1970). Geochemistry of black shale deposits - a summary report. *Econ. Geol.*, 65, 253-272.
- Vinogradov, A. P. (1962). Average contents of chemical elements in the principal types of igneous rocks of the earth's crust. *Geochemistry*, 7, 641-664.
- von Gehlen, K., Nielsen, H., Chunnett, I., and Rozendaal, A. (1983). Sulphur isotopes in metamorphosed Precambrian Fe-Pb-Zn-Cu sulphides and baryte at Aggeneys and Gamsberg, South Africa. *Mineralog. Mag.*, 47, 481-486.
- Vorma, A. (1976). On the petrochemistry of rapakivi granites with special reference to the Laitila Massif, southwestern Finland. *Bull. geol. Surv. Finland*, 285, 98pp.
- Walker, R. G. (1979). Turbidites and associated coarse clastic deposits, 91-104. *In: Walker, R. G., Ed., Facies models*. Ainsworth Press, Ontario, 211pp.
- Walker, R. G. and Cant, D. J. (1979). Sandy fluvial systems, 23-31. *In: Walker, R. G., Ed., Facies models*. Ainsworth Press, Ontario, 211pp.
- Walker, R. G. and Middleton (1979). Eolian sands, 33-41. *In: Walker, R. G., Ed., Facies models*. Ainsworth Press, Ontario, 211pp.
- Watanabe, T., Yui, S, and Kato, A. (1970). Metamorphosed bedded manganese deposits of the Noda-Tamagawa mine. *In: Tatsumi, T., Ed., Volcanism and ore genesis*, University Tokyo Press, Tokyo, 143-152.
- Waters, D. J. (1986). Metamorphic zonation and thermal history of pelitic gneisses from western Namaqualand, South Africa. *Trans. geol. Soc. S. Afr.*, 89, 97-102.
- Waters, D. J. and Whales, C. J. (1984). Dehydration melting and the granulite transition in metapelites from southern Namaqualand, S. Africa. *Contr. Miner. Petrol.*, 88, 269-275.
- Watkeys, M. K. (1986). The Achab Gneiss: a "floor" in Bushmanland or a flaw in Namaqualand? *Trans. geol. Soc. S. Afr.*, 89, 103-116.
- Wedepohl, K. H. (1972). Zinc. *In: Wedepohl, K. H., Ed., Handbook of Geochemistry*, Springer-Verlag Publishing Company, Berlin, 30-B-1 - 30-H-3.

- Welke, H. J. and Smith, C. B., (1984). Lead isotope characterization of the Aggeneys-Gamsberg ore bodies in relation to possible source rocks, with implications for Bushmanland metallogenesis. *Abs., Conference on Middle to Late Proterozoic lithosphere evolution, Precambr. Res. Unit, Univ. Cape Town, p.8-9.*
- White, D. E. (1965). Saline waters of sedimentary rocks. *Am. Ass. Petrol. Geologists, Mem. 4, 342-366.*
- White, J. C., and White, S. H. (1983). Semi-brittle deformation within the Alpine fault zone, New Zealand. *J. struct. Geol., 5, 579-589.*
- Wildeman, T. R. and Haskin, L. (1965). Rare-earth elements in ocean sediments. *J. Geophys. Res., 70, 2905-2910.*
- Williams, N. (1978). Studies of the base metal sulfide deposits at McArthur River, Northern Territory, Australia: II. The sulfide-S and organic-C relationships of the concordant deposits and their significance. *Econ. Geol., 73, 1036-1056.*
- Willis, I. L., Barnes, R. G., Stevens, B. P. J., Stroud, W. J. and Brown, R. E. (1988). Comments and replies on "Sedimentary model for the giant Broken Hill Pb-Zn deposit, Australia". *Geology, 16, 567.*
- Wilson, J. D. (1981). The geology of the Broken Hill deposit, Aggeneys, north west Cape. *Abs., South African geodynamics symposium, Geocongress '81, 231-233.*
- Winkler, H. J. F. (1976). *Petrogenesis of metamorphic rocks.* Springer-Verlag, New York, 334pp.
- Wright, J. V., Haydon, R. C. and McConachy, G. W. (1987). Sedimentary model for the giant Broken Hill Pb-Zn deposit, Australia. *Geology, 15, 598-602.*
- Zierenberg, R. A. and Shanks, W. C. III, (1986). Isotopic constraints on the origin of the Atlantis II, Suakin and Valdivia brines, Red Sea. *Geochim. Cosmochim. Acta, 50, 2205-2214.*